

PHOTOCURABLE HYDROGELS FOR TISSUE ENGINEERING APPLICATIONS

*Original*

PHOTOCURABLE HYDROGELS FOR TISSUE ENGINEERING APPLICATIONS / Zanon, Michael. - (2023 May 29), pp. 1-185.

*Availability:*

This version is available at: 11583/2978994 since: 2023-06-01T08:41:33Z

*Publisher:*

Politecnico di Torino

*Published*

DOI:

*Terms of use:*

Altro tipo di accesso

This article is made available under terms and conditions as specified in the corresponding bibliographic description in the repository

*Publisher copyright*

(Article begins on next page)



Politecnico  
di Torino

ScuDo  
Scuola di Dottorato ~ Doctoral School  
WHAT YOU ARE, TAKES YOU FAR

Doctoral Dissertation  
Doctoral Program in Material Science and Technology (35<sup>th</sup> Cycle)

# Photocurable Hydrogels for Tissue Engineering Applications

Michael Zanon

**Supervisors:**

- Prof. Marco Sangermano, Supervisor, Politecnico di Torino, Department of Applied Science and Technology (Torino, Italy)
- Dr. Annalisa Chiappone, Co-Supervisor, Università degli Studi di Cagliari, Department of Chemical and Geological Sciences (Cagliari, Italy)

**Doctoral Examination Committee:**

- Prof. Francesco Secci, *Referee*, Università degli Studi di Cagliari, Department of Chemical and Geological Sciences (Cagliari, Italy)
- Dr. Valentina Olivieri, *Referee*, Università degli Studi di Catania, Department of Chemical Sciences (Catania, Italy)
- Prof. Paula Bosh, Consejo Superior de Investigaciones Científicas (CSIC), Institute of Polymer Science and Technology (Madrid, Spain)
- Prof. Victor Sans, Universitat Jaume I, Institute of Advanced Materials (Castellón de la Plana, Spain)
- Prof. Chiara Tonda-Turo, *President*, Politecnico di Torino, Department of Mechanical and Aerospace Engineering (Torino, Italy)

Politecnico di Torino  
2023



## **Declaration**

I hereby declare that, the contents and organization of this dissertation constitute my own original work and does not compromise in any way the rights of third parties, including those relating to the security of personal data.

Michael Zanon

2023

\* This dissertation is presented in partial fulfillment of the requirements for **Ph.D. degree** in the Graduate School of Politecnico di Torino (ScuDo).



*I would like to dedicate this thesis to my loving parents and sisters.*



# Acknowledgment

Words cannot express my gratitude to my supervisors Prof. Marco Sangermano and Dr. Annalisa Chiappone for their invaluable patience, support, trust, and feedback all over my doctoral program. The opportunity to work with you both grow me not just as a scientist but also as a human being, able to face countless problems while learning from them. That's the best gift I could ever asked for.

A special mention is necessary for two other people who deserve mi sincero agradecimiento, Prof. Paula Bosh and Dr. Laura Montalvillo-Jimenez. Their knowledge and experience guided me with success all over that winding path that is a chemical Lab. Your contribution was really important to me, making me even more bounded with Spain than what I already was.

I also want to thank all the collaborators that gave important contributions to my research, both in terms of research and suggestions: Nadia Garino, Marta Canta, Raquel Cue-López, Enrique Martínez-Campos Minna Hakkarainen, Francesca Frascella, Desirée Baruffaldi, Davy-Louis Versace and Ignazio Roppolo.

A special gratitude to my colleagues in Turin. We shared not just a journey but also our frustrations, success and most importantly friendship. You guys were fundamental to me. Lorenzo, Luisa, Camilla, Andrea, Luigi, Angelo, Merve, Rossella, Christian, Dumitru, Matteo, Carlo, Beatrice, Maria and Alejandra.

I would also like to thank my Spanish family in Madrid. It is extraordinary how you welcomed that weird guy from Italy without any hesitations. Bonds like that are really difficult to break. Paula, Javiera, Estefania, Larissa, Maria, Grazia, Sandro, Itsaso, Adrian, Ruben, Carol and Paco.



Thanks to my crazy and wild friends! What can I say more than the unconditional love I have for you? Let's just affirm that I owe you my mental health (I leave you decide in which way): Andrea P., Laura, Mauro, Maria, Nicola, Silvia, Stacy, Giusi, Stefano, Greta, Alessia and Andrea F.

Particular gratitude goes to the micio always on my side, Danny. No words can really express what a support and love you showed me during these three years. I just want to say that I will try from now on, even if it is impossible, to repay you in every way I can. Thank you pips.

I would also like to thank my entire family: Mum, Dad, Jessica and Sofia. You always encouraged and supported me to go further without any pressure but comprehension. We are just like a puzzle, different pieces of the same extraordinary pattern. I love you all.

Lastly but as it was the first, thanks to Ilaria Orlando. I definitely owe you this.

# Abstract

Every year millions of people around the world face serious medical complications due to tissues/organs damages/failure, still leading to death in a large number of cases. In fact, just in the European Union 21 patients die every day while waiting for an organ transplant. However, a chronic lack of donors is a global phenomenon with kilometric organs waiting lists; 150'000 patients were waiting for organ donation in 2018 just in the EU. The arrival of tissue engineering at the beginning of this century intended to give a solution to the problem, merging the principles of engineering and life science into an interdisciplinary field toward the development of biological substitutes able to replace, restore or maintain the tissue features. Hydrogels play a unique role within this field, thanks to their unique structure similarity with the mammalian extracellular matrix. Principally natural polymers-derived hydrogels formed by photopolymerization emerged in the last decades as a “greener” and sustainable option to create scaffolds. Indeed, while the natural sources origin and properties of natural polymers (often extracted from industrial wastes) are hardly reproducible in laboratory, the process of photopolymerization (especially performed with visible light) presents the physiological conditions of temperature, pH and solvent (aqueous, buffer or cell culture medium) necessary in biological applications. In this dissertation, a wide range of photocurable natural polymer-derived hydrogels are develop with applications in the tissue engineering field, exploiting both synthesis procedures and hydrogel characterization while pursuing, when possible, the creation of 3D-printed detailed geometries able to mimic the complex and intrinsic architectures characteristic of the human body.

After a brief overview on the hydrogels state of arts and historical progress (Chapter 1), the photo-crosslinking process and technologies are exploited on Chapter 2. The first experimental investigation (Chapter 3) exploits a green and sustainable manner to synthetize a photocurable methacrylated chitosan through microwave-assisted organic chemistry (MAOS). The low reagent amount used, coupled with a relatively high degree of substitution achieved makes the process a sustainable alternative compared to traditional thermal synthesis, giving rise to stiff and biodegradable hydrogels employable on in-vitro investigations for lung tumoral cells models.

However, just simple extruded grids were 3D-printed in the aforementioned experimental chapter on methacrylated chitosan, due to a poor reactivity of the compound in water environments. Within Chapter 4, the additional contribution of a natural derived quinizarin dyes on the pristine formulation tune up the methacrylated polysaccharide reactivity, enabling the creation of complex and detailed geometries with a DLP 3D-printer, both in terms of final structure resolution and CAD fidelity. Moreover, a biological characterization proved the maintenance of the hydrogels biocompatibility, favoring the implementation of the system toward the creation of scaffolds to be employed as substitutes for soft tissues applications.

Chapter 5 focus on the development of alginate hydrogels obtained through thiol-yne reactions. The reason of the study on “click chemistry” reactions reside on their shorter propagation rate of radicals, able to facilitate unintended cells necrosis behaviors. After incorporation of alkyne moieties on the alginate backbone with good results in terms of substitution, two different water-soluble dithiol crosslinkers were employed to create hydrogels through visible light photopolymerization. The subsequent biological characterization certifies the good biocompatibility of the system, validating the proposed direction for the development of surgical fillers/medical patches for tissue engineering applications.

A possible improvement to create photocurable hydrogel is presented on Chapter 6, where a fully modified alginate suitable for thiol-ene reactions was investigated. Apart for radicals, also a necrotic critical response to overwhelming chemical conditions done by small molecules can lead to an unprogrammed form of cells death, as in the case of the previous reported usage of dithiol crosslinkers. Within this chapter, various chemical approaches were investigated to synthesize two batches of ene/thiol-substituted alginate, resulting in the creation of the first thiol-ene hydrogel formed without the addition of external crosslinkers. The improved stiffness, as much as is good biocompatibility, asses the hydrogel employment in the creation of scaffolds for stiffer soft tissues, such as intestines or tendons.

Lastly, the incorporation of unmodified gelatin into a well-known biocompatible polymer (poly-ethylene glycol diacrylate) is the main focus of Chapter 7. In fact, natural polymers never possess intrinsic chromophore moieties suitable to create photopolymerizable crosslinked networks, so antecedent steps of synthesis are always required to make them processable with this technique. In

this framework, an easy and low-cost way to chemically incorporate gelatin within the polymer network, without previous modification, demonstrate an interesting method to create substrates or models able to promote cell attachment and proliferation for in-vitro studies.





# Table of content

<b>Acknowledgment .....</b>	<b>i</b>
<b>Abstract .....</b>	<b>iii</b>
<b>Hydrogels: Concept and History .....</b>	<b>1</b>
<b>1.1 Classification: Based on the crosslinking method .....</b>	<b>4</b>
1.1.1. Physical crosslinking .....	5
1.1.2. Chemical crosslinking .....	7
1.1.3. IPNs and double network crosslinking .....	10
<b>1.2. Classification: based on the material .....</b>	<b>12</b>
1.2.1. Synthetic polymers .....	12
1.2.2. Natural polymers .....	14
1.2.2.1. Polysaccharide: Chitosan .....	16
1.2.2.2. Polysaccharide: Alginate .....	16
1.2.2.3. Protein: Collagen/Gelatin .....	17
<b>1.3. Applications .....</b>	<b>18</b>
1.3.1. Tissue engineering .....	20
<b>Photocurable hydrogels for tissue engineering applications.....</b>	<b>23</b>
<b>2.1. Photo-crosslinking processes.....</b>	<b>23</b>
2.1.1. Radical photopolymerization .....	25
<b>2.2. Light-induced additive manufacturing in tissue engineering .....</b>	<b>29</b>
2.2.1. Extrusion-based technologies .....	29
2.2.2. Lithography-based technologies .....	32
<b>Chitosan hydrogels .....</b>	<b>35</b>
<b>3.1. Introduction .....</b>	<b>35</b>
<b>3.2. Materials and procedures .....</b>	<b>37</b>
Materials .....	37
Synthesis of methacrylated chitosan (CHI-MA) .....	37
Synthesis of mono/di-methacrylated quinizarin (Q-1MAc and Q-2Mac) .....	38
<b>3.3. Characterization methods .....</b>	<b>38</b>
Attenuated total reflectance-infrared spectroscopy and nuclear magnetic resonance spectroscopy analysis (ATR-FTIR and <sup>1</sup> H-NMR) .....	38
Q-1MAc and Q-2MAc characterization .....	39
Hydrogel characterization.....	39

Enzymatic degradation, cell viability, proliferation and migration .....	41
<b>3.4. Results and discussion .....</b>	<b>43</b>
Microwave-assisted methacrylation of chitosan .....	43
Hydrogel characterization.....	47
3D printing .....	52
Enzymatic degradation .....	52
Preliminary investigation of the photocurable formulation for DLP 3D-printing	54
Preliminary investigation of the methacrylated quinizarin formulations.....	57
Formulations preparation and hydrogel characterization .....	61
<i>3D-printing of the quinizarin-based formulations</i> .....	63
Cell viability, proliferation and migration on methacrylated chitosan for 3D in-	
vitro model for cancerous tissues.....	65
Cell viability and proliferation assays on quinizarin-loaded hydrogels for soft	
tissue substitutes scaffolds .....	66
<b>3.5. Conclusions .....</b>	<b>68</b>
<b>Alginate hydrogels.....</b>	<b>69</b>
<b>4.1. Introduction .....</b>	<b>69</b>
<b>4.2. Materials and procedures .....</b>	<b>71</b>
Materials .....	71
Synthesis of alginate-yne (SA-PA) .....	71
Synthesis of Thiolated Oxidized Alginate (TOSA) .....	72
Synthesis of Thiolated Alginate (SA-CYS and SA-CSA).....	73
Synthesis of ene Alginate (SA-NOR).....	73
Preparation of the Thiol-Yne photocurable hydrogel .....	74
Preparation of the Thiol-Ene photocurable hydrogel .....	74
<b>4.3. Characterization methods .....</b>	<b>74</b>
Quantification of the aldehyde content (potentiometric titration).....	74
Quantification of the thiol content (Ellman reagent titration) .....	75
Spectrometric analysis ( <sup>1</sup> H-NMR, <sup>13</sup> C-NMR, solid-state <sup>13</sup> C-NMR, ATR-FTIR and	
RAMAN spectroscopy) .....	76
Gel permeation chromatography .....	77
Hydrogel characterization.....	77
Cell viability and proliferation.....	78
<b>4.4. Results and discussion .....</b>	<b>79</b>
Synthesis of alkine alginate (SA-PA).....	79
Synthesis of thiolated alginate via oxidation, imine bond creation and reductive	
amination (TOSA).....	82
Synthesis of thiolated alginate via carbodiimide chemistry (SA-CSA and SA-CYS)	
.....	85
Ene modification of alginate via carbodiimide chemistry.....	87



Thiol-yne hydrogels characterization.....	89
Thiol-ene hydrogel characterization .....	95
Cell viability and proliferation .....	97
<b>4.5. Conclusions .....</b>	<b>99</b>
<b>Gelatin hydrogels .....</b>	<b>101</b>
<b>5.1. Introduction .....</b>	<b>101</b>
<b>5.2. Materials and procedures .....</b>	<b>102</b>
Materials .....	102
Formulations .....	102
3D printing .....	103
<b>5.3. Characterization methods .....</b>	<b>103</b>
Hydrogel characterization.....	103
Investigation on the gelatin incorporation .....	104
Hydrogel purification, cell viability and proliferation .....	105
<b>5.4. Results and discussion .....</b>	<b>106</b>
Preliminary investigation on the formulations .....	106
Hydrogels Characterization.....	108
Hydrogel purification, cell viability and proliferation .....	110
<b>5.5. Conclusions .....</b>	<b>115</b>
<b>General conclusions .....</b>	<b>117</b>
<b>Appendix A .....</b>	<b>121</b>
<b>A1 List of abbreviations .....</b>	<b>121</b>
<b>A2 List of figures.....</b>	<b>124</b>
Chapter 1 .....	124
Chapter 2 .....	124
Chapter 3 .....	125
Chapter 4 .....	127
Chapter 5 .....	128
Chapter 6 .....	128
<b>A3 List of tables.....</b>	<b>129</b>
Chapter 3 .....	129
Chapter 4 .....	129
Chapter 5 .....	130
<b>Appendix B.....</b>	<b>131</b>
<b>B1 List of publications .....</b>	<b>131</b>

Related to the PhD project .....	131
Unrelated to the PhD project.....	131
<b>B2 List of conferences attended by the author .....</b>	<b>131</b>
<b>References .....</b>	<b>133</b>



# Chapter 1

## Hydrogels: Concept and History

The first reported term “hydrogel” appeared in literature at the end of the XIX century to describe a silica gel obtained by sol-gel chemistry [1].

Since then, and especially around the decade 1940s-1950s, the theoretical study of gels and their properties were further explored and dominated by three main researchers, named L.R.G Treloar [2], M.L. Huggins [3,4], and the future Nobel Prize winner P.J. Flory [5–7]. In particular, Flory developed a mathematical theory for the polymerization of compounds with more than two functional groups, leading some years after to the Flory-Stockmayer theory of gelation and, with the previous contribution of W.H. Carothers, to the concept of polymer network [8–10]. For this reason, it is not surprising that at the same time (1936) one of the future first polymers used to create hydrogels was synthesized by the DuPont scientists (the same company who hosted at the beginning of their career both Carothers and his junior assistant Flory), called poly(2-hydroxyethyl methacrylate) or pHEMA [11]. Nevertheless, it wasn't until 1960 that the first hydrogels were reported by Wichterle and Lim in the way we know them nowadays, e.g., a three-dimensional hydrophilic polymer network able to absorb and retain a large amount of water without dissolving or losing their stability and withstanding properties. Curiously, they used exactly the polar (Hydroxyethyl)methacrylate or HEMA monomer to create “soft” contact lenses [12], opening the employment of hydrogels in one of the future main fields of application of these materials, that is biomedical engineering.

In the following two decades, the scientist's efforts were essentially concentrated on relatively easy thermoset synthetic polymer networks with the main applications concerning ophthalmic and simple drug delivery studies. The network structure was extensively investigated granting the modeling of different physio-chemical properties such as the drug/solute diffusivity or the crosslinking density. At this time, hydrogels were prevalently formed by the polymerization of water-soluble monomers in presence of multifunctional crosslinkers [13]. Indeed, the first creation of polyethylene glycol (PEG) and polyvinyl alcohol (PVA) hydrogels by gamma radiation [14,15] are dated 1970 and 1977 while Nalbandian et al. explored the Pluronic hydrogel release of silver nitrate/silver lactate as antimicrobial agents for thermal burns treatments in 1972 [16]. Also poly(acrylamide) (PAM) gained attention in the same years, even though employed mainly as agricultural gel [13]. It was from the mid-late 70s to the end of the 80s that the approach toward hydrogels changed radically from simple water-swollen macromolecular networks into stimuli-sensitive materials (mostly based on weak or physical interactions) able to change their characteristics based on the surrounding conditions such as pH, temperature, quality of solvent or high concentrations of biomolecules [17]. The first publication on pH-sensitive hydrogels is attributed to Kopeček et al. thanks to the introduction of ionogenic groups into HEMA hydrogels [18]. Thermo-responsive hydrogels, instead, were demonstrated in 1986 by Hoffman et al. [19] for selective removal of substances from aqueous solutions; one of the first publications using hydrogels for water treatment applications.

In the next stage the hydrogels investigation moved toward new systems, interactions and materials to enhance or finely tune the previous mechanical, thermal and biocompatible properties achieved, without forgetting to explore new chemical reactions and applications [13]. For example, it is dated 1987 the first evidence of stereocomplexation of PLLA and PDLA to create soft hydrogels [20]. In fact, in this period natural or natural-derived polymers started to gain increasingly attention in the formation of hydrogel, even though generally just entrapped into the polymer network [21–24]. Indeed, these studies anticipated a process that will become predominant in the next decades, the movement toward sustainability, circular economy and in general “green chemistry”. One of the most important applications emerged in these years (later intensively related with natural polymers) was tissue engineering, especially thanks to one of the first pioneers in this field, J.P. Vacanti [25–27]. Also the techniques to create hydrogels improved and evolved in this period; it is dated 1993 one of the first hydrogel produced by photopolymerization by Sawhney et al. [28][29], where a

PEG structured hydrogel was formed by exposure to visible light creating a scaffold suitable for contact with cells.

Nowadays, with the increasing knowledge in organic chemistry, a large number of chemically crosslinked hydrogels has been developed. These new materials, except for the outstanding properties and features (self-healing [30,31], multi-component [32,33], double-network [34,35], interpenetrated polymer networks [36,37], shape memory [38,39], minimal or absent biotoxicity [40,41], etc.), are designed and tailored exactly on the final application they were made for; this is the reason why they are called “smart hydrogels”. An historical resume of the main discoveries is reported as a timeline and shown in Figure 1.1.

Other than an historical differentiation, hydrogels can be classified based on the material origin (natural or synthetic), crosslinking method (physical or chemical crosslinking), composition (homopolymer or copolymer networks) and many other [27,42,43]. However, the first two categories are between the most used to classify these materials and so chosen in this dissertation.

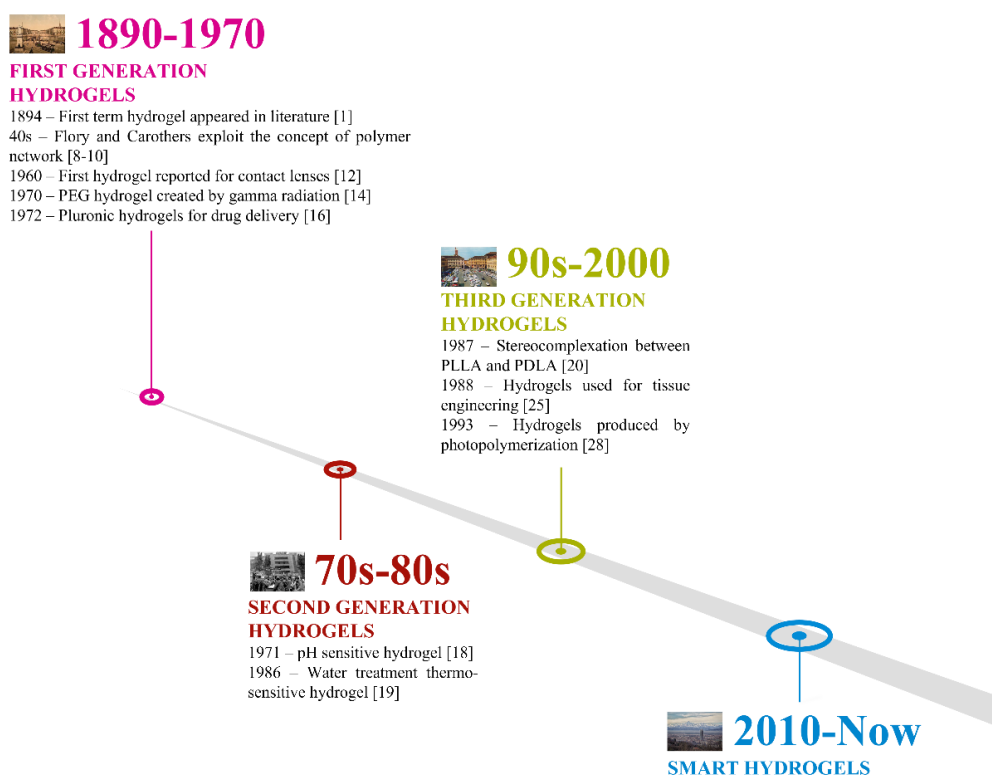


Figure 1.1: Historical timeline of the most important events in hydrogels investigation.

## 1.1 Classification: Based on the crosslinking method

As previously discussed, hydrogels are insoluble three-dimensional networks with the ability to absorb and retain a large amount of water [44–49]. As solid materials, hydrogels always present a clear elastic behavior, as shown by rheological analysis where the storage modulus ( $G'$ ) always show higher values than loss modulus ( $G''$ ) [50].

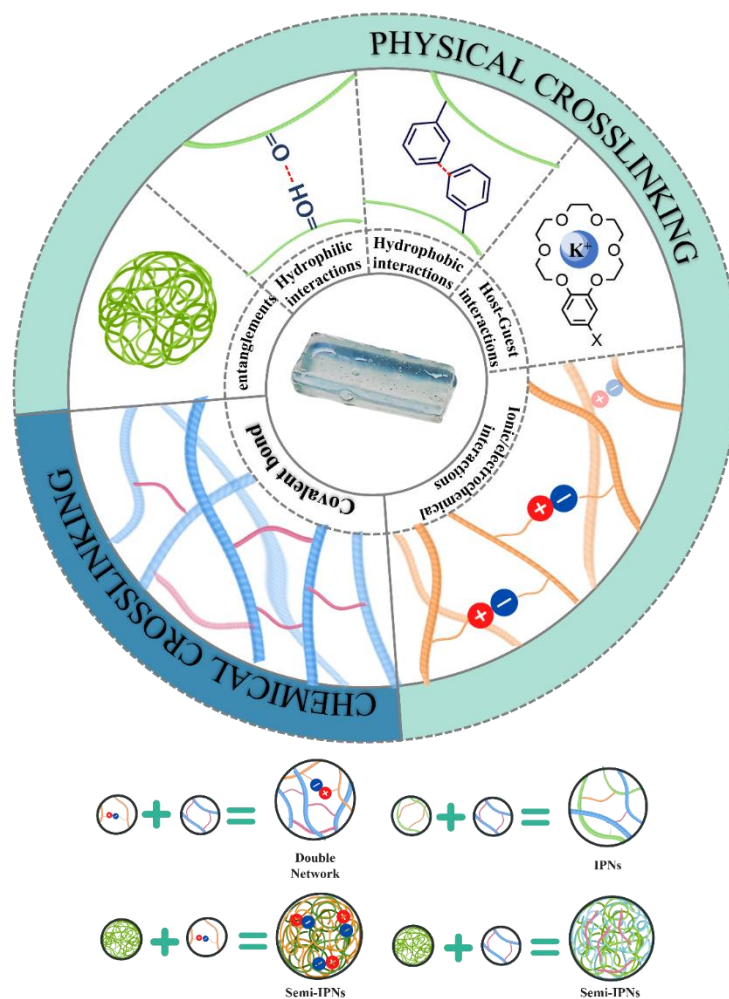


Figure 1.2: Crosslinking strategies for hydrogels formation. On the top of the image are reported the main typologies of crosslinking while on the bottom their eventual combinations.

Indeed, different type of networks and especially crosslinking methods are responsible of the insoluble characteristic of these class of materials. In fact, the crosslinking structure of hydrogels are characterized by tie-point or junctions, which may be formed from strong chemical bonds, ionic affinity between different functional groups and permanent or temporary physical entanglements, micro-crystallites presence, and weak interaction (mostly hydrogen bonds) [43][51,52]. The aforementioned methods are called respectively chemical (related to covalent chemical bonds) and physical crosslinking (any other interaction).

Moreover, the different types of crosslinking can be combined to grant properties not obtainable from the starting system. These solutions are known as interpenetrated polymer networks (IPNs), semi-IPNs or double networks. A scheme of the main crosslinking methods and their combinations is reported in Figure 1.2 while a brief resume of their different properties in Figure 1.3.

### **1.1.1. Physical crosslinking**

Physically crosslinked hydrogels are generally formed by intermolecular reversible interactions, i.e., ionic and electrostatic interaction, hydrogen bonds, polymerized entanglements, hydrophobic and hydrophilic interactions, crystallization or stereo-complex formation, metal coordination and  $\pi$ - $\pi$  stacking [53]. The first reason to choose this class of materials is generally the absence of crosslinking agents (with eventually the only exception of inorganic or non-toxic salts for electrostatic interaction). In fact, possible unreacted chemical molecules cannot just present a certain degree of cytotoxicity but also, subsequently, interact with the material or environment during the product operational life [54]. Moreover, the possibility of solubilizing or, in general, dissolve the hydrogels upon certain conditions gives the chance for the material recycling, thus having an increased sustainable process. Lastly, the opportunity to form the hydrogel directly “in-situ” make physically crosslinked gels the perfect choice for injectable materials [55].

Ionic/electrostatic interactions occur between two opposite electric charged macromolecules which interact between them to yield polyelectrolyte complexes [56]. If hydrogels are generated with ionic/electrostatic interactions, the polyelectrolyte complexes can be tuned with a large number of factors, including the polymer charge density, the concentration or mixed ratio of the macromolecule and the amount of each polymer if two different components are



blended, as well as the soluble microenvironment of polymer. Remarkable attention is only needed in the case the net charge of the formed complex is zero; this situation will influence the solubility, so the complex will precipitate. The peculiar advantage of ionic/electrostatic interactions is its intrinsic self-healing ability. Indeed, depending on the stress intensity, the eventual fracture of the physical network occurs but, thanks to the diffusion in solution of the macromolecules charged groups, the network can be reformed upon time once the stress is removed [53]. Metal coordination are a special kind of ionic interactions. The metal–ligand ionic interaction can be regarded as special Lewis’s acid–base, stronger than most noncovalent interactions, but weaker than typical covalent bonding interactions. Therefore, metal–ligand interactions can dynamically occur or disappear owing to their moderate bond energy that is responsible for the self-healing property [57–59].

Hydrophilic interactions and especially hydrogen bonds are the most important and stronger noncovalent bonds. Nevertheless, hydrogels created by one single type of hydrogen bond are generally not strong enough to support the entire structure formation. For this reason, hydrogels created by hydrophilic interactions need to exploit multiple multivalent hydrogen bonds. Different types of hydrophilic interaction need to be used at the same time, such as amide, urea, carboxylic acid, pyrrole, carbazole, thiol and hydroxyl groups. Alternatively, the addition of single molecules with multiple multivalent hydrophilic groups could lead to hydrogel formation; one example is ureidopyrimidinone (UPy) [60].

In contrast, hydrophobic interactions in water-soluble polymers occur when hydrophobic end or side groups are present in the main hydrophilic chain. The formation of stable interactions is generally thermally driven or induced by ultrasonic treatments. In fact, the hydrophobic moieties usually self-assemble into micelle structures when surrounded by the aqueous media, while the hydrophilic part of the polymer will be in direct contact with the solvent. Some polymers, however, at specific temperatures called lower critical solution temperature (LCST) and upper critical solution temperature (UCTS) are able to create bridges between micelles and lead to the formation of hydrogels. In the first case, at temperatures higher than LCST the polymer becomes insoluble and, while precipitating, leads to hydrogel creation [61]; one example of such a polymer is Poly(N-isopropylacrylamide) (PNIPAAm) [62]. In the second case, the situation is reversed and at temperatures higher than UCTS the micelles become water soluble [63]; an example here was reported by Fu et al., where a UCST-type thermosensitive ABA linear triblock copolymers composed of hydrophilic

poly(poly (ethylene glycol) methyl ether methacrylate) (PPEGMMA) middle block and a UCST-type thermosensitive poly(acrylamide-co-acrylonitrile) (P(AAm-co-AN)) outer block was synthesized [64]. Ultrasonic treated hydrogels formation is generally driven by phase variation. One example is silk fibroin, where the ultrasonic treatment in the solubilized protein can induce the generation of its characteristic hydrophobic  $\beta$ -sheet crystalline region and the subsequent self-assembly upon heat [65].

Remarkably, an important role in physical crosslinking regards host-guest interactions, where a specific polymer functional group can incorporate into other chemical species special cavities or spot. Numerous noncovalent interactions can smooth the host-guest inclusion, such as hydrogen bonding, electrostatics and van der Waals hydrophobic interactions as well as molecular shape (in aqueous solutions hydrophobic interactions are the most recurrent). Frequent host molecules are cyclodextrins (CDs), cucurbiturils (CBs), calixarenes (CAs) and crown ethers. This kind of interactions exhibits a strong and fixed directionality/binding of the two components, and more importantly are generally reversible changing the environment (e.g., pH) [66,67].

Lastly, physical polymeric entanglements and their possibility to create hydrogels resides in the random coils typical structure of polymers. In this case the hydrogel stability is given by topological interactions, strongly linked with high macromolecules molecular weights but also poor solvent affinity, temperature, and pH.

### **1.1.2. Chemical crosslinking**

Chemically crosslinked hydrogels involve covalent bonds among different macromolecules chains. Being thermoset materials, these linkages are extremely strong and permanent compared with physically crosslinked hydrogels, not permitting direct and simple recycling circles. Moreover, lower levels of biocompatibility are evidenced at the beginning of hydrogels creation due to the presence of isolated and not incorporated toxic molecules in solutions (e.g., crosslinking initiators or monomers). Nevertheless, compared with physically crosslinked hydrogels, covalently crosslinked hydrogels usually exhibit enhanced stability under physiological conditions and excellent mechanical properties with tunable degradation behavior. Lastly, even though a real price quantification between the different crosslinking technique appears difficult because of a large number of affecting factors (e.g., presence of various functionalization or

synthesis processes), the cost of hydrogels produced by chemical crosslinking is generally higher [68]. Among the different types of chemically crosslinked gels the most common are free radical polymerization induced crosslinks (mostly by photopolymerization), enzymatic induced crosslink, Diels-Alder “click” reaction, Schiff base formation, oxime formation and Michael-type addition (mostly involving thiols in the case of hydrogels) [53,54]. All the methodologies enounced will be briefly discussed below except for photoinduced radical crosslinking and Michael-type reactions which will be deeply analyzed in the next chapter.

Enzymatic crosslinking, enabling a free and fast (max 10 min) formation of gels just by modulating the enzyme concentration into the surrounding environment, is a promising route for totally biocompatible crosslinking processes for hydrogels creation [69,70]. One of the most common enzymatically catalyzed crosslinking methods involve transglutaminase (TG) along with calcium ions as cofactors; This enzyme can promote the formation of amide linkage between carboxamide and amine groups [71]. Another technique is the horseradish peroxidase (HRP)-catalyzed crosslinking reaction. HRP catalyzes the coupling of phenol [72], aniline [73] and their derivative tyramine [74] if hydrogen peroxide (H<sub>2</sub>O<sub>2</sub>) is present (low amount of hydrogen peroxide can be also beneficial for the human body [75]). Most of these enzymes are directly body produced, enabling the production of hydrogels in situ.

By “click chemistry” we refer to a group of reactions that possess many advantages such as rapidity, versatility, regiospecificity, easily usable and with high yields under mild conditions [76]. Diels-Alder reactions, Schiff base and oxime formations as well as Michael-type additions all fall in this category.

Diels-Alder reaction is a chemical reaction between a conjugated diene and a substituted alkene (generally termed as dienophile) highly regiospecific and with the absence of side-reactions or byproducts. Being a thermal highly selective [4 + 2] cyclization reaction don't need any initiators or additive to start, demonstrating in most cases enhanced biocompatibility [77]. For example, Nimmo et al., synthesized a furan functionalized hyaluronic acid (diene) to form a highly biocompatible hydrogel without any addition of additives/thermal initiators with the addition of a dimaleimide poly(ethylene glycol) (dienophile) linkers in aqueous solution [78].

Another example of cyclization is the copper(I)-catalyzed alkyne-azide cyclization (CuAAC) “click” reaction. The highly selective reaction involving the

cyclization of one alkyl/aryl azide and one alkyne, generally catalyzed by copper(I), was extensively studied by Huisgen, producing a mixture of 1,4 and 1,5-disubstituted products. The reaction gained increasing success in the last decades because its facility, extreme regioselectivity and possibility to work in many solvents (including water) [79].

Schiff-base reactions conventionally occur between amino and aldehyde groups to create an imine bond under physiological conditions. An important characteristic of these kind of reactions is the distinctive imine pseudo covalent bond. Indeed, if the bond is not reduced to amine the uncoupling and recoupling of the linkage can be tuned simply by pH (the bond is strongly dependent on the  $\text{H}_2\text{O}/\text{H}^+$  ratio), creating a recyclable hydrogel with self-healing capability [80]. Moreover, low concentrations of aldehyde groups into the scaffold can promote a further adhesion to tissues and organs, reducing a possible body rejection [81]. Nevertheless, being alkylating agents and prone to oxidation to carboxylic acids, free aldehydes carbonyl groups possess toxic profiles when used in high concentrations in vivo and in vitro [82,83].

Oxime formation needs the presence of an aminoxy/hydroxylamine group and an aldehyde or ketone and show a relative stability versus hydrolyzation as the equilibrium lies highly towards the oxime [84]. As much as the Diels-Alder reaction, the linkage is specific and selective between the two groups, even if other reactive species are present in solution. Under acid conditions the oxime formation proceeds through a condensation process which produces stoichiometric amounts of water [85]. The only drawback is a certain reversibility under some biological environments [86].

A special mention deserves dynamic covalent bond chemistry. Dynamic systems are a group of molecular components with the ability to reversibly assemble and disassemble upon an external stimulus [87,88]. Concretely, both physical interactions and chemical crosslinking systems can participate to create a dynamic bond. Examples of some physical interaction such as host-guest recognition, hydrogen bonding, hydrophobic interactions or ionic interaction are known as dynamic non-covalent bonds [89]. Nevertheless, covalent dynamic bonds gained increasing attention in the last years because of their properties considered a bridge between thermoset and thermoplastic polymers, with the same mechanical properties of the first category while permitting the recycle of the material as much as an increased workability. Dynamic covalent bonds on hydrogels include the Schiff base reaction or imine bond formation Diels-Alder

reaction, boronic ester formation, acylhydrazone bond and disulfide bond. The breakage and reconstruction of reversible dynamic bonds not only provide the hydrogels with high strength but also impart the hydrogels with self-healing properties and facilitate their applications in different fields [90]. Moreover, traditional covalently bonded hydrogels might release heat during formation and shrink (e.g., thiol-ene or CuAAC reactions). Dynamic bonds in this sense can also be used as sacrificial bond to dissipate energy, permitting a direct formation of the hydrogel in presence of living cells [91].



















	PHYSICAL CROSSLINKING		CHEMICAL CROSSLINKING
	Physical Interactions except ionic/electrochemical	Ionic/Electrochemical Interactions	Covalent bond
Mechanical resistance			
Biocompatibility			
Stability			
Workability			
Recyclability			
Price			

Figure 1.3: Main properties of the crosslinking strategies compared. Increasing number of indicators means a higher value of the property.

### 1.1.3. IPNs and double network crosslinking

To better understand the difference between the two class of materials, it's useful to analyse the definitions given in literature. An interpenetrated polymer network(s) or IPNs is “a polymer comprising two or more networks which are at least partially interlaced on a molecular scale but not covalently bonded to each other and cannot be separated unless chemical bonds are broken. A mixture of two or more pre-formed polymer networks is not an IPN [92]” while a “double

network or DN gel is characterized by a special network structure consisting of two types of polymer components with opposite physical natures: the minor component is an abundantly cross-linked polyelectrolytes (rigid skeleton) and the major component comprises of poorly cross-linked neutral polymers (ductile substance). The former and the latter components are referred to as the first network and the second network, respectively, since a synthesis step should be done in this order to realize high mechanical strength [93]". By definition, an IPNs is logically a combination between two chemically covalent crosslinked networks while a double network gel is given by the combination of a covalent and an ionic crosslinked network. The last sentence in the IPNs definition was constructed as a note to differentiate this class of materials from simple polymer blends. Moreover, if only one of the two IPNs components is crosslinked the material is called semi-IPN and the IUPAC definition changes into "Semi-interpenetrating polymer networks or semi-IPNs are distinguished from interpenetrating polymer networks because the constituent linear or branched polymers can, in principle, be separated from the constituent polymer network(s) without breaking chemical bonds; they are polymer blends [94]". In this case, the combination between crosslinking methods is given by covalent/ionic crosslinking from one side, and physical interactions from the other. Remarkable it's also the presence of interconnected network(s) or ICNs; the only difference from regular IPNs is the possibility of intermolecular covalent bonds between networks [95].

In hydrogels, the synergic effect searched from these combinations is to modify or enhance a specific characteristic property (or properties) not obtainable before from the two single polymers. A clear example of this behaviour resides in the glass transition temperature ( $T_g$ ) changes of the compound. Differently from polymer blends, in IPNs or DNs the  $T_g$  of the system (plotted as  $\tan\delta = E''/E'$  vs temperature) results in a broad and stocky curve (compared to the two different  $T_g$  curve ascribable to the two polymers); the reason is a deep, intricate and homogeneous multi-network where the two polymer structures are mixed at a molecular scale. However real IPNs or double networks generally have nanoscale network separation with "richer" domain of one or the other polymer (depending on the area) but resulting still in mediated properties between the two polymers, very different from the separated properties of polymer blends [95]. IPNs/DNs hydrogels are usually created to tune biological or biological-related properties such as mechanical resistance, bioadhesion, drug delivery capacity, cell compatibility or the possibility to make the gels stimuli-responsive [96].

## 1.2. Classification: based on the material

As already mentioned, another interesting method to differentiate between the existing window of hydrogels is by material. The classification is generally given by the source of these polymeric materials, so if they are natural or synthetic derived. To also mention the employment of both sources to give the hydrogel multiple features (a clear example can be found in IPNs or DNs hydrogels), usually called hybrid systems.

### 1.2.1. Synthetic polymers

The advantages on the employment of this category of polymers resides mainly on their synthetic source. Indeed, synthetic polymers or monomers are produced with a well-defined and repeatable structure, with known polymerization or crosslinking kinetics, with fine tunable degradation profiles as much as final mechanical properties. In other words, The artificial nature of synthetic hydrogels promote a easier creation of “smart hydrogels”, tailored for a specific application depending on the given external stimuli [97]. Numerous synthetic water-soluble polymers were employed over time to create hydrogels for different applications but the most used and reported are poly(ethylene glycol) (PEG) and derivatives, poly(acrylic acid) (PAA) and derivatives and poly(vinyl alcohol) (PVA).

PEG (or polyethylene oxide PEO, depending on its molecular weight) has been approved by EMA for several medical uses due to its biocompatibility and low toxicity [98]. PEG itself is a very hydrophilic polymer and can be synthesized at various molecular weight and geometries (linear, Y-shaped, branched, or multi-arm) from a ring opening polymerization of ethylene oxide. Having hydroxyl groups at its ends, PEG can easily be modified to include N-hydroxysuccinimide esters, thiols, carboxyl, alkyne, azide, or acrylic groups.

PAA and especially its derivative such as poly(2-hydroxyethyl methacrylate) (pHEMA) or Poly(N-isopropylacrylamide) (PNIPAAm) were extensively used as hydrogels in the past. While pHEMA was utilized in ophthalmic [12] and drug delivery [13], PNIPAAm can be potentially very attractive in biomedical science cause of its phase transition behavior above the lower critical solution temperature (LCST) at 32°C, matching almost perfectly the human body temperature [99]. NIPAAm (the initial monomer) is generally copolymerized starting from acrylic acid, methacrylic acid, or butylmethacrylic acid, depending on the desired final

applications [100]. However, limitations of these gels are the nondegradable cross-links; in fact, the vinyl monomers and cross-linking molecules are toxic, carcinogenic, or teratogenic [101,102].

PVA is usually obtained by hydrolysis, alcoholysis or aminolysis of poly(vinyl acetate) [103]. It's hydrophilicity and solubility in aqueous solutions strongly depends on the extend of hydrolysis and molecular weight. PVA can create hydrogels using the cytotoxic glutaraldehyde and epichlorohydrin as crosslinkers. However, due the high presence of hydroxyl groups in the macromolecule chain, a high number of hydrogen bonds are possible. This is the reason why repeated cycles of freezing/thawing lead to the formation of room temperature stable and highly elastic hydrogels [104]. Moreover, these types of interactions impart to the final hydrogels self-healing properties. Indeed Caprioli et al., developed a self-healing 3D printable hydrogel based on a IPN between PPA and PVA where after 2h of recovery, a moderately large deformation stretching could be subjected to the gel without any failure [105]. However, PVA is not easily degradable, especially in physiological conditions, so in biomedical science just long term or permanent scaffold can be designed [104]. The molecular repetitive unit of these three polymers is reported on Figure 1.4.

#### Synthetic polymers

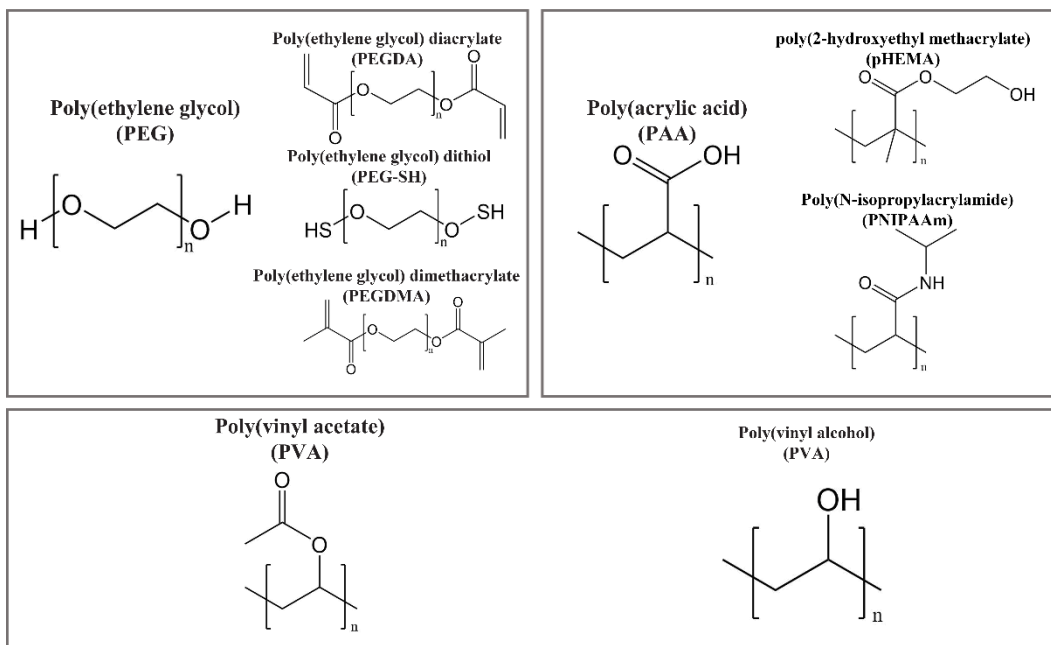


Figure 1.4: Most common synthetic polymer and derivatives for hydrogel creation.



### 1.2.2. Natural polymers

Compared with synthetic polymers, due to their incredible biocompatibility and biodegradability, hydrogels based on natural polymers are considered the most promising candidates in the biomedical field [106]. When talking about hydrogels based on natural polymers, polysaccharides and protein are the main actors taking role on the stage. The reason is their similarity to the characteristic human extracellular matrix (ECM), a complex network system of proteins (e.g., collagen), glycosaminoglycans, and proteoglycans able to sustain cell growth and adhesion [107]. Moreover, natural polymers are abundant and easily extractable from renewable sources such algae or plants, cultures of microbes, as much as some animals (e.g., pigs, fishes, crabs and shrimps). Thus, they have a large variety of compositions and properties not easily mimicked in laboratory, and the ease of their production makes numerous polysaccharides cheaper than synthetic polymers. However, the natural sources intrinsic variability makes these polymers extremely not predictable in term of molecular weight and polydispersity (changing batch to batch). Lastly, their mechanical properties once extracted frequently results poor and unforeseeable [108]. Many polysaccharides were used to create soft hydrogels; however, the most used and easily available are cellulose, starch, alginate, chitosan, and hyaluronic acid. Between protein instead, collagen or its derivative gelatin are still the most used and famous hydrogel precursor [109]. Once numerous natural polymers are described within this paragraph, chitosan, alginate and collagen/gelatin will be discussed in the next sections because important for this dissertation.

Cellulose, as the most abundant natural polymer on earth, is a polysaccharide directly involved in the structure creation and support of the entire tissue architecture of plants. Formed by a large number of repeating D-glucose units linked by  $\beta$ -1,4 glycosidic bonds, cellulose presents outstanding hydrophilicity and chemically modifying capacity. Acid hydrolysis and mechanical treatments, necessary to extract cellulose from natural sources, often result in the production of cellulose with different degree of crystallinity (i.e., microcrystalline cellulose, nanocrystalline cellulose and nanofibrillated cellulose) [110]. Even though these treatments make possible the extraction and separation of cellulose from lignin and hemicellulose, the resulted crystalline moieties are generally insoluble in aqueous solutions. However, further functionalization of cellulose involving the substitution of some hydroxyl groups lead to extremely lower degree of crystallization, the solubilization in water and, thus, the possible creation of hydrogels. An example is carboxymethyl-cellulose (CMC) obtained by a partial

substitution of 2, 3, and 6 hydroxyl groups of cellulose with carboxymethyl functional groups [49].

Starch is another abundant polysaccharide present with ranges between 20 and 30% in a large number of food commodities such as wheat, rice, rye, potato, maize, or cassava. It consists in two main D-glucose polymers; a linear  $\alpha$ -1,4 linked amylose and a branched  $\alpha$ -1,4- $\alpha$ -1,6 branch-linked amylopectin [44,111]. Due to its high tendency to crystallize, in order to produced stable aqueous solution, also starch often needs a previous treatment, called gelatinization [112]. Briefly, when heated and in presence of water, starch undergoes an irreversible transition where its preformed granules swell, absorb water (which act as plasticizer), loose crystallinity and start to solubilize [113].

Hyaluronic acid is an unbranched and water-soluble glycosaminoglycane formulated by two repeating disaccharide units: a  $\alpha$ -(1 $\rightarrow$ 4) D-glucuronic acid and a  $\beta$ -(1 $\rightarrow$ 3) N-acetylglucosamine. It is generally synthetized industrially from the bacteria streptococci but can be also extracted from animal connective tissues. In the human body hyaluronic acid is primarily responsible of lubricate the tissues but also to block the spread of invading microorganisms [108].

A brief summary to visualize the differences in terms of properties between synthetic and natural polymers is reported on Figure 1.5.



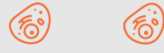


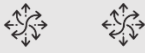

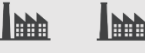
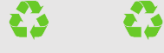


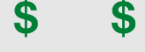
	Natural Polymers	Synthetic Polymers
Mechanical resistance		
Biocompatibility		
Versatility		
Workability		
Recyclability		
Price		

Figure 1.5: Main properties of the two material sources polymers compared. Increasing number of indicators means a higher value of the property.

### 1.2.2.1. Polysaccharide: Chitosan

The natural polysaccharide chitosan derives from a partial deacetylation by alkaline or enzymatic hydrolysis of a characteristic compound extracted from crab/shrimp shells: chitin (Chemical structure reported in Figure 1.6). Being the second most abundant polysaccharide on earth and often discarded after processing, the employment and usage of chitin result in an extremely sustainable process. To remove the acetyl group and free the amino group, chitin is subjected to a N-deacetylation (generally using sodium hydroxide, potassium hydroxide solutions, mixtures of anhydrous hydrazine, and hydrazine sulfate) of its constitutional repeating unit, N-acetyl-D-glucosamine. The resulting random backbone (chitosan) is formed partly by the antecedent N-acetyl-D-glucosamine and the new D-glucosamine unit: commercial chitosan usually owns a degree of deacetylation between 70 to 90% [114,115]. Many polar groups are present in the repetitive units; apart from the amino group, two more hydroxylic group (primary and secondary) are distinctive on the backbone. The amino group possess a pKb value of  $\approx 6.5$  which lead to an improper solubility in physiological solutions, due to possible hydrophilic interactions formed with the hydroxylic groups, thus to a partial aggregation of the material. However, the amino groups protonation in acidic solutions make chitosan easily water soluble; the ammonium cation ( $R-NH_3^+$ ), partly present even at neutral pH, is also responsible for the antimicrobial natural activity of chitosan, especially at low molecular weight. Moreover, the  $-NH_3^+$  group can promote hydrogel formation when chitosan is mixed with other negatively charged molecules (e.g., alginate or hyaluronic acid), creating an electrostatic compound held together by ionic interactions. Even chemical crosslinking is possible, upon modification of the easily functionable amino group [116]. Other than that, chitosan has excellent properties, such as biocompatibility, biodegradability, anti-inflammatory activity, antioxidant effect, and it can diminish foreign body reaction with little or no fibrous encapsulation [117].

### 1.2.2.2. Polysaccharide: Alginate

Alginate is a natural polysaccharide generally extracted by treatment with alkali solutions (NaOH usually) from brown algae or synthesized by some bacteria (Chemical structure reported in Figure 1.6). Considering that the class of brown algae exhibit more than 1500 species of algae, it is not surprising the intense and thorough study carried about alginate in the last decade [118]. It consists of a variable sequence of (1 $\rightarrow$ 4) linked  $\beta$ -D-mannuronic acid (M) and  $\alpha$ -L-guluronic acid (G). The composition of the two repetitive units is also extremely variable

and depends strongly on the origin of the natural resource considered. The block structure is extremely important because it determines the physical properties of the subsequent hydrogel. For example, alginates rich in G blocks form resistant and brittle gels, whereas the predominance of M or M/G block leads to weak but really elastic hydrogels. Bacteria's alginates instead, often present substitution in the D-mannuronic block in the 2nd and/or 3rd position with 0-acetyl groups [119]. Both the blocks comprise carboxylic groups able to deprotonate at physiological conditions, resulting in a perfectly water-soluble natural polymer (the minimum in solubility is around a pH of 3-3,5 due to the protonation of the carboxylic groups and the polar interactions onset). However, the creation of hydrogels by ionic interactions with divalent cations ( $\text{Ca}^{2+}$  and  $\text{Ba}^{2+}$  generally) is attributed just to the guluronic unit and that's the reason of the different properties of the resulting hydrogels. At the same way, a possible functionalization on the G block results more favorable to create chemical crosslinked hydrogels. Even though alginate hydrogels are indissolubly considered biocompatible, no bioactivity is generally evidenced; this is the reason why alginate gels are called bioinert [120]. At the same way, low levels of in-vivo biodegradability are reported cause of an unpredictable dissociation of the saccharide units, releasing high molecular weight strands on the organism not removable from the kidney and difficulty degraded from the mammalian body due to a lack of alginate degrading enzymes [121].

### **1.2.2.3. Protein: Collagen/Gelatin**

Collagen is the most abundant structural protein in the animal body. In humans, collagen include one third of the total proteins (three quarters in dry skin) and it's the prevalent component of the ECM. For industrial uses, it is generally extracted from animal waste such as skin, bones, or tendons. The defined structure is a combination of a three parallel left-handed polypeptide strands with a polyproline II-type (PPII) helical conformation coil where each other, with a one-residue stagger, form a right-handed triple helix. The tight packing of PPII helices mandates that every third residue is a Glycine, resulting in a repeating XaaYaaGly sequence, where Xaa and Yaa can be any amino acid. Even though the most common combination results to be (2*S*)-proline/4-hydroxyproline/glycine (10.5% of the times) [122]. However, collagen in adult animals always present a certain degree of crosslinking making impossible a simple extraction of the raw material [123]. Moreover, during the heated alkaline or acidic hydrolysis from animal raw tissue, the separation of collagen always involves a breakage of its structure; the resulting extremely heterogeneous material is called gelatin. Gelatin, because of its low cost and excellent water solubility is generally used to form transparent

hydrogels. The presence of numerous functional groups, which depends on the variable amino acids present in the starting collagen, makes gelatin easily modifiable to create covalent bonded hydrogels. Lastly, because gelatin directly derive from the animal ECM it presents the highest levels of biocompatibility [124].

The repetitive unit of the natural polymers listed above are schematized in Figure 1.6. Collagen/Gelatin is not reported cause of the different amino acids unpredictable structure, strongly dependent on the extraction tissue/source.

### Natural polymers

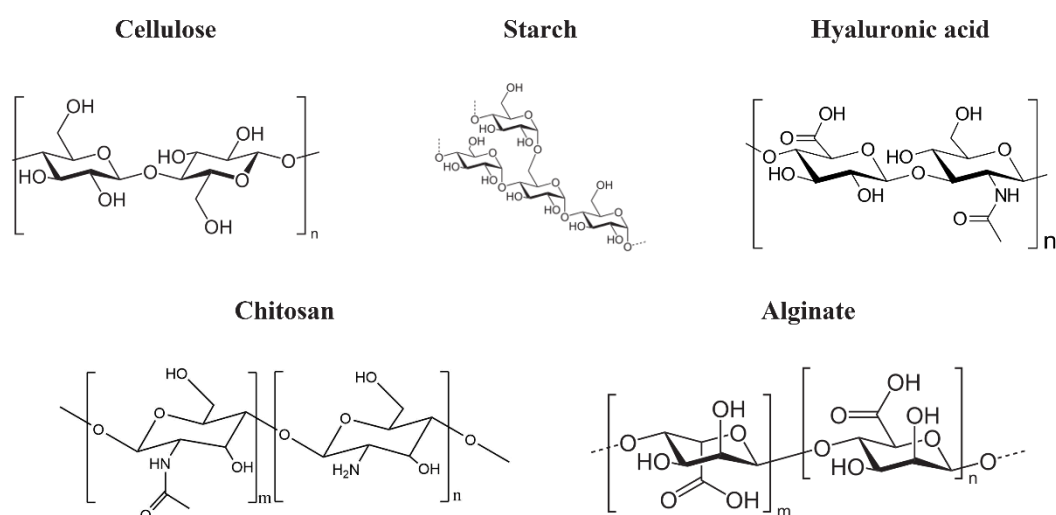


Figure 1.6: Most common natural polymers used for hydrogel creation. Collagen/Gelatin is not reported cause the different amino acids unpredictable structure, strongly dependent on the extraction tissue/source.

### 1.3. Applications

As a polymeric 3D network able to incorporate and retain a large amount of water, hydrogels find applications in various disciplines. From agriculture to water treatment or from batteries to sensors, hydrogels were historically designed and employed. But, especially in the biomedical field and cosmetics, this class of materials showed its natural collocation; one example is the creation of drug delivery systems or scaffolds.

In agriculture, hydrogels are generally employed as slow-release fertilizers. In this conformation, water-soluble urea or other fertilizers are entrapped within the hydrogels network and released locally and at low rates upon swelling. For this reason, after raining the water adsorbed both by the hydrogel and the ground starts the diffusion into the wet ground and enable the plant nutrient assumption [125]. For example, Zheng et al., prepared an intelligent agrochemical carrier (Ca-Alg-gP(NIPAm-co-NDEAm)/SC) able to release half of the glyphosate entrapped in the network in 15 h. The hydrogel was designed and synthesized by redox copolymerization and ion cross-linking methods using Alginate with pH sensitivity, poly(N-isopropyl acrylamide-co-N,N-diethylacrylamide) with temperature responsiveness, and photothermal material semi-coke with light susceptibility [126].

Hydrogels with unreacted functional groups are usually exploited to absorb pollutant from wastewaters [127,128]. Indeed, Noè et al., synthesized an UV curable starch hydrogel based on methacrylated starch and  $\gamma$ -cyclodextrin where the torous-shaped structure of cyclodextrins was able to successfully entrap the pollutant methylene blue inside of the network [129].

Nowadays, the parallel development of wearable electronics/sensors, such as smartphone or virtual reality tools, and their size and weight reduction powered up the need of storage devices with high energy and power density. Aqueous rechargeable batteries are between the cheapest and environmentally friendly options even though evident technical difficulties for large-scale integrations (especially for portable/wearable devices) such as the ability to perform under a wide range of temperatures and solicitations. The integration of hydrogels gives increased flexibility to the device thanks to their elastomeric behavior without affecting the ionic conductivity given by the aqueous electrolytes. Moreover, the hydrogel matrix functionalization or the employments of additives could increase even further the batteries capabilities [130,131]. For example, Ye et al. fabricated a wearable or implantable tissue-like battery made entirely of polyacrylamide/carbon nanotube hydrogel. Successive steps of hydrating and dehydrating grant the battery energy storage while suitable mechanical properties and biocompatibility certified the hydrogel application in tissue engineering [132].

At the same way, drug delivery systems often employ hydrogels due to their slow-release features upon swelling or presence of reactive functional groups, both able to retard and modulate the medicine absorption into the human body. Many strategies were developed to control the drug release such as through pH,

degradation, or mechanical deformations [133]. For example, ester bonds are degradable into the human body by hydrolysis and for this reason O'Shea et al., prepared a PEG-based hydrogel with the ability to achieve extremely slow protein release, with half-lives of up to 17 days [134].

Lastly, hydrogels are employed in cosmetics or for medical purposes [135,136]. From the antioxidant effects of Aloe Vera hydrogels to the usage of hyaluronic acid as surgical filler, the popularity of hydrogels in cosmetics is well known [137,138]. Interestingly, studies also report the usage of Vasalgel™ (a commercial product made of synthetic polymers) as masculine contraceptive filler. The gel injection into the testicular/urethra canal avoids the sperms passage for a maximum of 2 years, with the possibility of dissolving the gel upon a sodium bicarbonate solution injection [139].

### **1.3.1. Tissue engineering**

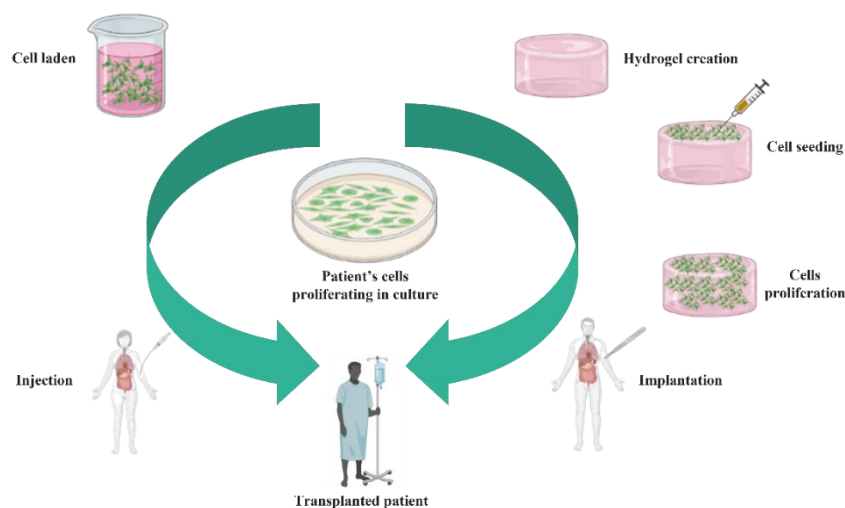
Every year, millions of people around the world suffer of organs and tissues damage or failure due to accidents or diseases. Tissue or organ transplantation is generally recommended in these situations to treat the injured patients. However, a chronic lack of donors is a global phenomenon, resulting in an average of 21 patients dying every day while waiting for an organ transplant in Europe. The same trend is evidenced in the organ/tissue waiting list where the demand for organs always exceeds the number of organs available; just in the EU, in 2018, over 150'000 patients were waiting for organ donation [140].

Considered the urge, it is not surprising the international direction on engineered tissue, directly based on the patient need. This area of research, commonly called tissue engineering, usually exploits polymeric network with properties similar to the extracellular matrix (ECM). A particular and smart approach is to combine these materials (called scaffold) with the patient's own cells to recreate the needed organ/tissue. The way the cells are collocated into the network defines the type of solution for transplant. If a cell-laden process is performed, the cells are premixed into the hydrogels precursor and polymerized in situ; this strategy is necessary for injectable hydrogels. If the cells are placed on the hydrogel surface and let migrate into the bulk, a cell-seeding technique is accomplished, and the implantation of the entire hydrogel is carried out when cells successfully colonize the entire structure [141]. A scheme of the two strategies is reported in Figure 1.7. A large variety of tissues were engineered following these strategies, including fabricated artery, bladder, skin, cartilage,

bone, ligament, and tendon; moreover, some of them are now at or close to clinical uses [104].

The critical bottleneck in all the tissue engineering approaches is the polymeric scaffold. In fact, the scaffold potentially mimics many features of the ECM and to find the possible requirements for a good, engineered tissue, a clear view of its role is necessary. ECMs are made of various proteins and sugar-based macromolecules and are able to support cells and control the tissue structure, regulate the function of the cells, and allow the diffusion of nutrients, metabolites, and growth factors [104]. Therefore, the scaffold requirements in tissue engineering are [142]:

- **Biocompatibility:** cells must adhere, migrate, and proliferate within the polymer network. Moreover, after implant the scaffold must elicit a negligible immune reaction in order to prevent severe inflammatory response, a reduced healing or cause rejection by the body.
- **Biodegradability:** Scaffold should not mean to be eternal and cells during their metabolic life should be capable of replace the engineered ECM. At the same way, the side products produced during degradation should be nontoxic and able to be expelled from the body.
- **Mechanical properties:** In order to permit a clear ad successful cell adhesion, the scaffold resistance must match the physiological mechanical properties of the native tissue.
- **Porosity:** A certain degree of space is always necessary inside of the polymeric network. In fact, cells must be able to migrate into the scaffold and have the possibility to subsequently vascularize the creating tissue.



*Figure 1.7: Cell-laden/cell-seeding clinic procedure*





## **Chapter 2**

# **Photocurable hydrogels for tissue engineering applications**

A large variety of techniques has been investigated to create hydrogels for tissue engineering such as temperature or chemical, physical, or ionic interactions. Chemical crosslinked hydrogels formation, especially because of the extremely toxic reaction conditions (e.g., heat generation, acid/basic pH, toxic reagents, etc.), can be tricky and challenging, even though their superior stability and mechanical resistance.

Talking about photochemically crosslinked hydrogels, the interaction of compounds called photo-initiators (PhI) with visible, or UV light can generate radicals able to start the polymerization and lead to the formation of chemically crosslinked hydrogels. This configuration presents numerous advantages such as fast and effective polymerization, good spatio-temporal control of hydrogel formation, and the possibility to perform the reaction at room temperature with minimal heat generation and under physiological conditions. Moreover, the short time of irradiation (in all the cases less than 10 minute, with peaks of few seconds) and the employment of non-toxic photo-initiators are compatible with cell laden hydrogel formation strategies. The application of laparoscopic devices, catheters or subdermal injection with transdermal irradiation also permit the creation of hydrogels in situ, starting from a liquid formulation [29].

### **2.1. Photo-crosslinking processes**

Since the discovery of the first photo-induced reaction on vinyl bromide by Hoffman, the valid mechanism proposed and accepted to describe the creation of

polymers is based on one-photon absorption (OPA) [143]. Briefly, the absorbed photon induces the promotion of one electron of the sensitizer from its ground state ( $S_0$ ) to a short-life excited singlet state ( $S_1$ ) maintaining its spin (otherwise the law of conservation of the angular momentum would be violated). The deactivation of this last state can follow two main different paths (Jablonski diagram, Figure 2.1):

- Return to  $S_0$  by radioactive decay (fluorescence) or non-radiative internal conversion emissions (IC, thermal).
- Relaxing into a temporary lower energetic triplet state ( $T_1$ ) undergoing spin inversion, process called intersystem crossing (ISC). The further deactivation to the stable  $S_0$  is driven by another ISC process or by phosphorescence emission. In both cases, the spin inversion implies longer times of existence of the triplet state. At this point, the longer lifetime of the triplet state combined with its higher energy orbital may create a reactive specie able to participate into primary photochemical reactions.

The eventual reactive specie generated after deactivation, which promote the polymerization after light irradiation, can be radicals or ions (cations/anions) and the occurring phenomenon are called radical or anionic/cationic photopolymerization, respectively [144–146]. While anionic photopolymerization is highly instable and rarely lead to a formed polymer, the other two mechanisms are currently and extensively used to create bulky polymers or coatings [147]. However, cationic polymerization usually refers to reactions highly affected by moisture, incompatibles with the watery structure of hydrogels, [148] for this reason this reaction will not be discussed in this manuscript. Once formed, the reactive specie promotes addition reactions on unsaturated hydrocarbons, such as alkenes, alkynes and some aromatic compounds. The electrophilic addition occurring on these compounds is related to their higher electron density (once compared with saturated bonds, i.e., alkanes) where a  $C=C$   $\pi$  bond breaks into two  $\sigma$  links, promoting a functional group addition and starting the process of photopolymerization [149,150].

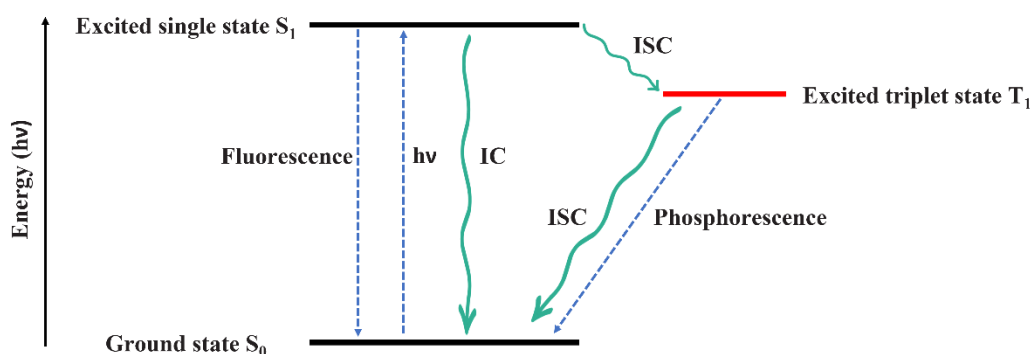


Figure 2.1: Jablonski diagram illustrating the electronic states and transitions upon the one-photon absorption mechanism.

### 2.1.1. Radical photopolymerization

As already pointed out, the photoinduced formation of radicals is among the most investigated strategies to create chemically cured hydrogels. Two main mechanisms of radical generation are involved in the polymer formation, depending on the system where the radical is created during the photoinduced process.

Norrish type I reactions (NT1) presume a unimolecular photochemical cleavage in order to create two radical intermediates [151]. For example, lithium phenyl-2,4,6-trimethylbenzoylphosphinate (LAP), is an acylphosphine oxides that can undergo  $\alpha$ -scission upon UV or visible light irradiation (Figure 2.2). The homolytic scission involves the carbon-carbon (C-C) group ( $\alpha$  position) adjacent to the carbonyl (C=O) chromophore group and leads to the creation of phosphinoyl radical (a) and a benzoyl radical (b). The mechanism of this photo-initiator resembles strongly other water insoluble type I photo-initiators (e.g., bis[2,4,6 trimethylbenzoyl] phenylphosphine oxide) even though alkali and alkaline earth metal salts of phosphinic acid (as in the case of LAP) generally are water soluble and perfectly suitable for hydrogels [152]. Moreover, it has been demonstrated that LAP is cytocompatible and have a moderate absorption into the visible light region, thus can be used in scaffold fabrication [153].



Figure 2.2: Radical generation upon light irradiation on LAP photo-initiator.

Norrish type II reactions (NT2) assume a bimolecular photochemical mechanism where a chromophore (often a ketone or diketone) interacts with a hydrogen donor molecule or co-initiator specie (amines typically but also alcohols, ethers, phosphines or sulphides) to generate a radical upon hydrogen abstraction [151,154]. One example can be camphorquinone (CQ, Figure 2.3) where its excitation state (T1) upon UV-light absorption interacts with the co-initiator to create a complex called “exciplex”. The subsequential electron transfer from the co-initiator firstly generates two linked ions and then the intramolecular H-abstraction occurs from the electron donor specie. The two radical species created are one the relatively unreactive and stable CQ-ketyl radical involved in further own recombination and the other one is the co-initiator radical which will grant the radical polymerization [46]. CQ was largely applied in scaffolds preparation and dentistry [155,156].

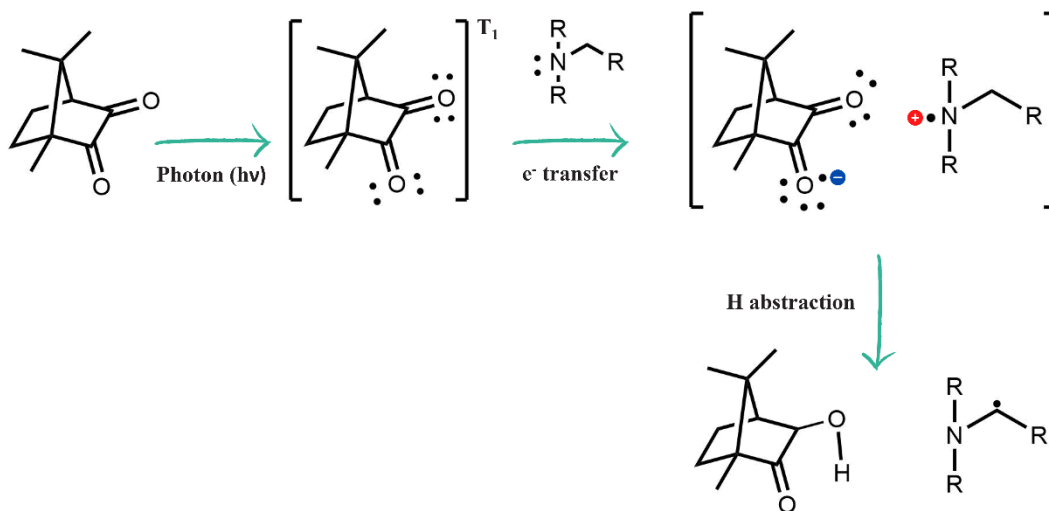


Figure 2.3: Radical generation upon light irradiation on CQ photo-initiator.

However, the photo-generation of radicals on the photo-initiator is just a part of the first step of polymerization which consist in three different stages of evolution until the hydrogel (or in general polymer) is created, named: initiation, propagation and termination.

In fact, the initiation is a two stages step where upon light exposure, the radical is generated on the photo-initiator following the NT1 And NT2 mechanisms. The rate of generation of radicals depends strongly on various parameters related to the applied chromophore and in particular to: 1) the light intensity, 2) PhI concentration and 3) the PhI quantum yield (function on its light absorption spectra). The radical then rapidly attack the unsaturated bond and the polymerization can start. It is important to consider that the radical generation is generally the slower stage of all process so the determining one.

The next step of propagation can proceed in two distinct manners, depending on the compound considered, called chain-growth (CGP) and step-growth (SGP) polymerization (Figure 2.4). If a chain-growth propagation occurs the reaction proceed by consequent addition on the forming network/chain until the hypothetical consumption of all the unsaturated moieties. Instead, step-growth propagation sees the contemporarily formation of different reacting sites until a final merging. Remarkably, the two propagation mechanisms imply a different increment on the average molecular weight ( $M_w$ , Figure 2.4); while a strong and fast increment of  $M_w$  is expected on CGP, the opposite phenomena is shown in SGP.

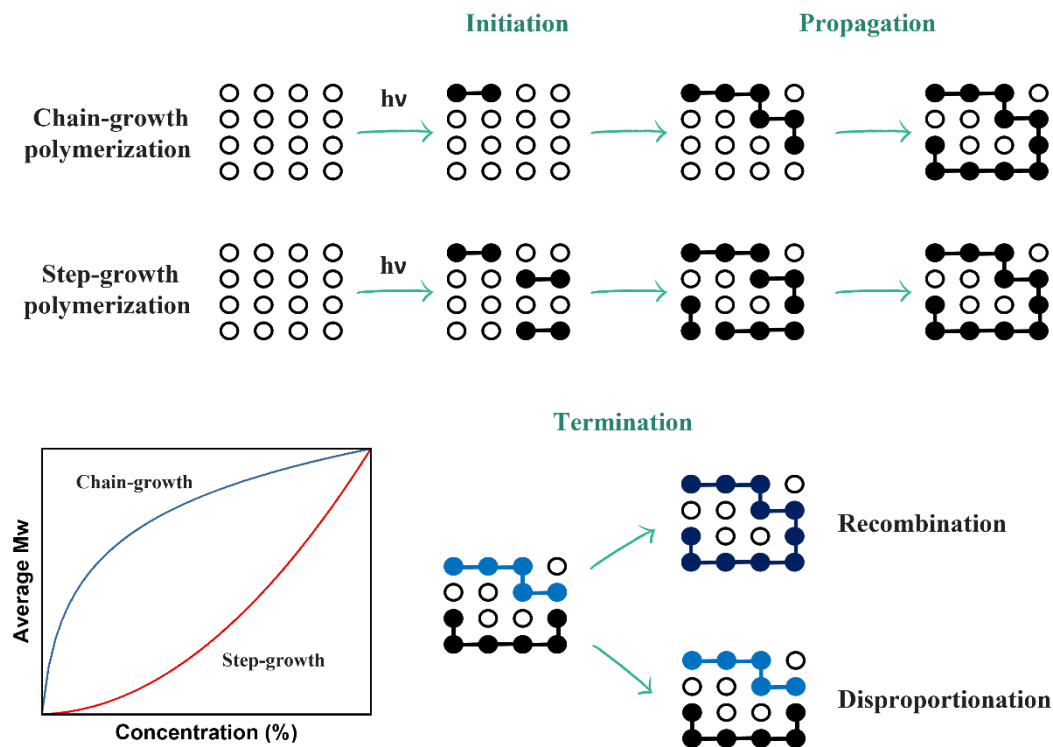


Figure 2.4: Polymerization stages involved in the polymer network/chain formation.

Even though the propagation could ideally continue until the complete consumption of the unsaturated bonds, the high reactivity of radicals usually leads to formation of covalent bonds. The polymerization termination occurs mainly by two different paths (Figure 2.4): 1) recombination (more frequent) where two reacting sites interact between themselves dampening two radicals (and eventually forming a bigger chain) or 2) disproportionation, where a H abstraction occurs in one reacting site giving a new unsaturated group and two "dead" sites [157,158].

Example of the CGP mechanism is given by (meth)acrylates (Figure 2.5 A). In this case, the unsaturated C=C bond can be attacked by the photo-initiator radical, starting the propagation. (Meth)acrylates are indubitably the most used system in photopolymerization due to their extreme versatility as much as their ease functionalization. However, some disadvantages are the short life of propagation radicals (leading to an incomplete C=C bond conversion), the shrinkage stress upon curing (very frequent in every CGP propagation systems, due to their crosslinking rapidity) and a certain degree of inhibition from atmospheric oxygen (oxygen cause a quenching of the T1 state in the PhI and also form peroxide reacting with free radicals) [159].

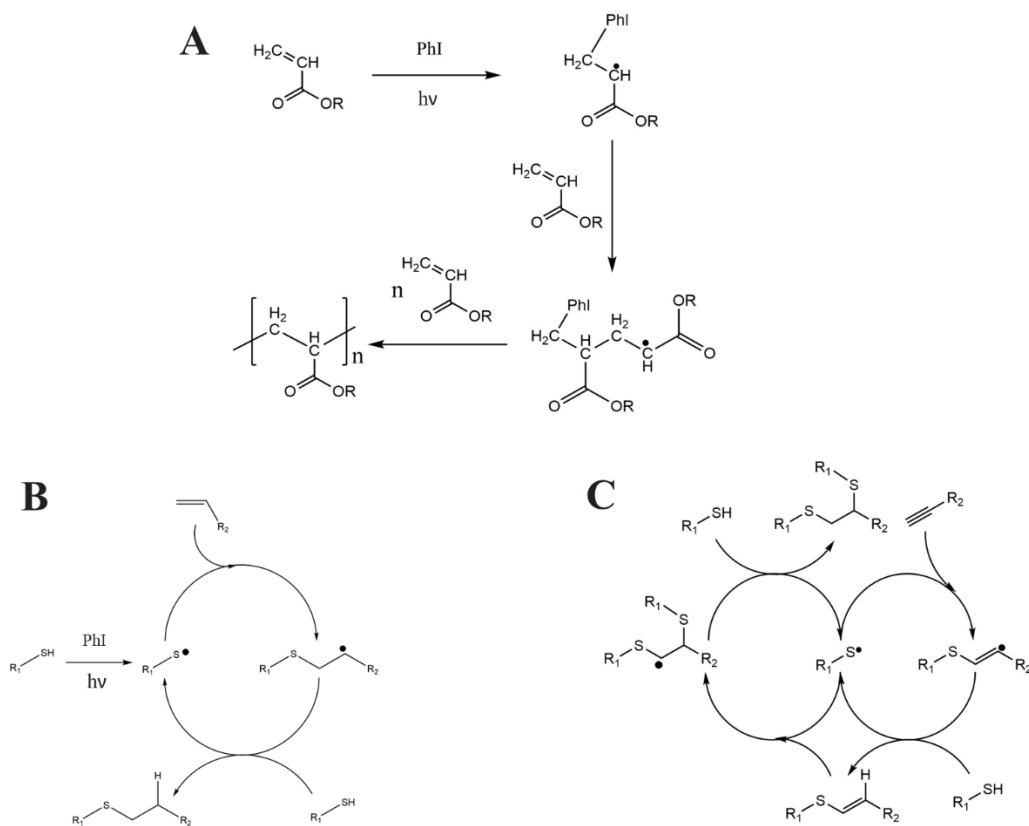


Figure 2.5: Initiation and propagation steps of methacrylates (A), thiol-ene (B), and thiol-yne reactions (C)

Instead, examples of SCP (also called Michael-like) are thiol-ene and thiol-yne reactions (Figure 2.5 B and C, respectively). These kinds of reactions fall in the category of “click-chemistry”, invented by Sharpless et al. and referring to high yield, stereospecific and orthogonal reactions [160]. Contrarywise to CGP, the slower propagation mechanism allows a slower shrinkage due to a higher time of relaxation and lower stress accumulation. Moreover, the system present insensibility to oxygen inhibition [161].

Thiol-ene reactions involve the presence of a thiol group and an unsaturated C=C bond. In this conformation, the photo-initiator generation of radicals upon light irradiation cause a H abstraction on the thiol moieties creating a thyl radical. Then, a subsequential attack on the C double bond may form a thioether bond and the creation of a carbon centered radical, able to react with a second thiol molecule by chain transfer and effectively forming a thiol-ene addition product [162]. Similarly, thiol-yne reactions present the same system apart from an unsaturated C triple bond, instead of C=C. However, unlike thioether generated in thiol-ene reactions, the vinyl sulfide may be capable of undergoing further reactions through addition of a second thyl radical. Indeed, at the end each alkyne

group is combined with two thiols to generate dithioethers and a thiol-yne addition product [163].

## **2.2. Light-induced additive manufacturing in tissue engineering**

The hydrogels creation, and especially their shaping, emerged in the last decade as one of extreme interest topic in the biomedical field. Until the only operative applications for this class of materials were simple polymeric networks (no matter of the geometry) or drug delivery systems, the basilar shaping using preformed mold was sufficient. However, as already pointed out, the need of scaffold mimicking the patient defected tissues and organs pushed the integration of hydrogel design/formation with additive manufacturing (AM).

To build such structures, AM techniques have required the skills combination of various fields, including biology, mechanical engineering, and material science. This new challenge, named biofabrication, employs the utilization of computer-aided design (CAD) files in STereo Lithography interface (STL) format permitting the automated formation of hydrogels (by layering the entire printing structure), with desired architectures and variable resolution in precise and reproducible manners. Moreover, if cells are directly mixed with the liquid formulation (cell-laden approach), the named technique is called bioprinting and the formulation bio-ink. Various light-based methods have been employed in the last years to create self-standing 3D printed hydrogels, categorized in the two main class of extrusion-based and lithography-based technologies [164].

### **2.2.1. Extrusion-based technologies**

Extrusion-based printers have been extremely successful in recent years to create bio-engineered hydrogels through simple extrusion and subsequent sterilization of the ink. The extraordinary popularity of this class of technologies resides mainly in their simplicity and predictability, with a large number of commercial bioprinters already available on the market at a relatively low budget, making these techniques extremely user-friendly [164]. The only foresight concerns the inks design, and especially their viscosity. In fact, relatively medium-high viscosity inks are generally required to control the extrusion process and to maintain a certain degree of mechanical stability until the geometry is photopolymerized; oscillatory shear stress experiments are usually performed on the non-cured formulation (e.g., amplitude sweep) to validate the behavior [165]. Moreover, while numerous natural inks already possess this feature (e.g., functionalized polysaccharides), the possible introduction of additives can easily



increase the viscosity; for this reason, one of the main advantages of these technologies are the high number of inks available [166]. Nevertheless, in comparison with the lithography-based techniques, extrusion-based printers' function at lower print speed and resolutions, decreasing the complexity of the formed geometries [164].

Three different set-ups can be used to 3D print biocompatible hydrogels, called "traditional", "embedded" and "in situ" (Figure 2.6) even though maintaining the same configuration. In all cases, an ink reservoir is previously filled with the formulation and let flow by various mechanisms (e.g., air pressure, mechanical force, etc.) through a small diameter needle (100-800  $\mu\text{m}$  usually) to dispense a filament which will create the first layer pattern. Once the first layer is formed, a vertical movement of the needle take place preparing the machines to the second layer pattern creation on top of the first. At the end, multiple layers are created one on top of the other to meet the final selected architecture. However due to the needle constriction, the ink is generally subjected to high shear stress during the flow. Importantly, if bio-inks are used to create hydrogels a lower viscosity is necessary to not reach out massive cell's death (viability can be reduced up to 80%). The light exposure, UV or visible, can be applied continuously during all printing process, after the entire architecture is created or with multiple photo crosslinking steps irradiating every single layer (depending on the formulation mechanical stability) [167].

A curious and interesting alternative to enable omnidirectional printing is the "embedded" configuration [168,169]. In this case, support baths are used to facilitate the deposition of the ink wherever in arbitrary 3D space, recovering rapidly once the needle is extracted or translate through them. Granules or slurries are generally used for this purpose; for examples gelatin microparticles slurries can effectively support the ink geometry creation by melting at the printing temperature of 37°C [170]. Moreover, at terminated printing, the bath material can be recycled (washed away generally) or sacrificed (by mechanical removal) depending on the chemical interactions established with the 3D-printed structure. This approach permits the fabrication of inks independent on the intrinsic viscosity, allowing the creation of hydrogels starting with very low viscosity formulation not suitable in the "traditional" case [171].

Lastly, the "in-situ" configuration is an evolution of the "traditional" method where the light irradiation occurs directly on the needle through a photo-permeable capillary, starting the photo-curing before deposition. This approach permits greater resolution of the final 3D printed hydrogels compared with the other techniques because of the enhanced mechanical stability of the layers [172].

The printing formulations consist of a mixture of different compounds to create the final hydrogel geometry, such as the monomer/oligomers/functionalized polymers, the solvent (generally water or physiological solutions), the photo-initiators and eventually additives that can impart non-Newtonian flow properties.

While the polymer precursors have been treated on the material section of Chapter 1, other materials include natural polymers functionalized with photocurable groups described in the previous section (2.1.1). Generally, the photo-initiators used are water-soluble such as LAP (or others phosphine derivatives) and Irgacure 2959 2-hydroxy-1-[4-(2-hydroxyethoxy) phenyl]-2-methyl-1-propanone (or other members of the Irgacure family) for NT1 reactions while Eosin-Y, Riboflavin and Camphorquinone derivatives are used for NT2 reactions; all at concentrations between 0.1 to 5 wt% (depending on the formulation reactivity) [173]. The non-Newtonian additives instead are able to switch the formulation behavior from low viscosity in proximity to the needle to high viscosity once deposited, giving shear-thinning properties to the resin; examples of these materials are nanosilicates and nanocellulose. Other compound inserted in the formulations are photosensitizers, molecules able to absorb and tune the photo-initiator reactivity toward different wavelength (such as the visible light, always preferred in tissue engineering to not cause DNA modification on cells) [164].

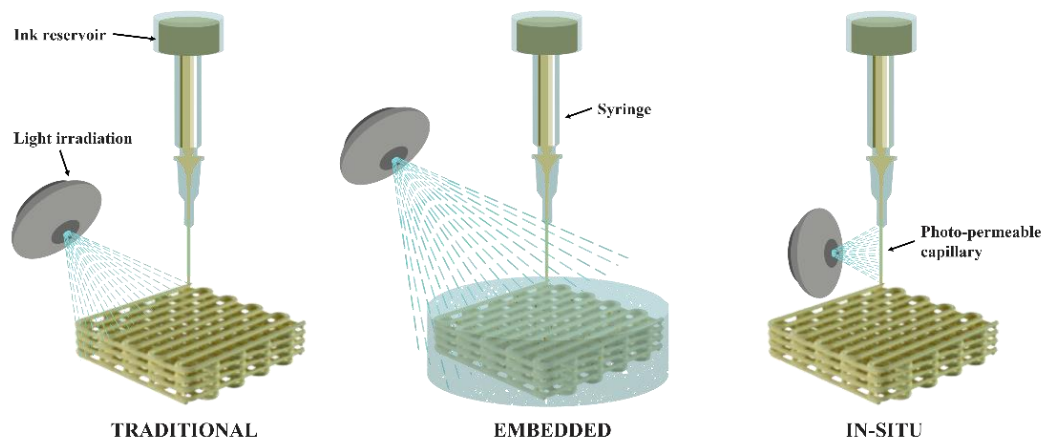


Figure 2.6: extrusion-based printers set-ups.

### 2.2.2. Lithography-based technologies

Lithography-based printers are nowadays the most evolved 3D-printing techniques on the market to produce complex structured hydrogels. These technologies are able to impart the best characteristics in terms of accuracy and precision of the spatially 3D construct, with resolutions around 25-50  $\mu\text{m}$  not achievable in all cases in extrusion-based systems [164]. Employing either a computer-controlled laser beam (Stereolithography, SLA) [174] or a digital light projector (Digital Light Processing, DLP) [175] the low viscosity liquid formulation is photocured onto a z direction moving platform to fabricate layer-by-layer the entire hydrogel geometry [176]. Both the printers utilize a similar concept for processing the hydrogel, based on a vat filled with the liquid resin (Figure 2.7).

SLA was invented in the 80s by Chuck Hull, where a concentrated laser beam photopolymerize the formulation in the vat, spot-by-spot, on the surface of the z-moving platform [177]. Normally, the laser is not focalized directly on the vat (so it's moving to create the geometry) but instead it is deflected by a fast-moving mirror which is responsible for the structure creation. After the first layer pattern is formed, the platform moves downward to let the formulation cover the second layer thickness; the process is then repeated until the final structure height [178].

Contrarywise, DLP printers employ a digital mirror device formed by millions of micro-mirrors that function as photomask for the light beam of the projector. This process grants the possibility to 3D print the entire layer once at a time by a single light exposure passing through the vat transparent bottom, speeding up extraordinarily the printing times independently to the x-y geometry complexity. Once the first layer is created a vertical movement of the building platform take place, the formulation is let flow under the platform, the second layer can be processed and so on. Curiously at printing completed, the resulted structure will be placed upside down on the platform, so a sufficient mechanical resistance is required [179,180].

It is clear that a low viscosity formulation is needed, otherwise an incomplete flow of the resin take place on/under the moving platform, generating an incomplete layer. The only drawback of these technologies is then the chronic lack of printing inks, due for the strict viscosity requirements which reduce the number of suitable formulations described for the extrusion-based printers. However, herein another class of molecules are often incorporated into the

printing formulations to reduce the possible light-scattering subsequent to the entire layer light irradiation, called photo-absorbers or dye. These molecules, usually water soluble to create hydrogels, are extremely useful to increase the printing resolution and are particularly needed to create porous or interconnected geometries; one of the most famous water soluble dye is brilliant green (BG) [164].

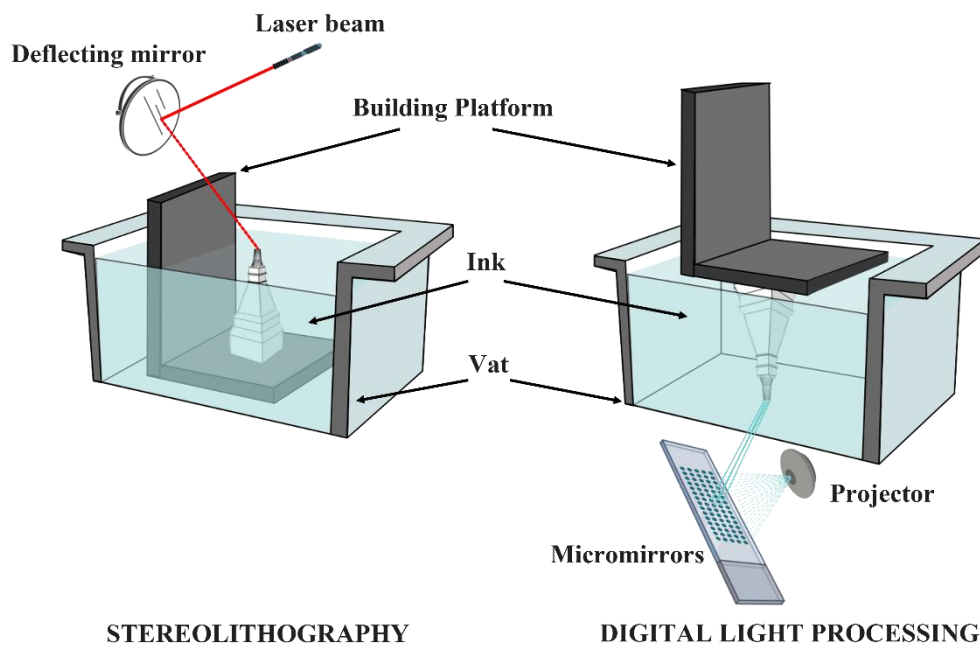


Figure 2.7: Lithography-based printers.



# Chapter 3

## Chitosan hydrogels

### 3.1. Introduction

Especially in the last decades, the field of material science has grown a large interest on natural polymers due to their characteristic physical-chemical properties and environmental sustainability, hardly reproducible in laboratory [27,43]. Their combination with photoactivated processing techniques, such as 3D printing, is also very attractive to reproduce scaffolds able to mimic any patient tissues defect or injuries [164,181]. As also pointed out on Chapter 1 (1.2.2. Natural polymers), the creation of scaffolds based on biopolymers is highly recommended in bioengineering applications, because of their enhanced biocompatibility [23].

To make them processable (e.g., photocurable), it must be considered that natural polymers often need various steps of functionalization generally driven by conventional thermal routes which employ external heating sources. Those techniques, despite their extensive application, present slow or hard to control heat transfer, inhomogeneous thermal gradients, not efficient reactions and generation of by-products [182]. Microwave-assisted organic synthesis (MAOS), exploiting the “microwave dielectric heating”, ensure a localized and targeted heating transfer based on the solvent/matrix ability to align its molecules dipoles on the direction of the oscillatory electric field [182,183]. Consequentially, reaction times and energy consumption experience drastic decreases, with economical beneficial effects. Moreover, this rapid and cheap method of synthesis presents less side reaction and generation of side products, making the whole process really useful for biomedical applications, moving also a further step toward green chemistry [184,185].

Moreover, as mentioned on Chapter 2 (subsection 2.2), additive manufacturing technologies are, and will be even more in the next future [186], extremely important in tissue engineering applications. Especially DLP printers, starting from liquid formulations, are able to create very well-defined structures in terms of details accuracy and resolution (15-50  $\mu\text{m}$ ), shaping personalized architectures on the patient tissue/organ defect [164]. However, low degree of substitution (range 23-33%) and limited solubility in water are often experienced while working with natural polymers, making the creation of complex DLP printed geometries very challenging [187–189].

Herein, chitosan (extensively treated on Chapter 1, subsection 1.2.2.1.) was functionalized for the first time using the MAOS process to incorporate methacrylic groups into the polysaccharide backbone, exploiting its easily modifiable amine moieties. Even though other natural polymers have already been modified using microwave [190], neither this technology have never been used to functionalize chitosan nor a deep study on the microwave parameter effect on the polymer degree of substitution has been proposed in literature.

Once modified, three synthesis batches at different degree of substitution were selected to mechanically characterize the scaffolds at different stiffnesses (to meet the different mechanical parameters of a multitude of human tissues) and swelling kinetics. Moreover, to test the hydrogels as 3D network for cancerous tissue progression in vitro models, the most substituted gel was selected for enzymatic degradation and biological characterization [191], while just simple 3D geometries were created using a traditional extrusion based printer due to the poor reactivity of the methacrylated chitosan solo hydrogels.

Then, we investigated a way to successfully create complex and detailed DLP printable hydrogels employing methacrylated chitosan as the main matrix. DLP printed methacrylated chitosan hydrogels have already been described in literature, but only with strong additions of synthetic crosslinkers, such as poly-(ethylene glycol) diacrylate and acrylamide [192,193], rendering any effort to create high biocompatible and totally bio-derived scaffolds. Since colored dyes are often employed in DLP formulation mainly to prevent light scattering inside of the building vat [194,195], the usage of low concentrated, bio-derived and biocompatible dyes to enhance the polymer reactivity could be a strategy to obtain well-detailed and stable printed structures.

The successful DLP printing of very detailed, stable, and defined structures was obtained thanks to the addition of a new methacrylated bio-derived colored dyes based on quinizarin [196] into both the microwave synthesized methacrylated chitosan (CHI-MA) and a polymer blend between CHI-MA and poly-(ethylene glycol) diacrylate (PEGDA). EPR experiments proved the quinone-like dyes (mono and di-methacrylated) possibility to create radicals upon light exposure, accelerating the polysaccharide polymerization kinetic and granting superior mechanical properties to the hydrogels. Moreover, the biological characterization

showed no cytotoxic effects of the printed hydrogels, promoting both cell adhesion and proliferation.

## 3.2. Materials and procedures

### Materials

Chitosan medium molecular weight (CHI, Mw = 190–310 KDa, 75–85% degree of N-deacetylation), methacrylic anhydride (MA, 94%), acetic acid ( $\geq 99\%$ ), lithium phenyl-2,4,6-trimethylbenzoylphosphinate (LAP,  $\geq 95\%$ ), Poly(ethylene glycol) diacrylate (PEGDA, average Mn 700), Brilliant Green (BG, hydrogen sulfonate Mw 482.63), Dimethyl sulfoxide (DMSO, anhydrous  $\geq 99.9\%$ ), Quinizarin (QZ, 96%), N-dimethylaminopyridine (DMAP,  $> 99\%$ ), 5,5-dimethyl-1-pyrroline N-oxide (DMPO), dialysis sacks (Avg. flat width 35 mm, MWCO 12 000 Da), phosphate-buffered solution (PBS, pH 7.4) and lysozyme from chicken egg white (LYS, protein  $\geq 90\%$ ,  $\geq 40\ 000$  units per mg protein) were purchased from Sigma-Aldrich and used as received without further purification.

### Synthesis of methacrylated chitosan (CHI-MA)

Table 3.1: Methacrylated chitosan microwave synthesis parameters. CHI = amino glucose ring of chitosan, MA = methacrylic anhydride.

Synthesis n°	Molar ratio (CHI:MA)	Max power (W)	Temperature (°C)	Launch time (s)	Reaction time (min)
1	1:1	800	100	30	5
2	1:2	800	100	30	5
3	1:4	800	100	30	5
4	1:6	800	100	30	5
5	1:1	800	80	30	5
6	1:1	800	60	30	5
7	1:1	800	100	60	5
8	1:1	800	100	120	5
9	1:1	800	100	30	10
10	1:1	800	100	30	15
11	1:1	800	80	60	10

Firstly, chitosan was dissolved at a concentration of 1.5wt% in a solution of DI water-2wt% of acetic acid and stirred overnight. Once homogeneous, methacrylic anhydride was added dropwise into a 100 mL clamped Teflon reactor



equipped with temperature and pressure probes. The molar ratio between the aminoglucose groups of chitosan and methacrylic anhydride (MA) was varied from 1:1 to 1:6. The solution was then placed into the microwave furnace (Milestone STARTSynth, Milestone Inc., Shelton, Connecticut) varying the characteristic machine parameters of temperature, launch time (i.e., the necessary time to gain the set temperature) and reaction time. The current power was let varying until a maximum of 800 W during the reaction to maintain the furnace set temperature. The synthesis tested, with the operative parameters, are summarized on Table 3.1. At the end the product was cooled down to RT for every synthesis batch. All the proposed synthesis combinations were reproduced in triplicate (with a variability of the results of  $\pm 1$ ), dialyzed 7 days against DI water, freeze dried and stored at 4° C.

### **Synthesis of mono/di-methacrylated quinizarin (Q-1MAc and Q-2Mac)**

The coloured dyes were kindly synthesized, characterized and shipped to our group from Prof. Versace of the Université Paris-Est Créteil (UPEC), according to a previously reported protocol [196]. The final yield obtained of Q-1MAc (mono-methacrylated) is 44% while a yield of 59% was achieved for Q-2MAc (di-methacrylated).

## **3.3. Characterization methods**

### **Attenuated total reflectance-infrared spectroscopy and nuclear magnetic resonance spectroscopy analysis (ATR-FTIR and <sup>1</sup>H-NMR)**

ATR-FTIR was used on freeze dried samples to evaluate the chemical composition of the synthesis products and to assess the successful incorporation of MA into the chitosan backbone, employing a Thermo Scientific Nicolet iS50 FTIR Spectrometer (Milano, Italy) furnished with a diamond crystal ATR accessory. The reported spectra are a mean of thirty-two scan with a resolution of 4 cm<sup>-1</sup> while neat chitosan was taken as reference.

<sup>1</sup>H-NMR spectra were used to confirm the presence of the double bond C=C on chitosan, recorded on a Bruker Avance DPX 400 MHz nuclear magnetic resonance spectrometer with samples dissolved in D<sub>2</sub>O (chitosan, with small amount of trifluoroacetic acid) at RT. The obtained spectra were evaluated by MestReNova software.

<sup>1</sup>H-NMR spectra were used to confirm the presence of the double bond C=C on quinizarin, recorded on a Bruker Avance DPX 400 MHz nuclear magnetic resonance spectrometer with samples dissolved in CDCl<sub>3</sub> (Q1-MAc and Q-2MAc) at RT. The obtained spectra were evaluated by MestReNova software.

### **Q-1MAc and Q-2MAc characterization**

Electron paramagnetic resonance (EPR) spin-trapping experiments were performed with a EMX spectrometer (standard TE<sub>102</sub> rectangular cavity (ER 4102 ST, Bruker)) or a EMXplus spectrometer (Bruker) equipped with the High Sensitivity Probe-head (Bruker) in the small quartz flat cell (Wilmad-LabGlass, WG 808-Q). Experiments have been done in dimethylsulfoxide (DMSO, anhydrous, Sigma-Aldrich) under argon at 295 K by direct irradiation of EPR resonator using LEDs@365 nm or LED@400 nm ( $\lambda_{\text{max}} = 385 \text{ nm}$  or  $400 \text{ nm}$ ; Bluepoint LED, Höppler UV Technology). The EPR spectra were recorded in situ during/after a defined exposure time as described elsewhere [334]. The experimental EPR spectra were analyzed by the WinEPR software (Bruker) and the calculations of spin-Hamiltonian parameters and relative concentrations of individual DMPO-adducts were performed with the EasySpin toolbox [335].

Absorption spectra of the methacrylated molecules at a concentration of  $10^{-4}$  M in a Water:DMSO solution (3:1, v/v) were collected using a Synergy HTX Multi-Mode Microplate Reader instrument (BioTek, Winooski, VM, USA) set in spectrum mode in the range between 300 to 700 nm and at a scan step of 10 nm.

### **Hydrogel characterization**

The viscosity of the formulations was evaluated with continuous flow measurements performed in triplicate with a range of shear rate from 0,01 to 1000 s<sup>-1</sup>, setting a gap between the two plates of 0.5 mm

The real-time photorheological measurements were performed using an Anton PAAR Modular Compact Rheometer (Physica MCR 302, Graz, Austria) in parallel-plate mode (25 mm diameter) where the visible-light source was provided by a bottom positioning of the light guide of the visible Hamamatsu LC8 lamp under the bottom plate. During the measurements, the gap between the two glass plates was maintained at 0.2 mm, while the sample was kept under a constant shear frequency of 1 Hz. The irradiating light was switched on after 60 s to allow the system to stabilize before the onset of polymerization. According to preliminary amplitude sweep measurements, all the tests were carried out in the linear viscoelastic region at a strain amplitude of 1%. The photo-rheology was studied as a function of the changes in the shear modulus ( $G'$ ) and in the loss modulus ( $G''$ ) of the sample versus the exposure time.

Amplitude sweep tests were performed on the cured hydrogels in the range between 1 and 1000% of strain, frequency of 1 Hz.

The crosslinking density was evaluated using the formula [44]:

$$\nu_e = \frac{G'N_a}{RT} \quad (1)$$

Where  $G'$  is the shear storage modulus obtained by the plateau region in the amplitude sweep measurements at 1% of strain,  $N_a$  the Avogadro number,  $R$  the ideal gas constant and  $T$  the photo-rheometer set temperature (37° C). The obtained values are a mean of three different tests.

The compression tests were conducted on a MTS QTestTM/10 Elite controller using TestWorks 4 software (MTS Systems Corporation, Eden Prairie, Minnesota, USA). A 10 N cell load in compression mode was used for the test with a compression speed of 1 mm min<sup>-1</sup> on cylindrical samples ( $D = 8$  mm,  $H = 7$  mm). The data acquisition rate was set as 20 Hz while the compressive modulus was calculated by TestWorks 4 software. The compressive modulus ( $E$ ) was estimated as the slope of the linear region of the stress–strain curves between 0 and 15% of deformation while the ultimate compression strength (UCS) and the elongation at rupture ( $\epsilon_r$ ) were extrapolated from the plots. All the experiments were performed on triplicate.

The different photocured samples ( $D = 8$  mm,  $H = 7$  mm) were weighted and soaked in DI water to evaluate the swelling capability and kinetics. The samples were taken out at different time point and weighted once the surface droplets were wiped off with paper until constant weight. The swelling ratio ( $Sw\%$ ) was calculated as:

$$Sw (\%) = \frac{W_t - W_0}{W_0} * 100 \quad (2)$$

$W_t$  is the weight of the hydrogel sample at a specific time, and  $W_0$  is the weight of the dried sample recorded as the initial weight. All tests were performed in triplicate.

To determine the gel content (GC) of the CHI-MA hydrogels, dried samples were held in a metal net, weighed, and then immersed in DI water (25° C) for 24 h to dissolve the uncrosslinked polymer. The samples were then dried for 24 hours (40° C) in a vacuum oven and weighed again. The gel content was determined as:

$$GC (\%) = \frac{W_i}{W_f} * 100 \quad (3)$$

Where  $W_i$  is the initial weight and  $W_f$  the weight after extraction.

The morphological characterization of the degraded samples was carried out by field emission scanning electron microscopy (FESEM, Zeiss Supra 40, Oberkochen, Germany). The samples were coated with a thin film of Pt/Pd 5 nm thick.

The Fickian diffusion or Peppas-Korsmeyer model was evaluated using the formula:

$$F = \frac{SwR_t}{SwR_e} = k_1 t^n \quad (4)$$

Where  $SwR_e$  and  $SwR_t$  are the swelling ratios at the swelling equilibrium and at the considered time  $t$ ,  $n$  is the solvent diffusion index where if  $n < 0.5$  the diffusion is Fickian (i.e., the relaxation rate of the chains is predominant over the solvent diffusion), If  $0.5 < n < 0.9$  the diffusion is non-Fickian (i.e., the two mechanisms are equally predominant) while if  $n > 0.9$  the diffusion of the solvent is faster than the relaxation of the polymer chains (with possible ruptures of the structure) and  $k_1$  is the swelling rate constants of the Peppas-Korsmeyer model.

The Schott's model was evaluated using the formula:

$$\frac{t}{SwR_t} = \frac{1}{k_2 (SwR_e^2)} + \frac{t}{SwR_e} \quad (5)$$

Where  $SwR_e$  and  $SwR_t$  are the swelling ratios at the swelling equilibrium and at the considered time  $t$  and  $k_2$  is the swelling rate constants of the Schott's model.

### **Enzymatic degradation, cell viability, proliferation and migration.**

The freeze dried and photocured CHI-MA DS 24 samples were firstly weighted, then immersed overnight in DI water to adjust the pH in the range of enzyme activity (6.0-9.0) and lastly sterilized 2 h in ethanol. Two solutions were prepared, the control solution containing PBS (pH 7.4) and the degradation solution containing PBS (pH 7.4) plus 1.5 mg/ml of LYS. The LYS amount was added based on the human physiological concentration in serum [197]. Crux shaped samples were prepared to evaluate the degradation change in geometry and transferred into an incubator with 5% CO<sub>2</sub> at 37° C for 1, 7, 14 and 21 days (replacing the mediums after 14 days, to avoid enzyme denaturation). After extraction, the samples were washed in water to eliminate the enzyme leftovers, freeze-dried, and weighted again. The weight loss percentage (D%) was followed using the equation:

$$D (\%) = \frac{W_0 - W_t}{W_0} * 100 \quad (6)$$

$W_t$  is the weight of the freeze-dried degraded sample at a specific time while  $W_0$  is the initial weight of the same dried sample. All the measurements were taken in triplicate.

The biological characterization was driven in two different ways depending on the final application: 3D in-vitro model for CHI-MA solo hydrogels and soft tissue substitutes material for the quinizarin-based dye loaded hydrogels.

In the first case thanks to the precious help of PolitoBIOMed Lab, scaffolds of diameter ranging from 5 to 8 mm, 5 mm height and with a 2 mm basin were produced. These dimensions resemble the 48 well cell culture plate and the basin allows the cell seeding. The scaffolds were then washed overnight in distilled water to neutralize the acidic pH, incompatible with the cell viability. Then, samples were sterilized by soaking for 2 h in a 70:30 solution of EtOH:DI water followed by 2 h in PBS added with 1% Penicillin/streptomycin and exposed 1h (30 min for each side) to UV light. For the migration assay, the scaffolds were positioned inside the 48 well cell culture plate (Greiner bio-one).  $4.5 \times 10^5$  cells were resuspended in 40  $\mu$ l and seeded on each scaffold basin. Cells were left 3 h attaching to the scaffold and then cell culture medium was added to completely cover the sample. After 96 h and 7D the scaffolds were washed with PBS, fixed with formalin free fixative solution (Sigma-Aldrich), permeabilized with 0.25% Triton x-100 (Sigma-Aldrich) for 30 min at RT and stained with 0.4 mM DAPI (Sigma-Aldrich) for 3 h at RT. Fluorescent images of the cells migrated inside the scaffold were collected using the microscope Eclipse Ti2 Nikon (Tokyo, Japan) equipped with a Crest X-Light spinning disk.

Chitosan-conditioned medium was produced for cell proliferation tests. The scaffolds were soaked in the cell medium (1,5 ml/scaffold) for 48 h in the dark at 37° C. Then the supernatant was filtered with a 0.22  $\mu$ M filter and used for cell seeding.  $3 \times 10^5$  cells/well were seeded on 48 well cell culture plate (Greiner bio one) in 500  $\mu$ l/well of normal and conditioned medium. After 24 h and 96 h of incubation cell proliferation was determined with Resazurin (Sigma-Aldrich). In particular, 50  $\mu$ l of Resazurin were added to each well and left 3 h in the dark at 37° C, 5% CO<sub>2</sub>. The fluorescence signal of the resazurin's reduced form resorufin (exc/em: 530/590) proportional to the number of living cells was detected by the Synergy<sup>TM</sup> HTX Multi-Mode Microplate Reader (BioTek, Winooski, VM, USA). The signal of the normal and conditioned medium without cells was used as background. The cell proliferation experiments were performed three times. Differences between groups were analyzed by two-way ANOVA using GraphPad PRISM 7.04 (GraphPad Software Inc.).

Instead, in the second case (thanks to the collaboration with UCM and CSIC of Madrid) before the cell viability and proliferation assays, all the hydrogels were sterilized in a 48-well plate (Corning) as follows: three initial 10 min washes with 70% ethanol were performed. Then, the samples were rinsed in PBS (phosphate buffer solution, Thermo Fisher) and sterilized with ultraviolet germicidal irradiation (UVGI) for 40 min. After a final rinse with PBS, the hydrogels were cover with DMEM 1X (Gibco) supplemented with 10% FBS (fetal bovine serum, Thermo Scientific) plus antibiotics 100 U mL<sup>-1</sup> penicillin and 100  $\mu$ g mL<sup>-1</sup> streptomycin sulphate (Sigma-Aldrich). Before the cell seeding, hydrogels were stored immersed in the culture medium at 37° C for 24 h.

Cell assays were performed using C166-GFP mouse endothelial cell line (ATCC CRL-2583<sup>TM</sup>, USA). C166-GFP were seeded over the different hydrogels

with a cell concentration of 10.000cells/hydrogel, covered with 500  $\mu$ L of complete culture medium and placed in an incubator at 37° C/5% CO<sub>2</sub>. Inverted fluorescence microscopy (Olympus IX51, FITC filter  $\lambda_{ex}/\lambda_{em}$  = 490/525 nm) was used daily to evaluate the culture attachment and proliferation over the surface of the hydrogels. After 72h, metabolic activity of the cells was measured using Alamar Blue assay, following the instructions of the manufacturer (Biosource).

This method is non-toxic and uses the natural reducing power of living cells, generating a quantitative measure of cell viability and cytotoxicity. Briefly, Alamar Blue dye (10 % of the culture volume) was added to each well, containing living cells seeded over hydrogels, and incubated for 90 minutes. Then, the fluorescence of each well was measured using a Synergy HT plate reader (BioTek) at 535/590 nm.

Finally, DNA quantitation of cells was determined by FluoReporter® Blue Fluorometric dsDNA Quantitation Kit fluorescent staining. This method is based on the ability of the bisbenzimidazole derivative Hoechst 33258 to bind to A-T-rich regions of double-stranded DNA. After binding to DNA, Hoechst 33258 exhibits an increase in fluorescence, which is measured at 360 nm excitation wavelength and 460 nm emission using a microplate reader (BioTek, Synergy HT).

## **3.4. Results and discussion**

### **Microwave-assisted methacrylation of chitosan**

Microwave-assisted organic synthesis (MAOS) is emerging in the last years as a most efficient and greener method to functionalize a wide range of materials, including natural polymers [190]. Considering its certified biocompatibility and easily modifiable structure [198], chitosan was selected as the matrix for the creation of photocurable and cytocompatible scaffolds for tissue engineering applications. Chitosan chemical structure, the reaction scheme to obtain the methacrylated polysaccharide and the photo-crosslinking process are displayed in Figure 3.1. Following reported literature, the methacrylate is expected to take

place both into the amine and hydroxylic moieties of the polymer [187].

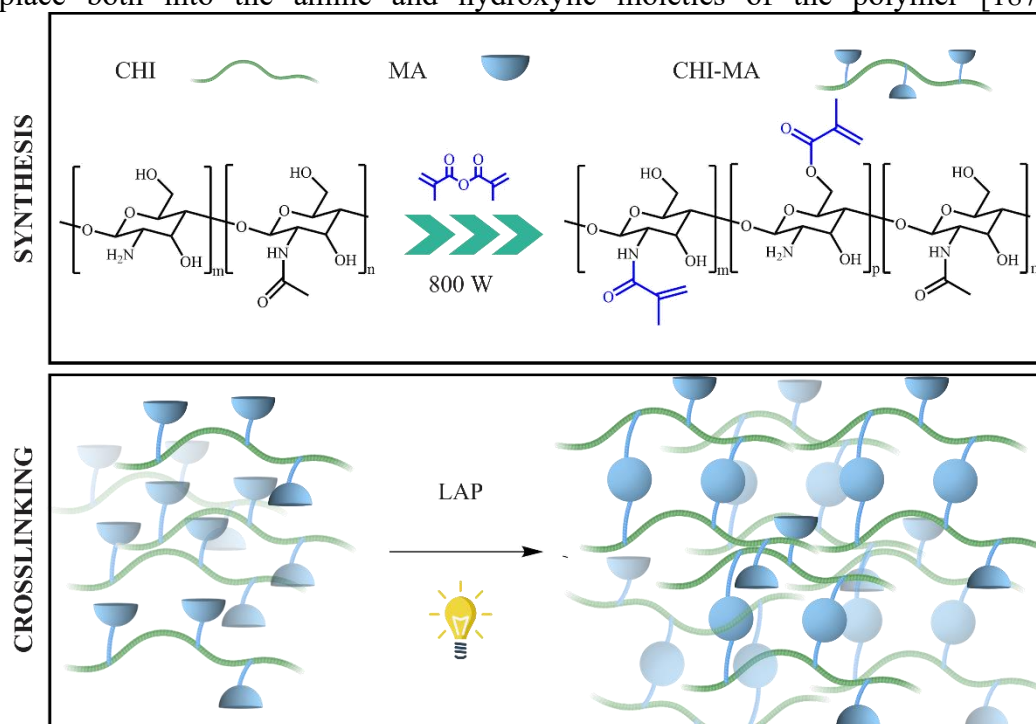


Figure 3.1: Chitosan chemical structure (CHI), reaction scheme to obtain methacrylated chitosan (CHI-MA) and photo-crosslinking process.

Different parameters were investigated to optimize the synthetic process, some related to the reaction (i.e., the molar ratio between MA and the amino glucose chitosan moieties) and some to the microwave equipment (i.e., reaction time, temperature and launch time). One parameters was varied at a time, starting from the molar ratio (CHI:MA = 1:1, 1:2, 1:4 and 1:6) and maintaining constant the other parameters (i.e. temperature = 100° C, launch time = 30 s, reaction time = 5 min, irradiation power = 800 W, based on other reported protocols [199,200]). In Figure 3.2 A are shown the FTIR spectra of CHI-MA at the proposed different molar ratios. The successful functionalization can be attributed to the presence of three peaks, related to the incorporation of MA into chitosan. The shifting at lower wavenumbers of the amine I stretching of CHI signal at 1620  $\text{cm}^{-1}$  (from its usual position around 1639  $\text{cm}^{-1}$ ) represents a first indication of the perturbation of the CHI amine reacting spot due to the incorporation of MA [40,187]. At the same way the appearance of the CO-NH peak at 3091  $\text{cm}^{-1}$  [201] and the formation of the ester band at 1710  $\text{cm}^{-1}$ , related to the incorporation of MA on the CHI hydroxyl groups [202], support the efficacious functionalization. To mention the disappearance of the ester band below a specific molar ratio (1:4), suggesting the CHI amines as the favourite spot of reaction over the hydroxyl moieties [203,204]. However, the certainty of MA

incorporation into the CHI backbone and its quantification was given by  $^1\text{H-NMR}$  (Figure 3.2 B). For every synthesis process, three new peaks appeared between 5.4 and 6 ppm; in fact, 5.4 and 5.6 ppm peaks are associated with the methylene group of MA reacted on the amine moieties while 5.6 and 6 ppm peaks to the reaction on the hydroxyl ones [187,189,205]. Analysing and integrating the peaks, the degree of substitution was evaluated for all samples obtained at different molar ratio between the amino glucose rings of CHI and MA (Figure 3.2 C). Almost a linear increase in the DS% was evidenced increasing the molar ratio between reagents, explained by the MA excess during reaction. However, after a DS% maximum at a molar ratio of 1:4 a sort of plateau (or shorter decrease) was evidenced, suggesting limitations due to steric hindrance. Even though, the obtained values are similar to previous reported works performed using the conventional thermal synthesis [187].

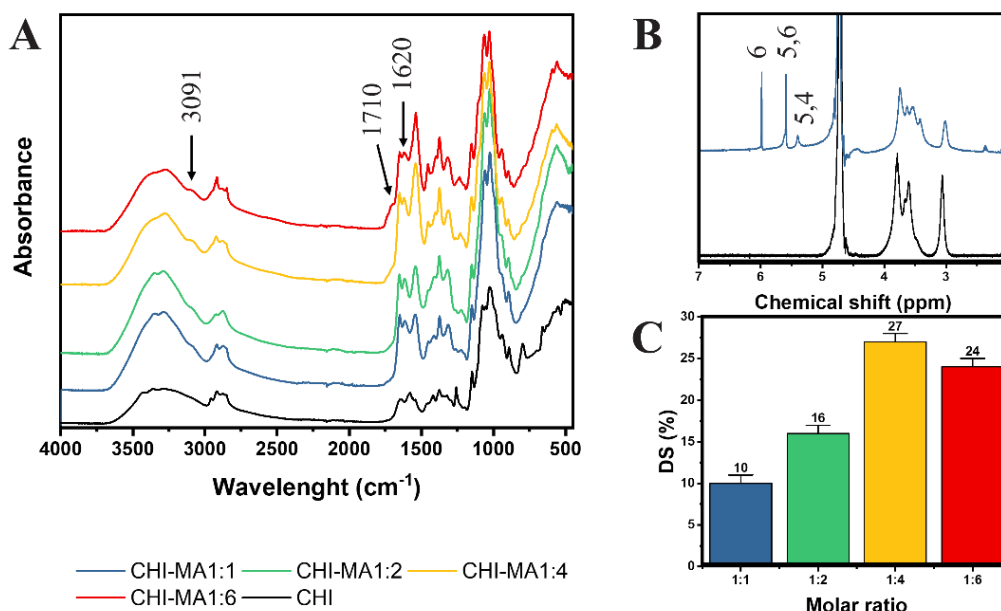


Figure 3.2: FT-IR spectra of CHI and CHI-MA obtained at different molar ratio between reagents (A) and the nuclear magnetic resonance spectroscopy analysis on CHI-MA (B). In Figure C are plotted the degree of substitution obtained at different molar ratio (1:1 to 1:6)

Once investigated the molar ratio effect on the CHI-MA degree of substitution, the study progressed on the optimization of the microwave characteristics parameters of temperature, launch and reaction time. Aiming to maintain the reaction as greener as possible, to limit the MA excess steric hindrance effects and to isolate the possible beneficial contribution of the microwave parameters the lower molar ratio of 1:1 between reagents was chosen for the chitosan methacrylation. In Figure 3.3 are plotted in column mode the



obtained degree of substitution varying the reaction temperature (synthesis n° 1, 5 and 6 of Table 3.1), the launch time (synthesis n° 1, 7 and 8 of Table 3.1) and the reaction time (synthesis n° 1, 9 and 10 of Table 3.1) while the synthesis performed with the coupled best parameters overall is shown separated (synthesis n° 11 of Table 3.1). This time, no linear trends were collected but rather two maximum values of DS% at 80° C, 60 s of launch time and 10 min of reaction time. While prolonged reaction times (i.e., 15 min) resulted in the gelation of the system, low values of DS% at mild conditions (low temperatures and high launch times) are explained by a less efficient reaction [206]. Instead, at severe conditions (high temperatures and low launch times) the results may be reconducted again to a not complete reaction efficiency and to a small degree of MA vaporization in the first instants due to the strong power heating ramp [200,206]. However, it can be stated that a correct optimization of the microwave parameters increases the final DS% at low molar ratio between reagents (1:1) to values comparable at much higher MA concentration into the reaction (e.g., 1:4 or 1:6) with a peak of 25% in correspondence to a launch time of 60 s.

Following the results, the best parameters overall (molar ratio 1:1, temperature 80° C, launch time 60 s, reaction time 10 min and 800 Watt of irradiation power; synthesis n°11 on Table 3.1) were used to synthesize a methacrylated chitosan with a DS% of  $24 \pm 1$  %. Those results indicated both that an efficient reaction can be conducted at 80° C as much as an extension of the launch time has a greater effect into the final DS% than the reaction time. Especially the second statement can be reconducted to the dropwise addition of the methacrylic product in conventional thermal baths; in fact, the addition of the functionalizing agent is often a critical parameter in traditional synthesis in order to avoid side products or inefficient reactions, so a proper and functional launch time might increase the reaction efficiency [45,207,208].

In conclusion, the application of MAOS can intrinsically reduce the total synthesis time while maintaining a certain degree of reproducibility and a low environmental impact. Considering that the tissue stiffness and composition always influence cell morphology, cytoskeletal structure, signaling and function, the step of hydrogel characterization was then performed on three synthesis batches at different degree of substitution (CHI-MA DS 24 = synthesis n°11, CHI-MA DS 17 = synthesis n°8 and CHI-MA DS 10 = synthesis n° 1) to meet different tissues properties [209–211].

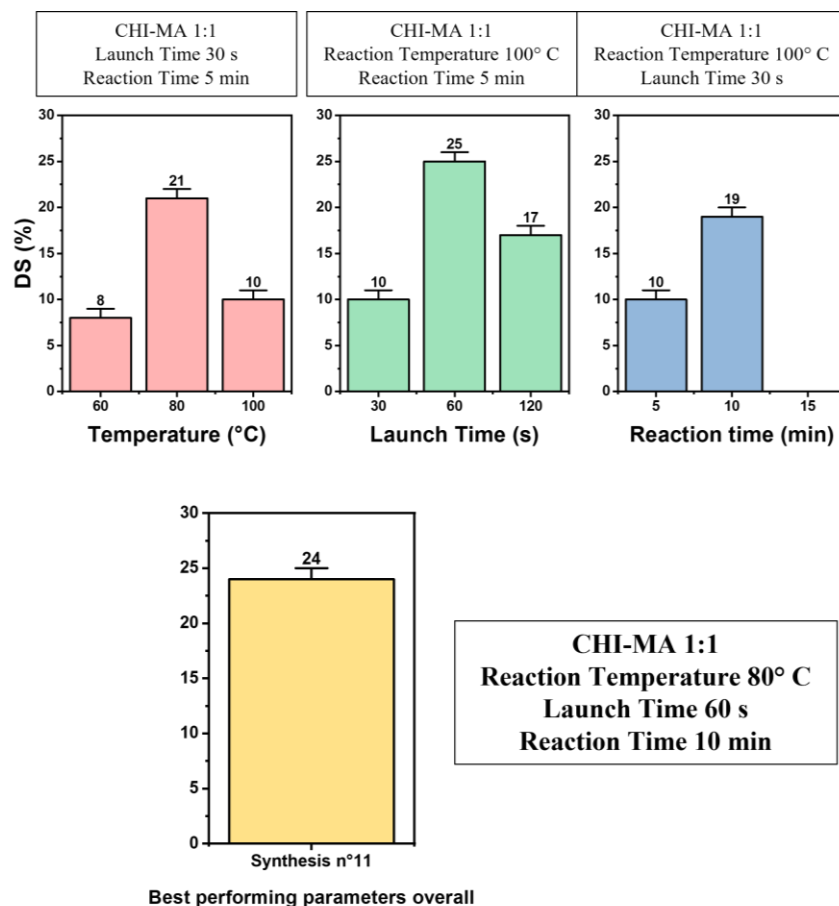


Figure 3.3: % Degree of substitution of all the synthesis batches varying the microwave parameters (i.e., temperature, launch and reaction time). The obtained DS% were measured by integration of each synthesis <sup>1</sup>H-NMR spectra.

## Hydrogel characterization

Firstly, the right CHI-MA concentration and viscosity were evaluated to allow an efficient 3D printing of the material using an extrusion deposition modelling machine. Two solution of CHI-MA DS 24 at different concentration, 2 wt% and 5 wt%, were prepared in DI water and tested through rheology to obtain information about their reactivity (by photo-rheology) and viscosity (Figure 3.4 A and B, respectively). Regarding the photo-rheology, the test is usually employed to evaluate the variation of the shear storage modulus  $G'$  over time of irradiation (herein started at 60 s, to give enough time to the system to stabilize). The three main information that can be extrapolated by the plot to evaluate the reactivity of the formulation are:

- The induction time, so the time corresponding to the initial increase of the  $G'$  curve.

- The slope of the increasing curve, related to the kinetic of reaction of crosslinking.
- The upper curve plateau, corresponding to the final mechanical properties of the hydrogel.

Herein, the three parameters in Figure 3.4 A show an increased behavior in terms of reactivity, mechanical properties, and stability of the final hydrogel for the CHI-MA 5 wt% formulation, with an instantaneous increase of the  $G'$  curve (compared with 44 s of delay for the CHI-MA 2 wt% formulation), a sharper initial curve slope and a clear and stable upper plateau. Moreover, an increased viscosity of the CHI-MA 5 wt% formulation was evidenced (Figure 3.4 B). Considering the formulation employment on extrusion 3D printing, high viscosity with a marked shear-thinning behavior and high shear storage modulus are often required to permit a constant flow through the printer nozzle and grant strong withstanding properties of the deposited printed layer; for these reasons a concentration of 5 wt% was selected for the three synthesis batches at different degree of substitution. In Figure 3.4 C are reported the photo-rheology tests on the selected formulations. All formulations showed instantaneous increase of  $G'$  (so 0 s of induction point) while the crosslinking kinetic and the final values of storage modulus respect the degree of substitution indicated, with nominal values comparable with literature [187]. The hydrogel stability over solicitations is reported in Figure 3.4 D by amplitude sweep measurements. The enhanced stiffness and relative fragility of CHI-MA DS 24 is confirmed by a higher initial  $G'$  value ( $\approx 3$  KPa) and yield point (the point where the hydrogel collapse and the mechanical properties start to decrease, 14% of strain for CHI-MA DS 24), compared with CHI-MA DS 17 ( $G' = 1$  KPa, yield point = 62% of strain) and CHI-MA DS 10 ( $G' = 0.75$  KPa, yield point = 121% of strain). The reason of the behavior is explained by a possible increment of crosslinking density, verified by the formula (1):  $v_e$  CHI-MA DS 10 =  $1.75 \cdot 10^{23} \text{ m}^{-3}$ ,  $v_e$  CHI-MA DS 17 =  $2.42 \cdot 10^{23} \text{ m}^{-3}$  and  $v_e$  CHI-MA DS 24 =  $7.42 \cdot 10^{23} \text{ m}^{-3}$  [212].

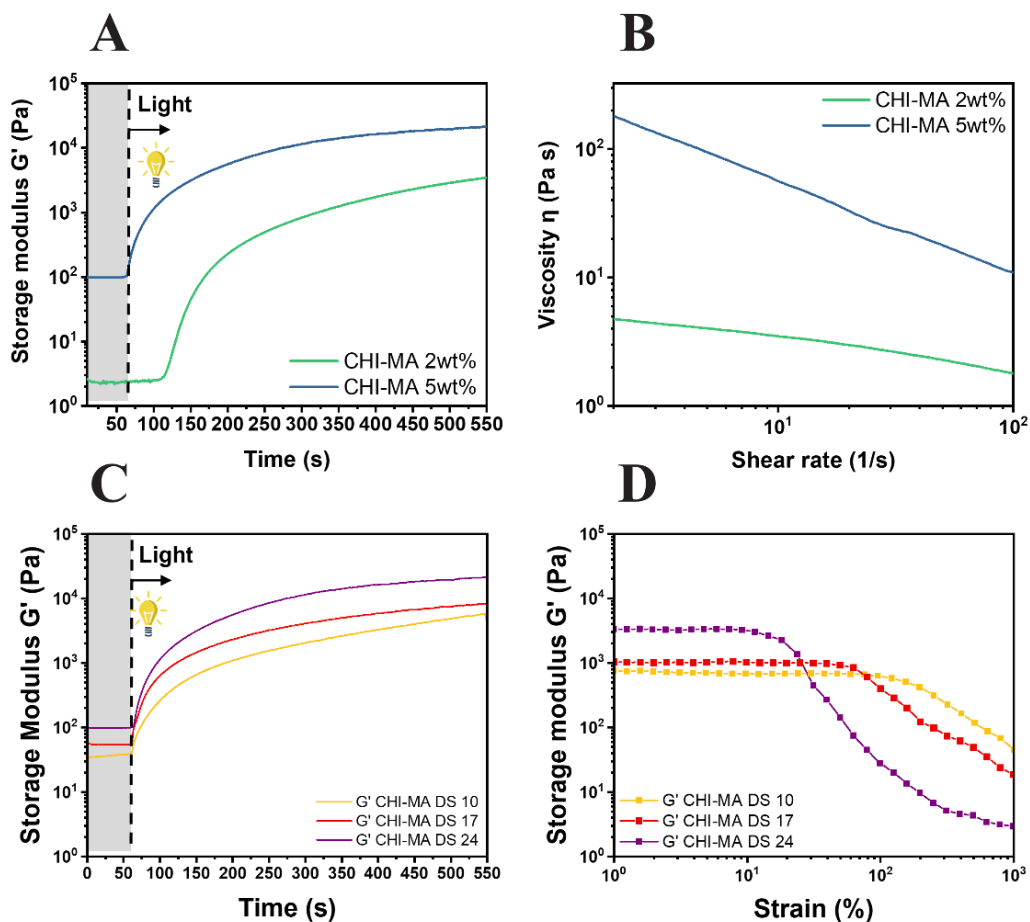


Figure 3.4: photo-rheology (A) and viscosity (B) calculated on CHI-MA DS 24 at different concentrations. On figure C and D are reported the photo-rheology and amplitude sweep plots of the CHI-MA at different degree of substitution, respectively.

The same formulations were then photocured in cylindrical molds to test the mechanical properties of the hydrogel at different degree of substitution over unconfined uniaxial compression (Figure 3. 5 A). The values of compressive storage modulus (E), ultimate compressive strength (UCS) and elongation at rupture ( $\epsilon_r$ ) are displayed on Table 3.2. With compression properties respecting the previously obtained trend based on the hydrogel degree of substitution and ranging from 20 KPa (CHI-MA DS 10) to 39 KPa (CHI-MA DS 24), stiffnesses suitable for soft tissues such as heart, lung or muscles tissues were achieved [213–215].

The same geometry shaped hydrogels were also subjected to swelling kinetics tests (Figure 3. 5 B). Considering that the maximum hydrogel capacity depends strongly on the affinity between the polymer and the used solvent [216–218], two opposite tendencies play a role in the swelling equilibrium of the hydrogel: i.e.,

the ordinary entropy gain subsequent to the polymer/solvent blending and the decreasing in entropy due to the distortion (here, expansion) of the 3D network [6]. So, apart for the constant polysaccharide hydrophilic moieties content (which favor the polysaccharide/aqueous solvent blending, constant on all samples) a major role is played by the hydrogel crosslinking density and its possibility to decrease the gel expansion. Effectively, the values of swelling equilibrium and gel content (reported on Table 3.2) support the proposed theory of an increase of crosslinking density along with the degree of substitution. The two models of Peppas-Korsmeyer and Schott's were also employed to evaluate the swelling kinetics of the CHI-MA hydrogels. Considering the adherence on the models (given by the  $R^2$  values, Table 3.2) and the values of  $n$  in the Peppas-Korsmeyer models (Table 3.2), suggesting a Fickian method of diffusion (i.e., the relaxation rate of the chains is predominant over the solvent diffusion, so no ruptures will occur during swelling), the hydrogels were deemed suitable for tissue engineering applications.

Moreover, the FESEM images of the crosslinked hydrogels (Figure 3. 5) collected on swollen samples show an interconnected porous structure, characteristic of all hydrogels and needed for the creation scaffolds able to be colonized by cells. However, increasing the degree of substitution a more close-packed and regular structure was evidenced, symptom again of an increased crosslinking density.

Even though all samples showed good scaffold characteristics, the employment of cancerous cells and their peculiar stiffer tissues properties [219,220] moved the selection of CHI-MA DS 24 for the further characterizations.

*Table 3.2: Storage modulus (E), ultimate compressive strength (UCS), compression at break ( $\epsilon_r$ ), swelling equilibrium (Sw eq) and Gel content (GC) with standard deviations of the hydrogels obtained from CHI-MA at different DS%. The values of  $R^2$  indicates the hydrogel behaviour's adhesion on the two proposed swelling kinetics models (only valid for  $SwRt/SwRe < 60\%$ ) while the value of  $n$  represents the Fickian or not method of solvent diffusion in the Peppas-Korsmeyer model.*

Sample	E (KPa)	UCS (KPa)	$\epsilon_r$ (%)	Sw eq (%)	GC (%)	Peppas-Korsmeyer model		Schott's model
						$R^2$	$n$	$R^2$
CHI-MA DS 10	20 ± 4	5,3 ± 0,7	46 ± 9	441 ± 87	69 ± 3	0,99	0,34	0,99
CHI-MA DS 17	24 ± 17	5,5 ± 3,8	51 ± 7	245 ± 45	79 ± 4	0,99	0,21	0,99
CHI-MA DS 24	39 ± 6	7,2 ± 0.5	59 ± 5	157 ± 21	87 ± 2	0,99	0,1	1

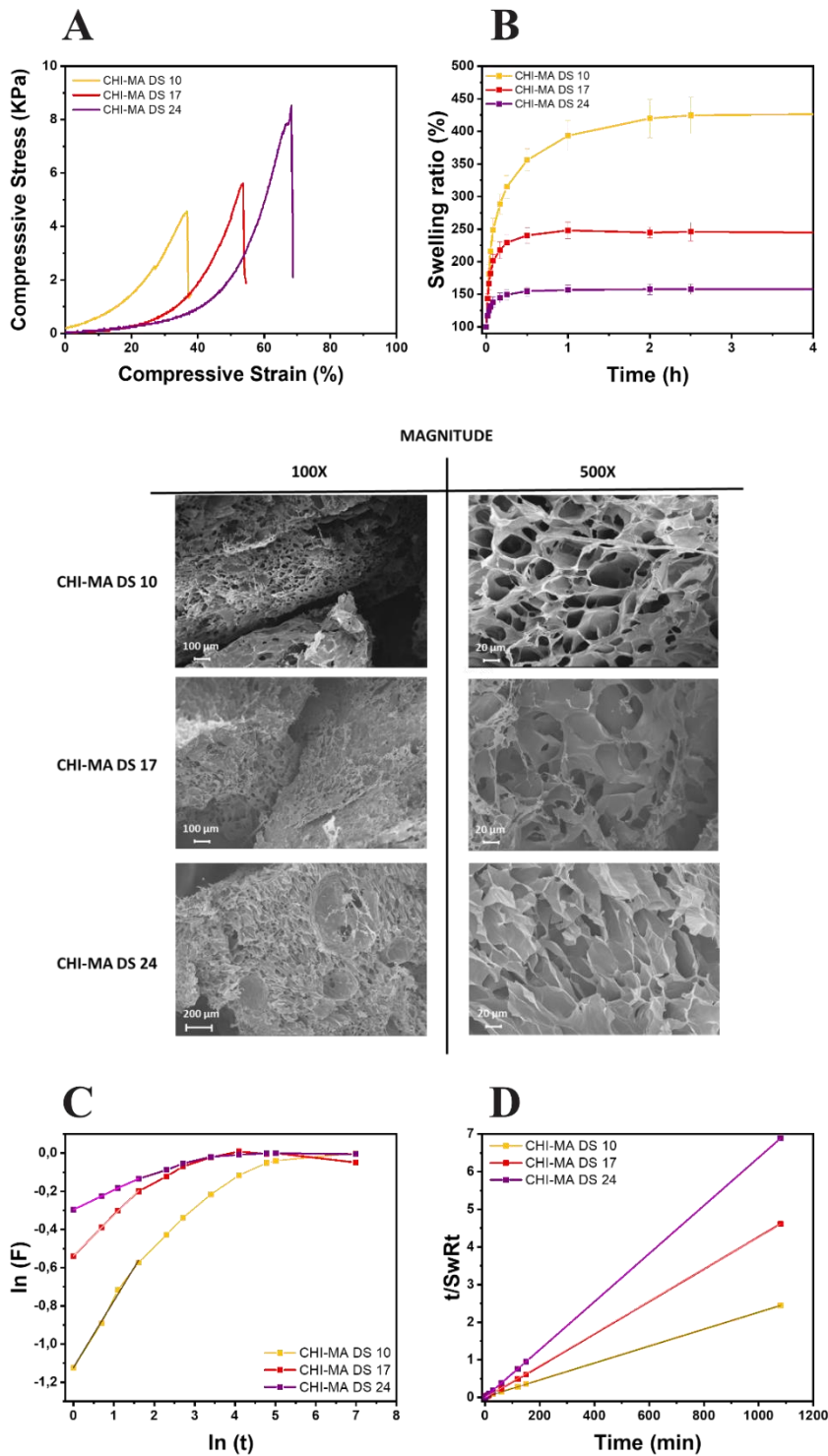


Figure 3. 5: Compression (A) and swelling (B) tests on the hydrogels at different degree of substitution. The FESEM images are displayed on the middle while at the bottom of the image the Peppas-Korsmeyer (C) and Shott's (D) models are reported.

## 3D printing

A 5 wt% formulation of CHI-MA DS 24 was selected for extrusion 3D printing thanks to its clear shear-thinning behavior and its ability to easily flow through the 0.8 mm printer needle. Before selecting the optimal printer parameters of extrusion pressure and needle speed various deposition attempts were made to ensure a continuous and rapid flow and to avoid the syringe clogging. While the printing temperature was set to 37° C and the deposition bed to 4° C (to maintain a certain filament shape after extrusion), various combinations of irradiation were tested. The instantaneous irradiation with the BIO-X embedded LED lamp (intensity < 5mW/cm<sup>2</sup>) resulted into a poor hydrogel crosslinking due to the low light intensity. Even though a slightly more consistent crosslinking was evidenced by using continuous deposition with an external lamp (50 mW/cm<sup>2</sup>), the deformation of the bottom layers led to a collapse of the structure. Instead, the usage of the external lamp with a photocuring time of 2 min per layer (while stopping the machine) permits the completion of a 4-layer grid with discreet resolutions (Figure 3.6). No dissolution in water was experienced after soaking the structure for one day (pH = 4), suggesting a good adhesion between layers and the stability of the gel. More complex structures were impossible to obtain with this extrusion-based technology.

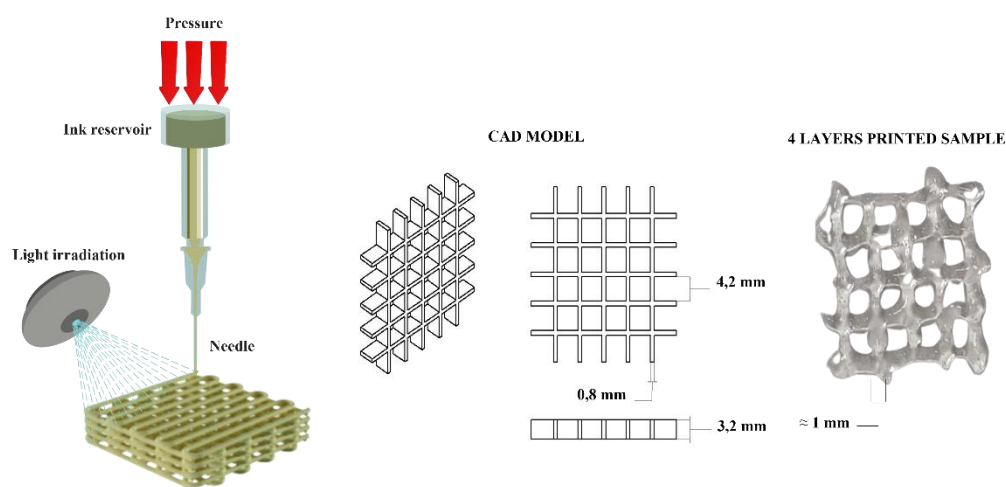


Figure 3.6: extrusion-based printer scheme, CAD model and the printed 4-layer grid.

## Enzymatic degradation

Into the mammalian body two routes generally drive the polysaccharide degradation, hydrolytic and enzymatic cleavage of the glycosidic bonds between units [221]. Even though the enzymatic route results faster and the degradation products are usually metabolized by the body or incorporated within proteoglycans [222], both the degradation path were explored to prove the

employment of CHI-MA scaffold in tissue engineering. Two solutions of PBS and PBS plus lysozyme were prepared to test the hydrolytic and enzymatic degradation, respectively. To appreciate the change in geometry the CHI-MA hydrogels were shaped in a crux-like form changing the media after 14 days of gel immersion into the media. In Figure 3.7 A, the gravimetric plot of the two hydrogel batches after freeze-drying are reported. As expected, the weight loss was more pronounced into the enzymatic batch, leading to a final net weight of 43% after 21 days compared with a 92% for the hydrolytic degraded hydrogels. Moreover, the degradation path led to a uniform weight loss maintaining the crux-like structure in both cases until 7 days. The results were further demonstrated by the morphological characterization of the degraded scaffolds (Figure 3.7 B). While no differences were noted in the PBS immersed hydrogels, the change into the pores dimension was evidenced from day 1 on the PBS+LIS solution, with pores enlargements from day 1 to 7, the emersion of smaller pores from day 14 and a complete destruction of the structure at day 21. This degradation pathway can explain the retard in lysozyme penetration into smaller pores and the architecture maintaining until 7 days [221].

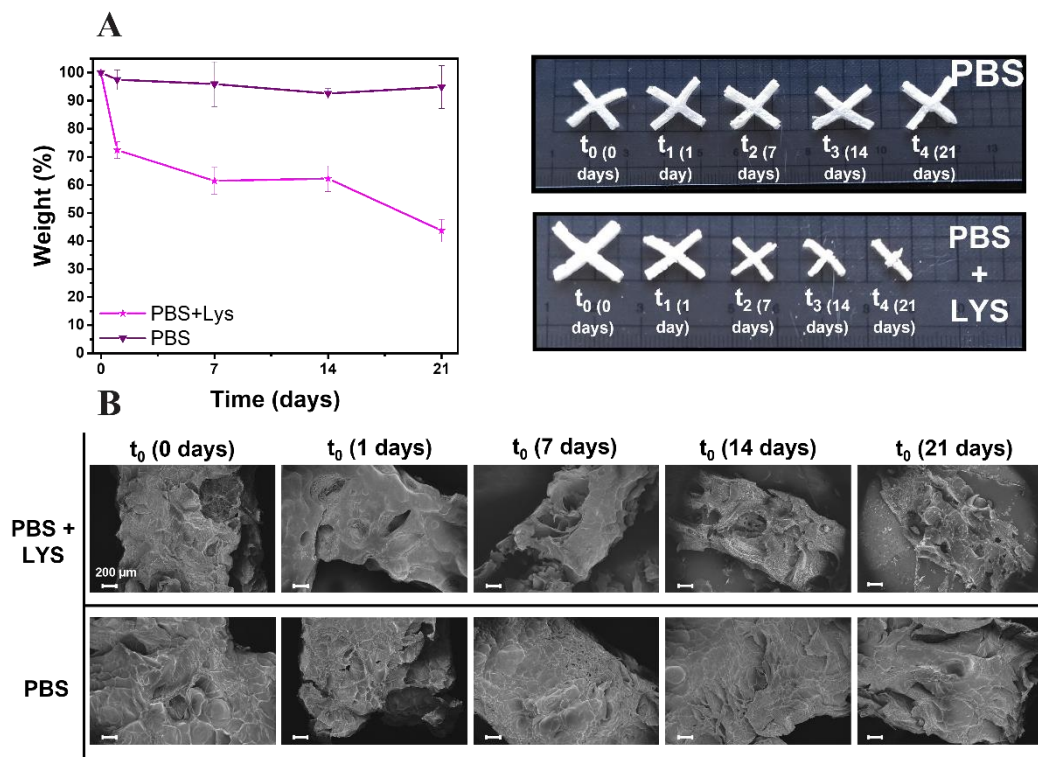


Figure 3.7: Degradation study through gravimetric curves (A) and morphological characterization (B).



## Preliminary investigation of the photocurable formulation for DLP 3D-printing

Once defined the right photoactive starting material (CHI-MA DS 24) and assessed the scaffold degradation path, we moved toward the optimization of a successfully DLP 3D printable chitosan-based formulation. Two kinds of formulations were used in the 3D printing process, one based entirely on methacrylated chitosan and one exploiting the addition of small quantities of crosslinkers in order to appreciate the differences in terms of print fidelity and resolution.

To ensure the printability of the formulation, the first step of characterization was performed using a well-known crosslinker employed in tissue engineering, PEGDA Mw 700 [153,223]. Moreover, a compromise between the amount of PEGDA over the CHI-MA content was required. Considering the similarity of CHI-MA with the extracellular matrix (ECM) glycosaminoglycans [224] and the application on tissue engineering of the final printed object, the lowest possible amount of PEGDA is suggested. The different formulations investigated are reported on Table 3. 3. The photo-initiator concentration was chosen based on similar work [189,225].

For each formulation the photo-rheology (to evaluate the reactivity of these formulation and the mechanical properties before and after the cross-linking), the viscosity (to match coherent values for DLP technology and a clear shear thinning behaviour), the amplitude sweep (to have information on the mechanical properties of the hydrogels), the gel content and the swelling properties of the hydrogels were investigated.

*Table 3. 3: Different CHI-MA:PEGDA investigated formulations.*

Formulation	Solvent	CHI-MA (wt%)	Photo-initiator	CHI-MA:PEGDA ratio (w/w)
1	Water	2	$3 \cdot 10^{-4}$ M LAP	1:2
2	Water	2	$3 \cdot 10^{-4}$ M LAP	1:1
3	Water	2	$3 \cdot 10^{-4}$ M LAP	2:1
4	Water	2	$3 \cdot 10^{-4}$ M LAP	100% CHI-MA

In Figure 3.8 are reported the photo-rheology (A), the viscosity of the formulations (B) and the amplitude sweep of the formed hydrogels (C). In DLP 3D printers, the final geometry is created upside-down in a custom fashioned layer-by-layer manner; for this reason, the first layers need to have reasonable reactivities and storage modulus to support the entire structure while a low shear-thinning viscosity is always necessary to permit the flow of the formulation under the moving platform [164]. Three main information can be extrapolated from photo-rheology, namely: a) the induction time of the reaction (the time corresponding to the initial increase of the G' curve) b) the slope of the increasing curve (related to the kinetic of reaction of crosslinking) and c) the mechanical stability of the final cross-linked product (by the upper plateau value). All the

studied formulations share a delay of 20 s from the initial irradiation (60 s) with the maximum storage modulus reached by sample 1 (21,6 KPa) after 200 s. Moreover, not only a decreasing trend in  $G'$  is evident while lowering the amount of PEGDA but also a rate of polymerization lag. Nevertheless, samples 2 and 3 present interesting storage modulus of the upper plateau (13,4 and 11,1 KPa) and acceptable reactivities (plateau reached after 230 and 260 s from the irradiation). Sample 4, instead, express the lowest storage modulus (9,9 KPa), and the impossibility to reach a clear plateau. Especially this last characteristic, strongly linked to a low rate of polymerization, makes CHI-MA formulation unapplicable for DLP 3D-printing, as already seen on the previous Chapter. Confirming the results, all photo-rheology plots are in good agreement with previous work [40,187,191].

Similar and DLP suitable low viscosities with a shear-thinning behaviour were evidenced for all the formulations [226].

The photo-rheology resulting hydrogels were then subjected to amplitude sweep to test their mechanical properties and stability upon a strain ramp. No major differences were observed in the four hydrogels apart from a small variation into the yield point (the point where the hydrogel collapse and the storage modulus fall, on Table 3.4). In fact, sample 1 and 2 have lower yield points, suggesting a more brittle behaviour [227]. The reason can be found into a denser and more cured structure due to the higher content of PEGDA.

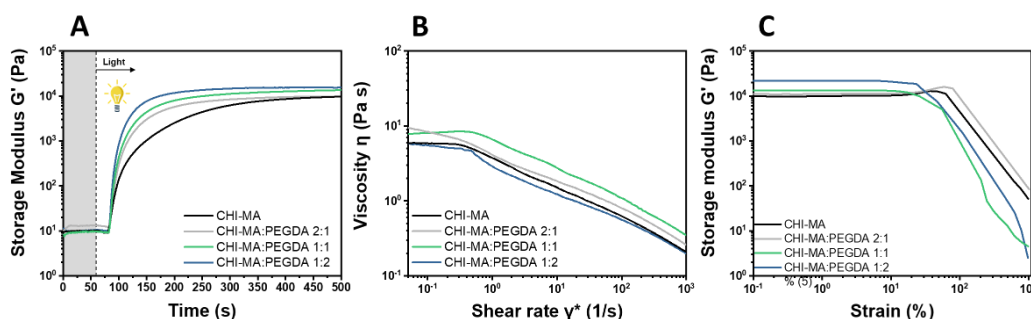


Figure 3.8: Photo-rheology (A) viscosity (B) and amplitude sweep (C) of the CHI-MA:PEGDA formulations.

The different formulations were casted into PDMS molds, irradiated for 5 minutes ( $50 \text{ mW/cm}^2$ ) to create cylindrical hydrogels ( $D = 5 \text{ mm}$ ,  $H = 3 \text{ mm}$ ) and let them dry overnight. Once dry the samples were weighted and soaked in DI water to evaluate the swelling capability and kinetics. On Figure 3.9 A are plotted the swelling kinetics of the different hydrogels while on Table 3.4 are expressed their swelling equilibrium and gel content. The swelling properties follow the PEGDA content of the different hydrogels. Indeed, the swelling equilibrium of the hydrogels increases from 151% of sample 1 to 186% of sample 4, probably due to a looser structure. At the same way, the time-to-plateau is almost equal for all the

samples (1 h) with the exclusion of CHI-MA (2 h). Considering the lower gel content of CHI-MA (75%) resulting in an emptier and more porous structure this behaviour is soon explained. Moreover, also gel contents follow the amount of PEGDA, suggesting again a denser and more crosslinked structure.

Table 3.4: Swelling equilibrium, gel content, storage modulus, yield point and crosslinking density of the CHI-MA:PEGDA hydrogels.

Sample	Swelling equilibrium (%)	Gel content (%)	Storage modulus G' (KPa)	Yield point (%)
1	151 ± 6	88 ± 4	21,6	13,9
2	154 ± 3	85 ± 1	13,4	17,5
3	167 ± 2	82 ± 2	11,1	79,1
4	186 ± 5	75 ± 1	9,9	62,5

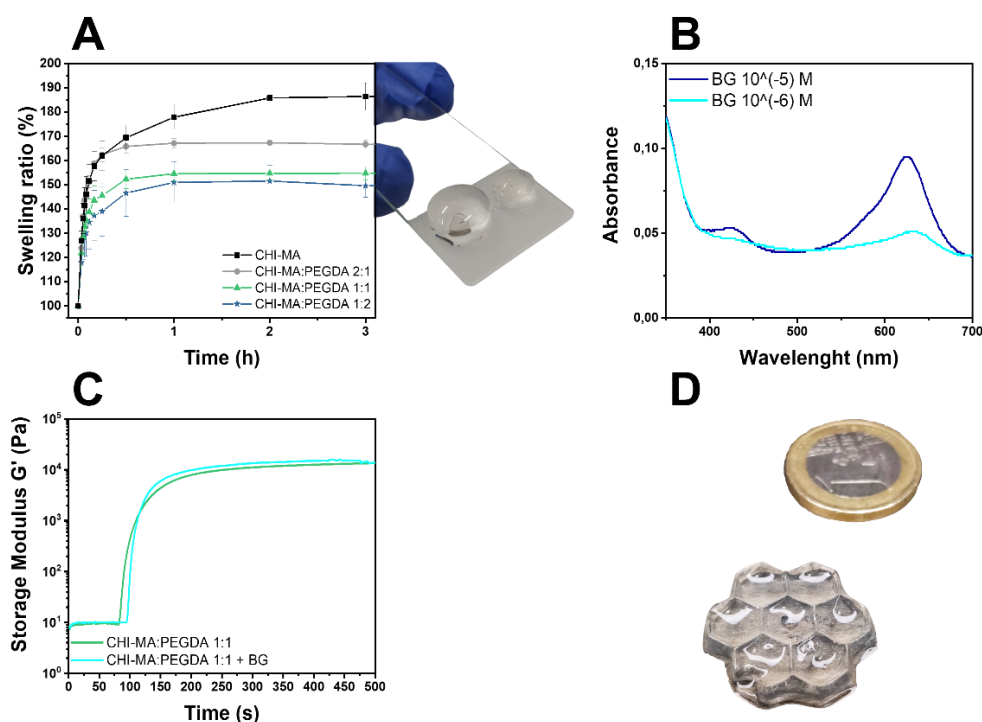


Figure 3.9: Swelling kinetics with a sample before and after swelling (A), absorption peaks of brilliant green (BG) at 440 and 640 nm [228,229] (B), photo-rheology of CHI-MA:PEGDA 1:1 and CHI-MA:PEGDA 1:1 with  $10^{-6}$  M of BG (C) and DLP 3D printed honeycomb structure (D).

The formulation printability was tested reproducing various CAD models using a VIS-Light DLP-3D printer Asiga PICO 2 (Asiga, Australia). Formulation 2 (CHI-MA-PEGDA 1:1, called CHI-PEG) was chosen as the best candidate because of different important characteristics, such as: a) proper induction time and rate of polymerization during photo-rheology, b) stable and acceptable mechanical properties both in photo-rheology and amplitude sweep, c) optimal swelling characteristics and d) good compromise between the amounts of CHI-MA and PEGDA. The first printing attempts without using any dye led to overcured structures, especially near the most complicated parts of the printed geometries. In these cases, the employment of coloured dyes at low concentrations avoids the light scattering in the vat and assure a reasonable resolution of the printed object [195,230–232]. For this reason, a greenish-blue water-soluble and visible light absorber dye (brilliant green, absorption peaks of brilliant green at 440 and 640 nm) was added to the formulation at a concentration ( $3 \cdot 10^{-6}$  M) able to mediate between over-polymerization and a massive dye absorption (absorption peak on Figure 3.9 B). The photo-rheology of this new formulation is reported on Figure 3.9 C, showing a similar trend in terms of rate of polymerization and final storage modulus. From the previous solution, only a 11 s delay in the induction time was evidenced, resolved during the printing process with just a little longer light exposure time. The printing parameters were optimized and reported on Table 3.5. Considering the high amount of water of the hydrogel, 96 wt%, the honeycomb printed geometry (Figure 3.9 D) presents a defined structure and stability. Despite this, more complicated architectures, such as hallow cubes, were impossible to print cause of a collapse and a detach of the structure from the building platform.

*Table 3.5: Printing parameters of the selected formulation.*

Formulation	BG concentration (M)	Light intensity (mW/cm <sup>2</sup> )	Layer thickness (μm)	Burn-in exposure time (s)	Layer exposure time (s)
CHI-PEG + BG	$3 \cdot 10^{-6}$	25	50	10	8

## **Preliminary investigation of the methacrylated quinizarin formulations**

Aiming to create a stiff and stable 3D printed hydrogel using the quinizarin-based colored dyes, a preliminary step of characterization of the two molecules (mono and di-methacrylated) is required. The molecules' structure and the <sup>1</sup>H-NMR spectra of the dyes are reported in Figure 3. 10. The protons of the methacrylic group are visible both in the mono (Q-1MAc at 6.46 and 5.87 ppm) and in the di-substituted quinizarin (Q-2MAc at 6.48 and 5.89 ppm). Additionally, the successful di-methacrylation of Q-2MAc is certified by the disappearance of

the hydroxylic group proton at 13.09 ppm, present in the Q-1MAc molecule but absent in Q-2MAc.

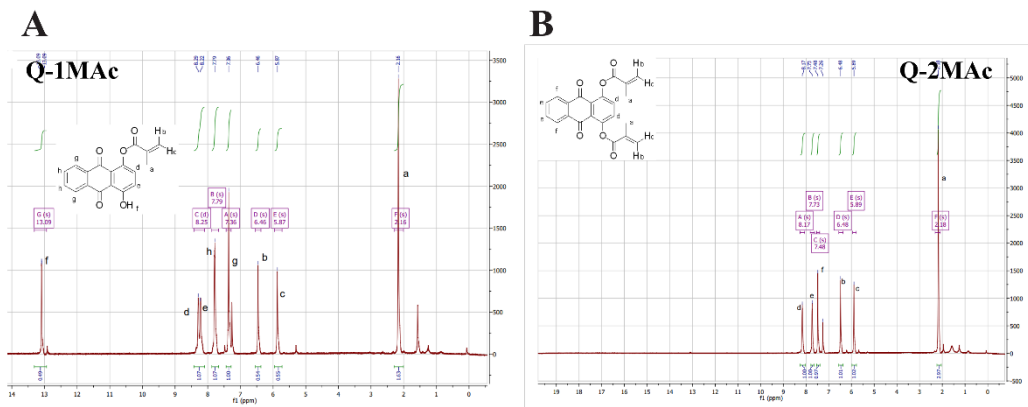


Figure 3. 10:  $^1\text{H-NMR}$  spectra of Q-1MAc (A) and Q-2MAc (B) in  $\text{CDCl}_3$ .

The EPR studies were conducted by irradiating the molecules in their maximum absorption region, to evaluate the possibility of Q-1MAc and Q-2MAc to generate carbon centered radicals. The LED@365 nm photoexcitation of Q-2MAc with DMPO under argon resulted in the formation of Q-2MAc-derived paramagnetic species. Upon irradiation of Q-2MAc/DMSO/Ar in the presence of DMPO spin trap, the generation of Q-2MAc-derived radical was again evidenced (Figure 3. 11 A), along with additional EPR signals demonstrating the generation of three spin-adducts: *i*) DMPO-adduct of carbon-centered radical ( $a_{\text{N}} = 1.450$  mT,  $a_{\text{H}^\beta} = 2.072$  mT;  $g = 2.0058$ ), *ii*) DMPO-adduct of acyl radical ( $a_{\text{N}} = 1.422$  mT,  $a_{\text{H}^\beta} = 1.637$  mT;  $g = 2.0058$ ), and *iii*) DMPO-adduct of oxygen-centered radical ( $a_{\text{N}} = 1.382$  mT,  $a_{\text{H}^\beta} = 1.164$  mT,  $a_{\text{H}^\gamma} = 0.075$  mT;  $g = 2.0059$ ) as shown in Figure 3. 11 B. The LED@400 nm irradiation of Q-1MAc in oxygen-free DMSO with DMPO spin adduct results in the formation of analogous three DMPO-adducts as found under analogous experimental conditions for derivative Q-2MAc (Figure 3. 11 A), along with the complex EPR signal of Q-1MAc-derived paramagnetic species representing superposition of Q-1MAc $^{\bullet-}$  with other Q-1MAc-derived paramagnetic species (Figure 3. 11 C and D).

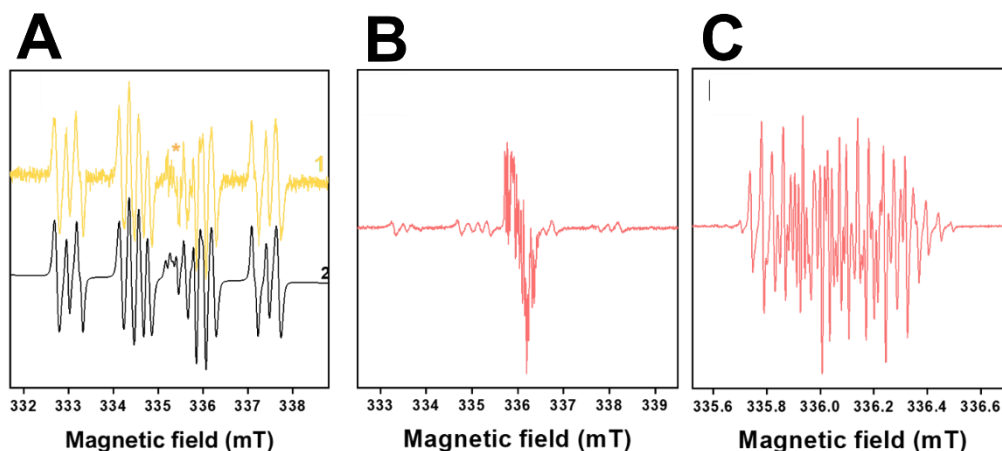


Figure 3. 11: The normalized experimental (yellow, 1) and simulated (black, 2) EPR spectra obtained during 450<sup>s</sup> in situ LED@365 nm exposure of Q-2MAc/DMSO with DMPO spin trap under argon. EPR spectrometer settings: microwave frequency, ~ 9.44 GHz; microwave power, 10.01 mW; center field, ~335.0 mT; sweep width, 7 mT; gain, 2.00\*10<sup>5</sup>; modulation amplitude, 0.05 mT or 0.025 mT; sweep time, 45 s; time constant, 10.24 ms; number of scans, 10. \* represents the Q-2MAc-derived radical species (B). The normalized experimental EPR spectra measured during in situ LED@400 nm irradiation of Q-1MAc/DMSO with DMPO spin trap under argon. Exposure: (C) 225 s; (D) 450 s. EPR spectrometer settings: microwave frequency, ~ 9.43 GHz; microwave power, 1.048 mW; center field, ~336.1 mT; sweep width, 7 mT or 1.2 mT; gain, 1.59\*10<sup>5</sup> or 1.00\*10<sup>4</sup>; modulation amplitude, 0.05 mT or 0.01 mT; sweep time, 45 or 90 s; time constant, 10.24 ms; number of scans, 5.

The UV-Vis spectra were collected to best assess the molecules absorption profiles, reported in Figure 3.12 A. Thanks to the electron donor effect of its hydroxylic group, Q-1MAc show the maximum absorption in the blue visible region (420 nm) while Q-2MAc, being completely substituted with the methacrylic group, present the maximum absorption around 335 nm but maintaining a moderate absorption until 500 nm [196].

The photo-active mechanism proposed for the quinizarin molecules implies an electron transfer process once irradiated, followed by a H-abstraction reaction when combined with tertiary amines and leading to the formation of aminoalkyl radical species (Norrish II type photo-initiators, see Chapter 2, 2.1.1. Radical photopolymerization) [196]. Depending on the degree of methacrylation, CHI-MA always keeps some unreacted primary amines and, even though those amines possess lower electron donor properties, they can likely be used as co-initiators in Norrish II reactions [46,233,234]. To test, compare the polymer crosslinking kinetic of Q-1MAc and Q-2MAc with the previous investigated CHI-PEG formulation and to assess their DLP printability, the two molecules were added into a solution 3:1 v/v of DI water:DMSO, at the same concentration chosen in the

preliminary formulation investigation for the LAP photo-initiator ( $3 \cdot 10^{-4}$  M). Once mixed homogeneously, the polysaccharide and the crosslinkers were added: 2 wt% of CHI-MA and 2 wt% of PEGDA 700, the previous CHI-PEG 3D printed formulation without the addition of BG. The photo-rheological measurements are reported in Figure 3.12 B.

The two formulations, called CHI-PEG Q-1MAc no LAP and CHI-PEG Q-2MAc no LAP (without the addition of any other photo-initiators), were tested. As visible in Figure 3.12 B, Q-1MAc and Q-2MAc actively work as photo-initiators forming hydrogels, even though demonstrating low reactivities not suitable for 3D-printing. In particular, Q-1MAc showed an induction time of 207 s while Q-2MAc reported 312 s for the same property. However around 500 s, the mechanical properties of the Q-2MAc hydrogel overcome the Q-1MAc, maintaining the same trend until the end of the test ( $\approx$  1h of irradiation). This behavior is not surprising because Q-2MAc, being di-methacrylated and acting as a cross-linker, compact the structure increasing the cross-linking density. On contrary, its lower light absorption in the UV spectra explain the increased induction time compared to Q-1MAc.

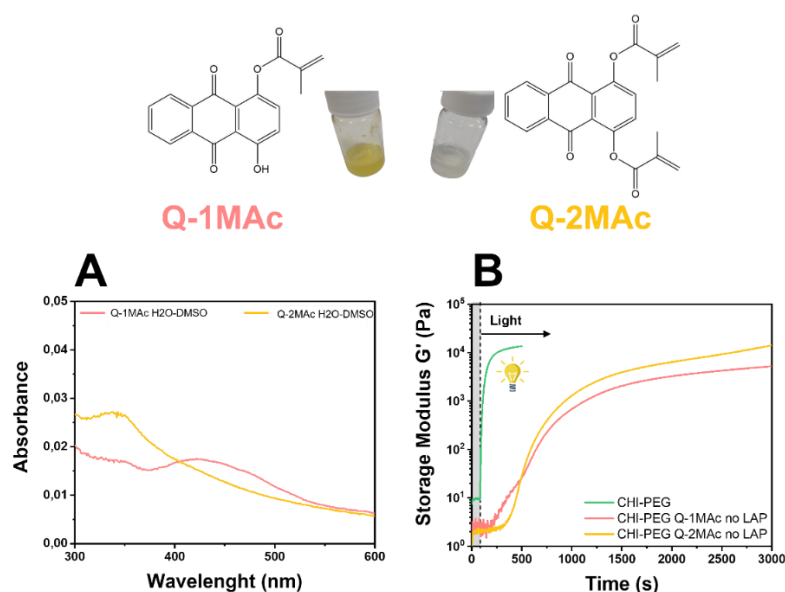


Figure 3.12: UV-Vis spectra of mono-methacrylated quinizarin (Q-1MAc, pink), di-methacrylated quinizarin (Q-2MAc, yellow) and structure of the methacrylated quinizarin dyes Q-1MAc (left) and Q-2MAc (Right) and the appearance of their solution in DI water:DMSO 3:1 v/v (A). In Figure B, the photo-rheological measurements of CHI-PEG Q-1MAc no LAP and CHI-PEG Q-2MAc no LAP compared with the CHI-PEG formulation using LAP photo-initiator at the same concentration of the dyes.

In conclusion, while the photo-activity of the quinizarin-based molecules was proven, their low reactivity doesn't allow any usage of the dyes as single photo-

initiator. However, the combination with other photo-initiators (such as LAP, a Norrish I type photo-initiator, see Chapter 2, 2.1.1. Radical photopolymerization) could be useful to increase even further the system reactivity while the incorporation of the methacrylated molecules into the polymer networks would enhance the hydrogel stiffness without releasing any cytotoxic substances, eventually making possible the 3D printing of the neat methacrylated chitosan.

## Formulations preparation and hydrogel characterization

As anticipated, two types of formulations were developed for each methacrylated quinizarin molecule: one based on the previous studied CHI-PEG formulation (without the addition of BG) and one of neat methacrylated chitosan. All the enounced formulations are reported in Table 3. 6, where in each case the viscosity, photo-rheology and amplitude sweep were evaluated.

Table 3. 6: *Quinizarin-based Q-1MAc and Q-2MAc loaded formulation in a solution of DI water-DMSO (3:1, v/v).*

	CHI-MA (wt%)	PEGDA (wt%)	LAP (mol/L)	Dye (mol/L)
CHI	2	--	$3 \cdot 10^{-4}$	--
CHI-PEG	2	2	$3 \cdot 10^{-4}$	--
CHI Q-1MAc	2	--	$3 \cdot 10^{-4}$	$3 \cdot 10^{-4}$
CHI-PEG Q-1MAc	2	2	$3 \cdot 10^{-4}$	$3 \cdot 10^{-4}$
CHI Q-2MAc	2	--	$3 \cdot 10^{-4}$	$3 \cdot 10^{-4}$
CHI-PEG Q-2MAc	2	2	$3 \cdot 10^{-4}$	$3 \cdot 10^{-4}$

In all cases no major differences in the formulation viscosity were evidenced, with defined and clear shear thinning behavior (Figure 3.13 A).

Figure 3.13 B and D report the photo-rheology plots of Q-1MAc and Q-2MAc solutions, respectively (compared with CHI and CHI-PEG formulations). In both cases, the crosslinking reaction starts immediately suggesting a coordinated action of the two photo-active molecules. Moreover, the sharper quinizarin-based molecules slope of the curves suggest a speed up of the whole reaction. The time-to-plateau of the different hydrogels (from the first light irradiation at 60 s) is 185 s and 193 s for CHI Q-1MAc and CHI Q-2MAc while 94 s and 108 s for samples CHI-PEG Q-1MAc and CHI-PEG Q-2MAc, confirming both an increased reactiveness of the hydrogels as well as their stability. PEG or CHI can likely act as H-donor molecule, as previously demonstrated with Eosin-PEG formulations [235]. Since Quinizarin derivatives can act as versatile photo-initiators or photosensitizers as previously remarked by the EPR results (Figure 3. 11), the combination of these phenomena can describe the reactivity increase of the quinizarin-based formulations. The mechanical properties, including the



hydrogels stability and their possibility to withstand over low solicitations or strains were measured by amplitude sweep and compression tests. The storage modulus and yields point in the amplitude sweep measurements (Figure 3.13 C and E, values reported on Table 3.7) indicate the mechanical stability of these gels at relatively high % strain compared to the corresponding CHI and CHI-PEG hydrogels, maintaining higher gel flexibility and  $G'$  modulus.

Table 3.7: photo-rheology induction time and time-to-plateau, amplitude sweep  $G'$  storage modulus and yield points, compressive  $E'$  storage modulus and swelling equilibrium of the proposed formulations.

	Induction time (s)	Time-to-plateau (s)	Storage modulus $G'$ (KPa)	Yield point (%)	Elastic modulus $E'$ (KPa)	Swelling Equilibrium (%)
CHI	+ 20 s	none	9,9	62,5	26 ± 4	186 ± 5
CHI Q-1MAc	0	185	24,1	32,1	47 ± 2	165 ± 2
CHI Q-2MAc	0	193	17,8	48,2	39 ± 2	175 ± 1
CHI-PEG	+ 20 s	170	13,4	17,5	37 ± 1	154 ± 3
CHI-PEG Q-1MAc	0	94	25,2	59,4	49 ± 5	131 ± 2
CHI-PEG Q-2MAc	0	108	17,9	73,5	44 ± 4	135 ± 7

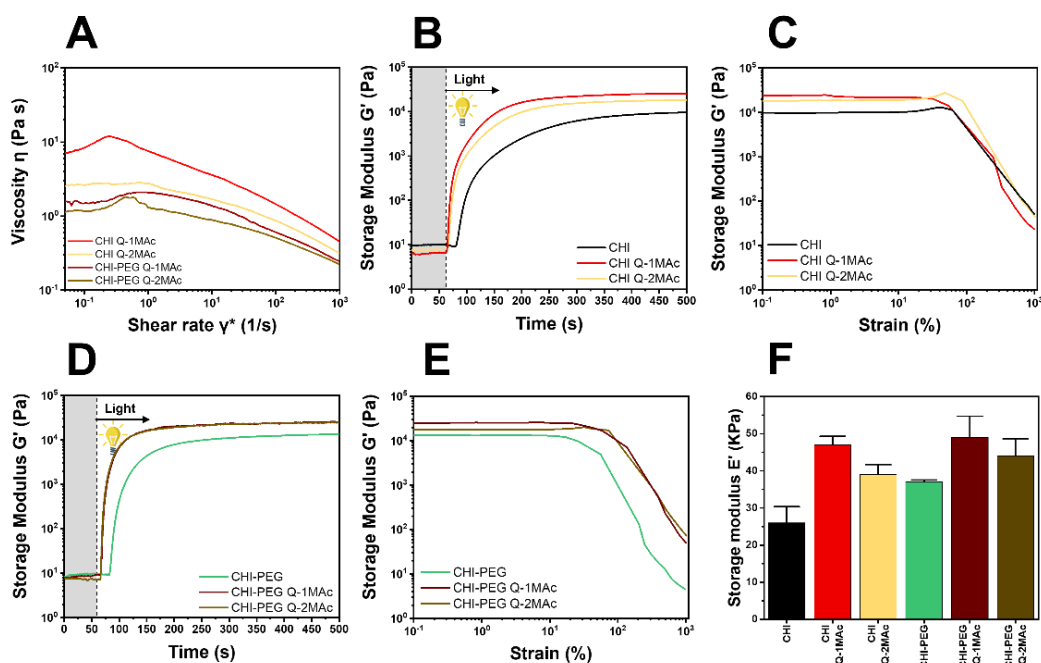


Figure 3.13: viscosity (A), photo-rheology and amplitude sweep of the CHI, CHI Q-1MAc and Q-2MAc formulations (B and C respectively), photo-rheology and amplitude sweep of the CHI-PEG, CHI-PEG Q-1MAc and CHI-PEG Q-2MAc formulations (D and E respectively) and compression  $E'$  storage modulus of all formulations.

Similarly, the compressive  $E'$  storage modulus obtained through cylindrical photocured hydrogels ( $D = 5$  mm,  $H = 3$  mm) and considering the first 10% of deformation of the stress-strain curve (Figure 3.13 F, values reported on Table 3.7) indicates increased mechanical properties of the quinizarin-based hydrogels, once compared with CHI and CHI-PEG gels. Moreover, the quinizarin loaded hydrogels possess stiffnesses comparable with intestines or tendons [236].

The swelling kinetic was evaluated thanks to cylindrical hydrogels ( $D = 5$  mm,  $H = 3$  mm) obtained casting the formulations into PDMS molds while irradiating 5 minutes ( $50$  mW/cm<sup>2</sup>). Once let the hydrogels dry overnight, the samples were firstly weighted and then soaked in DI water to test the swelling capability and kinetic, removing the samples and weighting them at every time point. Figure 3.14 A and B show the swelling kinetics of the quinizarin-based hydrogel (compared with the CHI and CHI-PEG hydrogels) while on Table 3.7 the swelling equilibriums are expressed. The time to swelling equilibrium didn't display any major differences (CHI based hydrogels  $\approx 2$  h and 1 h for the CHI-PEG based gels). However, decreased swelling equilibriums resulted once the methacrylated quinizarin compounds were added. This lower swelling capability may be justified firstly with an increased crosslinking density (as demonstrated by the higher  $G'$  and  $E'$  modulus) and secondly with the quinizarin low water affinity.

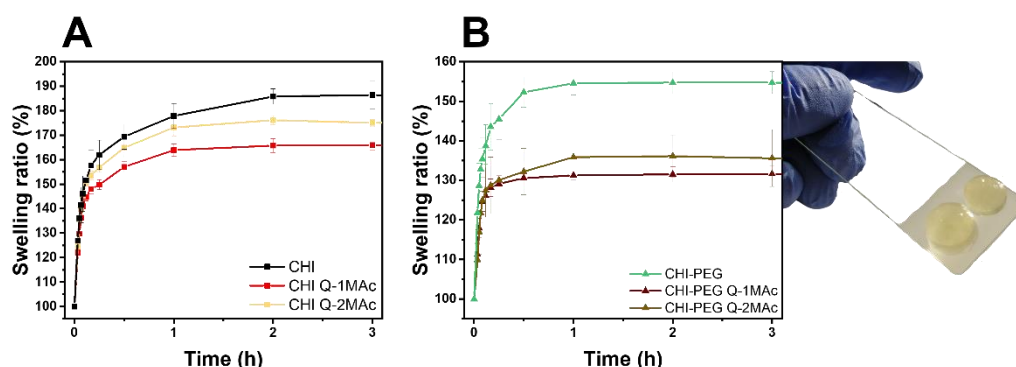


Figure 3.14: Swelling kinetic of the CHI, CHI Q-1MAc, CHI Q-2MAc, CHI-PEG, CHI-PEG Q-1MAc and CHI-PEG Q-2MAc hydrogels. The example sample before and after swelling is relative to CHI-PEG Q-2MAc.

### 3D-printing of the quinizarin-based formulations

The Quinizarin formulation printability was performed with the same equipment and conditions of the CHI-PEG solutions. Herein, all formulations were tested while three different geometries with increasing complexity were selected (i.e., honeycomb, hallow cube and light fountain). The no suspended structure 2.5 D honeycomb was chosen to set the minimum criteria in order to

define a formulation DLP printable [237], the hollow cube to certify the structure stability as much as the angles shape fidelity and in the end, the fountain light to test the ink's complex and interconnected internal hollow geometries creation.

The optimized printing parameters are reported on Table 3.8. The decreased printing times, compared with the CHI-PEG formulation are expressed, evidencing and supporting the photo-rheology results. In Figure 3.15, the printing attempts are expressed on a Table depending on the geometry complexity and object resolution. As predicted, the CHI-PEG solutions composed by a 96 wt% of water, resulted into more detailed geometries with exceptionally shaped angles and dimensions. Incredibly, the CHI-based formulations (CHI Q-1MAc or CHI Q-2MAc, 98 wt% of water) showed good-shaped and concrete structures with defined angles especially for the CHI Q-1MAc hydrogel. As pointed out before, the visible light absorption of Q-1MAc and its faster induction time explain the superior resolution of the corresponding 3D-printed hydrogels. This behaviour is also responsible of the increased mechanical properties of the mono-methacrylated biomolecule suggesting Q-1MAc as the best candidate for visible light 3D printing.

*Table 3.8: Printing parameters of the quinizarin-based formulation tested (all formulation contain LAP photo-initiator).*

	Light intensity (mW/cm <sup>2</sup> )	Layer thickness ( $\mu$ m)	Burn-in exposure time (s)	Layer exposure time (s)
CHI-PEG	25	50	10	8
CHI Q-1MAc	25	50	6	2
CHI-PEG Q-1MAc	25	50	6	2
CHI Q-2MAc	25	50	6	2
CHI-PEG Q-2MAc	25	50	6	2

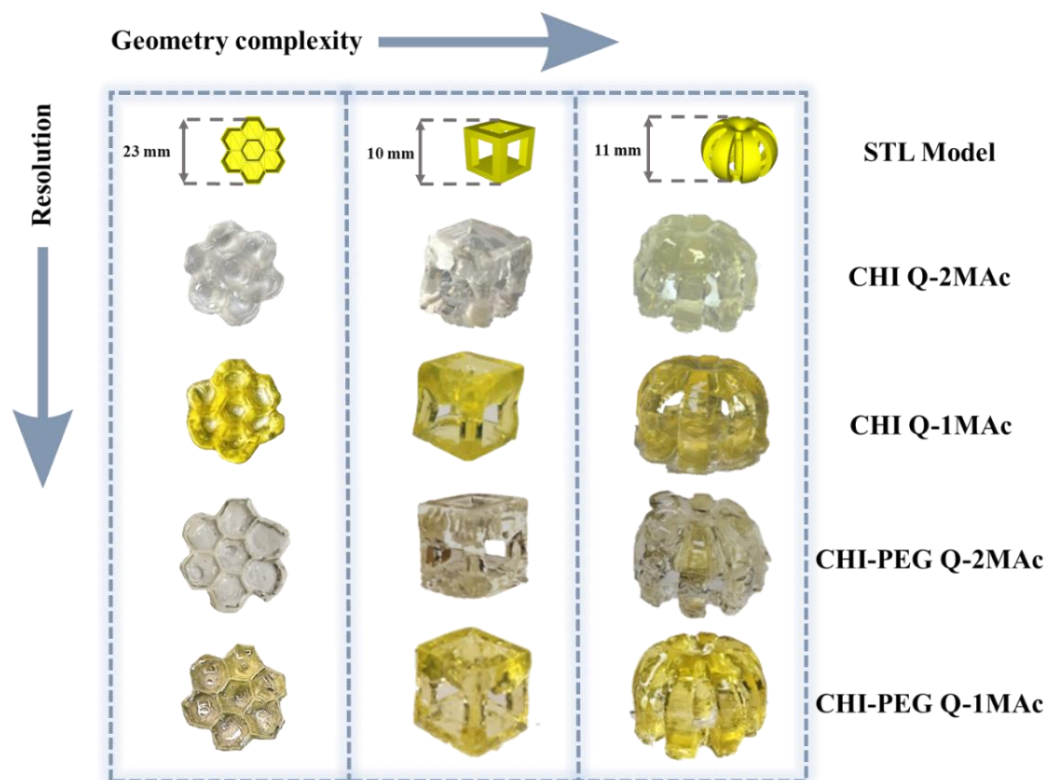


Figure 3.15: Hydrogels DLP printed with the quinizarin-based formulations. The printed objects are reported in order of resolution (top to bottom) and geometry complexity (left to right).

### Cell viability, proliferation and migration on methacrylated chitosan for 3D in-vitro model for cancerous tissues.

Firstly, the neat methacrylated chitosan (without the addition of any crosslinker or quinizarin based molecules) was biologically characterized to be used as 3D in-vitro model for cancerous tissues.

Even though chitosan is well described as a low toxic and bioactive biopolymer, different physio-chemical and biological properties (degree of deacetylation, molecular weight, porosity, adhesive surface, etc.) or modifications of the initial polysaccharide (DS%) must be deeply analyzed for applications in tissue engineering [198,238]. Firstly, cell viability was assessed through the contact between the chitosan conditioned medium and two different tumour cell lines (H1299 and A549 GFP-transduced) for 24 and 96 h, comparing the results with cell growth in normal culture conditions. As visible in Figure 3.16 A and B, the chitosan medium doesn't affect cell viability even at prolonged contact times,

suggesting no release of toxic substances and a bioactive behaviour of the scaffold by the high values of fluorescence.

Multiple hydrogels shaped to be inserted into a 48-well plate were seeded with cells on the top of the gels thanks to an upper basin created for the purpose. Cell growth and migration were followed for 4 to 7 days to appreciate any kind of proliferation or migration into the hydrogel inner structure (Figure 3.16 C). Fluorescence analysis demonstrated good attachment of both cell lines on the hydrogel surface and their proliferation. However, an effective migration until the hydrogel bottom was detected just for the H1299 cell line, compared with the movement of the A549 GFP limited to the central part of the gel. Although more investigation may be needed, this difference into the rate of migration could be ascribable to the nature of the former cell line. In fact, while A549 GFP cells derive from a lung adenocarcinoma, H1299 are isolated from a metastatic lymphatic site: the latter cells are well known for their rapid migration and invasion activities [239].

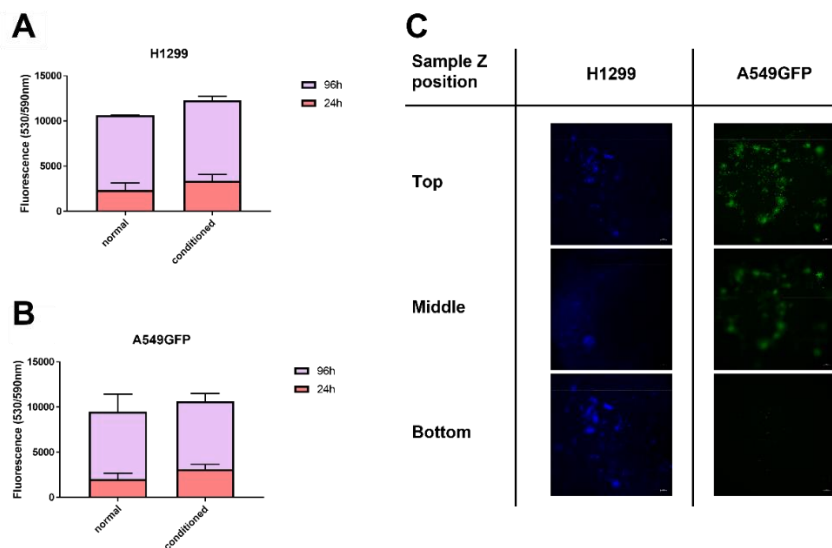


Figure 3.16: Cell proliferation of H1299 (A) and A549GFP (B) cell lines grown in normal and chitosan conditioned medium for 24 and 96 h. Cell migration of H1299 (DAPI stained) and A549GFP cell lines on chitosan scaffold after 7 days. The scale bar denotes 100  $\mu$ m for all images.

## Cell viability and proliferation assays on quinizarin-loaded hydrogels for soft tissue substitutes scaffolds

To recreate scaffold working as soft tissue substitutes, cells (Autofluorescent C166-GFP endothelial) were seeded on the top surface of the different quinizarin-

loaded hydrogels to assess their cytocompatibility. Figure 3.17 A reports the fluorescence micrographs after 72 h of contact. All hydrogels allowed the attachment and proliferation of the endothelial cells, reaching confluence in all samples after a growth of three days. To quantify cell viability and proliferation, metabolic activity (Alamar Blue) and DNA content (Fluoreporter) assays were performed (Figure 3.17 B and C, respectively). The higher values in terms of viability and growth were achieved with the CHI Q-2MAc hydrogel. The reason can be searched into a better incorporation of the Q-2MAc inside of the chitosan network, due to both its methacrylated extremities. However, the trend extracted from the data was very similar for all the samples in both tests, with no statistically significant differences among the different hydrogels. Indeed, it can be extracted that all 3D-printed hydrogels allowed attachment, growth, and proliferation of mammalian cells over their surface with no significant difference in term of biocompatibility once compared with CHI hydrogels and enabling a possible use in biomedical applications.

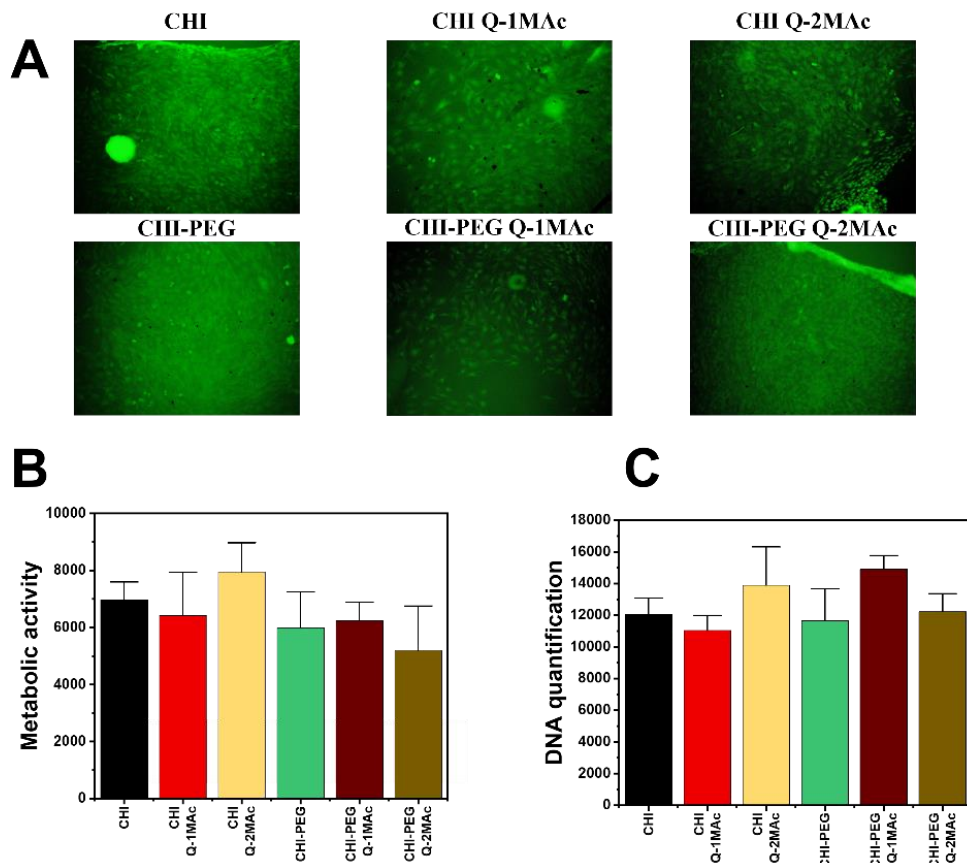


Figure 3.17: Micrographs of C166-GFP murine endothelial cells on the surface of the different hydrogels after 72 h of incubation (A). Metabolic activity values of the C166 cell cultures for the different hydrogels after 72 h of incubation (B). DNA quantitation values of C166 cell cultures for the different hydrogels after 72 h of incubation (C).

### 3.5. Conclusions

The cheap and easy production of methacrylated chitosan using the MAOS technology is here reported, enabling a drastic reduction of the reaction times (few minutes instead of hours) and energy consumption. Moreover, the mild synthesis conditions and the reduced usage of reagents assess this method of functionalization as green and sustainable. The functionalization success was validated by FT-IR and <sup>1</sup>H-NMR varying a wide range of microwave parameters, obtaining a methacrylated chitosan with degree of substitution in line with literature.

Tuning the degree of substitution, it was possible to obtain a wide range of hydrogel with increasing mechanical properties and stiffnesses comparable with human tissues such as heart, lungs, or muscles. Moreover, the direct extrusion 3D printing of the formulation was demonstrated. The porous structure and swelling response of the hydrogels enabled both to assess the hydrolytic/enzymatic degradation of the gels as much as their cell viability, proliferation, and migration with optimal biocompatibility.

3D-printed complex geometries of methacrylated chitosan were successfully obtained adding to the initial formulations two newly synthesized mono- and di-methacrylated quinizarin dyes, granting a detailed printability of both solo-methacrylated chitosan geometries (98wt% of water, not possible in absence of the quinizarin molecules) and the superior and defined printability of the poly(ethylene glycol) charged methacrylated chitosan formulations (96wt% of water).

Moreover, the different functionalities of the quinizarin-derivative as photosensitizer and dye were demonstrated. The resulted structures possess suitable mechanical properties, mechanical stability and swelling capability/kinetics to be employed as soft scaffold for tissue engineering. The exhibited reactivity under visible light and null cytotoxicity allows cell proliferation, as distinguishable by the metabolic activity and DNA quantification of the cells seeded hydrogels.

In conclusion, we demonstrated that the rapid, cheap, and mild microwave functionalization approach toward chitosan is a reliable and promising alternative to traditional thermal processing while the smart employment of dyes for different purposes (as light-scattering preventers and also as useful and participating agents in the 3D-printing of scaffolds) enhances the possibility to create engineered tissues of different materials perfectly designed and tailored on the patient's tissue defect requirements.

# Chapter 4

## Alginate hydrogels

### 4.1. Introduction

On Chapter 3 the employment of methacrylated Chitosan was extensively discussed for the creation of photocurable hydrogels in tissue engineering applications. However, even though acrylates and methacrylates functionalized natural polymers are nowadays between the most used matrix to create hydrogels suitable for biomedical purposes, a certain degree of cytotoxicity of (meth)acrylates at medium-high concentrations is commonly known [240,241]. As pointed out on Chapter 2 (2.1.1. Radical photopolymerization), there are two main kind of propagation steps in radical photopolymerization, called chain-growth (CGP) and step-growth photopolymerization (SGP) [157,158]. While reactions involving CGP propagation are among the most used in hydrogel formation because of their relatively easy synthesis processes and reactivity (methacrylates groups fall in the category) [159], SGP propagation reactions are experiencing nowadays an increasing interest. In fact, the main advantages of these reactions are the lower stress accumulation once the 3D hydrogel is formed and the usual lower cytotoxicity of the reacting moieties (due to a lower degree of radical propagation) [242,243]. “Click-chemistry” reactions are universally recognized as rapid, regiospecific and versatile systems, with high yields under mild conditions and enhanced biocompatibility of its reactive moieties [76,85,244]. Within this class, thiol-ene and thiol-yne reactions accomplish various features such as spatio-temporality, orthogonality and selectivity, giving rise to more homogeneous networks than (meth)acrylates.

Even though thiol-yne stoichiometric reaction between two thiols and one alkyne (see Chapter 2, 2.1.1. Radical photopolymerization) was extensively



discussed in literature, just few examples were reported to create hydrogels, especially for tissue engineering applications [161,245,246].

Sodium alginate, thanks to its easily modification of the carboxylic groups, was selected as matrix for the addition of the alkyne moieties [242,247]. As far as we know, no alginate hydrogels obtained by thiol-yne reactions were reported in literature making this study as the first investigation on the topic [248]. Once functionalized, two thiolated crosslinkers of different molecular length were chosen to create the polymer network, tuning the mechanical properties (Figure 4.1). At the end, a deep discussion about the formulation reactivity and the hydrogel swelling and morphological characterization was treated, demonstrating the usage of the material as surgical filler or patch.

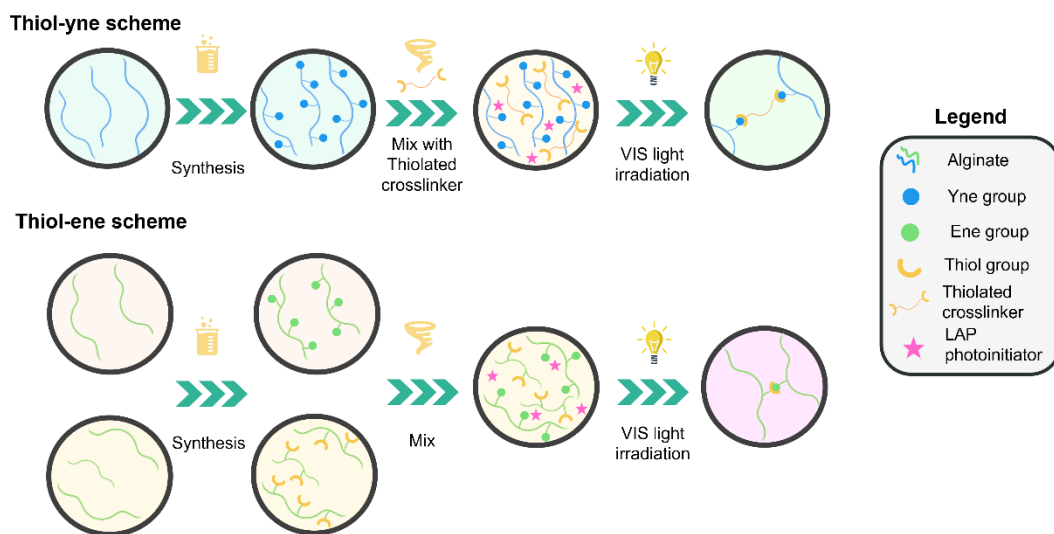


Figure 4.1: Scheme and crosslinking approaches of Thiol-Yne and Thiol-Ene reactions on Sodium Alginate.

However, the employment of small molecules able to interact with the cell walls (e.g., thiolated crosslinkers) can lead to various form of cell necrosis or apoptosis [249–251]. For this reason, a challenging approach in tissue engineering is to explore different crosslinking strategies, such as a complete modification of the matrix toward the incorporation of all the functional groups needed.

Again sodium alginate is selected as matrix to create soft hydrogels, thanks to its easy oxidation or modification of the carboxylic moieties [242,247]. Unlike thiol-yne hydrogels, the polysaccharide batches were modified separately adding both ene and thiol reactive functional groups to the alginate backbone, at different degree of substitution to achieve the synthesis of hydrogels with thiol-ene reactions, as schematized in Figure 4.1. Two different synthesis routes were explored to incorporate thiols into the polymer backbone; the first passing through a three-steps reaction to first oxidate alginate, followed by the creation of imide bond and a post-reductive amination on the previously formed aldehydes, while

the second exploiting the alginate carboxylic acids using the well-known carbodiimide chemistry [252,253]. Instead, the ene modification was performed through the addition of norbornene methylamine with carbodiimide chemistry, because of its increased reactivity [242].

Afterwards, for the first time an alginate-solo hydrogel was created via thiol-ene reaction without the addition of external crosslinkers. The robust and stiff hydrogel was created mixing the two different synthesis batches to meet the necessary soft tissue properties of other similar hydrogels, testing its mechanical, rheological and swelling behavior. At the end, cells adhesion and proliferation were tested by metabolic activity and DNA quantification, ensuring the enhanced biocompatibility of the gels, perfectly suitable for scaffolds in tissue engineering applications. This work was performed during the last period of the PhD program, so further investigations are needed before publication (i.e., corroboration of the obtained results on hydrogel characterization and 3D printing).

## 4.2. Materials and procedures

### Materials

Alginic acid sodium alginate from brown algae (SA, low viscosity), Propargylamine (PA, 98%), Cysteamine hydrochloride (CSA,  $\geq 98\%$ ), L-Cysteine (CYS, 97%), Sodium Periodate (SP, ACS reagent,  $\geq 99.8\%$ ), sodium borohydride (powder,  $\geq 98\%$ ), N-(3-Dimethylaminopropyl)-N'-ethylcarbodiimide hydrochloride (EDC,  $\geq 98\%$ ), N-Hydroxysuccinimide (NHS), 1,4-Dithiothreitol (DTT), Poly(ethylene glycol) dithiol (PEG-SH, average Mn 1000), lithium phenyl-2,4,6-trimethylbenzoylphosphinate (LAP,  $\geq 95\%$ ), Hydroxylamine hydrochloride (HH, ACS reagent, 98.0%), Methyl orange (MO, for microscopy), sodium phosphate monobasic (reagentplus,  $\geq 99.0\%$ ), sodium phosphate dibasic (reagentplus,  $\geq 99.0\%$ ), Ethylenediaminetetraacetic acid (EDTA, BioUltra, anhydrous,  $\geq 99\%$ ) 5,5'-Dithiobis(2-nitrobenzoic acid) (DTNB or Ellman reagent, suitable for determination of sulfhydryl groups,  $\geq 98\%$ ), and hydrochloric acid solution (37%) were all purchased from Sigma-Aldrich and used as received without further purification. Sodium hydroxide pellets were purchased from Panreac, pre-wetted dialysis membranes (MWCO 3500 Da Spectra/Por6) from Spectrum Laboratories and 5-Norbornene-2-methylamine (NOR, mixture of isomers) from TCI Europe N.V.

### Synthesis of alginate-yne (SA-PA)

First, Sodium Alginate was solubilized at a concentration of 1.5 wt% in DI water into a round bottom flask, while stirring. Once the solution was homogeneous, HCl droplets were slowly added to the flask until reaching a pH=4. In a different vial, a 1:1 molar ratio between EDC and NHS was prepared and

added onto the alginate solution. The pH of the solution was then adjusted at a value of 5. After 2 h of stirring at RT the pH was increased until 8.5 by dropping the corresponding amount of a 0.5M NaOH solution and then PA was directly added into the flask. The reaction was let proceed 16h at RT in the darkness. Following this procedure, the synthesis was performed varying the molar ratio between reactants as SA/EDC/NHS/PA 1:1:1:1 (SA-PA-1) and 1:4:4:4 (SA-PA-4). The produced solution color, before dialysis of 4-6 days in DI water at RT in the dark with a 3,5 KDa membrane, turned pale-yellow after reaction.

## Synthesis of Thiolated Oxidized Alginate (TOSA)

As it will be clear in the results and discussion section, this synthetic route was not successful in terms of degree of functionalization of the final product (below). Anyway, the synthesis procedure and the discussion of the results will be reported for the sake of completeness. Alginate was oxidized at different molar ratios between the alginate polysaccharide unit SA and the sodium periodate SP (i.e., 5:1, 10:1, 20:1) for 3 h as shown in Table 4.1. Briefly, in a round bottom flask 0.5 g of Sodium Alginate were solubilized in 25 ml of distilled water (DI water) by stirring overnight at RT (2 wt%). At the same time, a solution of DI water and sodium periodate (0,285 M) was prepared. When both solutions were homogeneous an adequate aliquot of SP solution was taken (respect to the desired molar ratio with SA) and diluted with DI water to reach 25 mL of solution and lastly mixed with the alginate solution while stirring at room temperature in the darkness. The reactions were quenched after 30 min with a 10% v/v of ethylene glycol, while stirring. Once the reaction was quenched, the product (OSA, Oxidized Sodium alginate) was dialyzed 6 days with a 3.5 KDa membrane changing water every day and concentrated in vacuo at 37° C until complete evaporation of water.

*Table 4.1: Synthesis of OSA (oxidized sodium alginate). Degree of substitution obtained by potentiometric titration.*

Sample	Molar ratio (SA:NaIO <sub>4</sub> )	Degree of substitution (DS%)
OSA 1	5:1	33 ± 1
OSA 2	10:1	10 ± 1
OSA 3	20:1	4 ± 1

The synthesis was done as reported in literature using as starting material the most substituted oxidized alginate (OSA 1) [254]. Firstly, in a round bottom flask 0.5 g of freeze-dried OSA 1 was dissolved in 40 mL of 0.1 M phosphate buffer solution (PBS, 1.25 wt% at pH 7.4). At the same time, 1.2 g of cysteine (molar ratio of 1:4 between the alginate units and cysteine) were solubilized in 10 mL of water and added to the previous solution. Finally, the mixture was stirred at room

temperature for 28h in the darkness, under nitrogen atmosphere. Then, 0.4 g of sodium borohydride  $\text{NaBH}_4$  were added to the solution to reduce the imine bond formed between the alginate aldehydes and the cysteine amines (at a molar ratio 1:1 with the formed aldehydes of OSA 1, degree of substitution of 33%). The solution was stirred in the darkness for 15 h at room temperature under nitrogen atmosphere [255]. At the end, the product (TOSA, Thiolated Oxidized Sodium Alginate) was dialysed 4-6 days in the darkness at  $10^\circ\text{C}$  with a 3.5 KDa membrane under an acidic solution (pH 4 and 0,1 M of NaCl) to avoid thiol oxidation and disulphide bond creation [256,257].

### **Synthesis of Thiolated Alginate (SA-CYS and SA-CSA)**

In a round bottom flask, a 1,5 wt% sodium alginate (SA)/DI water solution was previously prepared. The pH was lowered with diluted HCl solution at a value of 4. In a vial, EDC and NHS were solubilized together in DI water, slowly added to the flask and the pH adjusted with diluted HCl until a value of 5. The solution was stirred 2 h at RT to allow the activation of the carboxylic acids of alginate. The pH was then adjusted at 4 if needed. The round-bottom flask was then capped to let an atmosphere of  $\text{N}_2$  bubbling directly into the solution for 15 min. CYS/CSA was solubilized in DI water and added to the solution with a syringe (while  $\text{N}_2$  was bubbling). The reaction was performed in the darkness under stirring and  $\text{N}_2$  atmosphere at RT for 24h to impede the self-reaction between thiol groups [255]. At the end of the reaction the color of the solution was equal of the one of the solubilized sodium alginate solo. The product (SA-CYS for alginate modified with CYS and SA-CSA for alginate modified with CSA) was then dialyzed 4-6 days in the darkness at  $10^\circ\text{C}$  with a 3,5 KDa membrane under an acidic solution (pH 4 and 0,1 M of NaCl) to avoid thiol oxidation and disulfide bond creation [256,257].

### **Synthesis of ene Alginate (SA-NOR)**

2 wt% SA was solubilized previously in 2-(*N*-morpholino)ethanesulfonic acid buffer (MES buffer, 0.1 M) into a Round bottom flask following a previously reported work with some modifications [242]. The pH was lowered with the HCl solution at a value of 4. In a vial, EDC and NHS/S-NHS were solubilized together in MES buffer. A solution of EDC (molar ratio of 1:2.4 between the SA carboxylic moieties and EDC) and S-NHS/NHS (molar ratio of 1:0.8 between the SA carboxylic moieties and S-NHS/NHS) was prepared in MES buffer and slowly added to the alginate solution. Then the pH was lowered again with the HCl solution until 5 and allowed to stir for 2h at RT. The pH was then adjusted at 8.5 with a 0.1 M solution of NaOH. After that, NOR was added and the reaction was stirred in the darkness, under  $\text{N}_2$  atmosphere, at RT for 24h. At the end of the reaction the color of the solution was yellowish. The reaction crude was dialysed 4-6 days in DI water at RT in the darkness with a 3,5 KDa membrane.

## Preparation of the Thiol-Yne photocurable hydrogel

The sodium alginate functionalized with yne moieties (SA-PA) was dissolved in DI water at a concentration of 5 wt%. Then, 2 phr (per hundred resins, respect to the SA-PA weight) of LAP photo-initiator were added to the solution and stirred in the darkness until complete dissolution. Two water-soluble crosslinkers, dithiothreitol (DTT) and poly-(ethylene glycol) dithiol (PEG-SH), were firstly solubilized in DI water and then added to the SA-PA 4 solution until complete homogenization. The formulation was poured into PDMS molds ( $\approx H = 3$  mm,  $D = 5$  mm) and irradiated for 5 min with polychromatic visible light from a Hg-Xe lamp (Hamamatsu LC8 Lightningcure™), provided with a cut-off filter for  $\lambda < 400$  nm and equipped with a light guide ( $50 \text{ mW/cm}^2$ ).

## Preparation of the Thiol-Ene photocurable hydrogel

Two solutions containing a 5 wt% of SA-NOR 2 and SA-CSA 2 were prepared separately in 10 mL of DI water and then mixed. Subsequently, 1 phr of LAP (40 mg) was added to the solution and let stirring until complete dissolution in the darkness. The formulation was then casted in molds of PDMS ( $\approx H = 3$  mm,  $D = 5$  mm), irradiated 5 min at  $50 \text{ mW/cm}^2$  with a visible light lamp (Hamamatsu LC8) furnished with a cut-off filter for  $\lambda < 400$  nm.

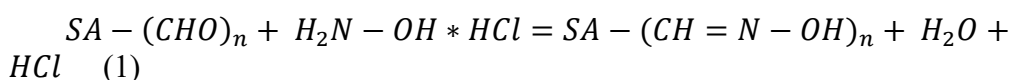
## 4.3. Characterization methods

### Quantification of the aldehyde content (potentiometric titration)

Briefly, 50 ml of a 0.25 M solution of hydroxylamine hydrochloride were prepared firstly adding 0.96 g of HH, under stirring, to 10 ml of DI water for 30 min. Once reached complete dissolution, 300  $\mu\text{L}$  of a methyl orange solution (1.5 mM) were added. Lastly the solution was topped with DI water to reach 50 ml and adjusted at pH 4. Then 20 mg of the OSA samples were dissolved in 5 ml of the titration solution where different amount of a NaOH solution (0,1 M) were added while measuring the pH.

The analytical reaction is as follows:

Reaction



Where  $SA - (CHO)_n$  is OSA and  $H_2N - OH * HCl$  is the hydroxylamine hydrochloride reagent.

Titration



Figure 4.2 A represents a typical plot of the pH variation over the volume of NaOH solution added in the OSA solution. The inflection points on this curve, this is, the maximum on the first derivative in Figure 4.2 B, reflects the necessary NaOH volume needed to neutralize the HCl in the solution, which allows the calculation of the aldehyde content into the alginate backbone. Moreover, the red-to-yellow methyl orange change of color at 4.3 pH, clearly evident in Figure 4.2 C, can give a first indication of the inflection point [258].

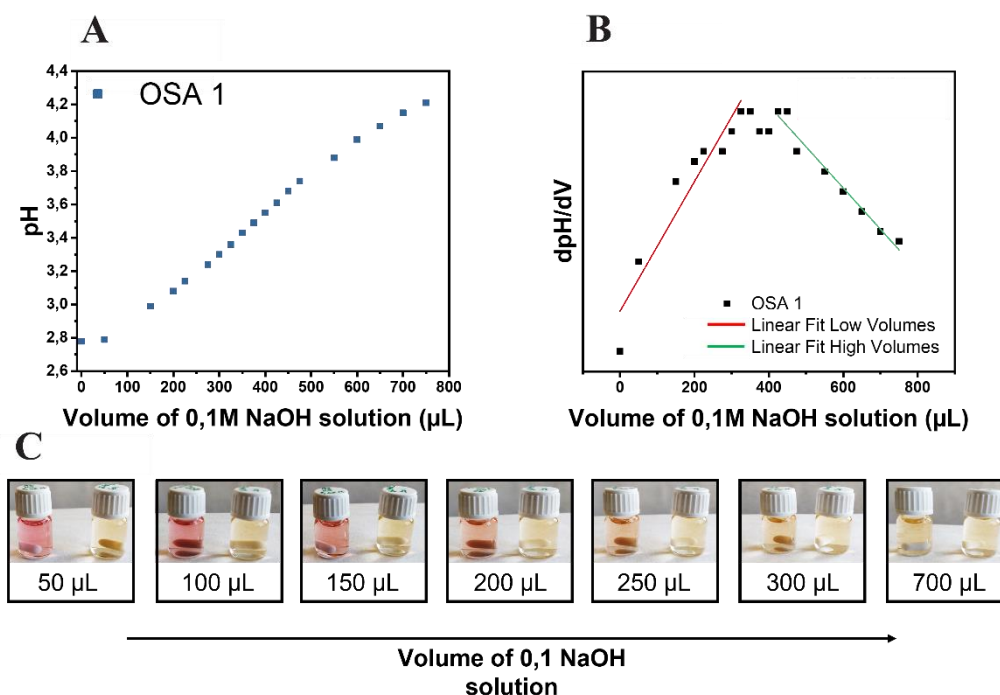


Figure 4.2: potentiometric titration of OSA 1 (A) and its first derivative (B). The image (C) shows the color change of methyl orange during NaOH titration, compared with a control sample.

At titration concluded, the aldehyde content was calculated by recording the amount of sodium hydrochloride consumed from following equation:

$$DO\% = \frac{\text{mol CHO}}{\text{mol SA}} * 100 = \frac{\text{mol NaOH into volume of solution at inflection point}}{\text{sample weight} / \text{molecular weight of SA repeating unit}} * 100 \quad (3)$$

### Quantification of the thiol content (Ellman reagent titration)

The content of free thiol groups was evaluated by the Ellman's reagent method. Firstly, a pH 8 phosphate buffer (0,1 M) was prepared using phosphate mono and dibasic salt and EDTA (0,001 M, to impede metal chelation of the thiol groups) [259]. In a different vial 4 mg of DTNB was solubilized manually in 1 ml

of the phosphate buffer. Then, in another vial, a solution of the desired thiolated alginate (TOSA, SA-CSA or SA-CYS) was prepared (around 10 mg/5mL of buffer). UV/Vis evaluation of samples was performed by triplicate measuring the intensity of the band at  $\lambda=412\text{nm}$  employing as blank and sample the following solutions:

- 1) Blank: 2,5 ml of buffer + 50  $\mu\text{L}$  of Ellman solution + 250  $\mu\text{L}$  of buffer
- 2) Sample: 2,5 ml of buffer + 50  $\mu\text{L}$  of Ellman solution + 250  $\mu\text{L}$  of TOSA/SA-CSA/SA-CYS solution

This procedure was performed in triplicate measuring the light absorption at 412 nm. The concentration of the thiol groups is obtained using the Lambert-Beer law:

$$A = \varepsilon \cdot l \cdot c \quad (4)$$

Where A is the difference in absorption between the blank and sample at 412 nm,  $\varepsilon$  is the molar extinction coefficient ( $1562 \text{ M}^{-1} \text{ cm}^{-1}$ . This value is obtained by reacting Ellman reagent solution with known concentrations of cysteine) and c is the pathlength (1 cm). Once obtained the concentration and the respective mol of thiol groups, the degree of substitution is obtained by:

$$DS\% = \left( \frac{\text{mol}_{SH}}{\text{mol}_{SA \text{ ring}}} \right) * 100 \quad (5)$$

### **Spectrometric analysis ( $^1\text{H-NMR}$ , $^{13}\text{C-NMR}$ , solid-state $^{13}\text{C-NMR}$ , ATR-FTIR and RAMAN spectroscopy)**

$^1\text{H-NMR}$  spectra was used to confirm the presence of aldehydes, yne and ene moieties on the alginate backbone, recorded on a Bruker Avance 400 MHz and on a Varian Mercury 400 MHz spectrometers with samples dissolved in  $\text{D}_2\text{O}$  at room temperature. Also  $^{13}\text{C-NMR}$  spectra was used to investigate the presence of yne moieties on a Varian Mercury 400 MHz spectrometer with samples dissolved in  $\text{D}_2\text{O}$  at RT.

The yne functionalization was further confirmed by ATR-FTIR spectra, recorded in a FTIR PerkinElmer Spectrum One spectrometer, and Raman spectroscopy, recorded in a Renishaw inVia Reflex system provided with a 515 nm state solid laser and a CCD detector. The Raman spectra were processed using Renishaw WIRE 3.4 software.

The solid-sate  $^{13}\text{C-NMR}$  measurements to confirm the presence of aldehydes groups were performed in a Bruker Avance 400 spectrometer equipped with an 89 mm wide bore, 9.4T superconducting magnet ( $^1\text{H}$  and  $^{13}\text{C}$  Larmor frequencies at 400.14 and 100.61 MHz respectively). The obtained spectra were in both cases evaluated by MestReNova software.

## Gel permeation chromatography

The molecular weight of commercial SA and its derivatives (OSA and TOSA) was determined by size exclusion chromatography (GPC) using a Shimadzu modular system comprising: DGU-20A3 solvent degasser, LC-20AD pump, column oven, HT- autosampler 20A HT, and RID-10A refractive index detector. The samples were dissolved (2 mg/mL) in the mobile phase based on Milli-Q water with NaNO<sub>3</sub> (0.2 M).

## Hydrogel characterization

Real-time photorheological measurements were performed using an Anton PAAR Modular Compact Rheometer (Physica MCR 302, Graz, Austria) in parallel-plate mode (25 mm diameter) and the visible-light source was provided by positioning the light guide of the visible Hamamatsu LC8 lamp under the bottom plate. During the measurements, the gap between the two glass plates was set to 0.2 mm, and the sample was kept under a constant shear frequency of 1 Hz. The irradiating light was switched on after 60 s to allow the system to stabilize before the onset of polymerization. According to preliminary amplitude sweep measurements, all the tests were carried out in the linear viscoelastic region at a strain amplitude of 50%. The photo-rheology was studied as a function of the changes in the shear modulus ( $G'$ ) and in the loss modulus ( $G''$ ) of the sample versus the exposure time.

Amplitude sweep tests were performed on the cured hydrogels in the range between 1 and 1000% of strain, frequency of 1 Hz.

The different photocured samples ( $\approx h = 3$  mm,  $d = 5$  mm) were washed and left to dry overnight. Once dry, the samples were weighed and soaked in DI water to evaluate the swelling capability and kinetics. The samples were taken out at different time intervals and weighed once the surface droplets were wiped off with wet paper until a constant weight was reached. The swelling ratio ( $Sw\%$ ) was calculated as:

$$Sw (\%) = \frac{W_t - W_0}{W_0} * 100 \quad (6)$$

where  $W_t$  is the weight of the hydrogel sample at a specific time, and  $W_0$  is the initial weight of the dried sample. All tests were performed in triplicate.

To determine the gel content (GC), previously dried samples were held in a metal net, weighed, and then immersed in DI water (25° C) for 24 h to dissolve the un-crosslinked polymer. The samples were then dried for 24 h (40° C) in a vacuum oven and weighed again. The gel content was determined as:

$$GC (\%) = \frac{W_i}{W_f} * 100 \quad (7)$$

where  $W_i$  is the initial weight and  $W_f$  is the weight after extraction.



The morphological characterization of the samples was carried out by field emission scanning electron microscopy (FESEM, Zeiss Supra 40, Oberkochen, Germany). The hydrogel samples were first frozen, sectioned in half, and lyophilized before coating with a 5 nm-thick, thin film of Pt/Pd.

Mechanical properties were evaluated by a dynamic compression test. Measurements were performed on photocured samples ( $\approx h = 9$  mm,  $d = 5$  mm) at RT using a universal test system, MTS QTest1/L Elite, a uniaxial testing machine equipped with a 10 N load cell in compression mode. Samples were placed between the compression plates. Each sample was subsequently deformed at 1 mm/min. All measurements were performed in triplicate.

## Cell viability and proliferation

Cell viability and proliferation was performed thanks to the collaboration with UCM and CSIC of Madrid. Before the cell viability and proliferation assays, all the hydrogels were sterilized in a 48-well plate (Corning, Corning, NY, USA). The hydrogels were stored in 70% ethanol for a week; carefully rinsed with PBS (phosphate-buffered saline, Thermo Fisher, Waltham, MA, USA); and then sterilized with ultraviolet germicidal irradiation (UVGI) for 40 min. After a final rinse with PBS, the hydrogels were covered with DMEM 1X (Gibco) supplemented with 10% FBS (fetal bovine serum, Thermo Scientific) and antibiotics (100 U mL<sup>-1</sup> penicillin and 100 µg/mL streptomycin sulfate (Sigma-Aldrich, St. Louis, MI, USA)). After 24 h of contact between the culture medium and the hydrogels at 37° C, the media containing soluble extracts were collected and kept in the freezer until further use.

Cell assays were performed using C166-GFP mouse endothelial cell line (ATCC CRL-2583™, (ATCC, Manassas, Virginia USA): 20,000 cells/mL were seeded in a 24-well culture plate and allowed to adhere and grow for 24 h. Then, the media were changed for mixtures (1:1 and 1:5) of complete DMEM and the medium that had been in contact with the hydrogels.

Inverted fluorescence microscopy (Olympus IX51, FITC filter  $\lambda_{ex}/\lambda_{em} = 490/525$  nm) was used daily to evaluate any changes in the cell culture morphology and proliferation that could indicate the leaching of toxins from the hydrogels. After 48 h, when the cell cultures reached confluency, the metabolic activity of the cells was measured using an Alamar Blue assay, following the instructions of the manufacturer (Biosource). This method is non-toxic and uses the natural reducing power of living cells, generating a quantitative measure of cell viability and cytotoxicity. Briefly, Alamar Blue dye (10% of the culture volume) was added to each well containing living cells and incubated for 90 min. Then, the fluorescence of each well was measured using a Synergy HT plate reader (BioTek, Winooski, VT, USA) at 535/590 nm.

Finally, the DNA quantitation of cells was determined by fluorescent staining with a FluoReporter® Blue Fluorometric dsDNA Quantitation Kit. This method is based on the ability of the bisbenzimidazole derivative Hoechst 33258 to bind to A-T-rich regions of double-stranded DNA. After binding to DNA, Hoechst 33258 exhibits an increase in fluorescence, which is measured at the 360 nm excitation wavelength and 460 nm emission wavelength using a microplate reader (BioTek, Synergy HT).

An unpaired Student's t-test (GraphPad Prism4) was performed to compare the metabolic activity and DNA content values of each sample. A p-value of less than 0.1 was considered statistically nonsignificant.

## 4.4. Results and discussion

### Synthesis of alkyne alginate (SA-PA)

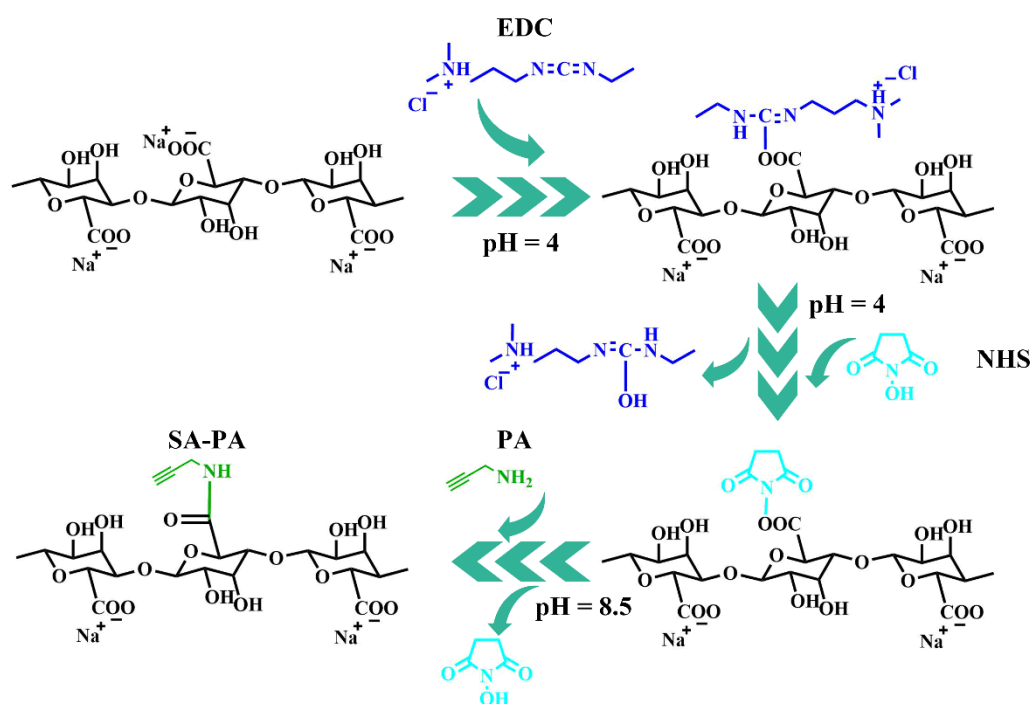


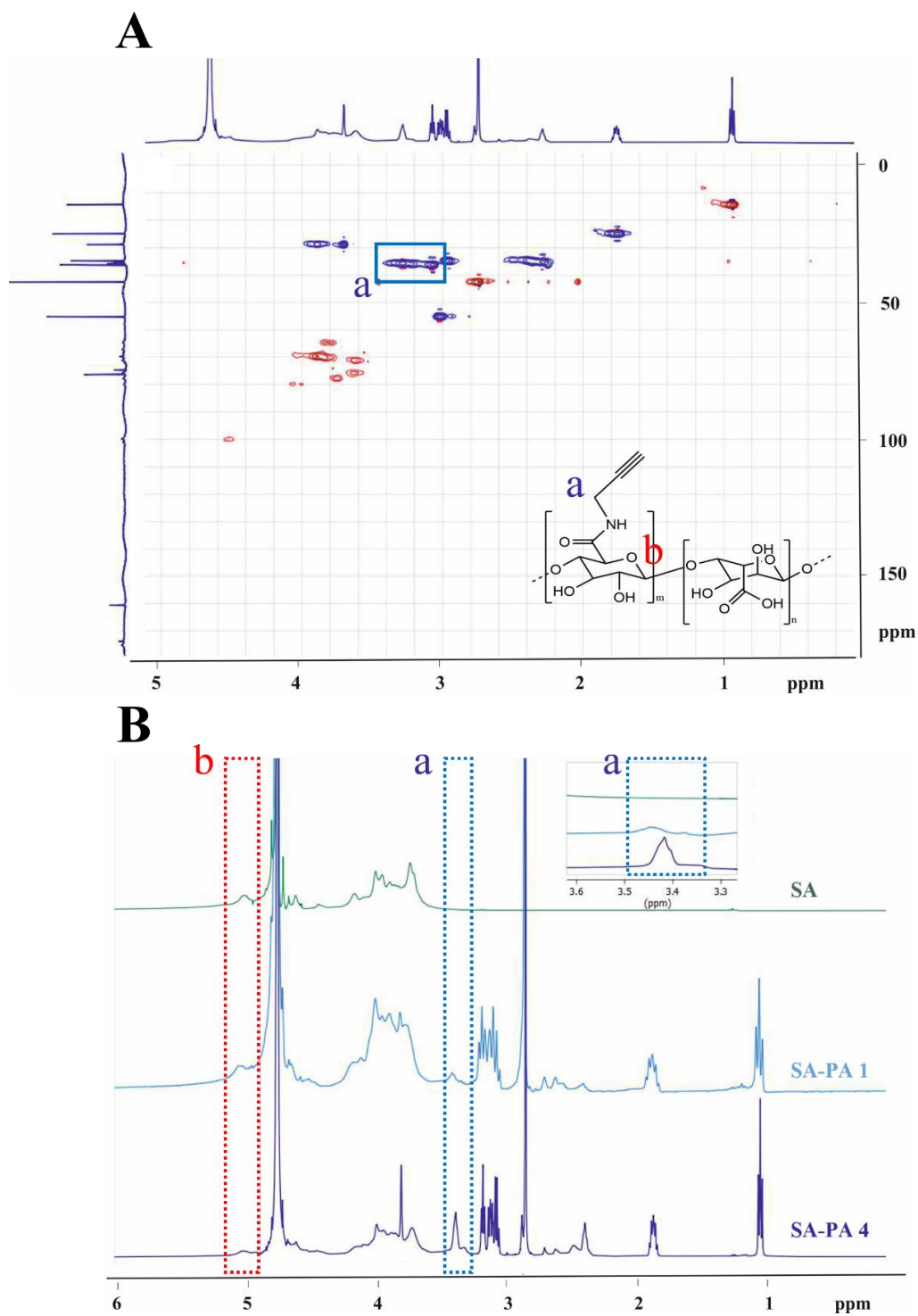
Figure 4.3: Two-step reaction scheme of the *yne* functionalization of sodium alginate (SA-PA) by carbodiimide chemistry.

Amidation reactions using the coupling mechanism of EDC/NHS to functionalize sodium alginate has a long history in chemistry [242,260,261]. In fact, the high number of carboxylic groups on the alginate backbone compared to other polysaccharides (see Chapter 1, subsection 1.2.2.2.) result as a favorable spot for the creation of the amino acid links. The alginate addition of

propargylamine in a two-step reaction is here proposed and summarized in Figure 4.3.

Once solubilized alginate, the resulting solution pH was lowered until 4 to ensure the protonation of the carboxylic groups [262]. The further EDC attack on the -COOH moieties, followed by NHS on the same sites, leads to the formation of a stable ester and to the subsequent amidation of PA. However, priorly to the addition of PA, the pH needs to be increased until 8.5 to enhance the amine nucleophilicity and make possible the successful reaction of PA on the NHS-ester (not possible in acidic or physiologic media) [253,263,264]. Considering a one-to-one reaction between PA and EDC/NHS, two molar ratios were selected for the investigation: equimolar (SA/EDC/NHS/PA 1:1:1:1, product called SA-PA 1) and with a four-fold excess of the alkyne reagent (SA/EDC/NHS/PA 1:4:4:4, product called SA-PA 4), based on the total amount of SA carboxylic groups.

Unfortunately, because of the  $^1\text{H-NMR}$  spectra position of the PA triple bond inside of the alginate backbone signal, no precise integration of the peak was possible. However, a more reliable signal to quantify the PA degree of substitution on SA was given by the alkyne reagent methylene. Its presence was identified determining the carbon-proton single-bond correlation by heteronuclear single quantum coherence experiment (HSQC, Figure 4. 4 A). In Figure 4. 4 A, -CH and -CH<sub>3</sub> groups are displayed in red while -CH<sub>2</sub> in blue. As highlighted, the 3.35 ppm signal on  $^1\text{H-NMR}$  and 35 ppm on  $^{13}\text{C-NMR}$  correspond to the PA methylene group, as reported in literature [264,265]. The integration of the 3.35 signal (Figure 4. 4 B), setting the anomeric -CH group of SA as internal standard (5.05 ppm), permits to estimate a degree of substitution of 2-3% for SA-PA 1 (difficult to interpret, due to the low intensity of the peak) and 28% for SA-PA 4. Due to the higher degree of substitution, SA-PA 4 was selected as the starting material for further investigations.



A further certification of the SA-PA 4 successful reaction was given by ATR-FTIR and Raman spectroscopy. In Figure 4. 5 A the Raman spectra certify the presence of the alkyne group with a sharp and defined peak at  $2122\text{ cm}^{-1}$  [266]. Even though Raman and FTIR spectroscopy are usually complementary, FTIR relies on the light transmission or absorption with a wide range of wavenumbers while Raman spectroscopy involves the inelastic scattering study from specific wavenumbers lamps. For this reason, especially if the proportion between chemical bonds is low such as in this case of alkynes, the intensity of the peaks results often more active and visible in Raman spectra [267]. Indeed, a really weak peak corresponding to the yne moieties at the same wavelength ( $2122\text{ cm}^{-1}$ , here compared with the PA spectra for completeness in Figure 4. 5 B) can be observed in the FTIR spectra. Nevertheless, both the techniques coupled with the nuclear magnetic resonance investigations suggest the successful linkage of PA within the SA backbone.

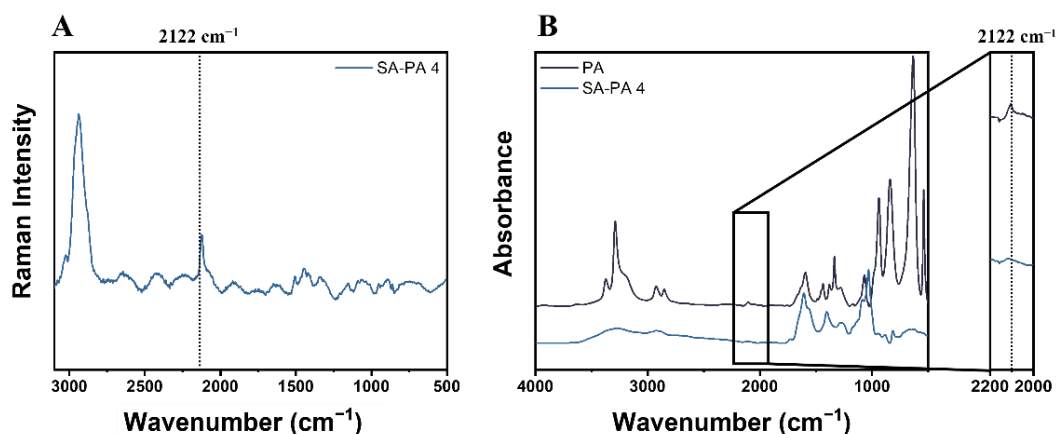


Figure 4. 5: Raman (A) and ATR-FTIR (B) spectroscopy of SA-PA 4 with the alkyne bond highlighted at  $2122\text{ cm}^{-1}$ .

### Synthesis of thiolated alginate via oxidation, imine bond creation and reductive amination (TOSA)

As already anticipated, two routes were initially selected to incorporate thiol moieties into the alginate backbone, in order to obtain the maximum degree of substitution. One interesting way to successfully functionalize polysaccharides with thiol groups exploits oxidation, imine bond creation and reductive amination of the initial natural polymer ( $1^{\circ}$  step, Figure 4.6). The oxidative modification of alginate, often performed with sodium periodate, takes place on the hydroxyl groups at C-2 and C-3 positions on the glucose rings, generating two aldehydes groups on the alginate backbone [247,268]. The reductive amination step was performed using sodium borohydride instead of Sodium triacetoxyborohydride

(STAB) to follow and compare the results with an already reported procedure [254].

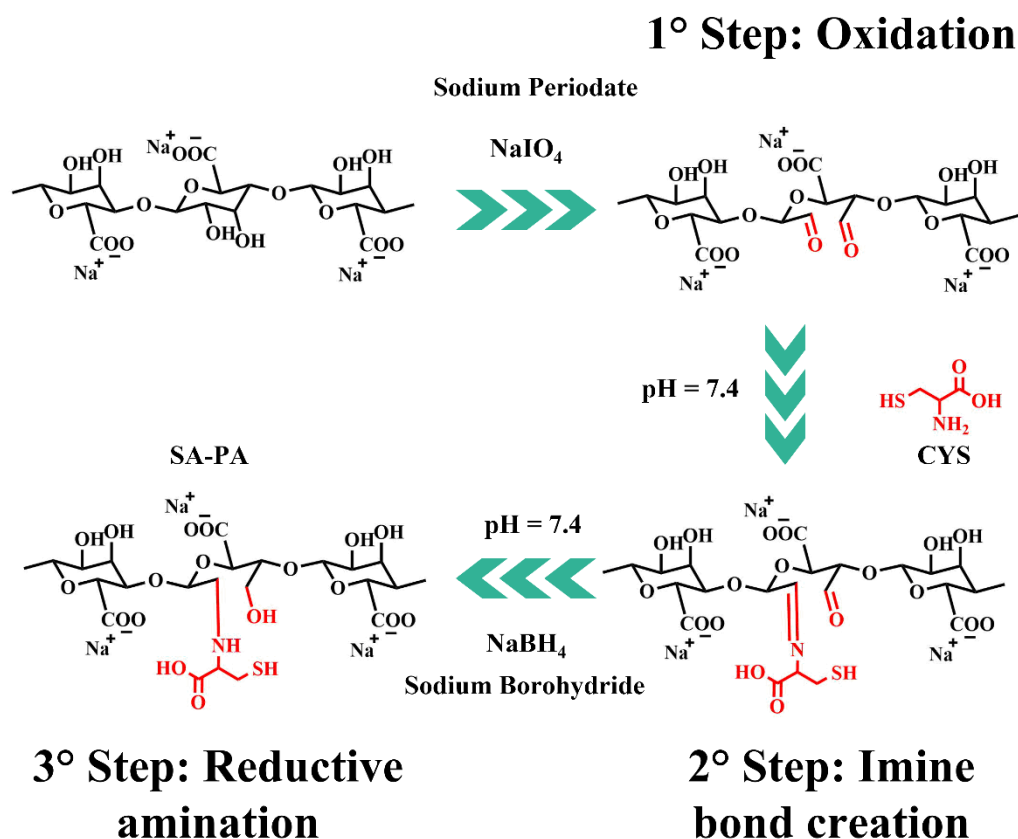


Figure 4.6: Scheme of the three-steps of reaction to obtain the thiolated oxidized sodium alginate (TOSA).

In the first step of reaction (oxidation) three different molar ratios between the alginic ring and the oxidizer were investigated (i.e., SA:SP = 5:1, 10:1, 20:1). After quenching with ethylene glycol [247] the aldehyde content was evaluated by potentiometric titration [247,269].

Using the formula (3), the calculated degree of modification on respect to the total alginate rings for the three batches is 33, 10 and 4% for OSA 1, OSA 2 and OSA 3, respectively (also reported on Table 4.1). However, considering the formation of two aldehydes groups for each cleavage on the alginate backbone and the amount of SP added, the theoretical degree of substitution for the three synthesis batches would have been 40, 20 and 10% (respectively on OSA 1, OSA 2 and OSA 3). However, not only the effective aldehydes generation occurs during the reaction; in fact, once formed, aldehyde groups are highly reactive and

can interact with proximal intra and intermolecular hydroxylic groups, generating hemiacetals and decreasing the available aldehydes groups [270]. Considering the higher degree of substitution, OSA 1 was selected for further investigations.

The presence of aldehydes on OSA 1 was further evidenced by ATR FT-IR,  $^1\text{H-NMR}$  and solid-state  $^{13}\text{C-NMR}$  (Figure 4. 7). While the FT-IR spectra confirm the appearance of the ester bond around  $1720\text{ cm}^{-1}$  (Figure 4. 7 A) [247], the  $^1\text{H-NMR}$  (Figure 4. 7 B) and solid-state  $^{13}\text{C-NMR}$  (Figure 4. 7 C) show the characteristics aldehydes peaks at 5.31-5.61 ppm and 92 ppm, respectively [254,271].

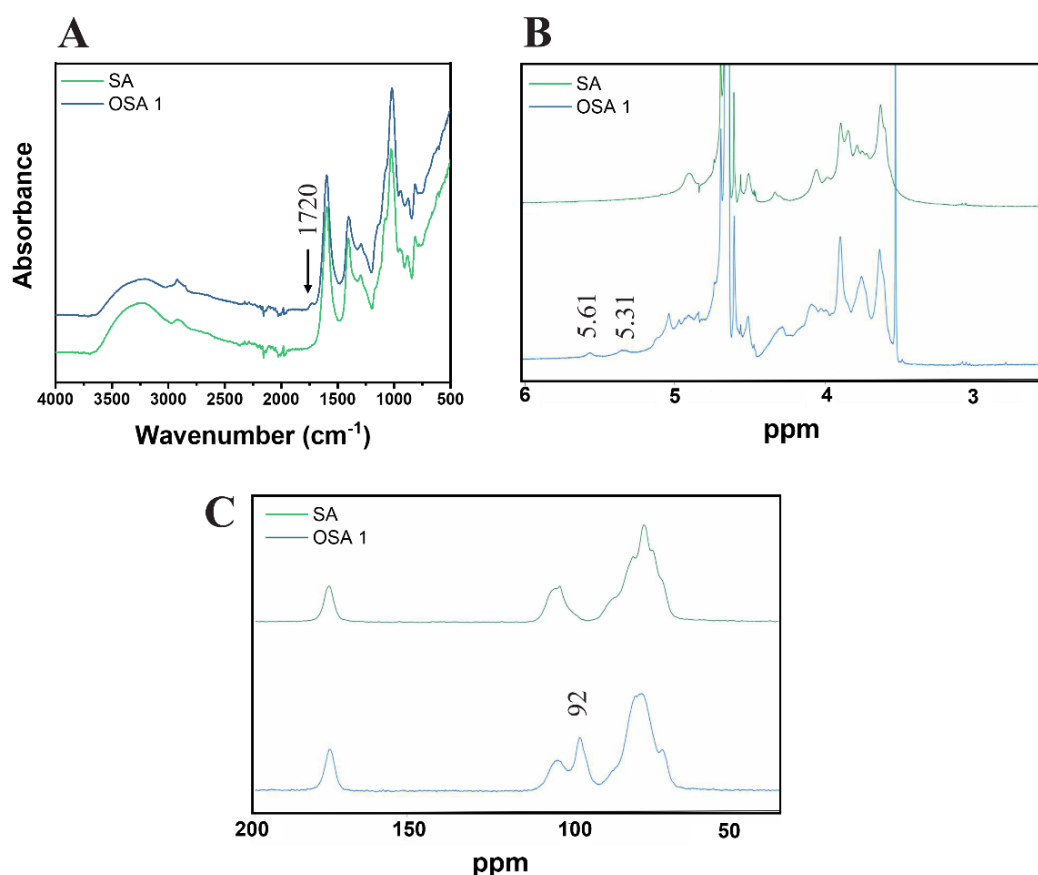


Figure 4. 7: ATR FT-IR (A),  $^1\text{H-NMR}$  (B) and solid-state  $^{13}\text{C-NMR}$  (C) of OSA 1.

Lastly, even if not directly modifying the number of aldehydes groups, oxidative reaction often leads to further cleavages of the alginate macromolecule, decreasing the molecular weight and chain stiffness [272]. The three synthesis batches and raw sodium alginate were so subjected to gel permeation chromatography to prevent an excessive fall in the molecular weight. On Table 4. 2 are expressed the values of retention time, number average molecular weight ( $M_n$ ), weight average molecular weight ( $M_w$ ) and their ratio. As expected, in all

cases the molecular weights of the final product decrease with the ratio between alginate rings and sodium periodate, suggesting reactions of chain breaking. However, considering the acceptable final molecular weight of OSA 1 and its higher level of modification, both in line with previous reported works and needed for the second synthesis step [252,272], this batch was selected for the next step of reductive amination.

Table 4. 2: Gel permeation chromatography data of sodium alginate (SA) and the three oxidized sodium alginate synthetic batches (OSA).

Sample	Retention time (min)	M <sub>n</sub>	M <sub>w</sub>	M <sub>w</sub> /M <sub>n</sub>
OSA 1	22.681	16228	36196	2.23
OSA 2	21.013	38686	97741	2.52
OSA 3	20.427	46131	130663	2.83
SA	19.689	58537	194641	3.33

After aldehyde formation, the thiolation reaction was performed following also a previous reported synthesis, using cysteine as functionalizing agent [254,273]. Briefly, the Schiff base formation, is given by the nucleophilic addition of the cysteine primary amine onto the OSA aldehyde groups [274]. The carbinolamine intermediate evolve later into condensation of water and the creation of the imine bond between the two reagents. The reaction, spontaneous, needs however a second step of reductive amination of the unstable imine bond in order to fix the functional group created [275,276]. The addition of sodium borohydride at a molar ratio 1:4 between the carbonyl group of OSA and the reducing agent is so necessary for the required product, the thiolated oxidized sodium alginate (TOSA). All reactions were performed under a N<sub>2</sub> atmosphere and in the darkness, to avoid disulfide bond formation or thiol oxidation [277]. The degree of substitution is evaluated by the Ellman reagent protocol using the equation (5); the mol<sub>SH</sub> value was obtained using the molar attenuation coefficient  $\epsilon$  (1562 M<sup>-1</sup> cm<sup>-1</sup>) previously obtained by UV-Vis spectra calibration with cysteine. Unfortunately, the degree of substitution measured by absorption on the UV-VIS spectra resulted  $0.5 \pm 0.1$  %, evaluated as too low for any further reaction of crosslinking. The reason could be ascribable to some sort of steric hindrance of the carboxylic group of cysteine as much as a not effective reduction amination reaction and to a possible hydrolysis of the imine group during dialysis [254,278].

### Synthesis of thiolated alginate via carbodiimide chemistry (SA-CSA and SA-CYS)

The other synthetic route to functionalize sodium alginate (eventually with thiol groups) involves the activation of carboxylic groups *via* carbodiimide



chemistry This two-steps amidation reactions involves the progressive reaction of EDC and NHS as activating agents [277,279,280]. Two different molecules to functionalize the polysaccharide were tested, cysteine (CYS) and cysteamine (CSA), at the same molar ratio of 1:4 (1:4=SA:CYS/CSA). The reaction schemes are reported in Figure 4.8.

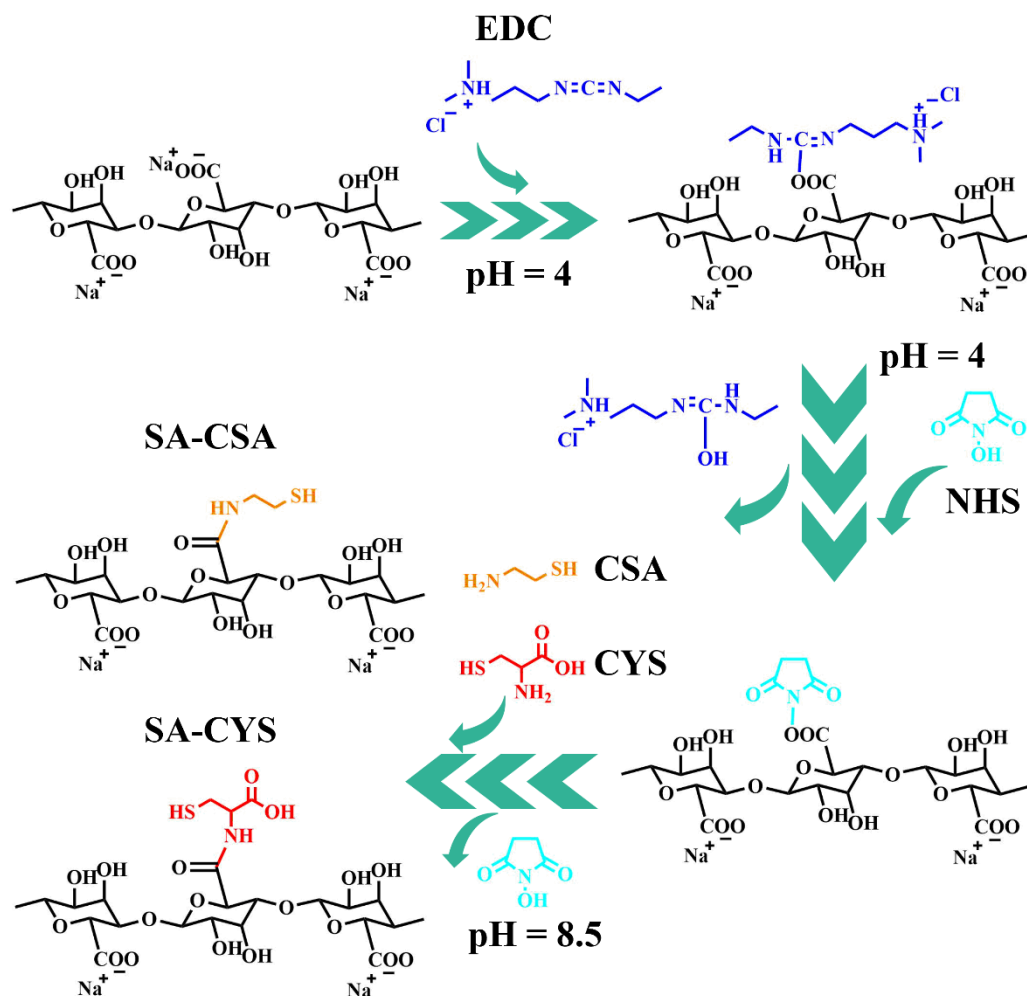


Figure 4.8: Scheme of the two-step of reaction to obtain SA-CYS/SA-CSA.

Within this reaction, alginate doesn't need any oxidation step because functionalization occurs between the natural polymer carboxylic groups and the reagents amines. The only requirement relates into the acidic pH of the reacting solution (generally around 4), in order to protonate the carboxylic moieties and catalyze the first attack by EDC. This step leads to the formation of an unstable intermediate, followed by the reaction of NHS to form a more stable ester [281,282]. After a reasonable activation time for the two agents (2 h), the thiol molecules were added and the reaction was let stirring at RT, at the same pH, under a N<sub>2</sub> atmosphere and darkness. While the pH is necessary to prevent thiols

deprotonation, the darkness and the N<sub>2</sub> atmosphere were demanded to prevent, during reaction, the creation of thiyl radicals and the formation of disulphides or thiols oxidation [283]. Functionalized SA-CYS (if cysteine was used) and SA-CSA (if cysteamine was used) polymers obtained were purified by dialysis against water using a 3.5 KDa membranes. The degree of substitution was measured by the Ellman reagent protocol using the previous reported  $\epsilon$ . In the case of cysteine, a degree of substitution of  $4.5 \pm 0.3$  % was achieved. Compared to the previous synthetic route, considerably higher degrees of substitution were achieved ( $4.5 \pm 0.3\%$  = SA-CYS and  $14 \pm 2$  % = SA-CSA vs  $0.5 \pm 0.05\%$  = TOSA), probably because of the absence of the restrictive step of reductive amination and the increased stability of the herein formed functional group. At the end SA-CSA was selected as the first component to create alginate hydrogels via thiol-ene reactions.

### Ene modification of alginate via carbodiimide chemistry

To modify sodium alginate with ene moieties, again carbodiimide chemistry was selected as an efficient method of synthesis, as reported also in literature [242].

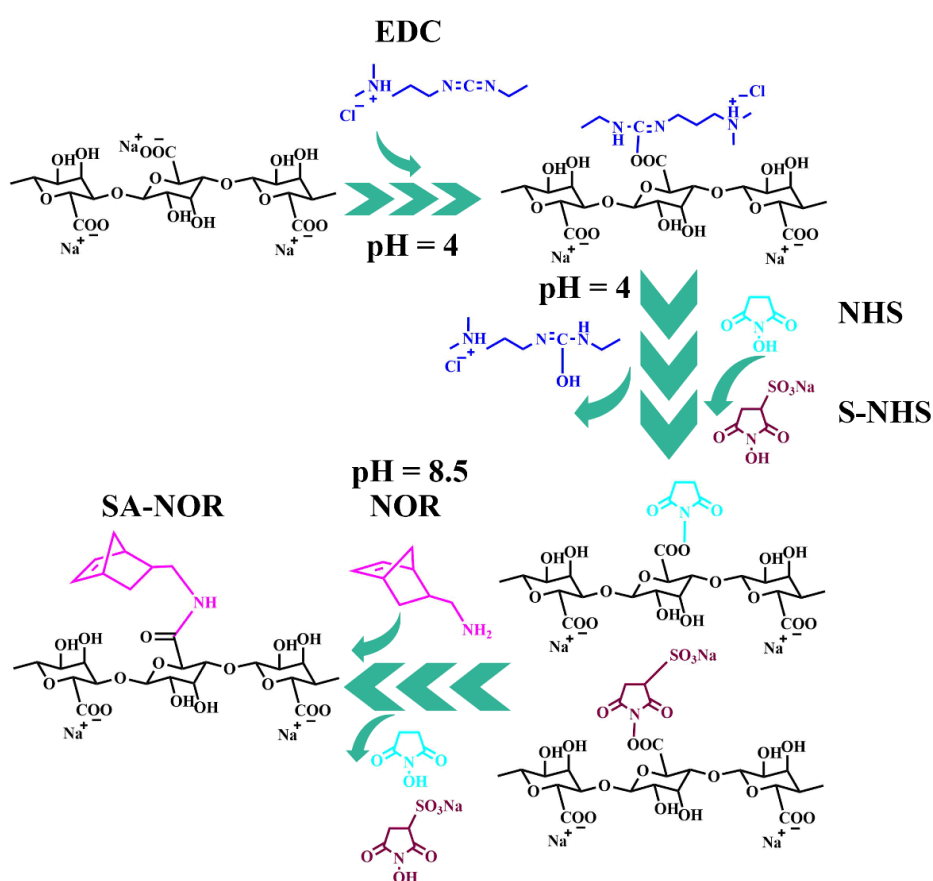


Figure 4.9: Scheme of the two-step of reaction to obtain SA-NOR.

After solubilization of sodium alginate in MES buffer (0.1 M), the pH of the solution was decreased until 4 to activate the carboxyl groups of the natural polymer. MES buffer was selected as the best solvent, following a recently reported work [242]. After the addition of the coupling agents and 2 h of reaction, the pH was increased till 8.5 to increase the amine nucleophilicity of Norbornene methylamine (NOR) and make possible its attack on the intermediate NHS-ester, favored at basic pH [253,264]. While EDC was maintained as the first coupling agent, two types of Hydroxysuccinimide reactive molecules were selected to form the second intermediate in reaction, NHS and S-NHS. Both molecules have already been tested to incorporate NOR into the alginate backbone, but to the best of our knowledge, no studies have been reported comparing the final degree of functionalization obtained [242,284–286]. Reaction was performed under argon atmosphere to prevent excessive self-reaction of the NOR molecules. The reaction scheme is reported in Figure 4.9. Once successfully dialyzed, the products SA-NOR 1 (synthesized using S-NHS) and SA-NOR 2 (using NHS) were analyzed by  $^1\text{H-NMR}$  (Figure 4.10). Similar degrees of functionalization were evidenced for the products checking the characteristics peaks at 6.02 and 6.27 ppm, corresponding at the two methylene of the norbornene double bond [242]. SA-NOR 2 showed a slightly better functionalization (15% vs 12% of SA-NOR 1), similar to its correlative SA-CSA counterpart (14%); for this reason, SA-NOR 2 was selected as the second reactive component for the creation of thiol-ene hydrogels.

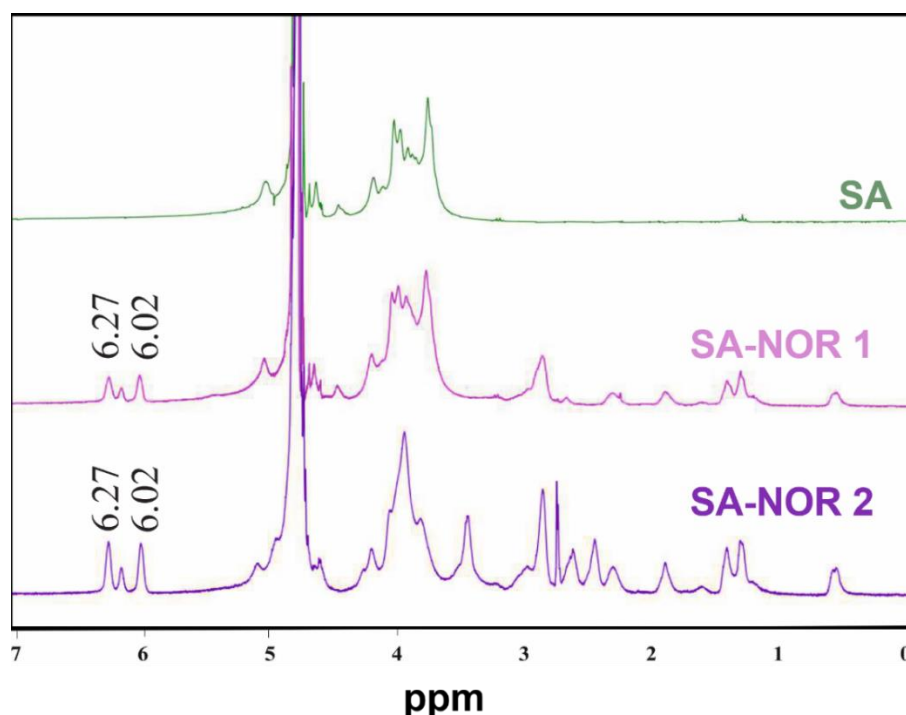


Figure 4.10:  $^1\text{H-NMR}$  of SA-NOR.

## Thiol-yne hydrogels characterization

As mentioned, two biocompatible dithiol water-soluble crosslinkers of different chain length dithiothreitol (DTT, chain length = 4, Mw 155) and poly(ethylene glycol) dithiol (PEG-SH, chain length  $\approx$  24, average Mn 1000) were employed to form the thiol-yne hydrogel [287]. Following the thiol-yne reaction (see Chapter 2, 2.1.1. Radical photopolymerization), one thiol reacts with a single alkyne to form a vinyl sulfide; then, if a second thiol approaches the reactive specie, a second thyl radical addition takes place, and a dithioether is formed [288]. Consequently, four formulations based on DTT and four based on PEG-SH were solubilized in DI water with incremental amounts of crosslinkers, as shown in Table 4.3.

*Table 4.3: Formulations prepared to form thiol-yne hydrogels. All formulations included: 5 wt% SA-PA-4, 2 phr (with respect to the amount of SA-PA 4) of LAP photo-initiator and were irradiated for 5 min.*

Sample	Crosslinker (HS-R-SH)	Molar Ratio (SA-PA:HS-R-SH)
0.05 DTT	DTT	1:0.05
0.1 DTT	DTT	1:0.1
0.2 DTT	DTT	1:0.2
0.3 DTT	DTT	1:0.3
0.05 S-PEG	PEG-SH	1:0.05
0.1 S-PEG	PEG-SH	1:0.1
0.2 S-PEG	PEG-SH	1:0.2
0.3 S-PEG	PEG-SH	1:0.3

While LAP photo-initiator was selected because of its recognized biocompatibility [289] the amount of crosslinkers was chosen to tune the hydrogel rigidity to meet different stiffnesses (the stoichiometric ratio between thiols and alkynes correspond to the 0.3 DTT or S-PEG formulations). Photo-rheology was used to assess the network formation, the system reactivity, and the optimal irradiation (Figure 4.11 A and C). An initial system stabilization time of 60 s was granted priorly to visible light irradiation, recording afterwards the increment of the shear storage modulus  $G'$  over time. The S-PEG formulations gel points (the solution gelation timepoint, represented when visible by the crossover between  $G'$  and  $G''$ , on Table 4.4) present lower values than the DTT molecules formulations in all cases. A minimum value of 95 s for S-PEG 0.2 was recorded, indicating a higher reactivity for this crosslinker. In addition, the S-PEG formulations sharper curve slope and the stable and defined upper plateau suggest an increased rate of polymerization using this crosslinker, even though the slightly better shear storage modulus of 0.1 DTT hydrogel. The reason resides probably into the shorter

molecular length of DTT crosslinkers, so to the consequent increased final mechanical rigidity [290]. At the same way, the lower DTT crosslinkers molecular weight might also explain the systems reduced reactivity. Indeed, once the molecule is one-side bonded, its reactivity decreases significantly due to a lack of mobility, especially compared to the high-molecular-weight crosslinkers. Instead, long-molecular-chain crosslinkers possess long and flexible chains, increasing the possibility of meeting a second alkyne reactive site [291].

The induction time, polymerization rate, and final  $G'$  value best properties were obtained from the 0.1 DTT and 0.2 S-PEG hydrogels, respectively (experimental data reported on Table 4.4). Amplitude-sweep measurements (Figure 4.11 B and D) support the previous results, considering the lowest yield points (Table 4.4) accomplished for 0.1 DTT and 0.2 S-PEG hydrogels. For this reason, a higher crosslinked structure is proposed for 0.2 S-PEG, while a shorter length between crosslinks is suggested for 0.1 DTT. To support this theory the increased fragility of 0.1 DTT hydrogel, measured by the lower yield point [227].

*Table 4.4: Rheological and mechanical properties of the thiol-yne hydrogels.*

Sample	Gel Point (s)	Induction Point (s)	Time to Plateau (s)	Storage Modulus $G'$ (KPa)	Yield Point (%)
0.05 DTT	237	153	/	0.03	1110
0.1 DTT	139	87	/	3.8	89
0.2 DTT	153	97	/	0.81	337
0.3 DTT	142	87	/	0.3	613
0.05 S-PEG	129	100	$\approx 200$	0.11	570
0.1 S-PEG	100	86	$\approx 200$	1.7	185
0.2 S-PEG	95	86	$\approx 200$	2.3	266
0.3 S-PEG	98	86	$\approx 200$	1.1	377

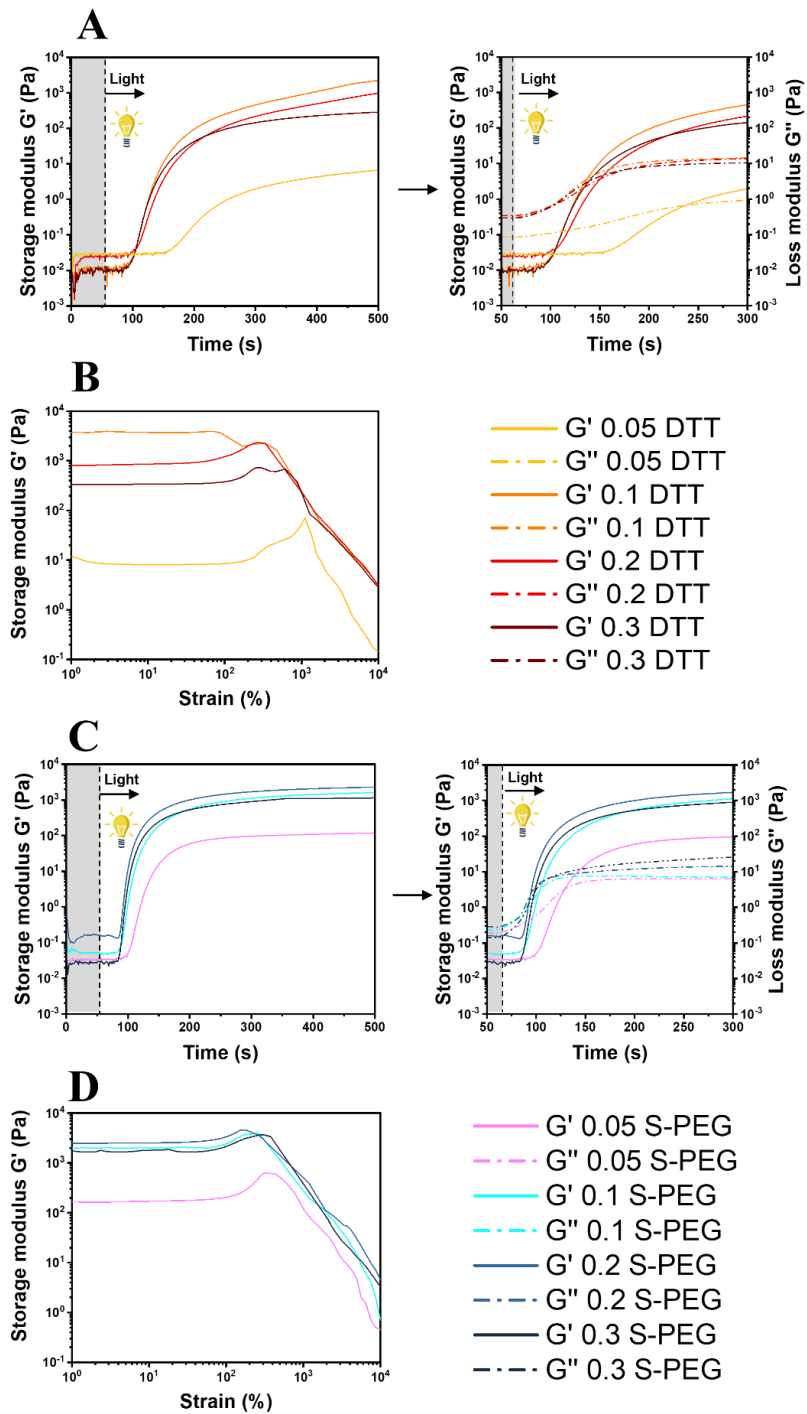


Figure 4.11: Photo-rheology (A and C) and amplitude sweep measurements (B and D) of the DTT/S-PEG formulations, respectively.

Since SA-PA 4 degree of the substitution is 28%, the best properties overall were expected from 0.3 DTT and 0.3 S-PEG hydrogels (respectively), considering the thiol-yne reaction mechanism. Nevertheless, while worst properties were expected for 0.05 DTT, 0.05 S-PEG, and 0.1 S-PEG (the hydrogels at lower molar ratio between the functionalized alginate and the crosslinkers) because of a non-complete network formation (validated by a low value of gel content, Table 4.5), slightly decreased properties were evidenced also for 0.2 DTT, 0.3 DTT, and 0.3 S-PEG formulations. This behaviour can reside in two different mechanisms:

The first mechanism involves the radical-scavenging properties of thiols in water environments (the human body is an example). Indeed, a great number of studies proved the radical-scavenging effect of thiols under physiological conditions, mostly related to beneficial effects to prevent biological free radicals formation [292–295]. The most common radical-scavenging path follows the reaction:



The reaction is kinetically driven toward the direction of thiyl radicals' removal through a rapid reaction with thiolate anions (always present at a physiological pH in water, contrary to bulk polymerization). If the  $SS\bullet^-$  product come into contact with oxygen, a near diffusion controlled rate irreversible reaction occurs [283]. Additionally, it was reported that dithiols, especially DTT, are more effective as radical scavengers [296,297]. To further support the hypothesis, the hydrogels were not optically transparent after photopolymerization (especially with DTT) but mildly turbid, a symptom of disulfide formation [298]. In Figure 4.12 are illustrated the 0.2 S-PEG hydrogel before (right after photopolymerization) and after water washing. The hydrogel appearance could support the idea of disulfide creation between crosslinkers and, consequently, their removal after swelling, also suggested by the low gel content observed in all hydrogels (Table 5.3).

Table 4.5: swelling properties of the thiol-yne hydrogels.

Sample	Swelling Equilibrium (%)	Swelling Time to Plateau (h)	%GEL (%)
0.05 DTT	1045 ± 26	1	41 ± 6
0.1 DTT	781 ± 63	1	72 ± 1
0.2 DTT	835 ± 46	1	62 ± 0.5
0.3 DTT	932 ± 16	1	53 ± 4
0.05 S-PEG	/	1	33 ± 4
0.1 S-PEG	802 ± 37	1	70 ± 3
0.2 S-PEG	791 ± 47	1	75 ± 2
0.3 S-PEG	1306 ± 222	1	57 ± 4

The second mechanism proposed resides into the chain transfer effects of thiols in free-radical polymerization, especially in aqueous solutions [299–302]. In fact, high thiol concentrations could lead to a great radical chain transfer phenomena and to a subsequent decrease in the crosslinking density, explaining the lower mechanical properties at high molar ratios.

Moreover, thiol-yne reactions always exhibit a certain degree of homopolymerization between the alkynes and vinyl sulfides, even if the optimal one yne/two thiols stoichiometric ratio is respected [288].

The combination of the three mechanisms might explain the lower photo-rheological properties in thiol-yne stoichiometric conditions.

The swelling kinetics and capability of the different hydrogels are reported on Figure 4.12 A and B, while the experimental data of swelling equilibrium and time to plateau in Table 4.5. Cylindrical hydrogels were immersed in DI water and weighted at different time points. The same photo-rheology trend was observed. Indeed, 0.1 DTT and 0.2 S-PEG presented the lowest swelling capability in their categories, supporting the proposed radical scavenging/chain transfer effects mechanism of thiols. Within these two hydrogels, similar swelling equilibrium values were observed (781% for 0.1 DTT and 791% for 0.2 S-PEG). Curiously, the obtained swelling equilibriums exhibit higher values compared with (meth)acrylate photocured alginate hydrogels [303–306].



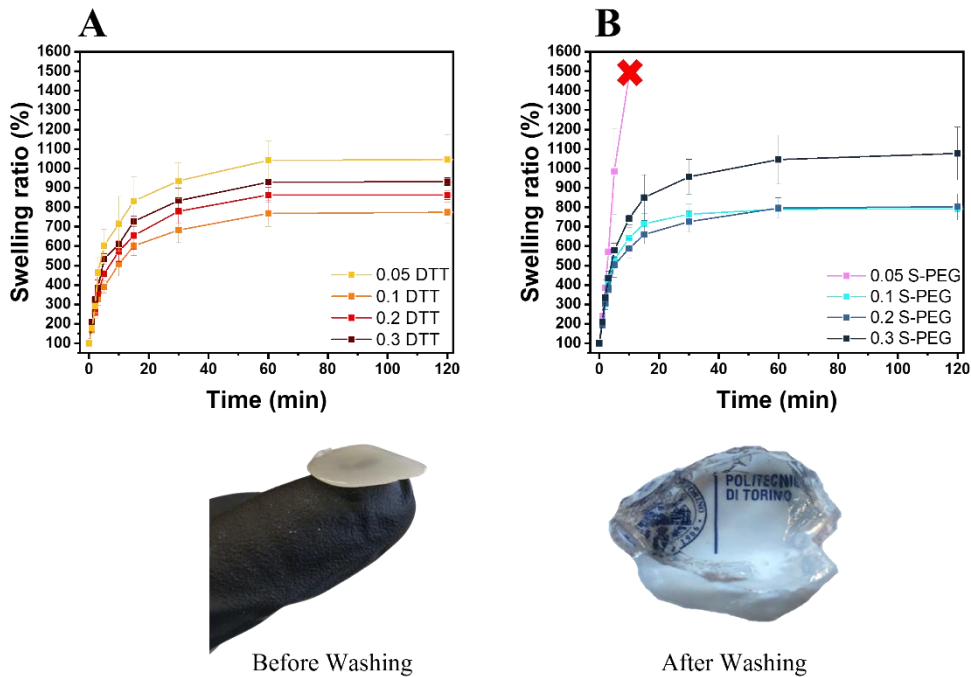


Figure 4.12: swelling kinetics of DTT (A) and S-PEG hydrogels (B). On the bottom of the image 0.2 S-PEG hydrogel before and after washing in DI water.

Considering their photo-rheological, mechanical, and swelling properties 0.1 DTT and 0.2 S-PEG hydrogels were chosen for further investigations.

The 0.1 DTT and 0.2 S-PEG freeze-dried hydrogels inner morphology was further investigated through field emission scanning electron microscopy (FESEM). The typical hydrogel required porous structure was observed in both samples envisaging a scaffold/filler application in tissue engineering. As visible in Figure 4.13 A and B, 0.2 S-PEG sample shows a more compact network with regular porosity while 0.1 DTT sample presents a less homogeneous structure.

The two hydrogels mechanical properties were also tested by compression test in a cylindrical shape ( $D = 5$  mm,  $H = 9$  mm). Storage modulus ( $E'$ ), ultimate compression strength, and deformation at break of the same order of magnitude were recorded for 0.2 S-PEG and 0.1 DTT hydrogels (Figure 4.13 C). Moreover, absolute mechanical values comparable to other proposed alginate hydrogels obtained using methacrylates [307,308] or thiol-ene reactions [242] were evidenced. The better values obtained for 0.2 S-PEG compared to 0.1 DTT could be attributed to a more homogeneous network, as assessed by FESEM images, and to a more deformable crosslinked structure (due to the higher molecular weight of the PEG crosslinker).

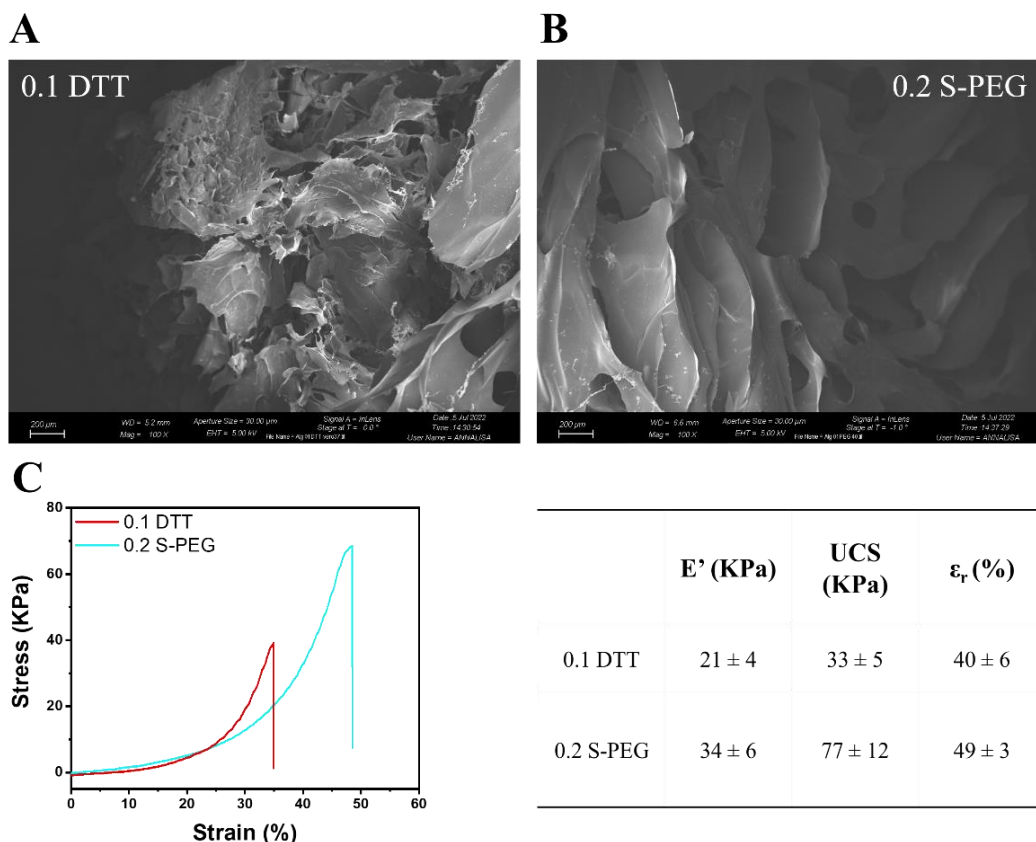


Figure 4.13: FESEM morphology of 0.1 DTT (A) and 0.2 S-PEG (B) hydrogels with a scale bar of 200 $\mu$ m. Compression test using the two water-soluble crosslinkers; the right table shows the experimental obtained values of compression elastic modulus ( $E'$ ), ultimate compression strength (UCS), and elongation at rupture ( $\epsilon_r$ ). Standard deviation is reported for all data.

## Thiol-ene hydrogel characterization

After the production of alginate-based hydrogels exploiting synthetic thiol crosslinkers, the production of fully alginate hydrogels has been pursued. Preliminary tests on the possibility to exploit SA-PA (alkyne functionalized alginate) and SA-CSA (thiol functionalized alginate) to create hydrogels did not lead to any successful results; thus, the use of a SA-NOR (alkene functionalized alginate) was preferred with SA-CSA.

Thiol-ene reactions are commonly known as highly regiospecific, highly reactive, and insensitive to oxygen and aqueous environments [160]. Equimolecular quantities of SA-CSA and SA-NOR 2 were mixed together in DI water at a total polymer concentration of 10 wt% trying to obtain a 1:1 regiospecific reaction between the thiol and ene functional groups (5 wt% of each component). The total concentration of 10 wt% was chosen in order to create

stiff and self-standing hydrogels with appropriate mechanical properties. Instead, 1 phr of LAP photoinitiator (as compared to the total amount of polysaccharide) was selected for its low cytotoxic effects on living cells and visible light absorption [289].

Photorheology was exploited to investigate photoreactivity of the selected formulation (Figure 4.15 A). No delay was observed. Unfortunately, no gel point (referred in photo-rheology as the crossover point between  $G'$  and  $G''$ ) could be detected cause of the medium-high viscosity of the formulation, so a not clear indication of the hydrogel network formation can be observed. However, the almost vertical increment of the  $G'$  curve suggest again the high reactivity of the system and the consequent network formation. Lastly, the thiol-ene hydrogel (TE Hydrogel) doesn't show any clear upper plateau, suggesting an ongoing progression of the reaction after 440 s of irradiation, even though the upper  $G'$  values ( $\approx 10^3$  Pa) are comparable with other reported hydrogel used in tissue engineering [44,187]. However, long irradiation times are not suitable if the polymerization of cells laden gels is envisaged, because of the possible carcinomic effects on cells by light [309].

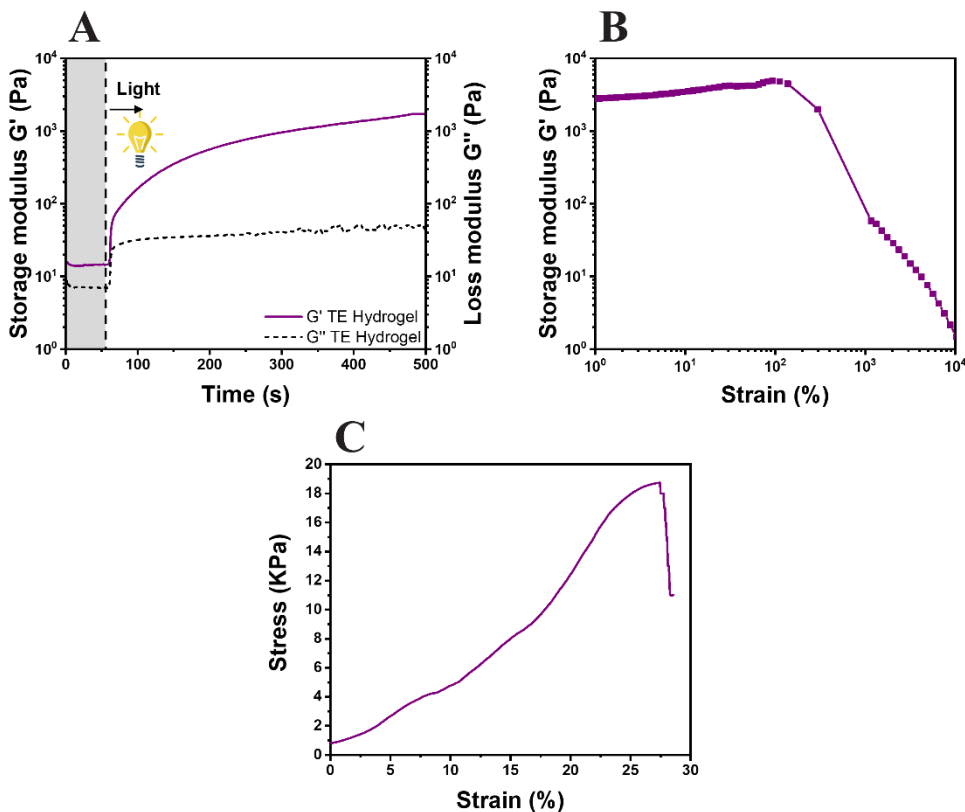
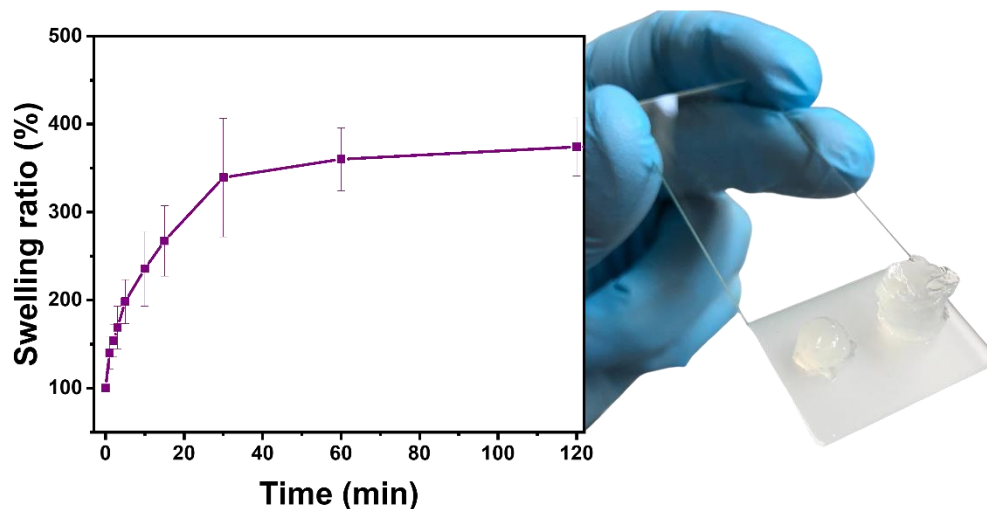


Figure 4.14: Photo-rheology (A), amplitude sweep (B) and compression tests of the thiol-ene hydrogel (TE hydrogel).

The mechanical properties of the formed hydrogel were tested both by amplitude sweep measurements and compression test (Figure 4.14 B and C). The hydrogel stability over an incremental strain is measured by amplitude sweep, with the yield point suggesting the maximum strain point applicable before the hydrogel collapse. In this system, the yield point at a 138% of strain compared with thiol-yne hydrogels suggest a strong behavior of the hydrogel, with an effective crosslinked network [227]. Furthermore, the compressive elastic modulus of  $44 \pm 3$  KPa place the resulted hydrogel into the stiffer soft tissues scaffolds, with properties comparable with the human intestine or tendons [236]. The increased stiffness compared with the thiol-yne hydrogels as well as a lower ultimate compressive strength ( $\approx 19$  KPa) and elongation at rupture  $\epsilon_r$  (27%) are ascribable to the higher polysaccharide concentration of the starting hydrogel and to a possible increase of crosslinking density.

The swelling behavior of the hydrogel was also evaluated. The hydrogels were produced in triplicate. As visible on Figure 4.15, the swelling plateau is reached after 30 min of immersion in DI water. The value of equilibrium,  $376 \pm 21\%$ , its way lower than the co-respective thiol-yne hydrogels reported but similar to other reported works [242,285,286] with analogue values and profile of swelling kinetics. The Gel content of the hydrogel, assessed in triplicate, showed a slightly better value of  $78 \pm 3\%$  compared to thiol-yne hydrogels. For this reason, the TE hydrogels were subjected to the biological characterization.



*Figure 4.15: Swelling kinetics of the TE hydrogel.*

## **Cell viability and proliferation**

The different hydrogels were sterilized as described and immersed in complete medium for 24 h at  $37^\circ$  C, before biological characterization. Laterally,

autofluorescent C166-GFP endothelial cells were seeded and allowed to adhere for 24 h in a 12-well plate. According to ISO 10993-5 recommendations, to ensure no toxic substances release from the hydrogels, the culture media in contact with the samples was added to the endothelial cells growing in a different culture plate. Cells proliferation was assessed via inverted bright-field microscopy for 48 h (Figure 4.16 A). Also, their metabolic activity and DNA content was quantified to assess hydrogel cytocompatibility (Figure 4.16 B and C, respectively).

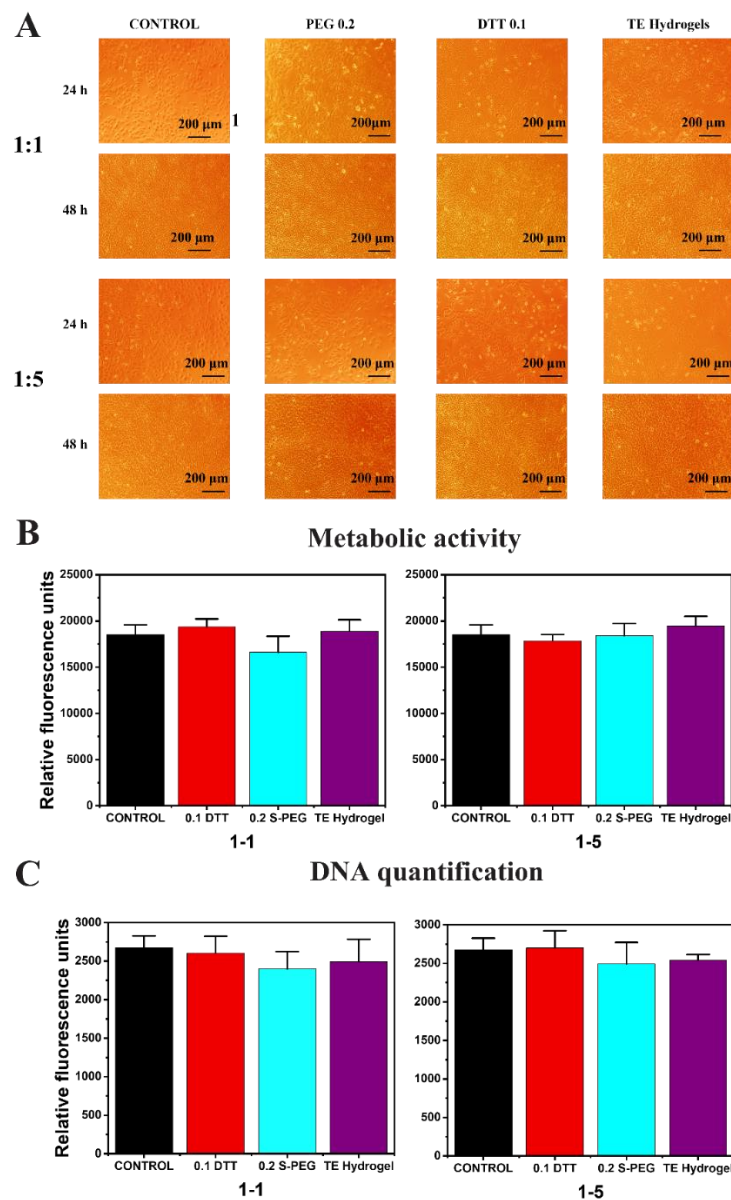


Figure 4.16: Bright-field microscopy (A), metabolic activity (B), and DNA quantification (C) of the hydrogels.

As evident in the micrographs (Figure 4.16 A), both no morphological changes and no detached cells or evidence of necrotic or apoptotic cell bodies were identified after culture media replacement. In all samples, a healthy and confluent cell monolayer was denoted. The mitochondrial metabolic analysis (Alamar Blue assay, Figure 4.16 B) showed proper levels of cell activity in all samples. Accordingly, the DNA proliferation analysis (Figure 4.16 C) certified the previous observations, with similar levels of DNA content for all conditions. Additionally, no statistically significant differences in the cultured cells were found when compared to a control, either in metabolic activity or in DNA content evaluation.

In summary, the thiol–yne alginate hydrogels don't show any signs of indirect in vitro cytotoxicity. These results open new possibilities of these hydrogels for clinical therapies. According to the obtained results and considering the presented mechanical properties, DTT alginate hydrogels (0.1 DTT) could be implemented for clinical indications with no strict structural requirements (e.g., protective dermal patches or other wound dressings [310]). Contrarywise, the 0.2 S-PEG hydrogels mechanical properties suggest the material as surgical fillers in cosmetic plastic surgery procedures or after tumour resections. Within these situations, alginate hydrogel fillers are already commonly used to maintain body structures or to sustain tissue proliferation and organism regeneration [120]. Considering their increased stiffness and mechanical properties, TE hydrogels may be employable in the creation of scaffolds for stiffer soft tissue as intestines or tendons.

## 4.5. Conclusions

Within this Chapter the successful and easy processing production of thiol–yne alginate hydrogels was proposed for the first time and a possible application in tissue engineering as wound-dressing patch or surgical filler was evidenced.

A two-step reaction using the well-known carbodiimide chemistry led to an alkyne degree of substitution of 28% on the alginate backbone, certified by NMR, Raman and FTIR spectra. The employment of two water-soluble dithiol crosslinkers (i.e., 1,4-dithiothreitol and poly-ethylene glycol dithiol) permitted to obtain hydrogels with tunable rheological, mechanical, swelling and morphological properties depending on the molar ratio between crosslinkers and yne moieties used. The formed gels presented similar or higher values compared to the standard and more cytotoxic (meth)acrylate photocured alginate hydrogels, supporting the proposed applications of these materials.

Lastly, the hydrogels obtained by thiol–yne reactions showed no signs of releasing cytotoxic byproducts that would impede their biomedical applicability. Cells in contact with culture media extracts exhibited optimal proliferation

measured in terms of metabolic activity and DNA content elevating the material as a good candidate for tissue engineering applications.

At the same way, the creation of the first fully modified alginate hydrogel without the addition of external crosslinkers via thiol-ene reactions was explored. The high regioselectivity towards ene moieties of thiol groups enabled the creation of stiff and porous scaffolds able to support cells attachment and proliferation, without the release of toxic substances.

Different routes of synthesis were investigated to obtain the two alginate counterparts able to crosslink to form the photocured thiol-ene hydrogel. Related to the thiol modified polysaccharide, the modification using carbodiimide chemistry resulted as the most promising way to incorporate thiol moieties into the alginate backbone while cysteamine granted higher degrees of substitution compared with cysteine, probably due to steric hindrance of the latter. The successful characterization of the products was confirmed by titration tests, as much as  $^1\text{H-NMR}$  and solid-state  $^{13}\text{C-NMR}$ . At the same way, the norbornene functionalized alginate obtained by carbodiimide chemistry showed comparable degrees of substitution using two different coupling agents, named NHS and S-NHS, validated by  $^1\text{H-NMR}$ .

Both the hydrogel formation and time of irradiation were characterized by photo-rheology while the mechanical properties were assessed by amplitude sweep (to check the hydrogel stability over increasing solicitation) and compression test. The evaluation of the swelling profile and gel content suggest an important internal porosity of the hydrogel, perfectly suitable for biological characterizations.

Lastly, the cell adhesion and proliferation confirm the possible employment of these scaffold for tissue engineering application, preferably for stiffer soft tissue as intestines or tendons.

# Chapter 5

## Gelatin hydrogels

### 5.1. Introduction

The mandatory functionalization of natural polymers is always a crucial step once a photocured hydrogels needs to be created, as extensively discussed on Chapter 2 and treated on the previous Chapters (3, 4, 5 and 6). The main drawbacks within this approach reside in the intrinsic characteristics of this class of materials, distinguished from synthetic polymers by the batch-to-batch variability in terms of molecular weight, polydispersity, or abundance of defined functional groups [97]. In fact, the natural polymer source and the extraction method highly influence the final functionalization uptake, leading to batches differentiations concerning the hydrogel degree of modification or mechanical properties [108]. Especially in DLP 3D printing, a predictable and effective reactivity, as much as the structure reproducibility, are a key formulation parameter to create hydrogels suitable for tissue engineering applications [179,180].

Herein, the implementation of a hybrid system based on a Norrish II photo-initiating reaction using PEGDA 700 as monomer and cold-water fish gelatin as co-initiator resulted into a reactive photocured 3D printable system, without previous polymer modifications [233]. The gelatin amine groups were used as reactive spot to initiate the Norrish II radical photopolymerization and make possible its direct incorporation into the poly-(ethylene glycol) diacrylate network [311–313]. The choice of the protein (cold-water fish gelatin) was driven by its low gelling point ( $<10^{\circ}\text{C}$ ) which enable its processability at RT, not possible with other sources type of gelatin (e.g., bovine gelatin, poorly processable at RT due to its sol-gel transition of  $37^{\circ}\text{C}$ ) [314].



The formulation printability with increased amount of gelatin was proven through photo-rheology while the protein incorporation was exploited by ATR-FTIR and gelatin release into a proper solvent. Furthermore, the mechanical, swelling, and morphological properties were tested assessing the hydrogel as good candidate for biological characterization. Finally, cell viability and proliferation was certified while the DLP 3D-printing showed defined and stable structures, indicating the proposed system as a facile and biocompatible system to create scaffolds for tissue engineering applications.

## **5.2. Materials and procedures**

### **Materials**

Gelatin from cold-water Fish skin (powder, gelling point  $<10^{\circ}\text{C}$ , CFG), poly(ethylene glycol) diacrylate (PEGDA, Mw 700), camphorquinone (Mw 166.22, CQ, 97%), Dulbecco's phosphate-buffered saline (DPBS, pH 7.0–7.3), and Brilliant Green (hydrogen sulfonate, Mw 482.63 BG) were purchased from Sigma-Aldrich (Milano, Italy) and used as received without further purification. A water-soluble hydroxyl-Phenylbis(2,4,6-trimethylbenzoyl)phosphine oxide (BAPO-OH) was kindly provided by ETH Zurich.

### **Formulations**

All formulation were kept with a constant PEGDA/DI water weight ratio of 35/65 wt%, according to preliminary test to maintain an optimal photocurable system. Firstly, CFG was dissolved in water while stirring at different weight ratio as displayed in Table 5. 1 (expressed on phr, respect to the PEGDA weight amount) due to the higher solubilization times. In a different container, BG (at different weight ratio to study its influence into the photocuring system) was added to the selected amount of PEGDA and let stir until complete homogenization. The PEGDA solution was then added into the previous obtained CFG/DI water solution and stirred. Lastly, the Norrish II photo-initiator CQ (also at different weight ratio to investigate its influence into the formulation reactivity) previously solubilized in ethanol (0.25 mg/ $\mu\text{L}$ ) to overcome its poor solubility in water, was added to the final solution. As reference was selected a formulation composed as follows: PEGDA 35 wt%, water 65 wt%, BAPO-OH 2 phr.

Table 5. 1: Formulations composition. \*phr=per hundred resin, referred to the PEGDA weight amount.

	PEGDA (wt%)	WATER (wt%)	CFG (phr)*	CQ (phr)*	BG (phr)*
CQ1	35	65	10	1	--
CQ2	35	65	10	2	--
CQ4	35	65	10	4	--
BG005	35	65	10	2	0.0005
BG01	35	65	10	2	0.001
BG02	35	65	10	2	0.002
CFG5	35	65	5	2	0.001
CFG10	35	65	10	2	0.001
CFG15	35	65	15	2	0.001
CFG30	35	65	30	2	0.001
CFG50	35	65	50	2	0.001

### 3D printing

The 3D printing tests were performed with an Asiga PICO 2 DLP-3D printer (Asiga, Australia) equipped with a LED light source emitting at 405 nm (nominal XY pixel resolution is 39  $\mu\text{m}$ , achievable Z-axis control is 1  $\mu\text{m}$ ). After printing, the 3D structures were soaked in distilled water for 1 minute and submitted to the post-curing process performed with a mercury lamp provided by Robotfactory (10 minutes, light intensity 10  $\text{mW}/\text{cm}^2$ ).

## 5.3. Characterization methods

### Hydrogel characterization

Real-time photorheological measurements were performed using an Anton PAAR Modular Compact Rheometer (Physica MCR 302, Graz, Austria) in parallel-plate mode (25 mm diameter). The visible-light source was provided by positioning the light guide of a Hamamatsu LC8 lamp (20  $\text{mW}/\text{cm}^2$ ), with a cut-off filter below 400 nm, under the bottom plate. During the measurements, the gap between the two glass plates was set to 0.2 mm, and the sample was kept under a constant shear frequency of 5 Hz. The irradiating light was switched on after 60 s to allow the system to stabilize before the onset of polymerization. According to preliminary amplitude sweep measurements (strain 0.01-100%, frequency 5 Hz), all the tests were carried out in the linear viscoelastic region at a strain amplitude

of 1%. The kinetics of photopolymerization was studied as a function of the shear modulus ( $G'$ ) versus the exposure time. Viscosity was measured with a range of shear rate from 0.01 to 1000 1/s. All the experiments were performed in triplicate.

For the swelling test, the 3D printed samples were first immersed in water at room temperature for 24 h to leach the unreacted-soluble fraction and/or the residues of CQ entrapped in the network and then dried overnight at 40° C in a vacuum oven. Then, the dried samples were immersed in deionized water at 37° C. The swelling kinetics was determined after taking out the soaked samples from water at different time intervals and weighing them once the surface droplets were wiped off with wet paper until constant weight. The swelling percentage (Sw%) was calculated as:

$$Sw (\%) = \frac{W_t - W_0}{W_0} * 100 \quad (1)$$

Where  $W_t$  is the weight of the hydrogel sample at a specific time, and  $W_0$  is the weight of the dried sample recorded as the initial weight. All tests were performed in triplicate.

DMTA measurements were performed in tensile mode on 3D printed dried thin and flat rectangular samples with a Tritec 2000 DMA (Triton Technology Ltd, London, UK). The tests were carried out in triplicate between -80° and +25° C, with the setting of a temperature ramp of 3 °C min<sup>-1</sup> and the application of a force to the sample with a constant frequency of 1 Hz. The concomitant changes of Tensile Storage Modulus  $E'$  and  $\tan\delta$  were measured as functions of the temperature.

A FESEM (Field-Emission Scanning Electron Microscopy) Supra 40 instruments manufactured by Zeiss operating at 30KW was used to investigate the samples' morphology and the cell distribution. The 3D printed samples prepared for SEM microscopy were washed twice with PBS, then they were incubated with 2% glutaraldehyde in PBS for 1h at room temperature. After, they were dehydrated using increasing amounts of ethanol-water (50%, 70%, 85%, and 100%) for 15 min each. At last, the samples were air-dried and coated with a 5 nm thick Pt layer.

## Investigation on the gelatin incorporation

To evaluate the gel content, previously dried 3D printed samples were held in a metal net, weighed, and then immersed in water (25° C) for 24 h to dissolve the uncrosslinked polymer. The samples were then dried overnight (40° C) in a vacuum oven and weighed again. The gel content was determined as:

$$GC (\%) = \frac{W_i}{W_f} * 100 \quad (2)$$

Where  $W_i$  is the initial weight and  $W_f$  the weight after extraction.

Attenuated total reflectance-infrared spectroscopy (ATR-FTIR) was conducted on 3D printed dried samples using Thermo Scientific Nicolet iS50 FTIR Spectrometer (Milano, Italy) equipped with a diamond crystal ATR accessory. Thirty-two ATR spectra were collected with a resolution of  $4\text{ cm}^{-1}$  in the range of  $4000\text{--}600\text{ cm}^{-1}$  for each sample. The spectrum of physically crosslinked CFG was taken as a reference.

## **Hydrogel purification, cell viability and proliferation**

This characterization was performed in collaboration with PolitoBIOMed Lab. The evaluation of the amount of unreacted CQ was performed through leakage in distilled water. Crosslinked samples (diameter 25 mm, thickness 2.5 mm) were immersed in 9 ml of deionized water for different times (1, 2, 4, and 6 days, in triplicate). For each time point, the water was withdrawn, replaced, and analyzed with the UV-Vis spectroscope Synergy™ HTX Multi-Mode Microplate Reader instrument (BioTek, Winooski, VM, USA). The spectrum mode was set in the range between 350 and 600 nm with a scan step of 2 nm. The experiments were performed on 1 ml of the different solutions using a 24-well plate. To quantify the amount of CQ extracted a calibration line was created starting from different concentrations of CQ in DI water.

For cellular studies, lung carcinoma epithelial cells, A549, and normal lung fibroblasts, MRC-5 were used. A549, kindly provided by Valentina Monica from the Oncology Department of the University of Turin, were cultured in RPMI 1640 GlutaMAX medium (Gibco, ThermoFisher) supplemented with 10% FBS and 1% penicillin/streptomycin (all from Sigma-Aldrich). MRC-5, kindly provided by Chiara Tonda Turo from Department of Mechanical and Aerospace Engineering, Politecnico of Torino, were maintained in EMEM GlutaMAX medium (Gibco, ThermoFisher) supplemented with 10% FBS, 1% Sodium pyruvate, and 1% penicillin/streptomycin (all from Sigma-Aldrich).

To test toxicity, the cell medium was conditioned for 72 h within the printed samples, previously sterilized for 30 min under UV light. Then,  $1 \times 10^4$  A549 or MRC-5 were seeded into a 96-well plate and cultured with a conditioned medium. After 24 and 48 h of incubation, MTT (10% SDS, 0.01 M HCl in  $\text{H}_2\text{O}$  from Sigma-Aldrich) was added at the concentration of 0.5 mg/ml and incubated for 2 h at  $37^\circ\text{C}$ . Then, the same amount of MTT solvent was added to solubilize the formazan crystal. After 1 h, the plate was read with a Synergy-HTX Multi-Mode Microplate Reader (BioTek, Winooski, VM, USA) at a wavelength of 570 and 650 nm. For microscopy, A549 and MRC-5 were seeded on printed disk (diameter 25 mm, height 2 mm) at  $3 \times 10^5$  cells/disk density. After 24 h, samples were washed with PBS and fixed with formalin-free tissue fixative (Sigma-Aldrich) for 30 min. Cell nuclei were stained for 5 min with 0.3 mM DAPI (Invitrogen). Bright-field and fluorescence images were obtained with a microscope (Eclipse Ti2 Nikon, Tokyo, Japan) equipped with a Crest X-Light

spinning disk confocal microscope and a Lumencor SPECTRA X light. All images were displayed using the same scaling and were collected using a Plan Apo 10X 0.45 NA (Nikon, Tokyo, Japan).

## 5.4. Results and discussion

### Preliminary investigation on the formulations

A preliminary investigation on the formulation was necessary to optimize the right amount of gelatin, photo-initiator, and dye. Moreover, visible light photopolymerization is always preferable in tissue engineering applications [309]. Firstly, the influence of the CQ photo-initiator was studied on a photocurable system composed of an arbitrary amount of 10 phr of gelatin (compared with the total quantity of PEGDA). Three different phr of CQ were selected (i.e., 1, 2 and 4 phr, respectively formulations CQ1, CQ2 and CQ4 in Table 5. 1). In Figure 5.1 A are reported the photo-rheology plots of the different systems. While CQ1 showed both a slightly lower increase of the G' modulus on the first instants of irradiation and a decreased final shear storage modulus at the end of the test, no main differences were evidenced for the CQ2 and CQ4 formulations. However, even though a long time employment of CQ in dental applications is reported in literature [155,156,315], many studies proved the Norrish II photo-initiator cytotoxicity, genotoxicity and pro-apoptotic potential for cells, due to the generation of reactive oxygen species (ROS) and the subsequent DNA damage [316–318]. For this reason, the formulation containing 2 phr of CQ was selected.

To move toward DLP 3D printing, the water-soluble dye BG was added to the formulation (Figure 5.1 B). Indeed, the employment of dyes in vat 3D printing is commonly required to prevent light scattering and a possible loss in the final object resolution [319]. In the CQ2 formulation tested, different amounts of BG were added (reported on Table 5. 1). While 0.002 phr of BG resulted in a great increase of the induction time, a shorter difference was evidenced for the two other formulations both in terms of induction time and final shear storage modulus. Thus, a concentration of 0.001 phr was selected to compromise between the desired dye light absorption effect and the delay in polymerization.

Finally, the evaluation of the CFG content was assess increasing the amount of gelatin from 5 to 50 phr (Figure 5.1 C). The formulations, reported on Table 5. 1 as CFG sequence, showed optimal stability of the solution before irradiation with no precipitation of the protein. The trend in Figure 5.1 C shows a decrement in the induction time with the amount of gelatin, with minimum variations between CFG5 and CFG15 and a difference of 60 s in the delay between CFG5 and CFG50. However, sharper curves are evidenced at lower amount of gelatin (so higher rates of polymerization) probably due to the reaction mechanism. In fact, Norrish II photo-initiators (i.e., CQ) act via intermolecular H abstraction from a suitable hydrogen donors (called co-initiator) [154,320,321]. The co-

initiator role is to produce the radical by reduction of the photoinitiator (here one of the ketone group of CQ)[46]. Amines are reported as good co-initiators [154], thanks to their electron donor capacity. Then, the H-abstraction occurs if the aliphatic methylene groups are positioned in a alpha position to the amine, generating the initiating specie able to start the reaction [46]. This is why, higher initial amounts of co-initiators (gelatin) explain the lower induction time of CFG50. On contrary, the rate of polymerization depends strongly on the monomer accessibility to the forming network [322]. Moreover, high viscosity (characteristic at high gelatin/monomer ratios) strongly interfere with monomer diffusion, resulting in a decrease of rate of polymerization[323,324]. So gelatin plays a crucial role in the system reactivity as co-initiator, acting as binder into the bioink formulation [311,312] and increasing the viscosity. However, because of the excellent biocompatibility of gelatin [325], the formulations CFG50 and CFG15 were chosen as more representative for further investigations.

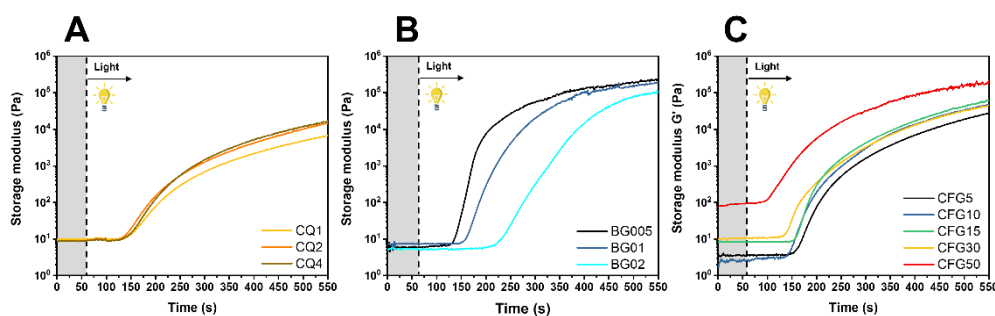


Figure 5.1: photo-rheology plots studying the influence of CQ (A), BG (B) and CFG (C) on the formulation reactivity.

The two formulations printability and viscosity were evaluated to move toward the creation of complex 3D printed structures [326]. The measured values of viscosity are reported on Table 5.2: CFG50 showed increased values due to the high amount of Gelatin, even though both formulations presented suitable values for DLP printers [226]. At this stage both the formulations were operatively tested to set the right printing parameters, reproducing simple geometries (i.e., parallelepiped or flat disks) while comparing the CAD design dimensions (Figure 5.2). In order to obtain the best CAD design fidelity, various parameters such as the light intensity, the layer thickness, and lastly, the burn-in (i.e., the time needed to ensure a full adhesion on the printing platform) and layer exposure times were optimized for the two formulations. All data are reported on Table 5.2. As comparison, a PEGDA-solo hydrogel obtained by the norrish type I initiator Bis(acyl)phosphane Oxide Photoinitiator was selected as reference [327,328]. Clearly compared to the neat PEGDA sample, long irradiation times were required for the CQ-initiated formulations to produce self-standing polymers. In particular, CFG50 hydrogel containing gelatin higher amounts showed faster reaction rate with respect to CFG15 with a reduction of the exposure time (20s

against 30s); this behavior agrees with the photo-rheology tests. Moreover, long printing times requested for the CFG50 formulation, led to a separation of gelatin clusters from the PEGDA monomer and to the production of samples presenting few inhomogeneities [329].

Table 5.2: Viscosities and optimized DLP printing parameters of the tested formulations.

	Viscosity $\eta$ ( $s^{-1}$ )	Light intensity ( $mW/cm^2$ )	Layer thickness ( $\mu m$ )	Burn-in exposure time (s)	Layer exposure time (s)
PEGDA	0.07	30	50	0.8	0.8
CFG 15	0.29	40	30	35	30
CFG 50	0.47	40	30	25	20

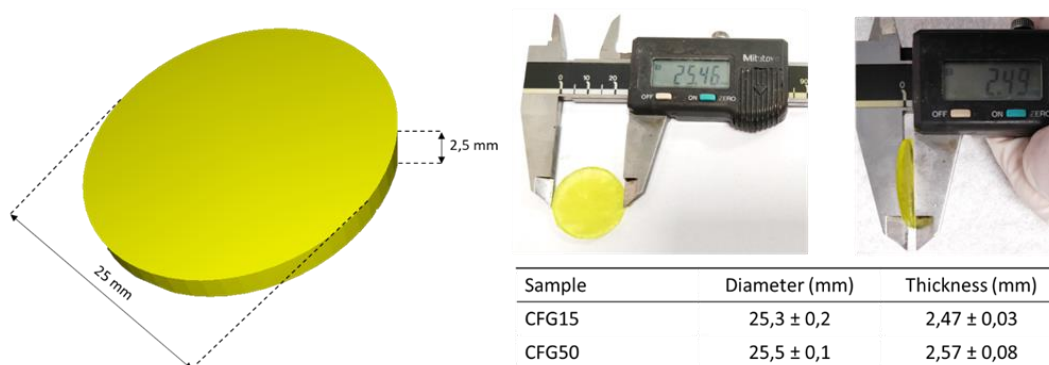


Figure 5.2: CAD fidelity of 3D printed flat disk geometry.

## Hydrogels Characterization

Once the 3D printed samples were prepared, the actual incorporation of gelatin inside of the PEGDA network was evaluated. To assess the formation of covalent bonds between the two-network component, the hydrogels were let swell in water to validate the gelatin unbounded chains extraction. The gel content (GC) was calculated and reported on Table 5.3: the crosslinking strategy is considered efficient if no or little loss of material occurs. The CFG15 and CFG50 samples were compared with hydrogels at the same reagents composition and weight ratio but using the Norrish type I photo-initiator BAPO-OH, where no covalent bonding of gelatin into the network is expected. The lower percentage of gel content for BAPO-OH photo-initiated samples (i.e., gel content of CFG15 BAPO-OH=  $93 \pm 0,3$ ; CFG50 BAPO-OH=  $79 \pm 7,2$ , compared with CFG15 and CFG50 data on Table 5.3) gives a first indication of the actual gelatin incorporation into the PEGDA network while the lower values for CFG50 (both

for CQ and BAPO-OH) are explained with a greater extraction of the clusters of unbonded gelatin.

The FT-IR spectra further confirmed the presence of gelatin inside the crosslinked network in ATR mode (Figure 5.3): the plot collected on samples CFG15 and CFG50 after extraction and drying still evidence the significant presence of the characteristic gelatin peaks ( $1650\text{ cm}^{-1}$  C=O stretching of amide I and  $1538\text{ cm}^{-1}$  N-H bending vibration of amide II) [46,330–332].

Table 5.3: Properties of the PEGDA-Gelatin hybrid networks.

	Photo-initiator	IF (%)	G' (KPa) <sup>(1)</sup>	Sw (%)	Tg (°C) <sup>(2)</sup>	E' (MPa) <sup>(2)</sup>
PEGDA	BAPO-OH	99 ± 0,6	--	90 ± 2	-34	4,5
CFG 15	CQ	97 ± 0,5	256	107 ± 1,1	-29	11,6
CFG 50	CQ	90 ± 3,9	196	73 ± 0,2	-31	62.6

(1) obtained from Amplitude sweep test on wet samples

(2) obtained from DMTA analyses after drying

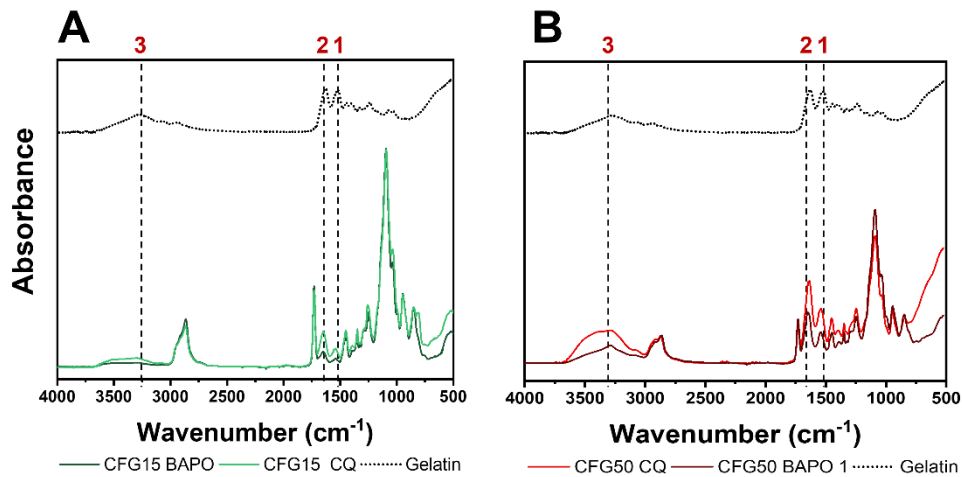


Figure 5.3: FT-IR complete spectra obtained in ATR mode of BAPO-OH and CQ photo-crosslinked CFG15 compared with gelatin and BAPO-OH and CQ photo-crosslinked CFG50 compared with gelatin. The bands relative to 1, 2 and 3 are the N-H stretching ( $3289\text{ cm}^{-1}$ ), the C=O stretching of amide I ( $1650\text{ cm}^{-1}$ ) and N-H bending vibration of amide II ( $1538\text{ cm}^{-1}$ ).

After confirming the covalent incorporation of gelatin into the hybrid system, the hydrogel properties were characterized. the first indication of the mechanical properties was certified by amplitude sweep tests (Figure 5.4 A). round and flat printed samples were employed for the test: wet CFG15 and CFG50 presented similar shear storage modulus G' values (Table 5.3) even though sample CFG 50 possess a more brittle behavior, suggested by a lower yield point [227], also clear



while handling the samples. Then, the hydrogels were dried and tested through DMTA analysis to evaluate the thermomechanical properties of the polymer network (Figure 5.4 B); on Table 7.3 are reported the  $E'$  storage modulus values at 20° C and the glass transition temperature ( $T_g$ ). Lower values of storage modulus  $E'$  are evidenced for CFG15 compared to CFG50 (CFG15 values comparable with human cartilage [236]); this behavior can be explained both with an improved crosslinking and with the higher amount of Gelatin in CFG50, considering its intrinsic modulus when dried [333]. Instead, no significant differences in the glass transition temperature were detected (variations around 4° C), probably indicating the PEGDA network's predominance, as already observed in previous works [46]. Dried samples underwent the swelling test to evaluate the network water capability; the samples containing Gelatin were compared to a neat PEGDA sample. The results show a clear difference between the different concentrations of gelatin and PEGDA hydrogels (used as reference). The swelling equilibrium (reported on Table 5.3) increased from a minimum of 73 wt% for CFG50 to 107 wt% for CFG15, while the PEGDA hydrogel showed a swelling ratio of 90 wt%. The lower absorption of water for CFG50 indicates that using Gelatin as a co-initiator enhances the crosslinking of the network. Contrarywise, CFG15 and the PEGDA hydrogel showed opposite results. The reason behind this behavior could be attributed to the stronger hydrophilicity of the gelatin chains, able to incorporate a more considerable amount of water. The faster swelling kinetic of CFG50 (Figure 5.4 C), reaching a swelling plateau after 20 min (compared to 2 h for CFG15), can support this thesis.

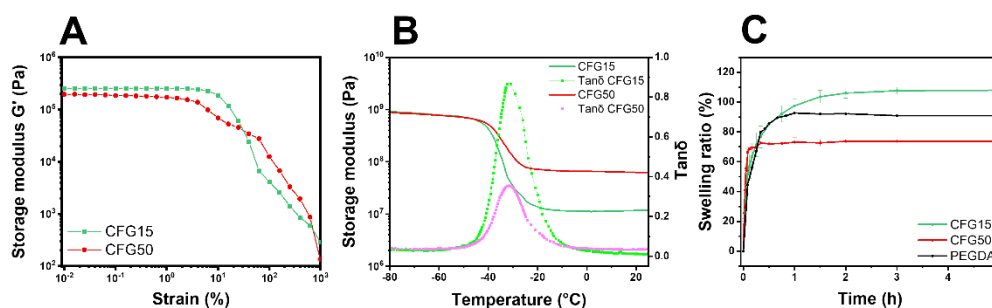


Figure 5.4: Amplitude sweep (A), DMTA analysis (B) and swelling kinetic of CFG15 and CFG50.

## Hydrogel purification, cell viability and proliferation

As visible on Figure 5.5 A, the crosslinked hydrogels after printing have an intense yellowish color due to the CQ photo-initiator. After swelling instead, the photo-initiator molecules are released in water, leaving an uncolored-opaque sample (Figure 5.5 B). As already mentioned, CQ possess cytotoxic properties, so a controlled washing of the sample is required for hydrogels dedicated to test the material's biocompatibility. To understand the time to obtain the complete

removal of residual CQ, the samples were firstly placed in 9 ml of distilled water. Envisaging the production of 3D structures water was preferred as washing solvent aiming to avoid fast evaporation of other solvents (e.g. ethanol) that may lead to the damage of the 3D shape. Considering the limited solubility of CQ in water [173], long time washings were performed. The solution was withdrawn, replaced, and analyzed with a UV-Vis spectroscope after different time intervals (1, 2, 4, and 6 days), searching for the characteristic peak of CQ around 472 nm (calibration curve on Figure 5.5 C) [334]. As expected, the peaks appeared less pronounced for each time point until no signal was detected after 6 days, while CFG15 and CFG50 samples, at the eye inspection, lost the yellowish color typical of CQ, indicating the extraction of the unreacted photo-initiator (Figure 5.5 D and E). The extracted amounts of CQ at 6 days were calculated of 59% and 47% (in respect to the initial quantity added) for CFG15 and CFG50, respectively. These values indicate that the CQ added during the preparation of the formulation is not completely consumed during the printing procedure but, on the other side, they suggest that gelatin plays a role into the CQ reaction, as theorized by the reaction mechanism.

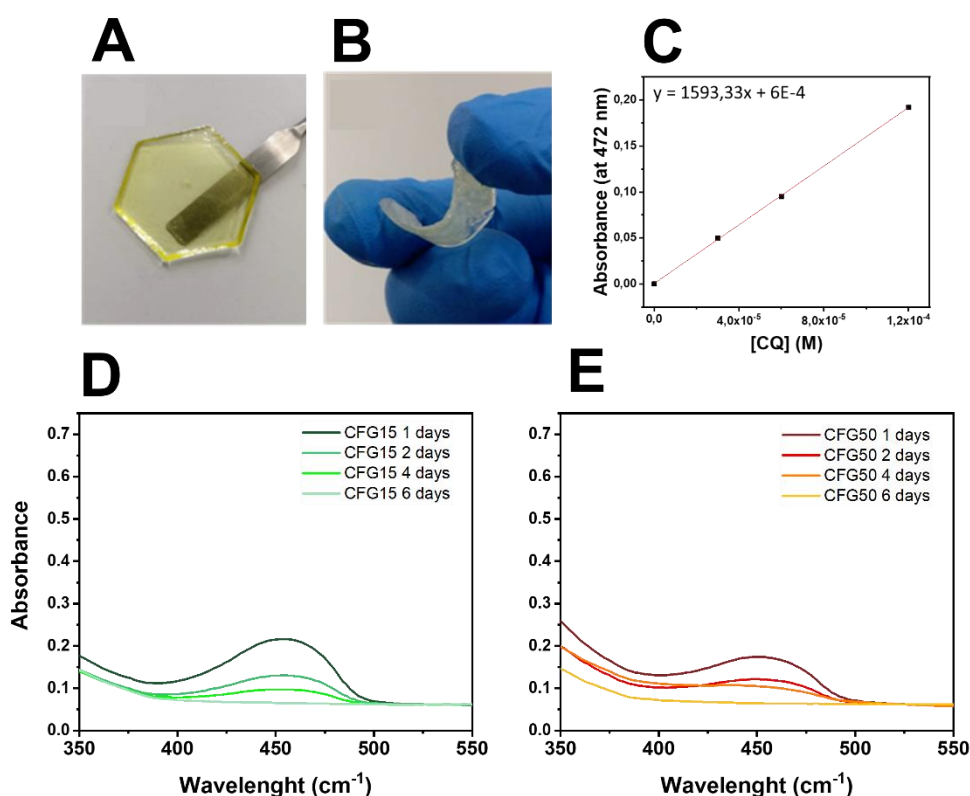


Figure 5.5: Samples before and after CQ washing (A and B, respectively). Calibration curve (C) and UV-VIS spectra at different time points for CFG15 (D) and CFG50 (E).

To test washing efficacy and the potential use of printed samples as scaffolds, proliferation was tested on cells incubated in a medium previously conditioned with PEGDA, CFG15, or CFG50. As shown in Figure 5.6, a slight decrease in cell viability was observed at 24 h for both the cell lines, even though it was less pronounced for CFG50. Nonetheless, A549 proliferation was maintained at 48 h, suggesting good biocompatibility of the scaffolds. Although MRC-5 did not show a substantial increase in proliferation, materials did not cause any cell death. Moreover, CFG50 showed higher biocompatibility compared to formulations with a lower amount of gelatin. This result suggests the removal of cytotoxic compounds from the printed samples, confirming the potential used as a substrate for cell culture. Next, A549 and MRC-5 were seeded onto printed samples and visualized at a fluorescence microscope. The two cell lines adhered better on CFG15 and CFG50, confirming the role of gelatin's adhesive moieties in cell attachment. Unfortunately, CFG50 printed disks were not homogeneous, causing cell growth in clusters (Figure 5.7).

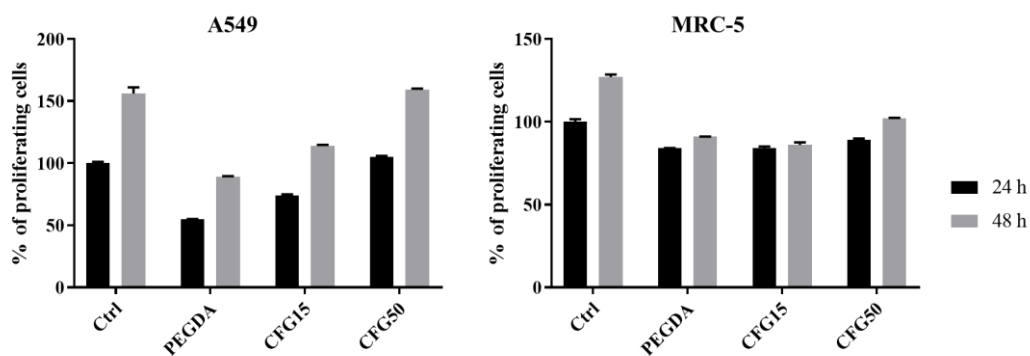
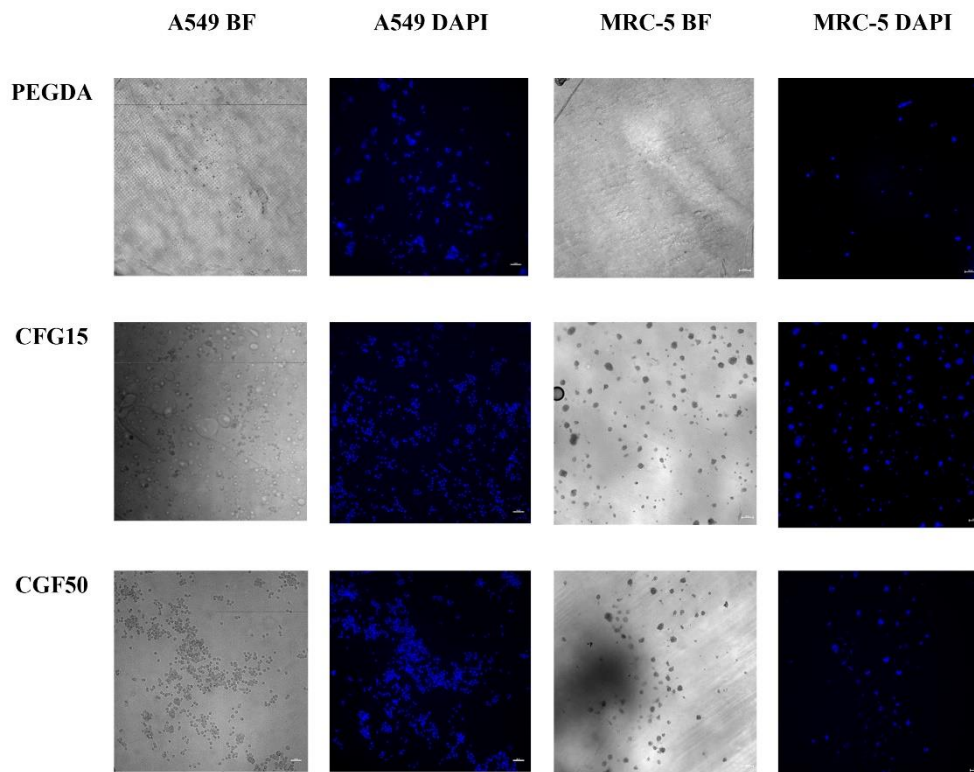
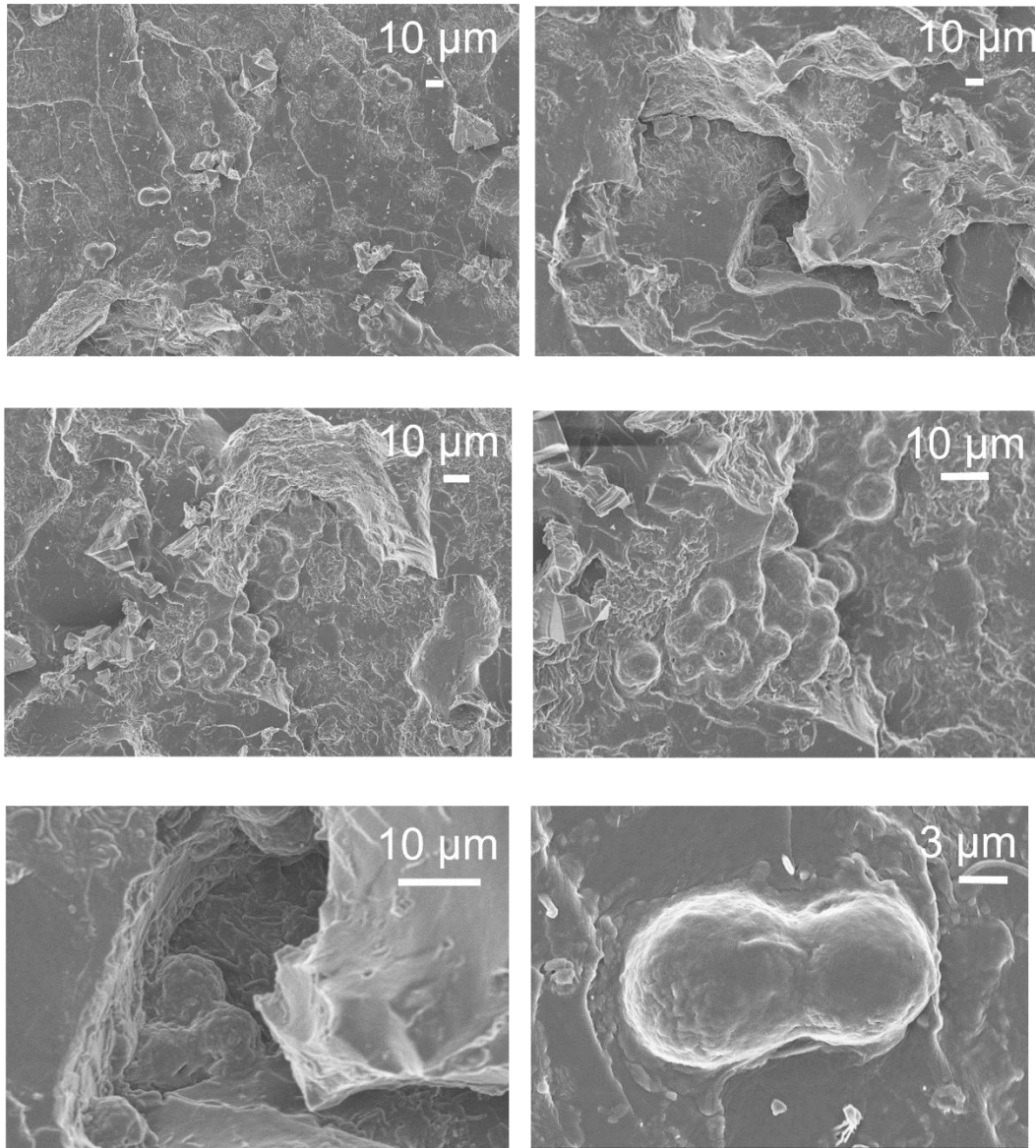


Figure 5.6: MTT assay on A549 and MRC-5 after 24h and 48h of incubation in medium conditioned with printed samples. Cells growth in a non-conditioned medium were used as the positive control. Error bars show mean SD.



*Figure 5.7: Phase-Contrast images and Fluorescence (DAPI – cell nuclei staining) of A549 and MRC-5 cell lines on the 3D printed disk prepared on PEGDA and PEGDA with different amounts of cold fish gelatin (CFG15 and CFG50). The scale bar denotes 50  $\mu\text{m}$  for all images.*

Considering the homogeneity and increased biocompatibility of CFG15, it was selected for further analysis with seeded A549 cells. The cells' morphology was investigated through FESEM images where the samples were incubated with glutaraldehyde in PBS for 1h at room temperature and then air-dried and coated 5 nm thick Pt layer. While a limited cell attachment was evidenced in the PEGDA samples, an increased number of round and healthy cells was found all over the CFG15 network, confirming the system's biocompatibility (Figure 5.8).



*Figure 5.8: FESEM images at different magnifications of A549 cell seeded CFG15 sample.*

Finally, the formulation CFG15 was selected to produce further and more complicated 3D printing geometries. The possibility to use such material with DLP printing, obtaining 3D shapes and defined patterns opens new possibilities for in vitro studies. Obviously, considering the higher PEGDA Mw 700 content, better formulation printability and final object resolution are expected compared with the chitosan hydrogels (Chitosan hydrogels), as visible also in the mechanical properties reported above. Several CAD models were successfully reproduced with the same parameters previously mentioned. The resulting

structures, such as honeycomb or hollow-lattice structures (Figure 5.9), showed defined details and the ability to withstand even after the complete water evaporation.

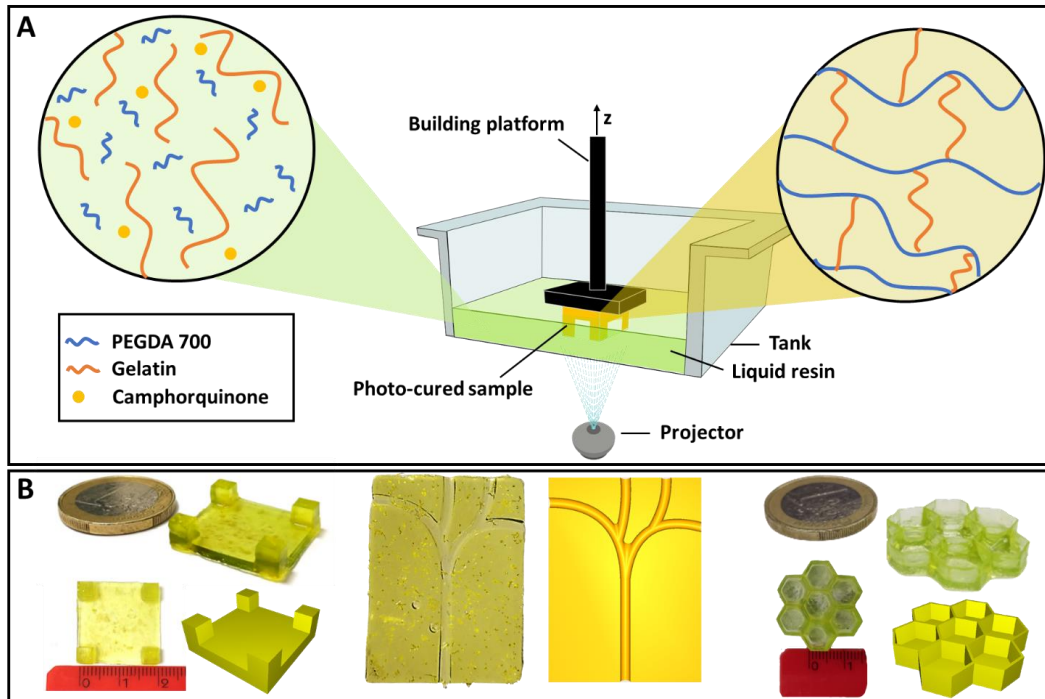


Figure 5.9: DLP scheme (A) and the CFG15 3D printed structure with the CAD as reference.

## 5.5. Conclusions

Within this chapter, the creation of hydrogels using natural polymers such as gelatin without previous modification was demonstrated. The smart implementation of this PEGDA-gelatin hybrid system using a Norrish II type photo-initiator led to the creation of stiff, biocompatible and 3D printed scaffolds for in-vivo cellular tests, with detailed and stable structures.

Modulating the formulation reagents, hydrogels with tunable photo-rheological, mechanical, swelling and biocompatible properties were created, certifying the actual incorporation of gelatin within the PEGDA network.

In conclusion, a facile and rapid method to create hydrogels for tissue engineering applications is here proposed, moving a step forward to create a promising candidate as 3D-printing ink for improved biomedical devices interfacing with cells.



# Chapter 6

## General conclusions

Within this dissertation, a wide range of chemically crosslinked hydrogels were produced through photopolymerization to create scaffolds or medical patches/surgical fillers. Indeed, the final idea of this PhD project was to expand the palette of biocompatible hydrogels materials suitable for tissue engineering applications. Among all the techniques to create crosslinked scaffold hydrogels, photopolymerization was selected as the most promising approach because it can occur at physiological conditions (pH, T, etc...).

From this starting point, the work was articulated firstly into the selection of different natural polymers (chitosan, alginate and gelatin, all exploiting advantageous features) and then to the investigation of different chemical modifications, trying to improve the synthesis steps in terms of efficiency, degree of substitution and amount of cytotoxic components employed. The photocurable methacrylic groups, the thiol-yne/ene reactions and the light-induced and spontaneous chemical incorporation of unmodified gelatin inside of a commercial ink were deeply studied. When possible, the DLP 3D printability was evaluated and optimized toward the creation of advanced patient specific scaffolds. In fact, apart for the design of new hydrogel materials, the parallel development of inks is extremely important to create detailed 3D-printed hydrogel structures able to reproduce the damaged or injured human tissues. The obtained scaffolds biocompatibility was assessed in all cases, confirming the possible employment of these material in tissue engineering applications.

The different materials and crosslinking strategies permitted to obtain numerous hydrogels presenting different and tuneable mechanical behaviours; especially these properties are really appetible for the scaffold material in order to select the most suitable choice for the target application. Indeed, tissue stiffness



can be considered as an important property able to determinate cell attachment [335]. A simple scheme of suitable human tissues matching the proposed prepared hydrogels is reported in Figure 6.1.

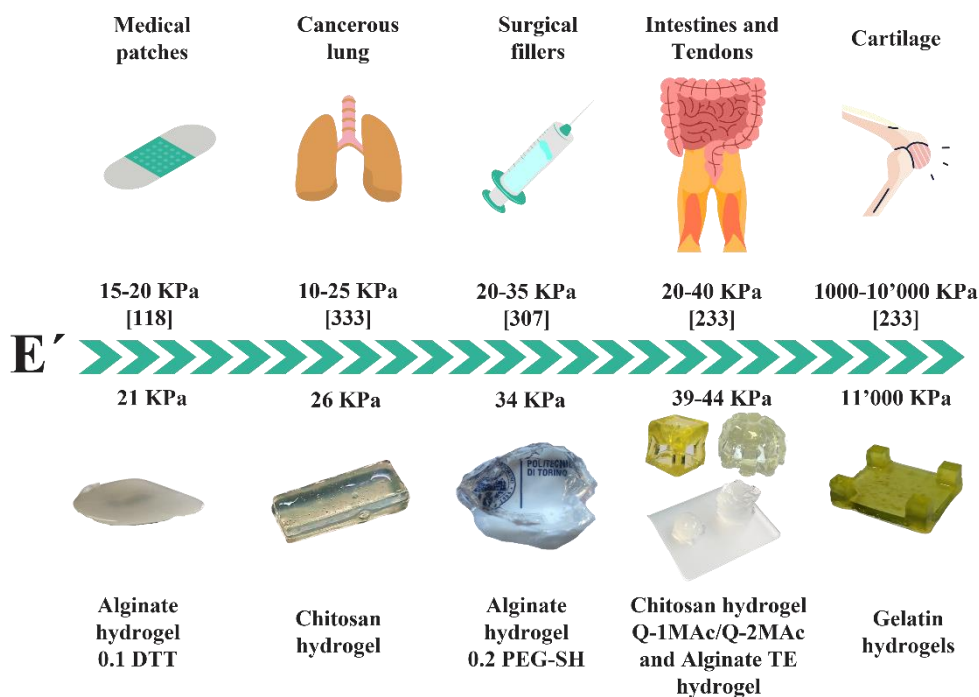


Figure 6.1: Scheme of of suitable human tissues matching the proposed prepared hydrogels [120,236,310,336].

In details, within this dissertation the successful creation of a photocurable methacrylated chitosan hydrogel is reported in the first experimental chapter (Chapter 3, Chitosan hydrogels) to promote lung cancer cell adhesion and proliferation in a 3D in-vitro model. One of the key point of this study was the employment and parameter optimization of microwave-assisted organic synthesis (MAOS) to obtain the first reported methacrylated chitosan using this technology. The product resulted in a greener and faster procedure, with low chemical waste and low energy consumption. Through this process, degree of substitution totally comparable with literature were reported using much lower molar ratios between the functionalizing agent and the aminoglucosidic ring of chitosan (stoichiometric). Then, the material was shaped by extrusion-based printing techniques. Unfortunately, the limited compound reactivity did not permit the good printability through DLP techniques. However, cell attachment and proliferation showed good results, with a strong cell colonization, certifying the enhanced biocompatibility of the synthesized material. Furthermore, the smart employment of photo-active and colored dyes extracted from the madder plant

root (quinizarin-based molecules) within the CHI-MA (methacrylated chitosan) formulation increased the system reactivity, making possible the DLP 3D printing of complex geometries. Conventionally, dyes in DLP printers are generally just used as light-scattering preventers but, herein, the choice of a photoactive molecule allowed the improvement of the crosslinking reactivity of the whole system.

The addition of the quinizarin-based dyes also enhanced the hydrogel stiffnesses and mechanical properties under sollicitation while decreasing at the same time the hydrogels swelling capability. Well-defined, structured and complex geometries were produced with a DLP 3D-printer with all the system tested, making this work the first crosslinkers-free DPL production of methacrylated chitosan hydrogels. Moreover, cell attachment and proliferation showed no differences compared to the pristine hydrogels, granting the employment of these material as scaffold in tissue engineering applications.

Nevertheless, (meth)acrylated photocurable systems are known for their reduced biocompatibility at medium-high concentrations due to their high radical propagation. “Click-chemistry” mechanisms emerged in the last years as bio-friendly reactions for the production of hydrogels in tissue engineering. On Chapter 4 (Alginate hydrogels) the implementation of a thiol-yne reaction to create alginate hydrogels is discussed. Firstly, the synthesis of an alginate-alkyne polymer was performed and optimised; afterwards two water-soluble crosslinkers (dithiothreitol and poly-ethylene glycol dithiol) were added to the solution and irradiated with visible light to form hydrogels suitable for tissue engineering applications. Modulating the type and amount of crosslinkers different rheological, mechanical, morphological, and swelling properties were obtained. The biological characterization on the two systems (cell metabolic activity and DNA quantification) proved their biocompatibility. However, small molecules such as monomers, oligomers or crosslinkers have the possibility to interact with living cells, causing the arise of cells necrosis. For this reason, the full modification of alginate incorporating both ene and thiol moieties was performed to create photocurable all-alginate hydrogels through thiol-ene reactions. Visible light irradiation enabled a facile and fast production of hydrogel with mechanical and swelling properties suitable for scaffolds while stiffnesses comparable with intestines or tendons were obtained. The biological characterization proved the high system biocompatibility and the successful usage for tissue engineering applications.

As pointed out before, natural polymers do not intrinsically possess any photo-reactive moieties, so a preliminary step of synthesis is always required. On Chapter 5 (Gelatin hydrogels) an interesting way to incorporate unmodified gelatin within a poly-ethylene glycol diacrylate network was investigated, also permitting the creation of complex DLP 3D-printed structures. Indeed, the amine groups of gelatin were employed as co-initiators in Norrish II radical photopolymerization to generate the radicals on the protein backbone through H-

abstraction and to initiate the reaction on the PEGDA oligomers. While all the hydrogels properties were evaluated (mechanical, rheological, morphological and swelling) at different amount of gelatin inside the polymer network, the successful incorporation of gelatin was assessed through ATR-FTIR spectra and comparing the hydrogel gel content with two different photo-initiators (BAPO-OH using a Norrish I radical photopolymerization and CQ). Detailed and stable structures were 3D-printed and biologically characterized, certifying the material biocompatibility and its implementation in tissue engineering.

To conclude, the results presented within this dissertation provided a complete and important contribution on two main directions emerged in the last years in tissue engineering applications: the creation of new bio-based hydrogel materials and the design of new 3D printable biocompatible inks able to reproduce finely the damaged patient tissues. Indeed, the obtained outcomes represent an interesting stimulus for future biological in-vivo test as much as clinical investigation targeting the herein proposed tissue/organs. Several tentative of in-vivo testing were already presented in literature during the last years (many of them are reported in the first chapter of this dissertation). However, a critical future challenge in the field faces the possibility of these polymeric hydrogels to promote blood vessels network formation after implantation. In fact, the possibility to transport and provide nutrients to the hydrogel formed cells colony is extremely important to integrate the engineered tissue with the rest of the body [104]. Two main techniques were recently exploited to accomplish the task: 1) local delivery of angiogenic factors (e.g., vascular endothelial growth factors [337], basic fibroblast growth factors [338], epidermal growth factors [339]), 2) co-transplanting of endothelial cells along with the target tissue cells (exploiting the unique feature of endothelial cells to spontaneously form capillary-like structures in appropriate environment [340]). The two techniques could be also integrated together during the hydrogel formation, alongside the initial gel components. Another field of application of the proposed hydrogels resides on the removal of pollutants into wastewater, due to their extreme water affinity and swelling properties. Indeed, the natural polymers considered within this manuscript possess intrinsic electrolyte moieties, able to naturally capture charged pollutants (e.g., organic molecules or heavy metals). An interesting non-related study was published by the author during the PhD considering methacrylated gelatin and chitosan for the removal of As(V) and Pb(II) from water. The results show really high removal efficiency of As(V) ions for methacrylated chitosan (98 and 92% in the case of  $C_0 = 1$  and 5 mg/L) and even better for the removal of Pb(II) by both the hydrogels (80% at  $C_0 = 75$  mg/L) [341].

# Appendix A

## A1 List of abbreviations

3D	Three dimensional
MAOS	Microwave assisted organic chemistry
DLP	Digital light processing
CAD	Computer aided design
pHEMA	Poly(2-hydroxyethyl methacrylate)
PEG	Polyethylene glycol
PVA	Polyvinyl alcohol
PAM	Poly(acrylamide)
PLLA	Poly-L-Lactic Acid
PDLA	Poly-D-Lactic Acid
IPNs	Interpenetrated polymer networks
semi-IPNs	Semi-interpenetrated polymer networks
LCST	Lower critical solution temperature
UCST	Upper critical solution temperature
PNIPAAm	Poly(N-isopropylacrylamide)
ABA	Acrylonitrile Butadiene Acrylate
PPEGMMA	Poly(poly(ethyleneglycol)methylether methacrylate)
P(AAm-co-AN)	Poly(acrylamideco-acrylonitrile)
CDs	Cyclodextrins
CBs	Cucurbiturils
Cas	Calixarenes
TG	Transglutaminase
HRP	Horseradish peroxidase

CuAAC	Copper(I)-catalyzed alkyne-azide cycloaddition
IUPAC	International Union of Pure and Applied Chemistry
T <sub>g</sub>	Glass transition temperature
DNs	Double networks
PAA	Poly(acrylic acid)
PEO	Polyethylene oxide
EMA	European medicines agency
PPA	Polyphthalamide
PEGDA	Poly(ethylene glycol) diacrylate
ECM	Extracellular matrix
CMC	Carboxymethyl-cellulose
PPII	Polyproline II-type
P(NIPAm-co-NDEAm)	Poly(N-isopropylacrylamide-co-N,N diethylacrylamide)
PhI	Photo-initiator
UV	Ultraviolet
OPA	One-photon absorption
S <sub>0</sub>	Electron ground state
S <sub>1</sub>	Electron short-life excited singlet state
T <sub>1</sub>	Electron temporary lower energetic triplet state
NTI	Norrish type I
NTII	Norrish type II
LAP	lithium phenyl-2,4,6-trimethylbenzoylphosphinate
CQ	camphorquinone
CGP	chain-growth polymerization
SGP	step-growth polymerization
AM	Additive manufacturing
STL	Strereolithography

Irgacure 2959	2-hydroxy-1-[4-(2-hydroxyethoxy)phenyl]-2-methyl-1-propanone
DNA	DeoxyriboNucleic Acid
<sup>1</sup> H-NMR	Proton nuclear magnetic resonance spectroscopy analysis
ATR-FTIR	Attenuated total reflectance-infrared spectroscopy
<sup>13</sup> C-NMR	Carbon nuclear magnetic resonance spectroscopy analysis
HSQC	Heteronuclear single quantum coherence spectroscopy
EPR	Electron paramagnetic resonance
LED	Light-emitting diode
D	Diameter
H	Height
UCS	Ultimate compression strength
$\epsilon_r$	Elongation at rupture
GC	Gel content
DI water	Deionized water
DS%	Degree of substitution %
FESEM	Field emission scanning electron microscopy
PDMS	Polydimethylsiloxane
GPC	Gel permeation chromatography
ISO	International organization for standardization
RT	Room temperature
MTT	3-(4,5-dimethylthiazol-2-yl)-2,5diphenyltetrazolium bromide
ROS	Reactive oxygen species
BAPO	Bis-acylphosphine oxide
DMTA	Dynamic thermo mechanical analysis

## **A2 List of figures**

### **Chapter 1**

Figure 1.1: Historical timeline of the most important events in hydrogels investigation.....	3
Figure 1.2: Crosslinking strategies for hydrogels formation. On the top of the image are reported the main typologies of crosslinking while on the bottom their eventual combinations. ....	4
Figure 1.3: Main properties of the crosslinking strategies compared. Increasing number of indicators means a higher value of the property. ....	10
Figure 1.4: Most common synthetic polymer and derivatives for hydrogel creation.....	13
Figure 1.5: Main properties of the two material sources polymers compared. Increasing number of indicators means a higher value of the property.....	15
Figure 1.6: Most common natural polymers used for hydrogel creation. Collagen/Gelatin is not reported cause the different amino acids unpredictable structure, strongly dependent on the extraction tissue/source. ....	18
Figure 1.7: Cell-laden/cell-seeding clinic procedure.....	21

### **Chapter 2**

Figure 2.1: Jablonski diagram illustrating the electronic states and transitions upon the one-photon absorption mechanism. ....	24
Figure 2.2: Radical generation upon light irradiation on LAP photo-initiator. ....	25
Figure 2.3: Radical generation upon light irradiation on CQ photo-initiator. ....	26
Figure 2.4: Polymerization stages involved in the polymer network/chain formation.....	27
Figure 2.5: Initiation and propagation steps of methacrylates (A), thiol-ene (B), and thiol-yne reactions (C) .....	28
Figure 2.6: extrusion-based printers set-ups. ....	31
Figure 2.7: Lithography-based printers. ....	33

### Chapter 3

Figure 3.1: Chitosan chemical structure (CHI), reaction scheme to obtain methacrylated chitosan (CHI-MA) and photo-crosslinking process. ....	44
Figure 3.2: FT-IR spectra of CHI and CHI-MA obtained at different molar ratio between reagents (A) and the nuclear magnetic resonance spectroscopy analysis on CHI-MA (B). In Figure C are plotted the degree of substitution obtained at different molar ratio (1:1 to 1:6) .....	45
Figure 3.3: % Degree of substitution of all the synthesis batches varying the microwave parameters (i.e., temperature, launch and reaction time). The obtained DS% were measured by integration of each synthesis <sup>1</sup> H-NMR spectra. ....	47
Figure 3.4: photo-rheology (A) and viscosity (B) calculated on CHI-MA DS 24 at different concentrations. On figure C and D are reported the photo-rheology and amplitude sweep plots of the CHI-MA at different degree of substitution, respectively. ....	49
Figure 3. 5: Compression (A) and swelling (B) tests on the hydrogels at different degree of substitution. The FESEM images are displayed on the middle while at the bottom of the image the Peppas-Korsmeyer (C) and Shott's (D) models are reported. ....	51
Figure 3.6: extrusion-based printer scheme, CAD model and the printed 4-layer grid. ....	52
Figure 3.7: Degradation study through gravimetric curves (A) and morphological characterization (B).....	53
Figure 3.8: Photo-rheology (A) viscosity (B) and amplitude sweep (C) of the CHI-MA:PEGDA formulations. ....	55
Figure 3.9: Swelling kinetics with a sample before and after swelling (A), absorption peaks of brilliant green (BG) at 440 and 640 nm [228,229] (B), photo-rheology of CHI-MA:PEGDA 1:1 and CHI-MA:PEGDA 1:1 with 10 <sup>-6</sup> M of BG (C) and DLP 3D printed honeycomb structure (D). ....	56
Figure 3. 10: <sup>1</sup> H-NMR spectra of Q-1MAc (A) and Q-2MAc (B) in CDCl <sub>3</sub> . ....	58
Figure 3. 11: The normalized experimental (yellow,1) and simulated (black, 2) EPR spectra obtained during 450 <sup>s</sup> in situ LED@365 nm exposure of Q-2MAc/DMSO with DMPO spin trap under argon. EPR spectrometer settings: microwave frequency, ~ 9.44 GHz; microwave power, 10.01 mW; center field, ~335.0 mT; sweep width, 7 mT; gain, 2.00*10 <sup>5</sup> ; modulation amplitude, 0.05 mT	



or 0.025 mT; sweep time, 45 s; time constant, 10.24 ms; number of scans, 10. \* represents the Q-2MAc-derived radical species (B). The normalized experimental EPR spectra measured during in situ LED@400 nm irradiation of Q-1MAc/DMSO with DMPO spin trap under argon. Exposure: (C) 225 s; (D) 450 s. EPR spectrometer settings: microwave frequency, ~ 9.43 GHz; microwave power, 1.048 mW; center field, ~336.1 mT; sweep width, 7 mT or 1.2 mT; gain,  $1.59 \times 10^5$  or  $1.00 \times 10^4$ ; modulation amplitude, 0.05 mT or 0.01 mT; sweep time, 45 or 90 s; time constant, 10.24 ms; number of scans, 5. ....59

Figure 3.12: UV-Vis spectra of mono-methacrylated quinizarin (Q-1MAc, pink), di-methacrylated quinizarin (Q-2MAc, yellow) and structure of the methacrylated quinizarin dyes Q-1MAc (left) and Q-2MAc (Right) and the appearance of their solution in DI water:DMSO 3:1 v/v (A). In Figure B, the photo-rheological measurements of CHI-PEG Q-1MAc no LAP and CHI-PEG Q-2MAc no LAP compared with the CHI-PEG formulation using LAP photo-initiator at the same concentration of the dyes. ....60

Figure 3.13: viscosity (A), photo-rheology and amplitude sweep of the CHI, CHI Q-1MAc and Q-2MAc formulations (B and C respectively), photo-rheology and amplitude sweep of the CHI-PEG, CHI-PEG Q-1MAc and CHI-PEG Q-2MAc formulations (D and E respectively) and compression E' storage modulus of all formulations. ....62

Figure 3.14: Swelling kinetic of the CHI, CHI Q-1MAc, CHI Q-2MAc, CHI-PEG, CHI-PEG Q-1MAc and CHI-PEG Q-2MAc hydrogels. The example sample before and after swelling is relative to CHI-PEG Q-2MAc.....63

Figure 3.15: Hydrogels DLP printed with the quinizarin-based formulations. The printed objects are reported in order of resolution (top to bottom) and geometry complexity (left to right). ....65

Figure 3.16: Cell proliferation of H1299 (A) and A549GFP (B) cell lines grown in normal and chitosan conditioned medium for 24 and 96 h. Cell migration of H1299 (DAPI stained) and A549GFP cell lines on chitosan scaffold after 7 days. The scale bar denotes 100 mm for all images.....66

Figure 3.17: Micrographs of C166-GFP murine endothelial cells on the surface of the different hydrogels after 72 h of incubation (A). Metabolic activity values of the C166 cell cultures for the different hydrogels after 72 h of incubation (B). DNA quantitation values of C166 cell cultures for the different hydrogels after 72 h of incubation (C). ....67

## Chapter 4

Figure 4.1: Scheme and crosslinking approaches of Thiol-Yne and Thiol-Ene reactions on Sodium Alginate.....	70
Figure 4.2: potentiometric titration of OSA 1 (A) and its first derivative (B). The image (C) shows the color change of methyl orange during NaOH titration, compared with a control sample. ....	75
Figure 4.3: Two-step reaction scheme of the yne functionalization of sodium alginate (SA-PA) by carbodiimide chemistry.....	79
Figure 4. 4: HSQC (A) and <sup>1</sup> H-NMR (B) of the alkyne functionalized sodium alginate. The propargylamine methylene is reported as (a), while the alginate anomeric methyl as (b). ....	81
Figure 4. 5: Raman (A) and ATR-FTIR (B) spectroscopy of SA-PA 4 with the alkyne bond highlighted at 2122 cm <sup>-1</sup> .....	82
Figure 4.6: Scheme of the three-steps of reaction to obtain the thiolated oxidized sodium alginate (TOSA).....	83
Figure 4. 7: ATR FT-IR (A), <sup>1</sup> H-NMR (B) and solid-state <sup>13</sup> C-NMR (C) of OSA 1. ....	84
Figure 4.8: Scheme of the two-step of reaction to obtain SA-CYS/SA-CSA. ....	86
Figure 4.9: Scheme of the two-step of reaction to obtain SA-NOR. ....	87
Figure 4.10: <sup>1</sup> H-NMR of SA-NOR. ....	88
Figure 4.11: Photo-rheology (A and C) and amplitude sweep measurements (B and D) of the DTT/S-PEG formulations, respectively. ....	91
Figure 4.12: swelling kinetics of DTT (A) and S-PEG hydrogels (B). On the bottom of the image 0.2 S-PEG hydrogel before and after washing in DI water. .	94
Figure 4.13: FESEM morphology of 0.1 DTT (A) and 0.2 S-PEG (B) hydrogels with a scale bar of 200μm. Compression test using the two water-soluble crosslinkers; the right table shows the experimental obtained values of compression elastic modulus (E'), ultimate compression strength (UCS), and elongation at rupture (ε <sub>r</sub> ). Standard deviation is reported for all data. ....	95
Figure 4.14: Photo-rheology (A), amplitude sweep (B) and compression tests of the thiol-ene hydrogel (TE hydrogel). ....	96
Figure 4.15: Swelling kinetics of the TE hydrogel. ....	97

Figure 4.16: Bright-field microscopy (A), metabolic activity (B), and DNA quantification (C) of the hydrogels. ....98

## Chapter 5

Figure 5.1: photo-rheology plots studying the influence of CQ (A), BG (B) and CFG (C) on the formulation reactivity. .... 107

Figure 5.2: CAD fidelity of 3D printed flat disk geometry. ....108

Figure 5.3: FT-IR complete spectra obtained in ATR mode of BAPO-OH and CQ photo-crosslinked CFG15 compared with gelatin and BAPO-OH and CQ photo-crosslinked CFG50 compared with gelatin. The bands relative to 1, 2 and 3 are the N-H stretching ( $3289\text{ cm}^{-1}$ ), the C=O stretching of amide I ( $1650\text{ cm}^{-1}$ ) and N-H bending vibration of amide II ( $1538\text{ cm}^{-1}$ ). .... 109

Figure 5.4: Amplitude sweep (A), DMTA analysis (B) and swelling kinetic of CFG15 and CFG50. .... 110

Figure 5.5: Samples before and after CQ washing (A and B, respectively). Calibration curve (C) and UV-VIS spectra at different time points for CFG15 (D) and CFG50 (E). .... 111

Figure 5.6: MTT assay on A549 and MRC-5 after 24h and 48h of incubation in medium conditioned with printed samples. Cells growth in a non-conditioned medium were used as the positive control. Error bars show mean SD. .... 112

Figure 5.7: Phase-Contrast images and Fluorescence (DAPI – cell nuclei staining) of A549 and MRC-5 cell lines on the 3D printed disk prepared on PEGDA and PEGDA with different amounts of cold fish gelatin (CFG15 and CFG50). The scale bar denotes  $50\text{ }\mu\text{m}$  for all images. .... 113

Figure 5.8: FESEM images at different magnifications of A549 cell seeded CFG15 sample. .... 114

Figure 5.9: DLP scheme (A) and the CFG15 3D printed structure with the CAD as reference. .... 115

## Chapter 6

Figure 6.1: Scheme of of suitable human tissues matching the proposed prepared hydrogels [120,236,310,336]. .... 118

## A3 List of tables

### Chapter 3

Table 3.1: Methacrylated chitosan microwave synthesis parameters. CHI = amino glucose ring of chitosan, MA = methacrylic anhydride.....	37
Table 3.2: Storage modulus (E), ultimate compressive strength (UCS), compression at break ( $\epsilon_r$ ), swelling equilibrium (Sw eq) and Gel content (GC) with standard deviations of the hydrogels obtained from CHI-MA at different DS%. The values of $R^2$ indicates the hydrogel behaviour's adhesion on the two proposed swelling kinetics models (only valid for $Sw_{Rt}/Sw_{Re} < 60\%$ ) while the value of n represents the Fickian or not method of solvent diffusion in the Peppas-Korsmayer model.....	50
Table 3. 3: Different CHI-MA:PEGDA investigated formulations.....	54
Table 3.4: Swelling equilibrium, gel content, storage modulus, yield point and crosslinking density of the CHI-MA:PEGDA hydrogels. ....	56
Table 3.5: Printing parameters of the selected formulation.....	57
Table 3. 6: Quinizarin-based Q-1MAc and Q-2MAc loaded formulation in a solution of DI water-DMSO (3:1, v/v). ....	61
Table 3.7: photo-rheology induction time and time-to-plateau, amplitude sweep $G'$ storage modulus and yield points, compressive $E'$ storage modulus and swelling equilibrium of the proposed formulations. ....	62
Table 3.8: Printing parameters of the quinizarin-based formulation tested (all formulation contain LAP photo-initiator).....	64

### Chapter 4

Table 4.1: Synthesis of OSA (oxidized sodium alginate). Degree of substitution obtained by potentiometric titration.....	72
Table 4. 2: Gel permeation chromatography data of sodium alginate (SA) and the three oxidized sodium alginate synthetic batches (OSA). ....	85
Table 4.3: Formulations prepared to form thiol-yne hydrogels. All formulations included: 5 wt% SA-PA-4, 2 phr (with respect to the amount of SA-PA 4) of LAP photo-initiator and were irradiated for 5 min.....	89
Table 4.4: Rheological and mechanical properties of the thiol-yne hydrogels. ....	90

Table 4.5: swelling properties of the thiol-yne hydrogels. ....93

## **Chapter 5**

Table 5. 1: Formulations composition. \*phr=per hundred resin, referred to the PEGDA weight amount. ....103

Table 5.2: Viscosities and optimized DLP printing parameters of the tested formulations. ....108

Table 5.3: Properties of the PEGDA-Gelatin hybrid networks. ....109

# Appendix B

## B1 List of publications

### Related to the PhD project

- [1] **M. Zanon** et al., Microwave-assisted methacrylation of chitosan for 3D printable hydrogels in tissue engineering, *Mater. Adv.* (2021).
- [2] **M. Zanon** et al., Visible light-induced crosslinking of unmodified gelatin with PEGDA for DLP-3D printable hydrogels, *Eur. Polym. J.* (2021).
- [3] **M. Zanon** et al., Photocurable Thiol-yne Alginate Hydrogels for Regenerative Medicine Purposes, *Polymers (Basel)*. (2022).
- [4] **M. Zanon** et al., Bioderived Dyes-Mediated Vat Photopolymerization 3D Printing of Chitosan Hydrogels for Tissue Engineering, *Additive Manufacturing* (2023).

### Unrelated to the PhD project

- [1] C. Noè, **M. Zanon** et al., UV-Cured Chitosan and Gelatin Hydrogels for the Removal of As(V) and Pb(II) from Water, *Polymers (Basel)*. (2022).

## B2 List of conferences attended by the author

- [1] **Conference Nanoday 2019**, Università degli studi di Milano Bicocca, Milan, ITA.
- [2] **Conference Virtual European Symposium of Photopolymer Science 2021**, (Poster session: Visible light induced crosslinking of unmodified gelatin with PEGDA for DLP 3D printable hydrogels).

- [3] **Conference l'era delle 3R 2021**, (Poster session: Visible light induced crosslinking of unmodified gelatin with PEGDA for DLP 3D printable hydrogels).
- [4] **Conference European Symposium of Photopolymer Science 2022**, Istanbul Technical University, Istanbul, TUR (Oral Presentation: Sustainable chitosan DLP 3D-printable hydrogels using Quinizarin-based functional “bio-dyes” for tissue engineering applications).
- [5] **Conference NGChem 2022**, Università degli studi di Cagliari, Cagliari, ITA (Oral Presentation: DLP 3D-printing of sustainable chitosan hydrogels using Quinizarin-based functional “bio-dyes” for tissue engineering applications).

# References

- [1] J.M. van Bemmelen, Das Hydrogel und das krystallinische Hydrat des Kupferoxyds, *Zeitschrift Für Anorg. Chemie.* 5 (1894) 466–483. <https://doi.org/10.1002/zaac.18940050156>.
- [2] L.R.G. Treloar, The thermodynamic study of rubber-like elasticity., *Proc. R. Soc. London. Ser. B.* 139 (1952) 506–512. <https://doi.org/10.1098/rspb.1952.0026>.
- [3] M.L. Huggins, Theory of Solutions of High Polymers, *J. Am. Chem. Soc.* 64 (1942) 1712–1719. <https://doi.org/10.1021/ja01259a068>.
- [4] M.L. Huggins, Properties of Rubber Solutions and Gels, *Ind. Eng. Chem.* 35 (1943) 216–220. <https://doi.org/10.1021/ie50398a020>.
- [5] P.J. Flory, Thermodynamics of high polymer solutions, *J. Chem. Phys.* 9 (1941) 660–661. <https://doi.org/10.1063/1.1750971>.
- [6] P.J. Flory, Network structure and the elastic properties of vulcanized rubber, *Chem. Rev.* 35 (1944) 51–75. <https://doi.org/10.1021/cr60110a002>.
- [7] P.J. Flory, Molecular Size Distribution in Three Dimensional Polymers. VI. Branched Polymers Containing A-R-Bf-1 Type Units, *J. Am. Chem. Soc.* 74 (1952) 2718–2723. <https://doi.org/10.1021/ja01131a008>.
- [8] Y. Gu, J. Zhao, J.A. Johnson, Polymer Networks: From Plastics and Gels to Porous Frameworks, *Angew. Chemie - Int. Ed.* 59 (2020) 5022–5049. <https://doi.org/10.1002/anie.201902900>.
- [9] W.H. Carothers, Polymers and polyfunctionality, *Trans. Faraday Soc.* 32 (1936) 39–49. <https://doi.org/10.1039/TF9363200039>.
- [10] W.H. Stockmayer, Theory of molecular size distribution and gel formation in branched polymers: II. General cross linking, *J. Chem. Phys.* 12 (1944) 125–131. <https://doi.org/10.1063/1.1723922>.
- [11] E.I. du P. de Nemours, Methacrylate Resins, *Ind. Eng. Chem.* (1936) 10–13.
- [12] O. Wichterle, D. Lim, Hydrophilic Gels for Biological Use, *Nature.* 185 (1960) 117–118. <https://doi.org/10.1038/185117a0>.



- [13] S.J. Buwalda, K.W.M. Boere, P.J. Dijkstra, J. Feijen, T. Vermonden, W.E. Hennink, Hydrogels in a historical perspective: From simple networks to smart materials, *J. Control. Release.* 190 (2014) 254–273. <https://doi.org/10.1016/j.jconrel.2014.03.052>.
- [14] J.W. Stafford, The radiation induced reactions of aqueous polyethylene oxide solutions. I. Theory of gelation, *Die Makromol. Chemie.* 134 (1970) 57–69. <https://doi.org/10.1002/macp.1970.021340105>.
- [15] Y. Ikada, T. Mita, F. Horii, I. Sakurada, M. Hatada, Preparation of hydrogels by radiation technique, *Radiat. Phys. Chem.* 9 (1977) 633–645. [https://doi.org/10.1016/0146-5724\(77\)90177-7](https://doi.org/10.1016/0146-5724(77)90177-7).
- [16] R.M. Nalbandian, R.L. Henry, H.S. Wilks, Artificial skin. II. Pluronic F-127 silver nitrate or silver lactate gel in the treatment of thermal burns, *J. Biomed. Mater. Res.* 6 (1972) 583–590. <https://doi.org/10.1002/jbm.820060610>.
- [17] J. Kopeček, Hydrogels: From Soft Contact Lenses and Implants to Self-Assembled Nanomaterials, *J. Polym. Sci. Part A Polym. Chem.* 47 (2009) 5929–5946. <https://doi.org/https://doi.org/10.1002/pola.23607>.
- [18] J. Kopeček, J. Vacík, D. Lím, Permeability of membranes containing ionogenic groups, *J. Polym. Sci. Part A-1 Polym. Chem.* 9 (1971) 2801–2815. <https://doi.org/10.1002/pol.1971.150091005>.
- [19] A.S. Huffman, A. Afrassiabi, L.C. Dong, Thermally reversible hydrogels: II. Delivery and selective removal of substances from aqueous solutions, *J. Control. Release.* 4 (1986) 213–222. [https://doi.org/10.1016/0168-3659\(86\)90005-2](https://doi.org/10.1016/0168-3659(86)90005-2).
- [20] Y. Ikada, K. Jamshidi, H. Tsuji, S.H. Hyon, Stereocomplex Formation between Enantiomeric Poly(lactides), *Macromolecules.* 20 (1987) 904–906. <https://doi.org/10.1021/ma00170a034>.
- [21] M.G. Cascone, B. Sim, D. Sandra, Blends of synthetic and natural polymers as drug delivery systems for growth hormone, *Biomaterials.* 16 (1995) 569–574. [https://doi.org/10.1016/0142-9612\(95\)91131-H](https://doi.org/10.1016/0142-9612(95)91131-H).
- [22] M. Santin, G. Peluso, S. Iannaces, L. Ambrosios, L. Nicolais, Synthesis and characterization of a new interpenetrated gelatin composite polymer, *Biomaterials.* 17 (1996) 1459–1467.
- [23] J.L. Drury, D.J. Mooney, Hydrogels for tissue engineering: Scaffold design variables and applications, *Biomaterials.* 24 (2003) 4337–4351.

[https://doi.org/10.1016/S0142-9612\(03\)00340-5](https://doi.org/10.1016/S0142-9612(03)00340-5).

- [24] A.G.A. Coombes, E. Verderio, B. Shaw, X. Li, M. Griffin, S. Downes, Biocomposites of non-crosslinked natural and synthetic polymers, *Biomaterials*. 23 (2002) 2113–2118. [https://doi.org/10.1016/S0142-9612\(01\)00341-6](https://doi.org/10.1016/S0142-9612(01)00341-6).
- [25] J.P. Vacanti, M.A. Morse, W.M. Saltzman, A.J. Domb, A. Perez-Atayde, R. Langer, Selective cell transplantation using bioabsorbable artificial polymers as matrices, *J. Pediatr. Surg.* 23 (1988) 3–9. [https://doi.org/10.1016/S0022-3468\(88\)80529-3](https://doi.org/10.1016/S0022-3468(88)80529-3).
- [26] J.P. Vacanti, R. Langer, Tissue engineering: The design and fabrication of living replacement devices for surgical reconstruction and transplantation, *Lancet*. 354 (1999) 32–34. [https://doi.org/10.1016/s0140-6736\(99\)90247-7](https://doi.org/10.1016/s0140-6736(99)90247-7).
- [27] B. V. Slaughter, S.S. Khurshid, O.Z. Fisher, A. Khademhosseini, N.A. Peppas, Hydrogels in regenerative medicine, *Adv. Mater.* 21 (2009) 3307–3329. <https://doi.org/10.1002/adma.200802106>.
- [28] A.S. Sawhney, C.P. Pathak, J.A. Hubbell, Photopolymerized Polyethylene glycol-co-poly( -hydroxy, *Macromolecules*. 26 (1993) 581–587.
- [29] K.T. Nguyen, J.L. West, Photopolymerizable hydrogels for tissue engineering applications, *Biomaterials*. 23 (2002) 4307–4314. [https://doi.org/10.1016/S0142-9612\(02\)00175-8](https://doi.org/10.1016/S0142-9612(02)00175-8).
- [30] L. Cai, S. Liu, J. Guo, Y.G. Jia, Polypeptide-based self-healing hydrogels: Design and biomedical applications, *Acta Biomater.* 113 (2020) 84–100. <https://doi.org/10.1016/j.actbio.2020.07.001>.
- [31] J. Chen, S. Li, Y. Zhang, W. Wang, X. Zhang, Y. Zhao, Y. Wang, H. Bi, A Reloadable Self-Healing Hydrogel Enabling Diffusive Transport of C-Dots Across Gel–Gel Interface for Scavenging Reactive Oxygen Species, *Adv. Healthc. Mater.* 6 (2017) 1–10. <https://doi.org/10.1002/adhm.201700746>.
- [32] V.M.P. Vieira, L.L. Hay, D.K. Smith, Multi-component hybrid hydrogels-understanding the extent of orthogonal assembly and its impact on controlled release, *Chem. Sci.* 8 (2017) 6981–6990. <https://doi.org/10.1039/c7sc03301j>.
- [33] N. Falcone, T. Shao, N.M.O. Andoy, R. Rashid, R.M.A. Sullan, X. Sun, H.B. Kraatz, Multi-component peptide hydrogels-a systematic study incorporating biomolecules for the exploration of diverse, tuneable biomaterials, *Biomater. Sci.* 8 (2020) 5601–5614.

<https://doi.org/10.1039/d0bm01104e>.

- [34] Q. Chen, L. Zhu, C. Zhao, Q. Wang, J. Zheng, A robust, one-pot synthesis of highly mechanical and recoverable double network hydrogels using thermoreversible sol-gel polysaccharide, *Adv. Mater.* 25 (2013) 4171–4176. <https://doi.org/10.1002/adma.201300817>.
- [35] Y. Huang, P.B. Jayathilaka, M.S. Islam, C.B. Tanaka, M.N. Silberstein, K.A. Kilian, J.J. Kruzic, Structural aspects controlling the mechanical and biological properties of tough, double network hydrogels, *Acta Biomater.* 138 (2022) 301–312. <https://doi.org/10.1016/j.actbio.2021.10.044>.
- [36] H.M.M. Nizam El-Din, A.W.M. El-Naggar, Radiation synthesis of acrylic acid/polyethyleneimine interpenetrating polymer networks (IPNs) hydrogels and its application as a carrier of atorvastatin drug for controlling cholesterol, *Eur. Polym. J.* 48 (2012) 1632–1640. <https://doi.org/10.1016/j.eurpolymj.2012.06.014>.
- [37] J. Liu, Q. Li, Y. Su, Q. Yue, B. Gao, Characterization and swelling-deswelling properties of wheat straw cellulose based semi-IPNs hydrogel, *Carbohydr. Polym.* 107 (2014) 232–240. <https://doi.org/10.1016/j.carbpol.2014.02.073>.
- [38] H. Guo, W. Dai, Y. Miao, Y. Wang, D. Ma, W. Xue, Sustained heparin release actuator achieved from thermal and water activated shape memory hydrogels containing main-chain LC units, *Chem. Eng. J.* 339 (2018) 459–467. <https://doi.org/10.1016/j.cej.2018.02.009>.
- [39] J.M. Korde, B. Kandasubramanian, Naturally biomimicked smart shape memory hydrogels for biomedical functions, *Chem. Eng. J.* 379 (2020) 122430. <https://doi.org/10.1016/j.cej.2019.122430>.
- [40] C. Tonda-Turo, I. Carmagnola, A. Chiappone, Z. Feng, G. Ciardelli, M. Hakkarainen, M. Sangermano, Photocurable chitosan as bioink for cellularized therapies towards personalized scaffold architecture, *Bioprinting.* 18 (2020) e00082. <https://doi.org/10.1016/j.bprint.2020.e00082>.
- [41] C. Garcia, A. Gallardo, D. López, C. Elvira, A. Azzahti, E. Lopez-Martinez, A.L. Cortajarena, C.M. González-Henríquez, M.A. Sarabia-Vallejos, J. Rodríguez-Hernández, Smart pH-Responsive Antimicrobial Hydrogel Scaffolds Prepared by Additive Manufacturing, *ACS Appl. Bio Mater.* 1 (2018) 1337–1347. <https://doi.org/10.1021/acsabm.8b00297>.
- [42] S. Thakur, V.K. Thakur, O.A. Arotiba, History, Classification, Properties

and Application of Hydrogels: An Overview, Springer Singapore, 2018. [https://doi.org/10.1007/978-981-10-6077-9\\_2](https://doi.org/10.1007/978-981-10-6077-9_2).

- [43] N.A. Peppas, P. Bures, W. Leobandung, H. Ichikawa, Hydrogels in pharmaceutical formulations, *Eur. J. Pharm. Biopharm.* 50 (2000) 27–46. [https://doi.org/10.1016/S0939-6411\(00\)00090-4](https://doi.org/10.1016/S0939-6411(00)00090-4).
- [44] C. Noè, C. Tonda-Turo, A. Chiappone, M. Sangermano, M. Hakkarainen, Light processable starch hydrogels, *Polymers (Basel)*. 12 (2020) 1359. <https://doi.org/10.3390/POLYM12061359>.
- [45] G. Melilli, I. Carmagnola, C. Tonda-Turo, F. Pirri, G. Ciardelli, M. Sangermano, M. Hakkarainen, A. Chiappone, DLP 3D printing meets lignocellulosic biopolymers: Carboxymethyl cellulose inks for 3D biocompatible hydrogels, *Polymers (Basel)*. 12 (2020) 1–11. <https://doi.org/10.3390/POLYM12081655>.
- [46] A. Cosola, A. Chiappone, C. Martinengo, H. Grützmacher, M. Sangermano, Gelatin type A from porcine skin used as co-initiator in a radical photo-initiating system, *Polymers (Basel)*. 11 (2019) 1–9. <https://doi.org/10.3390/polym11111901>.
- [47] Y. Yang, L. Xu, J. Wang, Q. Meng, S. Zhong, Y. Gao, X. Cui, Recent advances in polysaccharide-based self-healing hydrogels for biomedical applications, *Carbohydr. Polym.* 283 (2022) 119161. <https://doi.org/10.1016/j.carbpol.2022.119161>.
- [48] B. Peña, M. Laughter, S. Jett, T.J. Rowland, M.R.G. Taylor, L. Mestroni, D. Park, Injectable Hydrogels for Cardiac Tissue Engineering, *Macromol. Biosci.* 18 (2018) 1–22. <https://doi.org/10.1002/mabi.201800079>.
- [49] D. Cafiso, A.A. Septevani, C. Noè, T. Schiller, C.F. Pirri, I. Roppolo, A. Chiappone, 3D printing of fully cellulose-based hydrogels by digital light processing, *Sustain. Mater. Technol.* 32 (2022). <https://doi.org/10.1016/j.susmat.2022.e00444>.
- [50] G. Stojkov, Z. Niyazov, F. Picchioni, R.K. Bose, Relationship between structure and rheology of hydrogels for various applications, *Gels*. 7 (2021). <https://doi.org/10.3390/gels7040255>.
- [51] N.A. Peppas, N.K. Mongia, Ultrapure poly ( vinyl alcohol ) hydrogels with mucoadhesive delivery characteristics, 43 (1997) 51–58.
- [52] N.A. Peppas, E.W. Merrill, Poly(vinyl Alcohol) Hydrogels: Reinforcement of Radiation-Crosslinked Networks by Crystallization, 14 (1976) 441–457.

- [53] W. Hu, Z. Wang, Y. Xiao, S. Zhang, J. Wang, Advances in crosslinking strategies of biomedical hydrogels, *Biomater. Sci.* 7 (2019) 843–855. <https://doi.org/10.1039/c8bm01246f>.
- [54] W.E. Hennink, C.F. van Nostrum, Novel crosslinking methods to design hydrogels, *Adv. Drug Deliv. Rev.* 64 (2012) 223–236. <https://doi.org/10.1016/j.addr.2012.09.009>.
- [55] L. Voorhaar, R. Hoogenboom, Supramolecular polymer networks: Hydrogels and bulk materials, *Chem. Soc. Rev.* 45 (2016) 4013–4031. <https://doi.org/10.1039/c6cs00130k>.
- [56] X. Wang, F. Liu, X. Zheng, J. Sun, Water-Enabled Self-Healing of Polyelectrolyte Multilayer Coatings \*\*, (2011) 11378–11381. <https://doi.org/10.1002/anie.201105822>.
- [57] U.S. Schubert, C. Eschbaumer, Macromolecules containing bipyridine and terpyridine metal complexes: Towards metallosupramolecular polymers, *Angew. Chemie - Int. Ed.* 41 (2002) 2892–2926. [https://doi.org/10.1002/1521-3773\(20020816\)41:16<2892::AID-ANIE2892>3.0.CO;2-6](https://doi.org/10.1002/1521-3773(20020816)41:16<2892::AID-ANIE2892>3.0.CO;2-6).
- [58] H. Li, P. Yang, P. Pageni, C. Tang, Recent Advances in Metal-Containing Polymer Hydrogels, *Macromol. Rapid Commun.* 38 (2017) 1–9. <https://doi.org/10.1002/marc.201700109>.
- [59] J. Brassinne, F.D. Jochum, C.A. Fustin, J.F. Gohy, Revealing the supramolecular nature of side-chain terpyridine-functionalized polymer networks, *Int. J. Mol. Sci.* 16 (2015) 990–1007. <https://doi.org/10.3390/ijms16010990>.
- [60] H. Hofmeier, R. Hoogenboom, M.E.L. Wouters, U.S. Schubert, F. Polymers, T.N.O.I. Technology, D. Rondon, P.O. Box, High Molecular Weight Supramolecular Polymers Containing Both Terpyridine Metal Complexes and Ureidopyrimidinone Quadruple Hydrogen-Bonding Units in the Main Chain, (2005) 2597–2601.
- [61] S.J. Lue, C. Chen, C. Shih, Tuning of Lower Critical Solution Temperature (LCST) of Poly(N-Isopropylacrylamide-co-Acrylic acid) Hydrogels, *J. Macromol. Sci. Part B.* 50 (2011) 563–579. <https://doi.org/10.1080/00222341003784550>.
- [62] M.A. Haq, Y. Su, D. Wang, Mechanical properties of PNIPAM based hydrogels: A review, *Mater. Sci. Eng. C.* 70 (2017) 842–855. <https://doi.org/10.1016/j.msec.2016.09.081>.

- [63] L. Klouda, A.G. Mikos, Thermoresponsive hydrogels in biomedical applications, *Eur. J. Pharm. Biopharm.* 68 (2008) 34–45. <https://doi.org/10.1016/j.ejpb.2007.02.025>.
- [64] W. Fu, B. Zhao, Thermoreversible physically crosslinked hydrogels from UCST-type thermosensitive ABA linear triblock copolymers, *Polym. Chem.* 7 (2016) 6980–6991. <https://doi.org/10.1039/c6py01517d>.
- [65] X. Wang, J.A. Kluge, G.G. Leisk, D.L. Kaplan, Sonication-induced gelation of silk fibroin for cell encapsulation, *Biomaterials.* 29 (2008) 1054–1064. <https://doi.org/10.1016/j.biomaterials.2007.11.003>.
- [66] X. Ma, Y. Zhao, Biomedical Applications of Supramolecular Systems Based on Host-Guest Interactions, *Chem. Rev.* 115 (2015) 7794–7839. <https://doi.org/10.1021/cr500392w>.
- [67] H. Frisch, P. Besenius, pH-Switchable Self-Assembled Materials, (2014) 346–363.
- [68] M.M. Elsayed, Hydrogel Preparation Technologies : Relevance Kinetics , Thermodynamics and Scaling up Aspects, *J. Polym. Environ.* 27 (2019) 871–891. <https://doi.org/10.1007/s10924-019-01376-4>.
- [69] R. Wang, X. Huang, B. Zoetebier, P.J. Dijkstra, M. Karperien, Enzymatic co-crosslinking of star-shaped poly(ethylene glycol) tyramine and hyaluronic acid tyramine conjugates provides elastic biocompatible and biodegradable hydrogels, *Bioact. Mater.* 20 (2023) 53–63. <https://doi.org/10.1016/j.bioactmat.2022.05.020>.
- [70] S. Toledano, R.J. Williams, V. Jayawarna, R. V. Ulijn, Enzyme-triggered self-assembly of peptide hydrogels via reversed hydrolysis, *J. Am. Chem. Soc.* 128 (2006) 1070–1071. <https://doi.org/10.1021/ja056549l>.
- [71] J. Chen, J.S. Caserto, I. Ang, K. Shariati, J. Webb, B. Wang, X. Wang, N. Bouklas, M. Ma, An adhesive and resilient hydrogel for the sealing and treatment of gastric perforation, *Bioact. Mater.* 14 (2022) 52–60. <https://doi.org/10.1016/j.bioactmat.2021.11.038>.
- [72] R. Jin, L.S. Moreira Teixeira, P.J. Dijkstra, M. Karperien, C.A. van Blitterswijk, Z.Y. Zhong, J. Feijen, Injectable chitosan-based hydrogels for cartilage tissue engineering, *Biomaterials.* 30 (2009) 2544–2551. <https://doi.org/10.1016/j.biomaterials.2009.01.020>.
- [73] S. Kobayashi, Enzymatic Polymerization, *Polym. Sci. A Compr. Ref.* 10 Vol. Set. 5 (2012) 217–237. <https://doi.org/10.1016/B978-0-444-53349->

4.00137-0.

- [74] R. Jin, C. Hiemstra, Z. Zhong, J. Feijen, Enzyme-mediated fast in situ formation of hydrogels from dextran-tyramine conjugates, *Biomaterials*. 28 (2007) 2791–2800. <https://doi.org/10.1016/j.biomaterials.2007.02.032>.
- [75] B.H. Y, M. Veronique, L. Hua, Hydrogen peroxide in the human body, 486 (2000) 14–17.
- [76] C.D. Hein, X. Liu, D. Wang, Expert Review Click Chemistry , A Powerful Tool for Pharmaceutical Sciences, 25 (2008) 2216–2230. <https://doi.org/10.1007/s11095-008-9616-1>.
- [77] S. Otto, J.B.F.N. Engberts, Hydrophobic interactions and chemical reactivity, (2003) 2809–2820.
- [78] C.M. Nimmo, S.C. Owen, M.S. Shoichet, Diels - Alder Click Cross-Linked Hyaluronic Acid Hydrogels for Tissue Engineering, (2011) 824–830.
- [79] L. Liang, D. Astruc, The copper(I)-catalyzed alkyne-azide cycloaddition (CuAAC) “click” reaction and its applications. An overview, *Coord. Chem. Rev.* 255 (2011) 2933–2945. <https://doi.org/10.1016/j.ccr.2011.06.028>.
- [80] J. Xu, Y. Liu, S. hui Hsu, Hydrogels based on schiff base linkages for biomedical applications, *Molecules*. 24 (2019) 1–21. <https://doi.org/10.3390/molecules24163005>.
- [81] N.L. Morozowich, J.L. Nichol, H.R. Allcock, Hydrogels Based on Schiff Base Formation Between an Amino-Containing Polyphosphazene and Aldehyde Functionalized-Dextrans, (2016) 1–8. <https://doi.org/10.1002/pola.28184>.
- [82] M. Grootveld, B.C. Percival, J. Leenders, P.B. Wilson, Potential adverse public health effects afforded by the ingestion of dietary lipid oxidation product toxins: Significance of fried food sources, *Nutrients*. 12 (2020) 1–50. <https://doi.org/10.3390/nu12040974>.
- [83] A. Ahmed Laskar, H. Younus, Aldehyde toxicity and metabolism: the role of aldehyde dehydrogenases in detoxification, drug resistance and carcinogenesis, Taylor & Francis, 2019. <https://doi.org/10.1080/03602532.2018.1555587>.
- [84] J. Kalia, R.T. Raines, Hydrolytic stability of hydrazones and oximes, *Angew. Chemie - Int. Ed.* 47 (2008) 7523–7526. <https://doi.org/10.1002/anie.200802651>.

- [85] G.N. Grover, J. Lam, T.H. Nguyen, T. Segura, H.D. Maynard, Biocompatible hydrogels by oxime click chemistry, *Biomacromolecules*. 13 (2012) 3013–3017. <https://doi.org/10.1021/bm301346e>.
- [86] F. Lin, J. Yu, W. Tang, J. Zheng, A. Defante, K. Guo, C. Wesdemiotis, M.L. Becker, Peptide-functionalized oxime hydrogels with tunable mechanical properties and gelation behavior, *Biomacromolecules*. 14 (2013) 3749–3758. <https://doi.org/10.1021/bm401133r>.
- [87] A. Chrisnandy, D. Blondel, S. Rezakhani, N. Broguiere, M.P. Lutolf, Synthetic dynamic hydrogels promote degradation-independent in vitro organogenesis, *Nat. Mater.* 21 (2022) 479–487. <https://doi.org/10.1038/s41563-021-01136-7>.
- [88] H.P. Lee, K.A. Deo, J. Jeong, M. Namkoong, K.Y. Kuan, L. Tian, A.K. Gaharwar, Injectable , Self-healing , and 3D Printable Dynamic Hydrogels, (n.d.). <https://doi.org/10.1002/admi.202201186>.
- [89] P. Heidarian, A. Kaynak, M. Paulino, A. Zolfagharian, R.J. Varley, A.Z. Kouzani, Dynamic nanocellulose hydrogels: Recent advancements and future outlook, *Carbohydr. Polym.* 270 (2021) 118357. <https://doi.org/10.1016/j.carbpol.2021.118357>.
- [90] C.H. Lu, C.H. Yu, Y.C. Yeh, Engineering nanocomposite hydrogels using dynamic bonds, *Acta Biomater.* 130 (2021) 66–79. <https://doi.org/10.1016/j.actbio.2021.05.055>.
- [91] K. Fukao, T. Nonoyama, J.P. Gong, K. Tanaka, R. Kiyama, Hydrogels toughened by biominerals providing energy-dissipative sacrificial bonds, *J. Mater. Chem. B*. 8 (2020) 5184–5188. <https://doi.org/10.1039/d0tb00833h>.
- [92] A.D. Jenkins, R.F.T. Stepto, P. Kratochvíl, U.W. Suter, Glossary of basic terms in polymer science (IUPAC Recommendations 1996), *Pure Appl. Chem.* 68 (1996) 2287–2311. <https://doi.org/10.1351/pac199668122287>.
- [93] J.P. Gong, Why are double network hydrogels so tough?, *Soft Matter*. 6 (2010) 2583–2590. <https://doi.org/10.1039/b924290b>.
- [94] P. Matricardi, C. Di Meo, T. Coviello, W.E. Hennink, F. Alhaique, Interpenetrating polymer networks polysaccharide hydrogels for drug delivery and tissue engineering, *Adv. Drug Deliv. Rev.* 65 (2013) 1172–1187. <https://doi.org/10.1016/j.addr.2013.04.002>.
- [95] M.S. Silverstein, Interpenetrating polymer networks : So happy together ?, *Polymer (Guildf)*. 207 (2020) 122929.



<https://doi.org/10.1016/j.polymer.2020.122929>.

- [96] E.S. Dragan, Design and applications of interpenetrating polymer network hydrogels . A review, *Chem. Eng. J.* 243 (2014) 572–590. <https://doi.org/10.1016/j.cej.2014.01.065>.
- [97] R.M. Costa, S. Rauf, C.A.E. Hauser, Towards biologically relevant synthetic designer matrices in 3D bioprinting for tissue engineering and regenerative medicine, *Curr. Opin. Biomed. Eng.* 2 (2017) 90–98. <https://doi.org/10.1016/j.cobme.2017.05.001>.
- [98] EMEA Committee for Veterinary Medicinal, Polyethylene Glycols - Summary Report, (n.d.) 8–10.
- [99] M. Heskins, J.E. Guillet, Solution Properties of Poly(Nisopropylacrylamide), *J. Macromol. Sci. Part A - Chem.* (1968) 1441–1455. <https://doi.org/http://dx.doi.org/10.1080/10601326808051910>.
- [100] L.E. Bromberg, Eyal S. Ron, Temperature-responsive gels and thermogelling polymer matrices for protein and peptide delivery, *Adv. Drug Deliv. Rev.* 31 (1998) 197–221.
- [101] R.A. Stile, W.R. Burghardt, K.E. Healy, Synthesis and characterization of injectable poly(N-isopropylacrylamide)-based hydrogels that support tissue formation in vitro, *Macromolecules.* 32 (1999) 7370–7379. <https://doi.org/10.1021/ma990130w>.
- [102] C.S. Brazel, N.A. Peppas, Pulsatile local delivery of thrombolytic and antithrombotic agents using poly(N-isopropylacrylamide-co-methacrylic acid) hydrogels, *J. Control. Release.* 39 (1996) 57–64. [https://doi.org/10.1016/0168-3659\(95\)00134-4](https://doi.org/10.1016/0168-3659(95)00134-4).
- [103] G.S. Park, Poly ( vinyl alcohol ) properties and applications, *Polymer (Guildf).* 15 (1974) 1974.
- [104] K.Y. Lee, D.J. Mooney, Hydrogels for tissue engineering, *Chem. Rev.* 101 (2001) 1869–1879. <https://doi.org/10.1021/cr000108x>.
- [105] M. Caprioli, I. Roppolo, A. Chiappone, L. Larush, C.F. Pirri, S. Magdassi, 3D-printed self-healing hydrogels via Digital Light Processing, *Nat. Commun.* 12 (2021) 1–9. <https://doi.org/10.1038/s41467-021-22802-z>.
- [106] Z. Bao, C. Xian, Q. Yuan, G. Liu, J. Wu, Natural Polymer-Based Hydrogels with Enhanced Mechanical Performances: Preparation, Structure, and Property, *Adv. Healthc. Mater.* 8 (2019) 1–11. <https://doi.org/10.1002/adhm.201900670>.

- [107] K.A. Kyburz, K.S. Anseth, Synthetic Mimics of the Extracellular Matrix: How Simple is Complex Enough?, *Ann. Biomed. Eng.* 43 (2015) 489–500. <https://doi.org/10.1007/s10439-015-1297-4>.
- [108] T. Coviello, P. Matricardi, C. Marianecchi, F. Alhaique, Polysaccharide hydrogels for modified release formulations, *J. Control. Release.* 119 (2007) 5–24. <https://doi.org/10.1016/j.jconrel.2007.01.004>.
- [109] M.E. Furth, A. Atala, M.E. Van Dyke, Smart biomaterials design for tissue engineering and regenerative medicine, *Biomaterials.* 28 (2007) 5068–5073. <https://doi.org/10.1016/j.biomaterials.2007.07.042>.
- [110] X. He, W. Lu, C. Sun, H. Khalesi, A. Mata, R. Andaleeb, Y. Fang, Cellulose and cellulose derivatives : Different colloidal states and food-related applications, *Carbohydr. Polym.* 255 (2021) 117334. <https://doi.org/10.1016/j.carbpol.2020.117334>.
- [111] Y. Zhong, J. Zhou, X. Liu, L. Ding, Y. Liu, E. Bertoft, B.L. Petersen, B.R. Hamaker, K. Henrik, A. Blennow, Different genetic strategies to generate high amylose starch mutants by engineering the starch biosynthetic pathways, *Carbohydr. Polym.* 287 (2022) 119327. <https://doi.org/10.1016/j.carbpol.2022.119327>.
- [112] R. Hoover, Composition , molecular structure , and physicochemical properties of tuber and root starches : a review, 45 (2001).
- [113] P.J. Jenkins, A.M. Donald, Gelatinisation of starch: A combined SAXS/WAXS/DSC and SANS study, *Carbohydr. Res.* 308 (1998) 133–147. [https://doi.org/10.1016/S0008-6215\(98\)00079-2](https://doi.org/10.1016/S0008-6215(98)00079-2).
- [114] M. Naveed, L. Phil, M. Sohail, M. Hasnat, M. Muhammad, F. Ashraf, A. Ullah, M. Shumzaid, M. Ullah, T. Mehmood, M. Imtiaz, Q. Zhou, International Journal of Biological Macromolecules Chitosan oligosaccharide ( COS ): An overview, *Int. J. Biol. Macromol.* 129 (2019) 827–843. <https://doi.org/10.1016/j.ijbiomac.2019.01.192>.
- [115] C. Choi, J.P. Nam, J.W. Nah, Application of chitosan and chitosan derivatives as biomaterials, *J. Ind. Eng. Chem.* 33 (2016) 1–10. <https://doi.org/10.1016/j.jiec.2015.10.028>.
- [116] M.L. Pita-López, G. Fletes-Vargas, H. Espinosa-Andrews, R. Rodríguez-Rodríguez, Physically cross-linked chitosan-based hydrogels for tissue engineering applications: A state-of-the-art review, *Eur. Polym. J.* 145 (2021). <https://doi.org/10.1016/j.eurpolymj.2020.110176>.

- [117] C. Shi, Y. Zhu, X. Ran, M. Wang, Y. Su, T. Cheng, Therapeutic Potential of Chitosan and Its Derivatives in Regenerative Medicine<sup>1</sup> This work was supported by “973” programs on severe trauma (NO. 1999054205 and NO. 2005CB522605) from the Ministry of Science and Technology of China., *J. Surg. Res.* 133 (2006) 185–192. <https://doi.org/10.1016/j.jss.2005.12.013>.
- [118] S.J. Bidarra, C.C. Barrias, P.L. Granja, Injectable alginate hydrogels for cell delivery in tissue engineering, *Acta Biomater.* 10 (2014) 1646–1662. <https://doi.org/10.1016/j.actbio.2013.12.006>.
- [119] P. Gacesa, Enzymic degradation of alginates, *Int. J. Biochem.* 24 (1992) 545–552. [https://doi.org/10.1016/0020-711X\(92\)90325-U](https://doi.org/10.1016/0020-711X(92)90325-U).
- [120] K.Y. Lee, D.J. Mooney, Alginate: Properties and biomedical applications, *Prog. Polym. Sci.* 37 (2012) 106–126. <https://doi.org/10.1016/j.progpolymsci.2011.06.003>.
- [121] S. Reakasame, A.R. Boccaccini, Oxidized Alginate-Based Hydrogels for Tissue Engineering Applications: A Review, *Biomacromolecules.* 19 (2018) 3–21. <https://doi.org/10.1021/acs.biomac.7b01331>.
- [122] M.D. Shoulders, R.T. Raines, Collagen structure and stability, *Annu. Rev. Biochem.* 78 (2009) 929–958. <https://doi.org/10.1146/annurev.biochem.77.032207.120833>.
- [123] T. Ahsan, F. Harwood, K.B. McGowan, D. Amiel, R.L. Sah, Kinetics of collagen crosslinking in adult bovine articular cartilage, *Osteoarthr. Cartil.* 13 (2005) 709–715. <https://doi.org/10.1016/j.joca.2005.03.005>.
- [124] K.B. Djagny, Z. Wang, S. Xu, Gelatin: A valuable protein for food and pharmaceutical industries: Review, *Crit. Rev. Food Sci. Nutr.* 41 (2001) 481–492. <https://doi.org/10.1080/20014091091904>.
- [125] Y. Liu, J. Wang, H. Chen, D. Cheng, Science of the Total Environment Environmentally friendly hydrogel: A review of classification, preparation and application in agriculture, *Sci. Total Environ.* 846 (2022) 157303. <https://doi.org/10.1016/j.scitotenv.2022.157303>.
- [126] D. Zheng, K. Wang, B. Bai, N. Hu, H. Wang, Swelling and glyphosate-controlled release behavior of multi-responsive alginate-g-P(NIPAm-co-NDEAm)-based hydrogel, *Carbohydr. Polym.* 282 (2022). <https://doi.org/10.1016/j.carbpol.2022.119113>.
- [127] G. Jing, L. Wang, H. Yu, W.A. Amer, L. Zhang, Recent progress on study

- of hybrid hydrogels for water treatment, *Colloids Surfaces A Physicochem. Eng. Asp.* 416 (2013) 86–94. <https://doi.org/10.1016/j.colsurfa.2012.09.043>.
- [128] Z. Zhang, H. Fu, Z. Li, J. Huang, Z. Xu, Y. Lai, Hydrogel materials for sustainable water resources harvesting & treatment : Synthesis , mechanism and applications, *Chem. Eng. J.* 439 (2022) 135756. <https://doi.org/10.1016/j.cej.2022.135756>.
- [129] C. Noè, A. Cosola, A. Chiappone, M. Hakkarainen, H. Grützmacher, M. Sangermano, From polysaccharides to UV-curable biorenewable organo/hydrogels for methylene blue removal, *Polymer (Guildf)*. 235 (2021). <https://doi.org/10.1016/j.polymer.2021.124257>.
- [130] P. Yang, J.-L. Yang, K. Liu, H.J. Fan, Hydrogels Enable Future Smart Batteries, *ACS Nano*. (2022). <https://doi.org/10.1021/acsnano.2c07468>.
- [131] S. Zhao, Y. Zuo, T. Liu, S. Zhai, Y. Dai, Z. Guo, Y. Wang, Q. He, L. Xia, C. Zhi, J. Bae, K. Wang, M. Ni, Multi-Functional Hydrogels for Flexible Zinc-Based Batteries Working under Extreme Conditions, *Adv. Energy Mater.* 11 (2021) 1–29. <https://doi.org/10.1002/aenm.202101749>.
- [132] T. Ye, J. Wang, Y. Jiao, L. Li, E. He, L. Wang, Y. Li, Y. Yun, D. Li, J. Lu, H. Chen, Q. Li, F. Li, R. Gao, H. Peng, Y. Zhang, A Tissue-Like Soft All-Hydrogel Battery, *Adv. Mater.* 34 (2022). <https://doi.org/10.1002/adma.202105120>.
- [133] J. Li, D.J. Mooney, Designing hydrogels for controlled drug delivery, *Nat. Rev. Mater.* 1 (2016) 1–18. <https://doi.org/10.1038/natrevmats.2016.71>.
- [134] T.M. O’Shea, A.A. Aimetti, E. Kim, V. Yesilyurt, R. Langer, Synthesis and characterization of a library of in-situ curing, nonswelling ethoxylated polyol thiol-ene hydrogels for tailorable macromolecule delivery, *Adv. Mater.* 27 (2014) 65–72. <https://doi.org/10.1002/adma.201403724>.
- [135] F. Ullah, M. Bisyrul, F. Javed, H. Akil, Classification , processing and application of hydrogels: A review, 57 (2015) 414–433. <https://doi.org/10.1016/j.msec.2015.07.053>.
- [136] M.E. Parente, A.O. Andrade, G. Ares, F. Russo, Bioadhesive hydrogels for cosmetic applications, (2015) 511–518. <https://doi.org/10.1111/ics.12227>.
- [137] J. Kablik, G. Monheit, L. Yu, G. Chang, J. Gershkovich, Comparative Physical Properties of Hyaluronic Acid Dermal Fillers, *Dermatologic Surg.* 2010 (2010) 471–473. [https://doi.org/10.1016/s0093-3619\(09\)79411-0](https://doi.org/10.1016/s0093-3619(09)79411-0).

- [138] A. Oryan, E. Alemzadeh, A.A. Mohammadi, A. Moshiri, Healing potential of injectable Aloe vera hydrogel loaded by adipose-derived stem cell in skin tissue-engineering in a rat burn wound model, (2019).
- [139] A. Colagross-schouten, M. Lemoy, R.I. Keesler, E. Lissner, C.A. Vandervoort, The contraceptive efficacy of intravas injection of Vasalgel™ for adult male rhesus monkeys, *Basic Clin. Androl.* (2017) 1–7. <https://doi.org/10.1186/s12610-017-0048-9>.
- [140] N. Scholz, Organ donation and transplantation. Facts, figures and European Union action, (2020) 1–12.
- [141] J. Malda, J. Visser, F.P. Melchels, T. Jüngst, W.E. Hennink, W.J.A. Dhert, J. Groll, D.W. Hutmacher, 25th anniversary article: Engineering hydrogels for biofabrication, *Adv. Mater.* 25 (2013) 5011–5028. <https://doi.org/10.1002/adma.201302042>.
- [142] F.J. O'Brien, Biomaterials & scaffolds for tissue engineering, *Mater. Today.* 14 (2011) 88–95. [https://doi.org/10.1016/S1369-7021\(11\)70058-X](https://doi.org/10.1016/S1369-7021(11)70058-X).
- [143] J.L.R. Williams, Photopolymerization and photocrosslinking of polymers, *Photochemistry.* (2006) 227–250. <https://doi.org/10.1007/bfb0051134>.
- [144] S. Chatani, C.J. Kloxin, C.N. Bowman, The power of light in polymer science: Photochemical processes to manipulate polymer formation, structure, and properties, *Polym. Chem.* 5 (2014) 2187–2201. <https://doi.org/10.1039/c3py01334k>.
- [145] T.F. Scott, C.J. Kloxin, D.L. Forman, R.R. McLeod, C.N. Bowman, Principles of voxel refinement in optical direct write lithography, *J. Mater. Chem.* 21 (2011) 14150–14155. <https://doi.org/10.1039/c1jm11915j>.
- [146] S. Dadashi-Silab, S. Doran, Y. Yagci, Photoinduced Electron Transfer Reactions for Macromolecular Syntheses, *Chem. Rev.* 116 (2016) 10212–10275. <https://doi.org/10.1021/acs.chemrev.5b00586>.
- [147] M. Sangermano, I. Roppolo, A. Chiappone, New horizons in cationic photopolymerization, *Polymers* (Basel). 10 (2018). <https://doi.org/10.3390/polym10020136>.
- [148] Y. Lin, J.W. Stansbury, Near-Infrared Spectroscopy Investigation of Water Effects on the Cationic Photopolymerization of Vinyl Ether Systems, *J. Polym. Sci. Part A Polym. Chem.* 42 (2004) 1985–1998. <https://doi.org/10.1002/pola.20040>.
- [149] R.D. Pike, D.A. Sweigart, Electrophilic reactivity of coordinated cyclic  $\pi$ -

- hydrocarbons, 1999. [https://doi.org/10.1016/S0010-8545\(98\)00231-8](https://doi.org/10.1016/S0010-8545(98)00231-8).
- [150] C.J. Li, Organic reactions in Aqueous media with a focus on carbon-carbon bond formations: A decade update, 2005. <https://doi.org/10.1021/cr030009u>.
- [151] C. Fouassier, Jean Pierre;Allonas, Xavier;Lalevée, Jacques;Dietlin, Photoinitiators for Free Radical Polymerization Reactions, 2010.
- [152] T. Majima, W. Schnabel, W. Weber, Phenyl-2,4,6-trimethylbenzoylphosphinates as water-soluble photoinitiators. Generation and reactivity of O=P(C<sub>6</sub>H<sub>5</sub>)(O<sup>-</sup>) radical anions, *Die Makromol. Chemie.* 192 (1991) 2307–2315. <http://dx.doi.org/10.1002/macp.1991.021921010%5Cnhttp://doi.wiley.com/10.1002/macp.1991.021921010>.
- [153] B.D. Fairbanks, M.P. Schwartz, C.N. Bowman, K.S. Anseth, Photoinitiated polymerization of PEG-diacrylate with lithium phenyl-2,4,6-trimethylbenzoylphosphinate: polymerization rate and cytocompatibility, *Biomaterials.* 30 (2009) 6702–6707. <https://doi.org/10.1016/j.biomaterials.2009.08.055>.
- [154] E. Andrzejewska, D. Zych-Tomkowiak, M. Andrzejewski, G.L. Hug, B. Marciniak, Heteroaromatic thiols as co-initiators for type II photoinitiating systems based on camphorquinone and isopropylthioxanthone, *Macromolecules.* 39 (2006) 3777–3785. <https://doi.org/10.1021/ma060240k>.
- [155] A.A. Pérez-Mondragón, C.E. Cuevas-Suárez, J.A. González-López, N. Trejo-Carbajal, A.M. Herrera-González, Evaluation of new coinitiators of camphorquinone useful in the radical photopolymerization of dental monomers, *J. Photochem. Photobiol. A Chem.* 403 (2020). <https://doi.org/10.1016/j.jphotochem.2020.112844>.
- [156] P. Makvandi, J.T. Gu, E.N. Zare, B. Ashtari, A. Moeini, F.R. Tay, L. na Niu, Polymeric and inorganic nanoscopic antimicrobial fillers in dentistry, *Acta Biomater.* 101 (2020) 69–101. <https://doi.org/10.1016/j.actbio.2019.09.025>.
- [157] C. Decker, A.D. Jenkins, Kinetic Approach of o<sub>2</sub> Inhibition in Ultraviolet and Laser-Induced Polymerizations, *Macromolecules.* 18 (1985) 1241–1244. <https://doi.org/10.1021/ma00148a034>.
- [158] Y. Yagci, S. Jockusch, N.J. Turro, Photoinitiated polymerization: Advances, challenges, and opportunities, *Macromolecules.* 43 (2010)

6245–6260. <https://doi.org/10.1021/ma1007545>.

- [159] J. Xu, K. Jung, A. Atme, S. Shanmugam, C. Boyer, A robust and versatile photoinduced living polymerization of conjugated and unconjugated monomers and its oxygen tolerance, *J. Am. Chem. Soc.* 136 (2014) 5508–5519. <https://doi.org/10.1021/ja501745g>.
- [160] C.E. Hoyle, C.N. Bowman, Thiol-ene click chemistry, *Angew. Chemie - Int. Ed.* 49 (2010) 1540–1573. <https://doi.org/10.1002/anie.200903924>.
- [161] J.C. Kloxin, F.T. Scott, N.C. Bowman, Stress relaxation via addition fragmentation chain transfer in a thiol-ene photopolymerization, *Macromolecules.* 42 (2009) 2551–2556. <https://doi.org/10.1021/ma802771b>.
- [162] C.E. Hoyle, A.B. Lowe, C.N. Bowman, Thiol-click chemistry: A multifaceted toolbox for small molecule and polymer synthesis, *Chem. Soc. Rev.* 39 (2010) 1355–1387. <https://doi.org/10.1039/b901979k>.
- [163] B.D. Fairbanks, T.F. Scott, C.J. Kloxin, K.S. Anseth, C.N. Bowman, Thiol-yne photopolymerizations: Novel mechanism, kinetics, and step-growth formation of highly cross-linked networks, *Macromolecules.* 42 (2009) 211–217. <https://doi.org/10.1021/ma801903w>.
- [164] K.S. Lim, J.H. Galarraga, X. Cui, G.C.J. Lindberg, J.A. Burdick, T.B.F. Woodfield, Fundamentals and Applications of Photo-Cross-Linking in Bioprinting, *Chem. Rev.* 120 (2020) 10662–10694. <https://doi.org/10.1021/acs.chemrev.9b00812>.
- [165] S. Kyle, Z.M. Jessop, A. Al-Sabah, I.S. Whitaker, ‘Printability’ of Candidate Biomaterials for Extrusion Based 3D Printing: State-of-the-Art,’ *Adv. Healthc. Mater.* 6 (2017) 1–16. <https://doi.org/10.1002/adhm.201700264>.
- [166] R. Levato, T. Jungst, R.G. Scheuring, T. Blunk, J. Groll, J. Malda, From Shape to Function: The Next Step in Bioprinting, *Adv. Mater.* 32 (2020). <https://doi.org/10.1002/adma.201906423>.
- [167] J.E. Trachtenberg, J.K. Placone, B.T. Smith, C.M. Piard, M. Santoro, D.W. Scott, J.P. Fisher, A.G. Mikos, Extrusion-Based 3D Printing of Poly(propylene fumarate) in a Full-Factorial Design, *ACS Biomater. Sci. Eng.* 2 (2016) 1771–1780. <https://doi.org/10.1021/acsbiomaterials.6b00026>.
- [168] L. Shi, H. Carstensen, K. Hölzl, M. Lunzer, H. Li, J. Hilborn, A.

- Ovsianikov, D.A. Ossipov, Dynamic Coordination Chemistry Enables Free Directional Printing of Biopolymer Hydrogel, *Chem. Mater.* 29 (2017) 5816–5823. <https://doi.org/10.1021/acs.chemmater.7b00128>.
- [169] T.J. Hinton, Q. Jallerat, R.N. Palchesko, J.H. Park, M.S. Grodzicki, H.J. Shue, M.H. Ramadan, A.R. Hudson, A.W. Feinberg, Three-dimensional printing of complex biological structures by freeform reversible embedding of suspended hydrogels, *Sci. Adv.* 1 (2015). <https://doi.org/10.1126/sciadv.1500758>.
- [170] A. Lee, A.R. Hudson, D.J. Shiwarski, J.W. Tashman, T.J. Hinton, S. Yerneni, J.M. Bliley, P.G. Campbell, A.W. Feinberg, 3D bioprinting of collagen to rebuild components of the human heart, 0 (2019) 482–487.
- [171] C.B. Highley, C.B. Rodell, J.A. Burdick, Direct 3D Printing of Shear-Thinning Hydrogels into Self-Healing Hydrogels, *Adv. Mater.* 27 (2015) 5075–5079. <https://doi.org/10.1002/adma.201501234>.
- [172] L. Ouyang, C.B. Highley, W. Sun, J.A. Burdick, A Generalizable Strategy for the 3D Bioprinting of Hydrogels from Nonviscous Photo-crosslinkable Inks, *Adv. Mater.* 29 (2017) 1–7. <https://doi.org/10.1002/adma.201604983>.
- [173] W. Tomal, J. Ortyl, Water-Soluble Photoinitiators in Biomedical Applications, *Polymers (Basel)*. 12 (2020) 1–30.
- [174] K. Arcaute, B. Mann, R. Wicker, Stereolithography of spatially controlled multi-material bioactive poly(ethylene glycol) scaffolds, *Acta Biomater.* 6 (2010) 1047–1054. <https://doi.org/10.1016/j.actbio.2009.08.017>.
- [175] K.S. Lim, R. Levato, P.F. Costa, M.D. Castilho, C.R. Alcala-Orozco, K.M.A. Van Dorenmalen, F.P.W. Melchels, D. Gawlitta, G.J. Hooper, J. Malda, T.B.F. Woodfield, Bio-resin for high resolution lithography-based biofabrication of complex cell-laden constructs, *Biofabrication*. 10 (2018). <https://doi.org/10.1088/1758-5090/aac00c>.
- [176] F.P.W. Melchels, J. Feijen, D.W. Grijpma, A poly(D,L-lactide) resin for the preparation of tissue engineering scaffolds by stereolithography, *Biomaterials*. 30 (2009) 3801–3809. <https://doi.org/10.1016/j.biomaterials.2009.03.055>.
- [177] C.W. Hull, Apparatus for Production of Three-Dimensional Objects By Stereo Lithography, Patent. (1984) 16. <https://patents.google.com/patent/US4575330>.
- [178] J. Huang, Q. Qin, J. Wang, A review of stereolithography: Processes and



- systems, *Processes*. 8 (2020). <https://doi.org/10.3390/PR8091138>.
- [179] S.H. Kim, Y.K. Yeon, J.M. Lee, J.R. Chao, Y.J. Lee, Y.B. Seo, M.T. Sultan, O.J. Lee, J.S. Lee, S. Il Yoon, I.S. Hong, G. Khang, S.J. Lee, J.J. Yoo, C.H. Park, Precisely printable and biocompatible silk fibroin bioink for digital light processing 3D printing, *Nat. Commun.* 9 (2018). <https://doi.org/10.1038/s41467-018-03759-y>.
- [180] N.A. Chartrain, C.B. Williams, A.R. Whittington, A review on fabricating tissue scaffolds using vat photopolymerization, *Acta Biomater.* 74 (2018) 90–111. <https://doi.org/10.1016/j.actbio.2018.05.010>.
- [181] M. Rajabi, M. Mcconnell, J. Cabral, M.A. Ali, Chitosan hydrogels in 3D printing for biomedical applications, *Carbohydr. Polym.* 260 (2021) 117768. <https://doi.org/10.1016/j.carbpol.2021.117768>.
- [182] C.O. Kappe, Controlled microwave heating in modern organic synthesis, *Angew. Chemie - Int. Ed.* 43 (2004) 6250–6284. <https://doi.org/10.1002/anie.200400655>.
- [183] G.A. Tompsett, W.C. Conner, K.S. Yngvesson, Microwave synthesis of nanoporous materials, *ChemPhysChem.* 7 (2006) 296–319. <https://doi.org/10.1002/cphc.200500449>.
- [184] J.D. Moseley, C.O. Kappe, A critical assessment of the greenness and energy efficiency of microwave-assisted organic synthesis, *Green Chem.* 13 (2011) 794–806. <https://doi.org/10.1039/c0gc00823k>.
- [185] F.A. Bassyouni, S.M. Abu-Bakr, M.A. Rehim, Evolution of microwave irradiation and its application in green chemistry and biosciences, *Res. Chem. Intermed.* 38 (2012) 283–322. <https://doi.org/10.1007/s11164-011-0348-1>.
- [186] V.S.D. Voet, J. Guit, K. Loos, Sustainable Photopolymers in 3D Printing: A Review on Biobased, Biodegradable, and Recyclable Alternatives, *Macromol. Rapid Commun.* 42 (2021) 1–11. <https://doi.org/10.1002/marc.202000475>.
- [187] Z. Feng, M. Hakkarainen, H. Grützmacher, A. Chiappone, M. Sangermano, Photocrosslinked Chitosan Hydrogels Reinforced with Chitosan-Derived Nano-Graphene Oxide, *Macromol. Chem. Phys.* 220 (2019) 1–6. <https://doi.org/10.1002/macp.201900174>.
- [188] O.M. Kolawole, W. Man, V. V Khutoryanskiy, Methacrylated chitosan as a polymer with enhanced mucoadhesive properties for transmucosal drug

- delivery, *Int. J. Pharm.* 550 (2018) 123–129. <https://doi.org/10.1016/j.ijpharm.2018.08.034>.
- [189] Y. Shen, H. Tang, X. Huang, R. Hang, X. Zhang, Y. Wang, X. Yao, DLP printing photocurable chitosan to build bio-constructs for tissue engineering, *Carbohydr. Polym.* 235 (2020). <https://doi.org/10.1016/j.carbpol.2020.115970>.
- [190] G. Irmak, T.T. Demirtaş, M. Gumusderelioglu, Highly Methacrylated Gelatin Bioink for Bone Tissue Engineering, *ACS Biomater. Sci. Eng.* 5 (2019) 831–845. <https://doi.org/10.1021/acsbiomaterials.8b00778>.
- [191] M. Zanon, A. Chiappone, N. Garino, M. Canta, F. Frascella, M. Hakkarainen, C.F. Pirri, M. Sangermano, Microwave-assisted methacrylation of chitosan for 3D printable hydrogels in tissue engineering, *Mater. Adv.* (2021). <https://doi.org/10.1039/d1ma00765c>.
- [192] Y. He, F. Wang, X. Wang, J. Zhang, D. Wang, X. Huang, A photocurable hybrid chitosan/acrylamide bioink for DLP based 3D bioprinting, *Mater. Des.* 202 (2021) 109588. <https://doi.org/10.1016/j.matdes.2021.109588>.
- [193] Y. Lu, F. Wang, Q. Shi, J. Zhang, Z. Xiang, N. Li, X. Huang, J. Song, Three-Dimensional Printing Chitosan-Based Bolus Used for Radiotherapy, *ACS Appl. Bio Mater.* 4 (2021) 7094–7102. <https://doi.org/10.1021/acsabm.1c00701>.
- [194] M. Pagac, J. Hajnys, Q. Ma, L. Jancar, J. Jansa, P. Stefek, J. Mesicek, A Review of Vat Photopolymerization Technology: Materials, *Polymers (Basel)*. 13 (2021) 598.
- [195] M. Gastaldi, F. Cardano, M. Zanetti, G. Viscardi, C. Barolo, S. Bordiga, S. Magdassi, A. Fin, I. Roppolo, Functional Dyes in Polymeric 3D Printing: Applications and Perspectives, *ACS Mater. Lett.* 3 (2021) 1–17. <https://doi.org/10.1021/acsmaterialslett.0c00455>.
- [196] L. Breloy, V. Brezová, Z. Barbieriková, Y. Ito, J. Akimoto, A. Chiappone, S. Abbad-Andaloussi, J.P. Malval, D.L. Versace, Methacrylated Quinizarin Derivatives for Visible-Light Mediated Photopolymerization: Promising Applications in 3D-Printing Biosourced Materials under LED@405 nm, *ACS Appl. Polym. Mater.* 4 (2022) 210–228. <https://doi.org/10.1021/acsapm.1c01210>.
- [197] T. Porstmann, Measurement of Lysozyme in Human Body Fluids" Comparison of Various Enzyme Immunoassay Techniques and Their Diagnostic Application, *Clin. Biochem.* 22 (1989) 349–355.

- [198] M.M. Islam, M. Shahruzzaman, S. Biswas, M. Nurus Sakib, T.U. Rashid, Chitosan based bioactive materials in tissue engineering applications-A review, *Bioact. Mater.* 5 (2020) 164–183. <https://doi.org/10.1016/j.bioactmat.2020.01.012>.
- [199] S.H. Kim, C.C. Chu, Synthesis and characterization of dextran-methacrylate hydrogels and structural study by SEM, *J. Biomed. Mater. Res.* 49 (2000) 517–527. [https://doi.org/10.1002/\(SICI\)1097-4636\(20000315\)49:4<517::AID-JBM10>3.0.CO;2-8](https://doi.org/10.1002/(SICI)1097-4636(20000315)49:4<517::AID-JBM10>3.0.CO;2-8).
- [200] L.F. Wang, S.S. Shen, S.C. Lu, Synthesis and characterization of chondroitin sulfate-methacrylate hydrogels, *Carbohydr. Polym.* 52 (2003) 389–396. [https://doi.org/10.1016/S0144-8617\(02\)00328-4](https://doi.org/10.1016/S0144-8617(02)00328-4).
- [201] S.E. Darmon, K.M. Rudall, Infra-red and X-ray studies of chitin, *Discuss. Faraday Soc.* 9 (1950) 251–260. <https://doi.org/10.1039/DF9500900251>.
- [202] S. Samani, S. Bonakdar, A. Farzin, J. Hadjati, M. Azami, A facile way to synthesize a photocrosslinkable methacrylated chitosan hydrogel for biomedical applications, *Int. J. Polym. Mater. Polym. Biomater.* 0 (2020) 1–12. <https://doi.org/10.1080/00914037.2020.1760274>.
- [203] E.M. Sletten, C.R. Bertozzi, Bioorthogonal chemistry: Fishing for selectivity in a sea of functionality, *Angew. Chemie - Int. Ed.* 48 (2009) 6974–6998. <https://doi.org/10.1002/anie.200900942>.
- [204] D.J. Trader, E.E. Carlson, Chemoselective hydroxyl group transformation: An elusive target, *Mol. Biosyst.* 8 (2012) 2484–2493. <https://doi.org/10.1039/c2mb25122a>.
- [205] B.G. Amsden, A. Sukarto, D.K. Knight, S.N. Shapka, Methacrylated glycol chitosan as a photopolymerizable biomaterial, *Biomacromolecules.* 8 (2007) 3758–3766. <https://doi.org/10.1021/bm700691e>.
- [206] S. Hajirahimkhan, P.J. Ragona, C. (Charles) Xu, Methacrylation of kraft lignin for UV-curable coatings: Process optimization using response surface methodology, *Biomass and Bioenergy.* 120 (2019) 332–338. <https://doi.org/10.1016/j.biombioe.2018.11.038>.
- [207] X. Huang, L. Jing, S. V. Kershaw, X. Wei, H. Ning, X. Sun, A.L. Rogach, M. Gao, Narrowing the Photoluminescence of Aqueous CdTe Quantum Dots via Ostwald Ripening Suppression Realized by Programmed Dropwise Precursor Addition, *J. Phys. Chem. C.* 122 (2018) 11109–11118. <https://doi.org/10.1021/acs.jpcc.8b01053>.

- [208] S.S. Stalling, S.O. Akintoye, S.B. Nicoll, Development of photocrosslinked methylcellulose hydrogels for soft tissue reconstruction, *Acta Biomater.* 5 (2009) 1911–1918. <https://doi.org/10.1016/j.actbio.2009.02.020>.
- [209] D.E. Discher, P. Janmey, Y.L. Wang, Tissue cells feel and respond to the stiffness of their substrate, *Science* (80-. ). 310 (2005) 1139–1143. <https://doi.org/10.1126/science.1116995>.
- [210] T. Yeung, P.C. Georges, L.A. Flanagan, B. Marg, M. Ortiz, M. Funaki, N. Zahir, W. Ming, V. Weaver, P.A. Janmey, Effects of substrate stiffness on cell morphology, cytoskeletal structure, and adhesion, *Cell Motil. Cytoskeleton.* 60 (2005) 24–34. <https://doi.org/10.1002/cm.20041>.
- [211] K. Xu, K. Ganapathy, T. Andl, Z. Wang, J.A. Copland, R. Chakrabarti, S.J. Florczyk, 3D porous chitosan-alginate scaffold stiffness promotes differential responses in prostate cancer cell lines, *Biomaterials.* 217 (2019). <https://doi.org/10.1016/j.biomaterials.2019.119311>.
- [212] U.G.T.M. Sampath, Y.C. Ching, C.H. Chuah, R. Singh, P.C. Lin, Preparation and characterization of nanocellulose reinforced semi-interpenetrating polymer network of chitosan hydrogel, *Cellulose.* 24 (2017) 2215–2228. <https://doi.org/10.1007/s10570-017-1251-8>.
- [213] V.C. Shukla, N. Higueta-Castro, P. Nana-Sinkam, S.N. Ghadiali, Substrate stiffness modulates lung cancer cell migration but not epithelial to mesenchymal transition, *J. Biomed. Mater. Res. - Part A.* 104 (2016) 1182–1193. <https://doi.org/10.1002/jbm.a.35655>.
- [214] B. Bhana, R.K. Iyer, W.L.K. Chen, R. Zhao, K.L. Sider, M. Likhitpanichkul, C.A. Simmons, M. Radisic, Influence of substrate stiffness on the phenotype of heart cells, *Biotechnol. Bioeng.* 105 (2010) 1148–1160. <https://doi.org/10.1002/bit.22647>.
- [215] G. Huang, L. Wang, S. Wang, Y. Han, J. Wu, Q. Zhang, F. Xu, T.J. Lu, Engineering three-dimensional cell mechanical microenvironment with hydrogels, *Biofabrication.* 4 (2012). <https://doi.org/10.1088/1758-5082/4/4/042001>.
- [216] R.K. Farag, R.R. Mohamed, Synthesis and characterization of carboxymethyl chitosan nanogels for swelling studies and antimicrobial activity, *Molecules.* 18 (2013) 190–203. <https://doi.org/10.3390/molecules18010190>.
- [217] S.M. Taghizadeh, G. Davari, Preparation, characterization, and swelling behavior of N-acetylated and deacetylated chitosans, *Carbohydr. Polym.* 64

- (2006) 9–15. <https://doi.org/10.1016/j.carbpol.2005.10.037>.
- [218] M. Davidovich-Pinhas, H. Bianco-Peled, A quantitative analysis of alginate swelling, *Carbohydr. Polym.* 79 (2010) 1020–1027. <https://doi.org/10.1016/j.carbpol.2009.10.036>.
- [219] S.H. Medina, B. Bush, M. Cam, E. Sevcik, F.W. Delrio, K. Nandy, J.P. Schneider, Biomaterials Identification of a mechanogenetic link between substrate stiffness and chemotherapeutic response in breast cancer, *Biomaterials.* 202 (2019) 1–11. <https://doi.org/10.1016/j.biomaterials.2019.02.018>.
- [220] K.R. Levental, H. Yu, L. Kass, J.N. Lakins, M. Egeblad, J.T. Erler, S.F.T. Fong, K. Csiszar, A. Giaccia, W. Weninger, M. Yamauchi, D.L. Gasser, Matrix Crosslinking Forces Tumor Progression by Enhancing Integrin Signaling, *Cell.* 139 (2009) 891–906. <https://doi.org/10.1016/j.cell.2009.10.027>.
- [221] K. Nawrotek, M. Tylman, A. Adamus-Włodarczyk, K. Rudnicka, J. Gatkowska, M. Wieczorek, R. Wach, Influence of chitosan average molecular weight on degradation and stability of electrodeposited conduits, *Carbohydr. Polym.* 244 (2020) 116484. <https://doi.org/10.1016/j.carbpol.2020.116484>.
- [222] T. Freier, H.S. Koh, K. Kazazian, M.S. Shoichet, Controlling cell adhesion and degradation of chitosan films by N-acetylation, *Biomaterials.* 26 (2005) 5872–5878. <https://doi.org/10.1016/j.biomaterials.2005.02.033>.
- [223] C. Warr, J.C. Valdoz, B.P. Bickham, C.J. Knight, N.A. Franks, N. Chartrand, P.M. Van Ry, K.A. Christensen, G.P. Nordin, A.D. Cook, Biocompatible PEGDA Resin for 3D Printing, *ACS Appl. Bio Mater.* 3 (2020) 2239–2244. <https://doi.org/10.1021/acsabm.0c00055>.
- [224] G. Sandri, S. Rossi, M.C. Bonferoni, D. Miele, A. Faccendini, E. Del Favero, E. Di Cola, A. Icaro Cornaglia, C. Boselli, T. Luxbacher, L. Malavasi, L. Cantu, F. Ferrari, Chitosan/glycosaminoglycan scaffolds for skin reparation, *Carbohydr. Polym.* 220 (2019) 219–227. <https://doi.org/10.1016/j.carbpol.2019.05.069>.
- [225] R. Lin, Y. Chen, R. Moreno-luna, A. Khademhosseini, J.M. Melero-martin, Biomaterials Transdermal regulation of vascular network bioengineering using a photopolymerizable methacrylated gelatin hydrogel, *Biomaterials.* 34 (2013) 6785–6796. <https://doi.org/10.1016/j.biomaterials.2013.05.060>.
- [226] M. Maturi, C. Pulignani, E. Locatelli, V. Vetri Buratti, S. Tortorella, L.

- Sambri, M. Comes Franchini, Phosphorescent bio-based resin for digital light processing (DLP) 3D-printing, *Green Chem.* 22 (2020) 6212–6224. <https://doi.org/10.1039/d0gc01983f>.
- [227] D. Holthusen, P. Pértile, J.M. Reichert, R. Horn, Controlled vertical stress in a modified amplitude sweep test (rheometry) for the determination of soil microstructure stability under transient stresses, *Geoderma*. 295 (2017) 129–141. <https://doi.org/10.1016/j.geoderma.2017.01.034>.
- [228] S. Medhekar, R. Kumar, S. Mukherjee, R.K. Choubey, Study of nonlinear refraction of organic dye by Z-scan technique using He-Ne laser, *AIP Conf. Proc.* 1512 (2013) 470–471. <https://doi.org/10.1063/1.4791115>.
- [229] V. V. Tuchin, I.Y. Yanina, G. V. Simonenko, Destructive fat tissue engineering using photodynamic and selective photothermal effects, *Opt. Tissue Eng. Regen. Med.* III. 7179 (2009) 7179C. <https://doi.org/10.1117/12.812164>.
- [230] T.D. Ngo, A. Kashani, G. Imbalzano, K.T.Q. Nguyen, D. Hui, Additive manufacturing (3D printing): A review of materials, methods, applications and challenges, *Compos. Part B Eng.* 143 (2018) 172–196. <https://doi.org/10.1016/j.compositesb.2018.02.012>.
- [231] M. Layani, X. Wang, S. Magdassi, Novel Materials for 3D Printing by Photopolymerization, *Adv. Mater.* 30 (2018). <https://doi.org/10.1002/adma.201706344>.
- [232] M. Rahal, B. Graff, J. Toufaily, T. Hamieh, F. Dumur, J. Lalevée, Design of keto-coumarin based photoinitiator for Free Radical Photopolymerization: Towards 3D printing and photocomposites applications, *Eur. Polym. J.* 154 (2021). <https://doi.org/10.1016/j.eurpolymj.2021.110559>.
- [233] M. Zanon, D. Baruffaldi, M. Sangermano, C.F. Pirri, F. Frascella, A. Chiappone, Visible light-induced crosslinking of unmodified gelatin with PEGDA for DLP-3D printable hydrogels, *Eur. Polym. J.* 160 (2021). <https://doi.org/10.1016/j.eurpolymj.2021.110813>.
- [234] J. Wu, P.S. Grant, X. Li, A. Noble, V.K. Aggarwal, Catalyst-Free Deaminative Functionalizations of Primary Amines by Photoinduced Single-Electron Transfer, *Angew. Chemie.* 131 (2019) 5753–5757. <https://doi.org/10.1002/ange.201814452>.
- [235] P. Sautrot-Ba, A. Contreras, S. Abbad Andaloussi, T. Coradin, C. Hélarly, N. Razza, M. Sangermano, P.E. Mazeran, J.P. Malval, D.L. Versace,

- Eosin-mediated synthesis of polymer coatings combining photodynamic inactivation and antimicrobial properties, *J. Mater. Chem. B.* 5 (2017) 7572–7582. <https://doi.org/10.1039/c7tb01358b>.
- [236] A.M. Handorf, Y. Zhou, M.A. Halanski, W.J. Li, Tissue stiffness dictates development, homeostasis, and disease progression, *Organogenesis.* 11 (2015) 1–15. <https://doi.org/10.1080/15476278.2015.1019687>.
- [237] S. Wang, Z. Shi, L. Liu, Z. Huang, Z. Li, J. Liu, Y. Hao, Honeycomb structure is promising for the repair of human bone defects, *Mater. Des.* 207 (2021) 109832. <https://doi.org/10.1016/j.matdes.2021.109832>.
- [238] P. Kumar, B.S. Dehiya, A. Sindhu, Comparative study of chitosan and chitosan–gelatin scaffold for tissue engineering, *Int. Nano Lett.* 7 (2017) 285–290. <https://doi.org/10.1007/s40089-017-0222-2>.
- [239] J.T. Pai, C.Y. Hsu, Y.S. Hsieh, T.Y. Tsai, K.T. Hua, M.S. Weng, Suppressing migration and invasion of H1299 lung cancer cells by honokiol through disrupting expression of an HDAC6-mediated matrix metalloproteinase 9, *Food Sci. Nutr.* 8 (2020) 1534–1545. <https://doi.org/10.1002/fsn3.1439>.
- [240] V. Ansteinsson, H.B. Kopperud, E. Morisbak, J.T. Samuelsen, Cell toxicity of methacrylate monomers-The role of glutathione adduct formation, *J. Biomed. Mater. Res. - Part A.* 101 (2013) 3504–3510. <https://doi.org/10.1002/jbm.a.34652>.
- [241] M. Suh, D. Proctor, G. Chappell, J. Rager, C. Thompson, S. Borghoff, L. Finch, R. Ellis-Hutchings, K. Wiench, A review of the genotoxic, mutagenic, and carcinogenic potentials of several lower acrylates, *Toxicology.* 402–403 (2018) 50–67. <https://doi.org/10.1016/j.tox.2018.04.006>.
- [242] H.W. Ooi, C. Mota, A. Tessa Ten Cate, A. Calore, L. Moroni, M.B. Baker, Thiol-Ene Alginate Hydrogels as Versatile Biinks for Bioprinting, *Biomacromolecules.* 19 (2018) 3390–3400. <https://doi.org/10.1021/acs.biomac.8b00696>.
- [243] S. Vanslambrouck, R. Riva, B. Ucakar, V. Pr at, M. Gagliardi, D.G.M. Molin, P. Lecomte, C. J r me, Thiol-ene reaction: An efficient tool to design lipophilic polyphosphoesters for drug delivery systems, *Molecules.* 26 (2021) 1–14. <https://doi.org/10.3390/molecules26061750>.
- [244] Y. Li, X. Wang, Y. Han, H.Y. Sun, J. Hilborn, L. Shi, Click chemistry-based biopolymeric hydrogels for regenerative medicine, *Biomed. Mater.*

- 16 (2021). <https://doi.org/10.1088/1748-605X/abc0b3>.
- [245] A. Bagheri, J. Jin, Photopolymerization in 3D Printing, *ACS Appl. Polym. Mater.* 1 (2019) 593–611. <https://doi.org/10.1021/acsapm.8b00165>.
- [246] S.C. Ligon, R. Liska, J. Stampfl, M. Gurr, R. Mülhaupt, Polymers for 3D Printing and Customized Additive Manufacturing, *Chem. Rev.* 117 (2017) 10212–10290. <https://doi.org/10.1021/acs.chemrev.7b00074>.
- [247] Z. Emami, M. Ehsani, M. Zandi, R. Foudazi, Controlling alginate oxidation conditions for making alginate-gelatin hydrogels, *Carbohydr. Polym.* 198 (2018) 509–517. <https://doi.org/10.1016/j.carbpol.2018.06.080>.
- [248] M. Zanon, L. Montalvillo-jim, P. Bosch, R. Cue-l, E. Mart, M. Sangermano, A. Chiappone, Photocurable Thiol – yne Alginate Hydrogels for Regenerative Medicine Purposes, *Polymers (Basel)*. 14 (2022). <https://doi.org/https://doi.org/10.3390/polym14214709>.
- [249] J. Wu, J. Ye, Q. Xie, B. Liu, M. Liu, Targeting Regulated Cell Death with Pharmacological Small Molecules: An Update on Autophagy-Dependent Cell Death, Ferroptosis, and Necroptosis in Cancer, *J. Med. Chem.* 65 (2022) 2989–3001. <https://doi.org/10.1021/acs.jmedchem.1c01572>.
- [250] Y. Bai, H.C. Lam, X. Lei, Dissecting Programmed Cell Death with Small Molecules, *Acc. Chem. Res.* 53 (2020) 1034–1045. <https://doi.org/10.1021/acs.accounts.9b00600>.
- [251] Z.S. Guo, P. Kalinski, H. Chen, Z. Zhu, Immunogenic cell death-inducing small molecule inhibitors: Potential for immunotherapy of cancer, *Clin. Transl. Discov.* 2 (2022) 10–13. <https://doi.org/10.1002/ctd2.69>.
- [252] R.G. Huamani-Palomino, C.R. Jacinto, H. Alarcón, I.M. Mejía, R.C. López, D. de O. Silva, E.T.G. Cavalheiro, T. Venâncio, J.Z. Dávalos, A.C. Valderrama, Chemical modification of alginate with cysteine and its application for the removal of Pb(II) from aqueous solutions, *Int. J. Biol. Macromol.* 129 (2019) 1056–1068. <https://doi.org/10.1016/j.ijbiomac.2018.09.096>.
- [253] S. Bian, M. He, J. Sui, H. Cai, Y. Sun, J. Liang, Y. Fan, X. Zhang, The self-crosslinking smart hyaluronic acid hydrogels as injectable three-dimensional scaffolds for cells culture, *Colloids Surfaces B Biointerfaces.* 140 (2016) 392–402. <https://doi.org/10.1016/j.colsurfb.2016.01.008>.
- [254] R.G. Huamani-Palomino, B.M. Córdova, L. Elvis Renzo Pichilingue, T. Venâncio, A.C. Valderrama, Functionalization of an alginate-based



- material by oxidation and reductive amination, *Polymers (Basel)*. 13 (2021) 1–15. <https://doi.org/10.3390/polym13020255>.
- [255] C.M.Q. Le, F. Morlet-Savary, A. Chemtob, Role of thiol oxidation by air in the mechanism of the self-initiated thermal thiol-ene polymerization, *Polym. Chem.* 12 (2021) 6594–6605. <https://doi.org/10.1039/d1py01301g>.
- [256] S.W. Griffiths, J. King, C.L. Cooney, The reactivity and oxidation pathway of cysteine 232 in recombinant human  $\alpha$ 1-antitrypsin, *J. Biol. Chem.* 277 (2002) 25486–25492. <https://doi.org/10.1074/jbc.M203089200>.
- [257] D. Schilter, Thiol oxidation: A slippery slope, *Nat. Rev. Chem.* 1 (2017) 1–2. <https://doi.org/10.1038/s41570-016-0013>.
- [258] J.S. Fritz, E.C. Bradford, S.S. Yamamura, Determination of Carbonyl Compounds, *Anal. Chem.* 31 (1959) 260–263. <https://doi.org/10.1021/ac60146a032>.
- [259] C. Mohan, A guide for the preparation and use of, (2014).
- [260] R.W. Barrs, J. Jia, M. Ward, D.J. Richards, H. Yao, M.J. Yost, Y. Mei, Engineering a Chemically Defined Hydrogel Bioink for Direct Bioprinting of Microvasculature, *Biomacromolecules*. 22 (2021) 275–288. <https://doi.org/10.1021/acs.biomac.0c00947>.
- [261] I.C. Carvalho, A.A.P. Mansur, S.M. Carvalho, R.M. Florentino, H.S. Mansur, L-cysteine and poly-L-arginine grafted carboxymethyl cellulose/Ag-In-S quantum dot fluorescent nanohybrids for in vitro bioimaging of brain cancer cells, *Int. J. Biol. Macromol.* 133 (2019) 739–753. <https://doi.org/10.1016/j.ijbiomac.2019.04.140>.
- [262] G. Lawrie, I. Keen, B. Drew, A. Chandler-Temple, L. Rintoul, P. Fredericks, L. Grøndahl, Interactions between alginate and chitosan biopolymers characterized using FTIR and XPS, *Biomacromolecules*. 8 (2007) 2533–2541. <https://doi.org/10.1021/bm070014y>.
- [263] N.V. Bhagavan, C.-E. Ha, *Essentials of Medical Biochemistry*, 2015.
- [264] J.C. Breger, B. Fisher, R. Samy, S. Pollack, N.S. Wang, I. Isayeva, Synthesis of “click” alginate hydrogel capsules and comparison of their stability, water swelling, and diffusion properties with that of Ca<sup>2+</sup> crosslinked alginate capsules, (2014) 1120–1132. <https://doi.org/10.1002/jbm.b.33282>.
- [265] F. Inagaki, K. Maeda, K. Nakazawa, C. Mukai, Construction of the Oxazolidinone Framework from Propargylamine and CO<sub>2</sub> in Air at

Ambient Temperature: Catalytic Effect of a Gold Complex Featuring an L2/Z-Type Ligand, *European J. Org. Chem.* 2018 (2018) 2972–2976. <https://doi.org/10.1002/ejoc.201800228>.

- [266] H. Durand, I. Baussanne, M. Demeunynck, J. Viger-Gravel, L. Emsley, M. Bardet, E. Zeno, N. Belgacem, J. Bras, Two-step immobilization of metronidazole prodrug on TEMPO cellulose nanofibrils through thiol-yne click chemistry for in situ controlled release, *Carbohydr. Polym.* 262 (2021). <https://doi.org/10.1016/j.carbpol.2021.117952>.
- [267] G. Mangiante, P. Alcouffe, B. Burdin, M. Gaborieau, E. Zeno, M. Petit-Conil, J. Bernard, A. Charlot, E. Fleury, Green nondegrading approach to alkyne-functionalized cellulose fibers and biohybrids thereof: Synthesis and mapping of the derivatization, *Biomacromolecules.* 14 (2013) 254–263. <https://doi.org/10.1021/bm3016829>.
- [268] M. Dalheim, A.S.T. Ulset, I.B. Jenssen, B.E. Christensen, Degradation kinetics of peptide-coupled alginates prepared via the periodate oxidation reductive amination route, *Carbohydr. Polym.* 157 (2017) 1844–1852. <https://doi.org/10.1016/j.carbpol.2016.11.068>.
- [269] H. Zhao, N.D. Heindel, Determination of Degree of Substitution of Formyl Groups in Polyaldehyde Dextran by the Hydroxylamine Hydrochloride Method, *Pharm. Res. An Off. J. Am. Assoc. Pharm. Sci.* 8 (1991) 400–402. <https://doi.org/10.1023/A:1015866104055>.
- [270] A. Jejurikar, X.T. Seow, G. Lawrie, D. Martin, A. Jayakrishnan, L. Grøndahl, Degradable alginate hydrogels crosslinked by the macromolecular crosslinker alginate dialdehyde, *J. Mater. Chem.* 22 (2012) 9751–9758. <https://doi.org/10.1039/c2jm30564j>.
- [271] C.G. Gomez, M. Rinaudo, M.A. Villar, Oxidation of sodium alginate and characterization of the oxidized derivatives, *Carbohydr. Polym.* 67 (2007) 296–304. <https://doi.org/10.1016/j.carbpol.2006.05.025>.
- [272] K.H. Bouhadir, K.Y. Lee, E. Alsberg, K.L. Damm, K.W. Anderson, D.J. Mooney, Degradation of partially oxidized alginate and its potential application for tissue engineering, *Biotechnol. Prog.* 17 (2001) 945–950. <https://doi.org/10.1021/bp010070p>.
- [273] S. Hauptstein, S. Dezorzi, F. Prüfert, B. Matuszczak, A. Bernkop-Schnürch, Synthesis and in vitro characterization of a novel S-protected thiolated alginate, *Carbohydr. Polym.* 124 (2015) 1–7. <https://doi.org/10.1016/j.carbpol.2015.01.049>.

- [274] C. Le-Tien, M. Millette, M. Lacroix, M.-A. Mateescu, Modified alginate matrices for the immobilization of bioactive agents, *Biotechnol. Appl. Biochem.* 39 (2004) 189. <https://doi.org/10.1042/ba20030054>.
- [275] A.B. Baxter, Ellen W.; Reitz, Reductive Aminations of Carbonyl Compounds with Borohydride and Borane Reducing Agents, *Org. React.* 59 (2001). <https://doi.org/10.1093/jaoac/36.3.1036>.
- [276] M. Dalheim, J. Vanacker, M.A. Najmi, F.L. Aachmann, B.L. Strand, B.E. Christensen, Efficient functionalization of alginate biomaterials, *Biomaterials.* 80 (2016) 146–156. <https://doi.org/10.1016/j.biomaterials.2015.11.043>.
- [277] A. Bernkop-Schnürch, Thiomers: A new generation of mucoadhesive polymers, *Adv. Drug Deliv. Rev.* 57 (2005) 1569–1582. <https://doi.org/10.1016/j.addr.2005.07.002>.
- [278] J. Battersby, R. Clark, W. Hancock, E. Puchulu-campanella, N. Haggarty, D. Poll, D. Harding, controlled release Sustained release of recombinant human growth hormone from dextran via hydrolysis of an imine bond, 42 (1996) 143–156.
- [279] S. Dünnhaupt, J. Barthelmes, C.C. Thurner, C. Waldner, D. Sakloetsakun, A. Bernkop-Schnürch, S-protected thiolated chitosan: Synthesis and in vitro characterization, *Carbohydr. Polym.* 90 (2012) 765–772. <https://doi.org/10.1016/j.carbpol.2012.05.028>.
- [280] T.F. Palmberger, K. Albrecht, B. Loretz, A. Bernkop-Schnürch, Thiolated polymers: Evaluation of the influence of the amount of covalently attached l-cysteine to poly(acrylic acid), *Eur. J. Pharm. Biopharm.* 66 (2007) 405–412. <https://doi.org/10.1016/j.ejpb.2006.11.017>.
- [281] E. Guzmán, R.G. Rubio, F. Ortega, A closer physico-chemical look to the Layer-by-Layer electrostatic self-assembly of polyelectrolyte multilayers, 282 (2020). <https://doi.org/10.1016/j.cis.2020.102197>.
- [282] A. Hansson, N. Hashom, P. Rousselle, O. Jordan, G. Borchard, In vitro evaluation of an RGD-functionalized chitosan derivative for enhanced cell adhesion, 90 (2012) 1494–1500. <https://doi.org/10.1016/j.carbpol.2012.07.020>.
- [283] U. Jakob, D. Reichmann, Oxidative stress and Redox regulation, *Oxidative Stress Redox Regul.* 9789400757 (2013) 1–483. <https://doi.org/10.1007/978-94-007-5787-5>.

- [284] J. Bolander, C. Mota, H.W. Ooi, H. Agten, M.B. Baker, L. Moroni, F.P. Luyten, Bioinspired Development of an In Vitro Engineered Fracture Callus for the Treatment of Critical Long Bone Defects, *Adv. Funct. Mater.* 31 (2021). <https://doi.org/10.1002/adfm.202104159>.
- [285] R.M. Desai, S.T. Koshy, S.A. Hilderbrand, D.J. Mooney, N.S. Joshi, Versatile click alginate hydrogels crosslinked via tetrazine-norbornene chemistry, *Biomaterials.* 50 (2015) 30–37. <https://doi.org/10.1016/j.biomaterials.2015.01.048>.
- [286] T. Geuens, F.A.A. Ruiters, A. Schumacher, F.L.C. Morgan, T. Rademakers, L.E. Wiersma, C.W. van den Berg, T.J. Rabelink, M.B. Baker, V.L.S. LaPointe, Thiol-ene cross-linked alginate hydrogel encapsulation modulates the extracellular matrix of kidney organoids by reducing abnormal type 1a1 collagen deposition, *Biomaterials.* 275 (2021) 120976. <https://doi.org/10.1016/j.biomaterials.2021.120976>.
- [287] C. Lin, C.S. Ki, H. Shih, Thiol – Norbornene Photoclick Hydrogels for Tissue Engineering Applications, 41563 (2015) 1–11. <https://doi.org/10.1002/app.41563>.
- [288] A.B. Lowe, E. Hoyle, C.N. Bowman, Thiol-yne click chemistry: A powerful and versatile methodology for materials synthesis, (2010) 4745–4750. <https://doi.org/10.1039/b917102a>.
- [289] B. Huber, K. Borchers, G.E.M. Tovar, P.J. Kluger, Methacrylated gelatin and mature adipocytes are promising components for adipose tissue engineering, *J. Biomater. Appl.* 30 (2016) 699–710. <https://doi.org/10.1177/0885328215587450>.
- [290] B. Wagner, R. Tharmann, I. Haase, M. Fischer, A.R. Bausch, Cytoskeletal polymer networks: The molecular structure of cross-linkers determines, (2006).
- [291] Y. Pan, Y. Guo, J. Liu, H. Zhu, G. Chen, Q. Liu, PDMS with Tunable Side Group Mobility and Its Highly Permeable Membrane for Removal of Aromatic Compounds, 211816 (2022). <https://doi.org/10.1002/anie.202111810>.
- [292] M.Z. Baker, R. Badiello, M. Tamba, M. Quintiliani, G. Gorin, Pulse radiolytic study of hydrogen transfer from glutathione to organic radicals, *Int. J. Radiat. Biol.* 41 (1982) 595–602. <https://doi.org/10.1080/09553008214550691>.
- [293] Y.S. Lim, M.K. Cha, H.K. Kim, T.B. Uhm, J.W. Park, K. Kim, I.H. Kim,

Removals of hydrogen peroxide and hydroxyl radical by thiol-specific antioxidant protein as a possible role in vivo, *Biochem Biophys Res Commun.* (1993). <https://doi.org/doi:10.1006/bbrc.1993.1410>.

- [294] P. Di Mascio, M.E. Murphy, H. Sies, Antioxidant defense systems: The role of carotenoids, tocopherols, and thiols, *Am. J. Clin. Nutr.* (1991). <https://doi.org/10.1093/ajcn/53.1.194S>.
- [295] T.A. Dreier, C.J. Ackerson, Radicals Are Required for Thiol Etching of Gold Particles, *Angew. Chemie - Int. Ed.* 54 (2015) 9249–9252. <https://doi.org/10.1002/anie.201502934>.
- [296] M. Baňasová, K. Valachová, I. Juránek, L. Šoltés, Dithiols as more effective than monothiols in protecting biomacromolecules from free-radical-mediated damage: In vitro oxidative degradation of high-molar-mass hyaluronan, *Chem. Pap.* 68 (2014) 1428–1434. <https://doi.org/10.2478/s11696-014-0591-1>.
- [297] M. Lin, J.Z. Yu, Dithiothreitol (DTT) concentration effect and its implications on the applicability of DTT assay to evaluate the oxidative potential of atmospheric aerosol samples, *Neotrop. Entomol.* 251 (2019) 938–944. <https://doi.org/10.1016/j.envpol.2019.05.074>.
- [298] D. Ko, H. Kim, H. Lee, C.T. Yavuz, H.R. Andersen, Y. Hwang, Applicability of disulfide-polymer particles surface embedded on alginate beads for cadmium removal from airport derived stormwater, *J. Environ. Chem. Eng.* 6 (2018) 4124–4129. <https://doi.org/10.1016/j.jece.2018.06.007>.
- [299] C. Hoffmann, V. Chiaula, L. Yu, M. Pinelo, J.M. Woodley, A.E. Dugaard, Simple Preparation of Thiol–Ene Particles in Glycerol and Surface Functionalization by Thiol–Ene Chemistry (TEC) and Surface Chain Transfer Free Radical Polymerization (SCT-FRP), *Macromol. Rapid Commun.* 39 (2018) 1–6. <https://doi.org/10.1002/marc.201700394>.
- [300] J.P.A. Heuts, T.P. Davis, G.T. Russell, Comparison of the Mayo and chain length distribution procedures for the measurement of chain transfer constants, *Macromolecules.* 32 (1999) 6019–6030. <https://doi.org/10.1021/ma990076j>.
- [301] W. Sattler, M.C.D. Carter, N.J. Irick, J. Defelippis, R.C. Even, End-Group Control in the Radical Polymerization of Methyl Methacrylate with tert-Butyl Peroxypivalate Initiator in the Presence of Thiol Chain Transfer Agents, *ACS Appl. Polym. Mater.* 2 (2020) 3936–3947. <https://doi.org/10.1021/acsapm.0c00598>.

- [302] C. Henríquez, C. Bueno, E.A. Lissi, M. V. Encinas, Thiols as chain transfer agents in free radical polymerization in aqueous solution, *Polymer (Guildf)*. 44 (2003) 5559–5561. [https://doi.org/10.1016/S0032-3861\(03\)00581-0](https://doi.org/10.1016/S0032-3861(03)00581-0).
- [303] O. Jeon, D.S. Alt, S.M. Ahmed, E. Alsberg, The effect of oxidation on the degradation of photocrosslinkable alginate hydrogels, *Biomaterials*. 33 (2012) 3503–3514. <https://doi.org/10.1016/j.biomaterials.2012.01.041>.
- [304] Y. Il Cho, S. Park, S.Y. Jeong, H.S. Yoo, In vivo and in vitro anti-cancer activity of thermo-sensitive and photo-crosslinkable doxorubicin hydrogels composed of chitosan-doxorubicin conjugates, *Eur. J. Pharm. Biopharm.* 73 (2009) 59–65. <https://doi.org/10.1016/j.ejpb.2009.04.010>.
- [305] O. Jeon, C. Powell, S.M. Ahmed, E. Alsberg, Biodegradable, photocrosslinked alginate hydrogels with independently tailorable physical properties and cell adhesivity, *Tissue Eng. - Part A*. 16 (2010) 2915–2925. <https://doi.org/10.1089/ten.tea.2010.0096>.
- [306] X. Wang, T. Hao, J. Qu, C. Wang, H. Chen, Synthesis of thermal polymerizable alginate-GMA hydrogel for cell encapsulation, *J. Nanomater.* 2015 (2015). <https://doi.org/10.1155/2015/970619>.
- [307] F. Araiza-Verduzco, E. Rodríguez-Velázquez, H. Cruz, I.A. Rivero, D.R. Acosta-Martínez, G. Pina-Luis, M. Alatorre-Meda, Photocrosslinked alginate-methacrylate hydrogels with modulable mechanical properties: Effect of the molecular conformation and electron density of the methacrylate reactive group, *Materials (Basel)*. 13 (2020). <https://doi.org/10.3390/ma13030534>.
- [308] M. Hasany, S. Talebian, S. Sadat, N. Ranjbar, M. Mehrali, G.G. Wallace, M. Mehrali, Synthesis, properties, and biomedical applications of alginate methacrylate (ALMA)-based hydrogels: Current advances and challenges, *Appl. Mater. Today*. 24 (2021) 101150. <https://doi.org/10.1016/j.apmt.2021.101150>.
- [309] U.P. Kappes, D. Luo, M. Potter, K. Schulmeister, T.M. Rüniger, Short- and long-wave UV light (UVB and UVA) induce similar mutations in human skin cells, *J. Invest. Dermatol.* 126 (2006) 667–675. <https://doi.org/10.1038/sj.jid.5700093>.
- [310] W. Lu, D. Bao, F. Ta, D. Liu, D. Zhang, Z. Zhang, Z. Fan, Multifunctional Alginate Hydrogel Protects and Heals Skin Defects in Complex Clinical Situations, *ACS Omega*. 5 (2020) 17152–17159. <https://doi.org/10.1021/acsomega.0c01108>.

- [311] K.E. Barış, L. Tanaçan, Improving the geopolymeric reactivity of Earth of Datça as a natural pozzolan in developing green binder, *J. Build. Eng.* 41 (2021). <https://doi.org/10.1016/j.jobe.2021.102760>.
- [312] J. Godleman, F. Leroux, S. Reynolds, J. Philpott, P.B. Cranwell, J.L. Harries, W. Hayes, H.M. Colquhoun, Progress in Organic Coatings Aromatic poly ( fluorocarbon ) s : Soluble , hydrophobic binders for inkjet formulations, *Prog. Org. Coatings.* 158 (2021) 106378. <https://doi.org/10.1016/j.porgcoat.2021.106378>.
- [313] T. Zheng, T. Zhang, M.S. de la Fuente, G. Liu, Aqueous emulsion of conductive polymer binders for Si anode materials in lithium ion batteries, *Eur. Polym. J.* 114 (2019) 265–270. <https://doi.org/10.1016/j.eurpolymj.2019.02.041>.
- [314] I.J. Haug, K.I. Draget, O. Smidsrød, Physical and rheological properties of fish gelatin compared to mammalian gelatin, *Food Hydrocoll.* 18 (2004) 203–213. [https://doi.org/10.1016/S0268-005X\(03\)00065-1](https://doi.org/10.1016/S0268-005X(03)00065-1).
- [315] A. Peutzfeldt, E. Asmussen, Hardness of restorative resins: Effect of camphorquinone, amine, and inhibitor, *Acta Odontol. Scand.* 47 (1989) 229–231. <https://doi.org/10.3109/00016358909007706>.
- [316] W. Geurtsen, F. Lehmann, W. Spahl, G. Leyhausen, Cytotoxicity of 35 dental resin composite monomers/additives in permanent 3T3 and three human primary fibroblast cultures, *J. Biomed. Mater. Res.* 41 (1998) 474–480. [https://doi.org/10.1002/\(SICI\)1097-4636\(19980905\)41:3<474::AID-JBM18>3.0.CO;2-I](https://doi.org/10.1002/(SICI)1097-4636(19980905)41:3<474::AID-JBM18>3.0.CO;2-I).
- [317] M. Wessels, G. Leyhausen, J. Volk, W. Geurtsen, Oxidative stress is responsible for genotoxicity of camphorquinone in primary human gingival fibroblasts, *Clin. Oral Investig.* 18 (2014) 1705–1710. <https://doi.org/10.1007/s00784-013-1178-x>.
- [318] J. Volk, C. Ziemann, G. Leyhausen, W. Geurtsen, Non-irradiated campherquinone induces DNA damage in human gingival fibroblasts, *Dent. Mater.* 25 (2009) 1556–1563. <https://doi.org/10.1016/j.dental.2009.07.009>.
- [319] M. Gastaldi, F. Cardano, M. Zanetti, G. Viscardi, C. Barolo, S. Bordiga, S. Magdassi, A. Fin, I. Roppolo, Functional Dyes in Polymeric 3D Printing: Applications and Perspectives, *ACS Mater. Lett.* 3 (2021) 1–17. <https://doi.org/10.1021/acsmaterialslett.0c00455>.
- [320] H.J. Hageman, For free radical polymerization 60, 6800, 13 (1985) 123–

- [321] H. Korhonen, A. Helminen, J. V. Seppälä, Synthesis of polylactides in the presence of co-initiators with different numbers of hydroxyl groups, *Polymer (Guildf)*. 42 (2001) 7541–7549. [https://doi.org/10.1016/S0032-3861\(01\)00150-1](https://doi.org/10.1016/S0032-3861(01)00150-1).
- [322] K.S. Anseth, C.M. Wang, C.N. Bowman, Kinetic Evidence of Reaction Diffusion during the Polymerization of Multi(meth)acrylate Monomers, *Macromolecules*. 27 (1994) 650–655. <https://doi.org/10.1021/ma00081a004>.
- [323] P. Leclercq, J.M. Buisine, X. Coqueret, On the polymer effect observed with macromolecular photoinitiators: A study of the viscosity effect on the starting polymerization rate, *Macromol. Chem. Phys.* 198 (1997) 2977–2984. <https://doi.org/10.1002/macp.1997.021980926>.
- [324] P.R. Dvornić, M.S. Jaćović, The Viscosity Effect on Autoacceleration of the Rate of Free Radical Polymerization, *Polym. Eng. Sci.* 21 (1981) 792–796.
- [325] D.A. Gyles, L.D. Castro, J.O.C. Silva, R.M. Ribeiro-Costa, A review of the designs and prominent biomedical advances of natural and synthetic hydrogel formulations, *Eur. Polym. J.* 88 (2017) 373–392. <https://doi.org/10.1016/j.eurpolymj.2017.01.027>.
- [326] H. Kumar, K. Sakthivel, M.G.A. Mohamed, E. Boras, S.R. Shin, K. Kim, Designing Gelatin Methacryloyl (GelMA)-Based Bioinks for Visible Light Stereolithographic 3D Biofabrication, *Macromol. Biosci.* 21 (2021) 1–17. <https://doi.org/10.1002/mabi.202000317>.
- [327] E. Fantino, I. Roppolo, D. Zhang, J. Xiao, A. Chiappone, M. Castellino, Q. Guo, C.F. Pirri, J. Yang, 3D Printing/Interfacial Polymerization Coupling for the Fabrication of Conductive Hydrogel, *Macromol. Mater. Eng.* 303 (2018) 1–8. <https://doi.org/10.1002/mame.201700356>.
- [328] G. Müller, M. Zalibera, G. Gescheidt, A. Rosenthal, G. Santiso-Quinones, K. Dietliker, H. Grützmacher, Simple one-pot syntheses of water-soluble Bis(acyl)phosphane oxide photoinitiators and their application in surfactant-free emulsion polymerization, *Macromol. Rapid Commun.* 36 (2015) 553–557. <https://doi.org/10.1002/marc.201400743>.
- [329] R.L. Monika Schuster, Claudia Turecek, Guenter Weigel, Robert Saf, Juergen Stampfl, Franz Varga, Gelatin-Based Photopolymers for Bone Replacement Materials, *J. Polym. Sci. Part A Polym. Chem.* 47 (2009)



7078–7089. <https://doi.org/10.1002/pola>.

- [330] H. Staroszczyk, J. Pielichowska, K. Sztuka, J. Stangret, I. Kołodziejaska, Molecular and structural characteristics of cod gelatin films modified with EDC and TGase, *Food Chem.* 130 (2012) 335–343. <https://doi.org/10.1016/j.foodchem.2011.07.047>.
- [331] Y. Zheng, Y. Liang, D. Zhang, X. Sun, L. Liang, J. Li, Y.N. Liu, Gelatin-Based Hydrogels Blended with Gellan as an Injectable Wound Dressing, *ACS Omega.* 3 (2018) 4766–4775. <https://doi.org/10.1021/acsomega.8b00308>.
- [332] Q. Xing, K. Yates, A. Bailey, C. Vogt, W. He, M.C. Frost, F. Zhao, Effects of local nitric oxide release on human mesenchymal stem cell attachment and proliferation on gelatin hydrogel surface, *Surf. Innov.* 1 (2013) 224–232. <https://doi.org/10.1680/si.13.00019>.
- [333] I. Yakimets, N. Wellner, A.C. Smith, R.H. Wilson, I. Farhat, J. Mitchell, Mechanical properties with respect to water content of gelatin films in glassy state, *Polymer (Guildf).* 46 (2005) 12577–12585. <https://doi.org/10.1016/j.polymer.2005.10.090>.
- [334] K. Ikemura, K. Ichizawa, Y. Jogetsu, T. Endo, Synthesis of a novel camphorquinone derivative having acylphosphine oxide group, characterization by UV-VIS spectroscopy and evaluation of photopolymerization performance, *Dent. Mater. J.* 29 (2010) 122–131. <https://doi.org/10.4012/dmj.2009-026>.
- [335] C.F. Guimarães, L. Gasperini, A.P. Marques, R.L. Reis, The stiffness of living tissues and its implications for tissue engineering, *Nat. Rev. Mater.* (n.d.). <https://doi.org/10.1038/s41578-019-0169-1>.
- [336] A. Miyazawa, S. Ito, S. Asano, I. Tanaka, M. Sato, M. Kondo, Y. Hasegawa, *SC, Biochem. Biophys. Res. Commun.* (2018). <https://doi.org/10.1016/j.bbrc.2017.12.115>.
- [337] Lee, K. Y., M.C. Peters, K.W. Anderson, D.J. Mooney, Controlled growth factor release from synthetic extracellular matrices, *Nature.* 408 (2000) 1–3. <https://doi.org/https://doi.org/10.1038/35050141>.
- [338] Y. Tabata, Y. Matsui, Y. Ikada, Growth factor release from amylopectin hydrogel based on copper coordination, *J. Control. Release.* 56 (1998) 135–148. [https://doi.org/10.1016/S0168-3659\(98\)00081-9](https://doi.org/10.1016/S0168-3659(98)00081-9).
- [339] N. ÇELEBI, N. ERDEN, B. GÖNÜL, M. KOZ, Effects of epidermal

- growth factor dosage forms on dermal wound strength in mice, *J. Pharm. Pharmacol.* 46 (1994) 386–387. <https://doi.org/10.1111/j.2042-7158.1994.tb03820.x>.
- [340] D.E. Ingber, D. Prusty, J. V. Frangioni, E.J. Cragoe, C. Lechene, M.A. Schwartz, Control of intracellular pH and growth by fibronectin in capillary endothelial cells, *J. Cell Biol.* 110 (1990) 1803–1811. <https://doi.org/10.1083/jcb.110.5.1803>.
- [341] C. Noè, M. Zanon, A. Arencibia, M.J. López-Muñoz, N.F. de Paz, P. Calza, M. Sangermano, UV-Cured Chitosan and Gelatin Hydrogels for the Removal of As(V) and Pb(II) from Water, *Polymers (Basel)*. 14 (2022). <https://doi.org/10.3390/polym14061268>.
- [342] P. Sautrot-Ba, V. Brezová, J.P. Malval, A. Chiappone, L. Breloy, S. Abbad-Andalousi, D.L. Versace, Purpurin derivatives as visible-light photosensitizers for 3D printing and valuable biological applications, *Polym. Chem.* 12 (2021) 2627–2642. <https://doi.org/10.1039/d1py00126d>.
- [343] S. Stoll, A. Schweiger, EasySpin, a comprehensive software package for spectral simulation and analysis in EPR, *J. Magn. Reson.* 178 (2006) 42–55. <https://doi.org/10.1016/j.jmr.2005.08.013>.